Illinois U. Library

ЖУРНАЛ
ЭКСПЕРИМЕНТАЛЬНОЙ И ТЕОРЕТИЧЕСКОЙ
ФИЗИКИ
АКАДЕМИЯ НАУК СССР

SOVIET PHYSICS

JETP

VOLUME 3 NUMBER 3

A Translation

of the

Journal of Experimental and Theoretical Physics

of the

Academy of Sciences of the USSR

OCTOBER, 1956

Published by the

AMERICAN INSTITUTE OF PHYSICS
INCORPORATED

SOVIET PHYSICS
JETP

A translation of the Journal of Experimental and Theoretical Physics of the USSR.

A publication of the

AMERICAN INSTITUTE OF PHYSICS

Governing Board

FREDERICK SEITZ, *Chairman*
ALLEN V. ASTIN
ROBERT F. BACHER
W. S. BAIRD
H. A. BETHE
R. T. BIRGE
FRANK D. DEXTER
I. C. GARDNER
S. A. GOUDSMIT
CHARLES KITTEL
HUGH S. KNOWLES
R. B. LINDSAY
WILLIAM F. MEGGERS
HARRY F. OLSON
R. R. PALMER
R. F. PATON
ERIC RODGERS
RALPH A. SAWYER
H. D. SMYTH
MARK W. ZEMANSKY

Administrative Staff

HENRY A. BARTON, *Director*
MARK W. ZEMANSKY, *Treasurer*
WALLACE WATERFALL, *Executive Secretary*
THEODORE VORBURGER, *Advertising Manager*
RUTH F. BRYANS, *Publication Manager*
ALICE MASTROPIETRO *Circulation Manager*
KATHRYN SETZE, *Assistant Treasurer*
EUGENE H. KONE, *Director of Public Relations*

American Institute of Physics Advisory Board on Russian Translation

ELMER HUTCHISSON, *Chairman*
DWIGHT GRAY, MORTON HAMERMESH, VLADIMIR ROJANSKY, VICTOR WEISSKOPF

Editor of SOVIET PHYSICS
ROBERT T. BEYER, DEPARTMENT OF PHYSICS, BROWN UNIVERSITY, PROVIDENCE, R.I.

SOVIET PHYSICS is a monthly journal published by the American Institute of Physics for the purpose of making available in English reports of current Soviet research in physics as contained in the Journal of Experimental and Theoretical Physics of the Academy of Sciences of the USSR. The page size of SOVIET PHYSICS will be 7⅞" x 10½", the same as other Institute journals.

Transliteration of the names of Russian authors follows the system employed by the Library of Congress.

This translating and publishing project was undertaken by the Institute in the conviction that dissemination of the results of researches everywhere in the world is invaluable to the advancement of science. The National Science Foundation of the United States encouraged the project initially and is supporting it in large part by a grant.

The American Institute of Physics and its translators propose to translate faithfully all the material in the Journal of EXPERIMENTAL AND THEORETICAL PHYSICS OF THE USSR appearing after January 1, 1955. The views expressed in the translated material, therefore, are intended to be those expressed by the original authors, and not those of the translators nor of the American Institute of Physics.

Two volumes are published annually, each of six issues. Each volume contains the translation of one volume of the Journal of EXPERIMENTAL AND THEORETICAL PHYSICS OF THE USSR. New volumes begin in February and August.

Subscription Prices:

Per year (12 issues)

United States and Canada	$60.00
Elsewhere	64.00

Back Numbers

Single copies	$ 6.00

Subscriptions should be addressed to the American Institute of Physics, 57 East 55 Street, New York 22, New York.

Copyright by American Institute of Physics 1956

SOVIET PHYSICS

JETP

SOVIET PHYSICS JETP VOLUME 3, NUMBER 3 OCTOBER, 1956

Toward New Successes of Soviet Physics

J. Exptl. Theoret. Phys. (U.S.S.R.) 30, 433-436 (March, 1956)

IN the summary report of the Central Committee of the Communist Party of the Soviet Union, Comrade Khrushchev expressed from the rostrum of the Congress deep gratitude to Soviet scientists for their fruitful work. This expresion of gratitude received general approval by the delegates to the congress. Outstanding among the successful accomplishments of our scientists is the work done by the Soviet physicists.

Describing the progress of Soviet science, Academician A. N. Nesmeianov, President of the U.S.S.R. Academy of Sciences, stated in his address to the Congress that "the brightest accomplishments are the recent successes in the field of atomic energy and its peaceful use. It must be noted, that we deal here not with any one particular discovery or disclosure of a secret, as it usually seems to the nonspecialist, but with a vigorous, well organized, rapid advance of the entire front of science in a field that is becoming recognized as predominant in the natural sciences.

"It was possible to organize this matter within a short period because the U.S.S.R. Academy of Sciences had already been working on radioactivity, cosmic rays, and nuclear phenomena. Thus, a certain "scientific inventory" of trained personnel was on hand to make possible this development. The success was based on the use of the entire arsenal of modern physics and the trails of investigation blazed by the theories of relativity and quantum mechanics, which are the foundations of modern physics. This unprecedented advance of science has included, as particular cases, many discoveries such as the principle (developed at the Academy of Sciences) for producing accelerators that enable charged particles to reach the colossal, indeed cosmic energies of 10 bev, and many other, no less important, discoveries.

"Even in the Sixth Five Year Plan, atomic power, though still used on an experimental scale, will produce more than twice the power generated by the stations of Tsarist Russia. Ahead of us is the mastery of control of thermonuclear reactions as a result of which one can hope that the reactions that take place in the hydrogen bomb and similar reactions will become available for the peaceful purposes of power engineering.

"A by product of this tremendous work cycle is the successful study of the application of isotopes – new elements produced by the atomic industry – to the logging of petroleum wells, to prospecting for other useful minerals, to performing gamma-ray inspection of metal articles and structures, to the preservation of health, and to the penetration of the deep mysteries of the living action of organism and its control. It is thus possible, for example, to arrest the growth of potatoes for months and conversely, to induce their growth by irradiation with gamma rays.

"In the twenties and thirties of this century, solid-state physics had been developing almost exclusively as an abstract science. Later, however, this development led to the creation of semiconductors for radio instruments, to thermocouple generators, and Rochelle-salt and photocell instruments. These instruments represent a new step in technological progress and are revolutionizing at the present time contempory communication, engineering, automation, computing and control machinery – literally every branch of modern engineering.

"The latest investigations of the thermoelectric

properties of semiconductors have uncovered great possibilities for power engineering, particularly in the field of direct conversion of waste products of heat into electricity. It can be hoped that the time is near when it will become possible to convert the heat and light of the deserts directly into electric energy."

The development of atomic physics and atomic power, which can now be truly considered as key sciences, was the subject of an address to the Congress by Academician I. V. Kurchatov. Academician Kurchatov reported to the Congress that he considers "the program of the Sixth Five Year Plan covering the utilization of atomic energy for peaceful purposes, will be fulfilled and overfulfilled by the Soviet people, as will be the entire Five Year Plan".

Kurchatov next told the Congress how the task, listed in the draft of the Directives, of generating 2000-2500 megawatts of electricity from atomic power will be solved in the current Five Year Plan. "The present level of nuclear engineering shows that although the capital investment per unit of installed capacity required for atomic electric stations is approximately 1.5 times that needed for coal-burning stations, the cost per kilowatt-hour generated by a large atomic and a coal-burning station can be approximately the same. This is mostly due to negligible low fuel consumption of the atomic electric. A 500-megawatt coal-burning station requires not less than 100,000 cars of coal per year, while for an atomic electric station of equal rating only several cars of uranium per year are enough.

"It is expedient to build atomic electric stations first in regions where fuel must be supplied from a distance. The present Five Year Plan calls for the construction of two atomic electric stations in the Urals with a total capacity of 1000 magawatts. A 400 magawatt atomic station will also be constructed near Moscow. The total capacity of the atomic electric stations which should be put into operation during the current Five Year Plan, is comparable with the capacity of some of the largest electric stations in the world, such as the one in Kuibyshev.

"The Congress must be told, however, although the installed capacity of the atomic electric stations is indeed large and, according to published data, exceeds the capacity of atomic electric stations planned in the U.S.A. and in England ,the atomic electric stations built under the current Five Year Plan are by nature still a large experiment, carried out by the government to determine the most technically reliable and economical ways of erecting atomic electric stations. We must determine reliably what share of the total power capacity of our socialist government must be allotted to atomic power in the Seventh and subsequent Five-Year Plans.

"Unlike the conventional coal and oil, the nuclear fuel burned in the atomic reactors yields new substances such as plutonium and others, which do not exist in nature and which in themselves are nuclear fuels. The quantity of the new products formed depends on the conditions under which the nuclear chain reaction is carried out. Under some conditions more new nuclear fuel is formed in greater quantities, than is initially consumed in the chain reaction. This process is called expanded breeding. It is as if you were to burn coal in a furnace, and recover still more coal among the ashes.

"The process of breeding nuclear fuel in atomic reactors guarantees the economic production of nuclear energy and makes possible the use of not only uranium but also thorium.

"Topics studied in detail to date are the dependence of fission probability of various atomic nuclei on the neutron velocity, the laws of transmutation of matter in neutron and gamma fields, and the laws of retardation of neutrons and their interaction with the fission products of uranium. Many such problems can be solved only in operating reactors of some type or another.

"The current Five Year Plan calls for construction of up to ten types of atomic reactors with capacities from 50 to 200 megawatts each. Reactors will be built with fast and intermediate neutrons; with medium-energy neutrons; with graphite, beryllium or heavy-water moderators; and with gas, water, and metal cooling. A large thorium reactor will be built.

"We are carrying on work on atomic reactors jointly with the scientists and engineers of the satellite nations who are producing at home, with the cooperation of the Soviet Union, atomic reactors for scientific purposes and who are planning the construction of atomic electric stations. Our joint work with the scientists of the satellite nations will increase in scope and will undoubtedly lead to outstanding results."

The concluding portion of the address by Academician Kurchatov was devoted to the tasks of Soviet scientists in the development of atomic physics. He said: "Before us is a large program of work on atomic electric stations and atomic power installations. But Soviet scientists and nuclear specialists must not restrict their activity to the solution of these problems alone. It is also essential to develop further theoretical nuclear science so as to blaze reliable new paths

for the future technology.

"We have before us an example of how Soviet scientists and engineers solved the problem of using the nuclear energy of uranium and other heavy elements. Our successes in this field are largely due to the fact that the institutes, with whose founding the great Lenin concerned himself as early as 1918-1920, carried on persistent theoretical work on the study of the laws of atomic structure, the laws of chain reactions, the laws of structure of the atomic nucleus – theoretical work that laid out the paths now followed by our nuclear engineering.

"Soviet scientists must discover new laws of nature and gain more and more knowledge of the properties of matter. We must discover the nature of the forces binding the protons and the neutrons to each other, and the basic structural elements of the atomic nuclei. It is essential to study the structure of the protons and neutrons themselves. We must construct giant accelerators for this purpose.

"The party and the government grant liberally the requests made by scientists. This year, for example, a powerful accelerator, capable of accelerating protons to an energy of 10 bev is scheduled to go into operation. The electromagnet of this installation, the greatest in the world, weighs 36,000 tons. Even larger accelerators, capable of accelerating particles to energies of 50 bev, are now being designed.

"Theoretical work on atomic and nuclear physics has uncovered the possibility of finding new ways of utilizing atomic energy for peaceful purposes, and realizing controllable thermonuclear reactions. These reactions of synthesis or fusion are now the most important general problem of science.

"The controllable thermonuclear reaction would obtain energy not from the reserves concentrated in the atomic nuclei of the rare elements uranium and thorium, but by producing helium from hydrogen, an element widely available in nature.

"The solution of this most difficult and greatest problem would relieve humanity forever of the worry over the energy resources needed for its existence on the earth.

"We now know how to create in the hydrogen bomb the conditions for the fusion of hydrogen into helium. But it is now necessary to control this reaction so as to prevent explosion.

"We, the Soviet scientists, would like to work on the solution of this scientific problem, of greatest importance to humanity, together with the scientists of all the countries in the world, including the American scientists, whose scientific and technical accomplishments we greatly value. To make this possible we need only one thing, that the government of the United States accept the proposal of the Soviet Union for which our party is constantly struggling, that the use of atomic and hydrogen weapons be outlawed."

In its Directives the Congress has adopted many important resolutions, which will contribute to the rapid development of both theoretical and practical knowledge, and will enable our physicists to develop their work even more and result in a further flowering of physical science.

Translated by J. G. Adashko
86

Meson Field Theory. III. Conservation of Physical Quantities

A. A. BORGARDT
Dnepropetrovsk State University

(Submitted to JETP editor November 17, 1954)
J. Exptl. Theoret. Phys. (U.S.S.R.) 30, 330-333 (February, 1956)

The paper investigates densities of physical quantities and conservation laws for meson fields with anticommuting matrices, whose general properties were described in previously published papers[1-3]

CONSERVATION laws for wave fields can be obtained using Noether's theorem.[4,5] This method is based on the use of the correspondence which exists between the invariance of the Lagrangian of the field with respect to coordinate transformations of the conformal group and the conservation of physical quantities.

In the present case, such a procedure is not convenient mainly because of the non-uniqueness of the variational principle. In obtaining the conservation laws it is therefore more expedient to go directly to the wave equations, since any conservation laws must be consistent with them. We choose the wave equations of the meson field in the form

$$\Gamma_\lambda \partial\Psi / \partial x_\lambda + k_0\Psi = Q, \tag{1}$$

$$-\partial\Psi^+ / \partial x_\lambda \Gamma_\lambda + k_0\Psi^+ = Q^+,$$

where the kinematic matrices Γ_μ anticommute:

$$^1/_2 \{\Gamma_\mu\Gamma_\nu\} - \delta_{\mu\nu}\cdot I = 0. \tag{2}$$

If we use a representation with real Γ_i and imaginary Γ_4, we can define the charge conjugate by means of the diagonal reflection matrix R_4

$$\Psi^+ = \Psi^* R_4 \qquad (R_\mu = 2\beta_\mu^2 - I). \tag{3}$$

The anticommuting matrices Γ_μ, which, together with their products, form the group G_{16}, are made up of two orthogonal 16'th-degree reducible representations of the Kemmer algebra:

$$\Gamma_\mu = \beta_\mu^{(1)} + \beta_\mu^{(2)}, \tag{4}$$

$$\beta_\mu\beta_\nu\beta_\rho + \beta_\rho\beta_\nu\beta_\mu - \beta_\mu\delta_{\nu\rho} - \beta_\rho\delta_{\nu\mu} = 0, \tag{5}$$

$$\beta_\mu^{(1)}\beta_\mu^{(2)} = 0 \text{ (n. s.)*}$$

The orthogonalization can be achieved most simply by using the matrix of the genalized Larmor transformation[2]:

$$\beta_\mu^{(2)} = -\Gamma_5\beta_\mu^{(1)}\Gamma_5. \tag{6}$$

where ($\Gamma_5 = \Gamma_1\Gamma_2\Gamma_3\Gamma_4$):

In addition to the group G_{16}, another group $\bar{G}_{16}$ generated by the anticommuting matrices $\bar{\Gamma}_\mu$

$$\bar{\Gamma}_\mu = \beta_\mu^{(1)} - \beta_\mu^{(2)}, \tag{7}$$

$$^1/_2 \{\bar{\Gamma}_\mu\bar{\Gamma}_\nu\} - \delta_{\mu\nu}\cdot I = 0, \ [\Gamma_\mu\bar{\Gamma}_\nu] = 0. \tag{8}$$

will play an important part.

It is easy to see that all elements of G_{16} and $\bar{G}_{16}$ commute with one another. The matrices Γ_μ and $\bar{\Gamma}_\mu$ are related simply via the reflection matrices: $\bar{\Gamma}_\mu = R_\mu\Gamma_\mu$ (n. s.)

From the field equations, we immediately obtain differential relations which are bilinear in the components of the undor** Ψ

$$\Psi^+ M\Gamma_\lambda\partial\Psi / \partial x_\lambda \tag{9}$$

$$\mp(\partial\Psi^+ / \partial x_\lambda)\Gamma_\lambda M\Psi + (1 \pm 1) k_0\Psi^+ M\Psi$$

$$= \Psi^+ MQ \pm Q^+ M\Psi,$$

where M is any matrix of G_{16} or $\bar{G}_{16}$.

Conservation laws are obtained from (9) in the

---

[1] A. A. Borgardt, Dokl. Akad. Nauk SSSR **78**, 1113 (1951).

[2] A. A. Borgardt, J. Exptl. Theoret. Phys. (U.S.S.R.) **24**, 24 (1953).

[3] A. A. Borgardt, J. Exptl. Theoret. Phys. (U.S.S.R.) **24**, 284 (1953).

[4] E. Bessel-Hagen, Math. Ann. **84**, 258 (1921).

[5] E. L. Hill, Revs. Mod. Phys. **23**, 253 (1951).

*n. s. means 'no summation.'

**By undor we designate a one-column matrix whose 16 elements consist of a scalar, a 4-vector, and the components of completely antisymmetric tensors of all ranks up to four.

two cases where M commutes, or anticommutes, with all the Γ_μ.

a). $[M\Gamma_\mu] = 0$. This can happen if M belongs to the ring $\bar{G}_{16}$; we get 16 conservation laws of the form

$$\partial(\Psi^+\bar{\Gamma}\Gamma_\lambda\Psi)/\partial x_\lambda = \Psi^+\bar{\Gamma}Q - Q^+\bar{\Gamma}\Psi, \tag{10}$$

where $\bar{\Gamma}$ is any element of $\bar{G}_{16}$.

The conserved quantities have the following physical meaning:

1. $\bar{\Gamma} = I,\ j_\mu = (e/2\mathscr{E}_0)\Psi^+\Gamma_\mu\Psi$

is the vector of the electric current density, and vanishes in a neutral field (the proof was given in Ref. 3, Eqs. 25-27; the problem is handled similarly in all other cases.)

2. $\bar{\Gamma} = \bar{\Gamma}_\mu,\ T'_{\mu\nu} = {}^1/_2\,\Psi^+\bar{\Gamma}_\mu\Gamma_\nu\Psi$

the symmetric energy-momentum tensor, does not vanish in a neutral field.

3. $\bar{\Gamma} = {}^1/_2[\bar{\Gamma}_\mu\bar{\Gamma}_\nu],\ \sigma'_{\mu\nu,\rho} = (c/4\mathscr{E}_0)\Psi^+[\bar{\Gamma}_\mu\bar{\Gamma}_\nu]\Gamma_\rho\Psi$,

the spin pseudovector, does not vanish in a neutral field. The form of the conservation equation is

$$\partial\sigma'_{\mu\nu,\lambda}/\partial x_\lambda = (c/4\mathscr{E}_0)(\Psi^+[\bar{\Gamma}_\mu\bar{\Gamma}_\nu]Q - Q^+[\bar{\Gamma}_\mu\bar{\Gamma}_\nu]\Psi) \tag{11}$$

and is expressed in three-dimensional form as

$$\partial\vec{\sigma}/c\partial t + \nabla, \ldots \tag{12}$$

Thus, strictly speaking, we are dealing simply with the mechanical equation of motion of an angular momentum.

The space divergence which appears on the left side of (12) represents the time derivative of the orbital angular momentum. Therefore we should distinguish (11) from the strict spin-conservation equation (continuity equation) which will be gotten later.

4. $\bar{\Gamma} = \bar{\Gamma}_5\bar{\Gamma}_\mu,\ M_{\rho\tau} = (e\hbar c/2\mathscr{E}_0^2)\Psi^+\bar{\Gamma}_5\bar{\Gamma}_\mu\Gamma_\nu\Psi$,

the antisymmetric tensor of the dipole moment, vanishes in a neutral field.

5. $\bar{\Gamma} = \Gamma_5,\ \sigma''_\mu = (ic/2\mathscr{E}_0)\Psi^+\bar{\Gamma}_5\Gamma_\mu\Psi$,

a spin pseudovector, vanishes in a neutral field since, like the current and the dipole moment, it is a quantity of the type ( ) − ( )*. Obviously, the spin σ''_μ (and not σ'_μ) is responsible for the formation of the kinematic dipole moment $M_{\mu\nu}$. In addition, σ'_μ and σ''_μ differ in the sign of terms containing ψ_0 and $\bar{\psi}_0$; in a purely transverse field, this difference disappears. The spin σ''_μ satisfies an equation of continuity of the form

$$\partial(\Psi^+\bar{\Gamma}_5\Gamma_\lambda\Psi)/\partial x_\lambda = \Psi^+\bar{\Gamma}_5Q - Q^+\bar{\Gamma}_5\Psi. \tag{13}$$

b). $\{M\Gamma_\mu\} = 0$. This can occur if M belongs to $R_5\bar{G}_{16}$; we get 16 conservation laws of the form

$$\partial(\Psi^+R_5\Gamma\Gamma_\lambda\Psi)/\partial x_\lambda + 2k_0\Psi^+R_5\bar{\Gamma}\Psi = \Psi^+R_5\bar{\Gamma}Q + Q^+R_5\bar{\Gamma}\Psi. \tag{14}$$

The conserved quantities differ from those considered in case a) by the presence of the matrix R_5 of reflection of proper time. Its effect on the density can be made clear from the following considerations. The matrix R_5 is used for splitting the wave function Ψ into a potential matrix Ψ^{I} and a field strength matrix Ψ^{II}[3]:

$$\Psi^{\mathrm{I}} = ({}^1/_2\,k_0)(I - R_5)\Psi, \tag{15}$$

$$\Psi^{\mathrm{II}} = {}^1/_2(I + R_5)\Psi.$$

Since $R_5^2 = I$, we get

$$R_5\Psi^{\mathrm{I}} = -\Psi^{\mathrm{I}},\quad R_5\Psi^{\mathrm{II}} = \Psi^{\mathrm{II}}. \tag{16}$$

Densities of physical quantities can be subdivided into those of "symmetrical" type

$$\rho_s(\Gamma) = \Psi^{+\mathrm{II}}\Gamma\Psi^{\mathrm{II}} + k_0^2\Psi^{+\mathrm{I}}\Gamma\Psi^{\mathrm{I}} = \rho^{\mathrm{II}} + k_0^2\rho^{\mathrm{I}} \tag{17}$$

and those of "antisymmetrical" type

$$\rho_{as}(\Gamma) = k_0(\Psi^{+\mathrm{II}}\Gamma\Psi^{\mathrm{I}} + \Psi^{+\mathrm{I}}\Gamma\Psi^{\mathrm{II}}). \tag{18}$$

The introduction of R_5, while it does not change the type of quantity, converts an antisymmetric density of the form ( ) + ( )* into a density of the form ( ) − ( )*, and vice versa; in the symmetric case, the sign of the part $\sim k_0^2$ is reversed.

The conserved quantities are:

1. $\bar{\Gamma} = I,\quad s_\mu = (c/2\mathscr{E}_0)\Psi^+R_5\Gamma_\mu\Psi$,

the action current vector, does not vanish in a neutral field.

2. $\bar{\Gamma} = \bar{\Gamma}_\mu,\ T''_{\mu\nu} = {}^1/_2\Psi^+R_5\bar{\Gamma}_\mu\Gamma_\nu\Psi$,

a symmetric energy-momentum tensor, does not vanish in a neutral field; it differs from $T'_{\mu\nu}$ in the sign of the part $\sim k_0^2$.

3. $\bar{\Gamma} = {}^1/_2[\Gamma_\mu\Gamma_\nu],\ \bar{\sigma}'_{\mu\nu,\rho}(c/4\mathscr{E}_0)\Psi^+R_5[\bar{\Gamma}_\mu\bar{\Gamma}_\nu]\Gamma_\rho\Psi$,

a spin pseudovector, differs from $\sigma'_{\mu\nu,\rho}$ in the fact that it vanishes in a neutral field.

4. $\bar{\Gamma} = \bar{\Gamma}_5\bar{\Gamma}_\mu,\ \bar{M}_{\rho\tau} = (e\hbar c/2\mathscr{E}_0^2)\Psi^+\Gamma_5\bar{\Gamma}_\mu\Gamma_\nu\Psi$,

an antisymmetric dipole moment tensor, differs from $M_{\rho\tau}$ in the sign of the part $\sim k_0^2$.

5. $\bar{\Gamma} = \bar{\Gamma}_5,\ \bar{\sigma}''_\mu = (ic/2\mathscr{E}_0)\Psi^+\Gamma_5\Gamma_\mu\Psi$

a spin pseudovector, differs from σ''_μ in the fact that it does not vanish for a neutral field.

In a purely transverse wave field, the equalities $\sigma'_\mu = \overline{\sigma}''_\mu$ and $\sigma''_\mu = \overline{\sigma}'_\mu$. hold. Thus the wave field possesses two spin densities, for each of which there is an equation of motion and an equation of continuity.

The use of two sets of anticommuting matrices Γ_μ and Γ_μ also simplifies the theory of ordinary meson fields. From (4) and (7), it follows immediately that the equations

$$\tfrac{1}{2}(\Gamma_\lambda + \overline{\Gamma}_\lambda)\,\partial\Psi/\partial x_\lambda + k_0\Psi = \tfrac{1}{2}(Q + \overline{Q}), \quad (19)$$

$$-\tfrac{1}{2}(\Gamma_\lambda + \overline{\Gamma}_\lambda)^T\,\partial\Psi^+/\partial x_\lambda + k_0\Psi^+ = \tfrac{1}{2}(Q + \overline{Q})^+$$

describe the usual vector-pseudoscalar field. Current, spin, energy, momentum and other quantities are formed from those considered above by symmetrizing with respect to Γ_μ and $\overline{\Gamma}_\mu$, at the same time preserving the parity of the quantity with respect to coordinate indices.

$$j_\mu = (e/4\mathscr{E}_0)\,\Psi^+(\Gamma_\mu + \overline{\Gamma}_\mu)\,\Psi = (e/2\mathscr{E}_0)\,\Psi^+\beta_\mu\Psi, \quad (20)$$

$$\sigma_\mu = (ic/4\mathscr{E}_0)\,\Psi^+(\Gamma_5\Gamma_\mu + \overline{\Gamma}_5\overline{\Gamma}_\mu)\,\Psi$$

$$= (ic/2\mathscr{E}_0)\,\Psi^+\beta_5\beta_\mu\Psi,$$

$$T_{\mu\nu} = \tfrac{1}{2}\Psi^+(\overline{\Gamma}_\mu\Gamma_\nu + \Gamma_\mu\overline{\Gamma}_\nu)\,\Psi$$

$$= \tfrac{1}{2}\Psi^+(\{\beta_\mu\beta_\nu\} - 2\delta_{\mu\nu}\cdot I)\,\Psi$$

etc. These same quantities for a pseudovector-scalar field are constructed by applying a generalized Larmor transformation to the operator of the corresponding quantity; this leaves the energy-momentum tensor unchanged.

In conclusion we must point out the following: In contrast to the equations obtained using Noether's theorem, the conservation equations given above contain explicitly only internal field quantities. However, it is easy to verify that this difference is a purely formal one.

We shall consider the conservation of the action current for a free electromagnetic field, and use vector notation. In this case, the quantity $s_\mu = (s, is_0)$,

$$\mathbf{s} = (1/c)\,[\mathbf{H}\cdot\mathbf{A}], \quad s_0 = -(1/c)\,\mathbf{E}\cdot\mathbf{A}, \quad (21)$$

satisfies a conservation law of the form of (14):

$$\partial s_\lambda/\partial x_\lambda = \partial s_0/c\partial t + \nabla\cdot\mathbf{s} = \tfrac{1}{2}c\,(\mathbf{E}^2 - \mathbf{H}^2). \quad (22)$$

On the other hand, using Noether's theorem, the invariance of the Lagrangian under reflection, $\delta x_\mu = a x_\mu$ leads to the conservation law

$$(\partial/\partial x_\lambda)\,(F_{\lambda\sigma}A_\sigma + x_\sigma T^{(k)}_{\lambda\sigma}) \quad (23)$$

$$= (\partial/c\partial t)\,(\mathbf{E}\cdot\mathbf{A}/c - \mathscr{E}^{(k)}t + \mathbf{p}^{(k)}\mathbf{x})$$

$$+ \nabla\cdot([\mathbf{H}\cdot\mathbf{A}]/c - \mathbf{S}^{(k)}t + \mathbf{T}^{(k)}\mathbf{x}) = 0,$$

where $\mathbf{p}^{(k)}$, $\mathbf{S}^{(k)}$, $\mathscr{E}^{(k)}$, $T^{(k)}_{ik}$, the momentum density, energy flux, energy density and stress tensor are components of the canonical energy-momentum tensor $T^{(k)}_{\mu\nu}$

In order to show the equivalence of (22) and (23), we substitute in (23) the quantity $\partial s_0/c\partial t + \nabla\cdot\mathbf{S}$ from (22), and integrate over the four-dimensional volume occupied by the field. We then obtain the obvious relation between the action, energy, and momentum of the field:

$$S = -t\int\mathscr{E}^{(k)}(d\mathbf{x}) + \int\mathbf{x}\mathbf{p}^{(k)}(d\mathbf{x}). \quad (24)$$

A similar equivalence proof can also be given in other cases.

Translated by M. Hamermesh
58

Generalized Form of the Diffusion Equation for a Single Particle

L. JANOSSY
Budapest

(Submitted to JETP editor October 15, 1954)
J. Exptl. Theoret. Phys. (U.S.S.R.) 30, 351-361 (February, 1956)

A general formulation is given of the diffusion equation for a single particle, from which follow a number of well known equations as special cases. By way of application, the scattering of particles in a homogeneous absorber is considered.

1. A general formulation of the diffusion equation for a single particle is given in the present paper. Other well known equations follow from it as special cases. The method applied in the present work is not here compared with other methods described in the literature; such a comparison will be given in a paper written by the author in collaboration with L. Pal and A. Bekesy. At the end of the paper, an application of the equation which represents practical interest will be examined.

The process of diffusion can be described by the function $\varphi(\mathbf{A}, \mathbf{U}, t)$, where $\mathbf{A} = A_1, A_2, \ldots, A_k$ are parameters which determine the state of the particle; in this case we do not limit ourselves only to such parameters which are strictly necessary for the determination of the state of the particle, but take into consideration other parameters, which depend in whole or in part on the rest; such parameters are included in order to determine their distribution. The vector $\mathbf{U}$, which has the components $\mathbf{U} = U_1, U_2, \ldots$, defines the intervals of the components of $\mathbf{A}$, and therefore, for each given state $\mathbf{A}$, we can determine whether it lies within $\mathbf{U}$ or not. Finally, t denotes the time and φ the probability that a particle, which is in the state $\mathbf{A}$ at the time $t' = 0$, is transferred at time $t' = t$ into such a state $\mathbf{A}'$ that

$$\mathbf{A}' \text{ lies within } \mathbf{U}. \tag{1}$$

The choice of intervals $\mathbf{U}$ has no importance for the solution of the problem that has been posed. For many purposes it is appropriate to choose some or even all of the components of $\mathbf{U}$ to be infinitely narrow. In the latter case we consider φ as the probability *density* relative to those components for which the interval is bounded in the fashion mentioned. In particular, if all the components of $\mathbf{U}$ are narrow, we have, in place of Eq. (1),

$$\mathbf{A}' = \mathbf{U}. \tag{2}$$

2. We choose the time as an independent variable, since any other choice of independent variable leads to difficulties, about which we shall say something below. The quantity φ must satisfy the following initial condition:

$$\varphi(\mathbf{A}, \mathbf{U}, t = 0) = \Delta(\mathbf{A}, \mathbf{U}), \tag{3}$$

where

$$\Delta(\mathbf{A}, \mathbf{U}) = \begin{cases} 1, & \text{if } \mathbf{A} \text{ is within } \mathbf{U} \\ 0 & \text{in any other case.} \end{cases}$$

In particular, if all the components of $\mathbf{U}$ lie in narrow intervals, then

$$\varphi(\mathbf{A}, \mathbf{U}, t = 0) = \delta(\mathbf{A} - \mathbf{U}). \tag{4}$$

If we had not chosen the time as the independent variable, but, say, the x coordinate of the particle, then, in place of an *initial* condition of type (3) or (4), it would have been necessary to furnish a *boundary* condition for x. It is not possible to give such a boundary condition arbitrarily; thus, for example, the boundary condition of the type

$$\varphi(\mathbf{A}, \mathbf{U}, x = 0) = \Delta(\mathbf{A}, \mathbf{U}) \tag{5}$$

leads to a contradiction. If the particle begins to move in the positive direction along the x axis, beginning from the point $x = 0$, then it can in general get back to the plane $x = 0$, while upon its return it can be shown to be outside of the interval $\mathbf{U}$. The probability of such a case is always finite, although in many cases it can be small. Thus a condition of type (5) can be imposed only for a single instant of time; hence it follows that it is not possible to lay down (5) as a boundary condition for an independent variable x.

Although, strictly speaking, it is not possible to choose x as the independent variable, nevertheless in a series of cases, such a choice can be shown to be a suitable approximation. In these cases, we

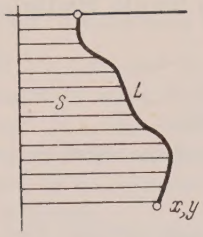

FIG. 1

neglect the errors which result from a possible rotation of the particle in the y,z plane from which it set out originally.

It is also possible to consider the length of path l as an independent variable. The difficulties which arise in this case are less serious than those in the choice of x as the independent variable; nevertheless, even in this case there remains the possibility that the velocity of the particle will finally reduce to zero. This leads to the appearance of singularities if l is chosen as the independent variable.

3. We consider the nature of the parameters **A**, while particular attention will be given to continuously and discontinuously varying quantities.

1) As components of **A** we can consider such quantities as the energy of the particle E, the momentum components p_x, p_y, p_z, the velocity components, etc. Such quantities change their values only in collisions (in each case, in the absence of an external field). Between collisions, these quantities remain fixed. In particular, it should be noted that the energy is often considered not as a continuously changing quantity rather than as a discontinuously changing one . It should be emphasized that such a treatment is of necessity approximate; ionizing losses are the result of many collisions, and in each collision, only a small part of the energy is lost. Thus the energy losses are discrete, and therefore we shall consider this process as discrete. Later it will be seen that, if we neglect certain small terms in our exact formula, we can obtain approximate formulas which result in the consideration of ionization as a continuous process.

2). We shall consider the components of **A** which change in a strictly continuous way. As such quantities, we have, for example, the coordinates x, y, z of the particle and the length l. An important quantity of this type is the area S between the trajectory of the particle and its projection on the x axis (Fig. 1). The latter quantities are not changed in a collision process, but change continuously in the interval between collisions. However, the derivatives of these quantities change discontinuously at the time of a collision. Thus, let

$$A_1 = v_x,\ A_2 = v_y,\ A_3 = x,\ A_4 = y,\ A_5 = S$$

(v_x, v_y are velocity components); then, between collisions, $A_1(t) = A_1(0)$, $A_2(t) = A_2(0)$, $A_3(t) = A_3(0) + A_1(0)t$, $A_4(t) = A_4(0) + A_2(0)t$, $A_5(t) = A_5(0) + A_3(0)t + {}^1/_2 A_1(0)A_2(0)t^2$ (for $0 \leqslant t < t_1$), where $A_k(t)$ is the value of the component A_k at $t \geq 0$, and under the condition that up to $t_1 > t$ no collision occurred.

3). If external forces act on the particle, then such parameters as the energy and momentum will change continuously between collisions, and discontinuously at collisions. A case of practical importance is the case of the deflection of a particle under the combined action of a magnetic field and diffusion.

In order not to introduce any limitations, we assume that, in general,

$$A_k(t) = A_k^{(0)}(0) + A_k^{(1)}(0)\,t + {}^1/_2 A_k^{(2)}(0)\,t^2 + \ldots$$

and consider all variables $A_k^{(l)}$ as stochastic variables which can change or not change upon collisions. However, we assume that a finite (and generally speaking, small) number of derivatives of $A_k^{(l)}$ will give a sufficiently accurate approximation*.

In what follows, when the symbol **A** is used, it will be assumed that all components $A_k^{(l)}$ are included in it, and correspondingly, that the vector **U** includes all components which relate to all the $A_k^{(l)}$. The quantities **A** thus introduced are certainly not all independent of each other; below, we shall have to deal with the question of the inclusion of certain of them in the course of the computation, but initially, we shall not take into account the possibility of the existence of a dependence between the quantities under consideration.

4). Variables which change continuously in accordance with the laws of probability will not be considered. Such quantities are not met with in practice and their introduction would provide an unnecessary complication. Those quantities which arbitrarily change "almost" continuously (for example, due to ionization losses), can be successfully considered as discontinuously changing quantities.

4. In order to write down the diffusion equation for φ it is necessary to introduce the collision cross section. We define

$$w(\mathbf{A}(t), \mathbf{A}'')\, d\mathbf{A}''\, dt \tag{5a}$$

* The method developed here has been generalized by L. Pal; he has deduced the diffusion equation for cases in which $\mathbf{A}(t)$ is an arbitrary function of time, while not making use of the power series expansion.

as the probability that a particle, whose state at time t is described by the vector $\mathbf{A}(t)$, undergoes such a collision in the time interval t, $t + dt$ that after the collision the particle is found in the interval $\mathbf{A}''$, $\mathbf{A}'' + d\mathbf{A}''$. It is obvious that

$$d\mathbf{A}'' = \prod_{k,l} dA_k^{(l)''}.$$

In place of $\mathbf{A}$ we write $\mathbf{A}(t)$, since the state of the particle changes even in the absence of a collision. Use of the vector $\mathbf{A}(t)$ denotes that all computed values of all essential time derivatives $d^l A_k(t)/dt^l$; are considered; this is important because the instantaneous value of only one of the parameters does not sufficiently determine the state of the particle.

Some of the parameters $A_k^{(l)}$ do not change abruptly in collisions. We denote those quantities which do change abruptly by $\mathbf{a}$, and those which do not so change by $\mathbf{b}$. Thus $\mathbf{A} = \mathbf{a}, \mathbf{b}$; we can separate $w(\mathbf{A}(t), \mathbf{A}'')$ in the following manner:

$$w(\mathbf{A}(t), \mathbf{A}'') = \overline{w}(\mathbf{A}(t), \mathbf{a}'')\,\delta(\mathbf{b}(t) - \mathbf{b}''(t)), \quad (6)$$

where the δ function is the product of δ functions for each of the components $\mathbf{b}$.

The function $\overline{w}$ can depend on the value of $\mathbf{b}(t)$ as shown above, but the function $\mathbf{b}(t)$ cannot change in collisions. An example of such a case is scattering in an inhomogeneous absorber. In this case, the cross section depends on the coordinates, in spite of the fact that the coordinates do not change in the collision. It would have been possible to write down the diffusion equation in terms of a regular $\overline{w}$ function, and thus avoid the application of δ functions. However, it is rather complicated to divide $\mathbf{A}$ into the groups $\mathbf{a}$ and $\mathbf{b}$; therefore we prefer to employ w and the δ function. In order to avoid difficulties connected with the application of the δ function, we can replace the actual δ function by regular functions, e.g., by the Gaussian function

$$\delta(x) = (2\pi\varepsilon)^{-1/2} \exp(-x^2/2\varepsilon), \; \varepsilon > 0, \quad (7)$$

where ϵ is small but different from zero. Substituting Eq. (7) in Eq. (6), we introduce an error which can be made sufficiently small if ϵ is chosen sufficiently small. In fact, let us consider as an example, the x component of a mixture. In this case, the introduction of Eq. (7) in place of the actual δ function is equivalent to the supposition that in each collision x changes discontinuously by an amount of order ϵ. If, for example, $\epsilon \sim 10^{100}$ cm, then such a supposition would undoubtedly have been allowable, since it does not lead to any noticeable effect. The mathematical consequence of such a supposition, which does not have any physical consequence, is the possibility of considering $u(\mathbf{A}, \mathbf{A}'')$ as a regular function.

5. We can now write down the diffusion equation for $u(\mathbf{A}, \mathbf{U}, t)$. We have

$$\varphi(\mathbf{A}, \mathbf{U}, t) = \varphi_0(\mathbf{A}, \mathbf{U}, t) + \varphi_1(\mathbf{A}, \mathbf{U}, t), \quad (8)$$

where φ_0 is the probability that the final state within $\mathbf{U}$ arises without a collision, and φ_1 is the probability that the final state within $\mathbf{U}$ arises as the result of one or more collisions.

The probability of an absence of a collision in the time interval from 0 to t' can be written as $\varphi_0(\mathbf{A}, t')$; the probability of an absence of a collision in the interval between t' and t is expressed as $\varphi(\mathbf{A}(t'), t - t')$. Thus the probability that no collision takes place during the entire interval is equal to

$$\varphi_0(\mathbf{A}, t) = \varphi_0(\mathbf{A}(0), t')\,\varphi_0(\mathbf{A}(t'), t - t'). \quad (9)$$

The general solution of Eq. (9) is

$$\varphi_0(\mathbf{A}, t) = \exp\left\{-\int_0^t w(\mathbf{A}(t''))dt''\right\}, \quad (10)$$

which can be established by substituting Eq. (10) in Eq. (9), where

$$w(\mathbf{A}(t'')) = \int_{\mathbf{A}''} w(\mathbf{A}(t''), \mathbf{A}'')\,d\mathbf{A}'' \quad (11)$$

and integration is carried out over all components of $\mathbf{A}''$. Equation (11) is so chosen that the entire probability of collision is equal to the value given by Eq. (5a).

Thus the first term on the right side of Eq. (8) is determined by the expression

$$\varphi_0(\mathbf{A}, \mathbf{U}, t) = \varphi_0(\mathbf{A}, t)\,\Delta(\mathbf{A}(t), \mathbf{U}). \quad (12)$$

The expression on the right side of Eq. (12) is equal to the product of the probability of the absence of a collision between 0 and t and the probability that a continuously changing $\mathbf{A}$ undergoes a transition into the interval $\mathbf{U}$ or remains there.

In order to determine $\varphi_1(\mathbf{A}, \mathbf{U}, t)$, we consider a case in which the first collision takes place in the interval $t - t''$, $t - t'' + dt''$. The probability of such an event is

$$\varphi_0(\mathbf{A}, t - t'')\,w(\mathbf{A}(t - t''), \mathbf{A}'')\,d\mathbf{A}''dt'',$$

where it is assumed that the first collision is such that the state of the particle is found within the interval $\mathbf{A}''$, $\mathbf{A}'' + d\mathbf{A}''$. The probability of

the passage of a particle into the interval U after a time t'' is $\varphi(A'', U, t'')$, and therefore the total probability that, as a result of one or more collisions, the particle is found in the interval U, is equal to

$$\varphi_1(\mathbf{A}, \mathbf{U}, t) = \int_0^t \int_{\mathbf{A}''} \varphi_0(\mathbf{A}, t-t'')\, w(\mathbf{A}(t-t''), \mathbf{A}'')\, \varphi(\mathbf{A}'', \mathbf{U}, t'')\, d\mathbf{A}''dt''. \tag{13}$$

Combining φ_0 and φ_1, we then obtain

$$\varphi(\mathbf{A}, \mathbf{U}, t) = \varphi_0(\mathbf{A}, t)\,\Delta(\mathbf{A}(t), \mathbf{U}) + \int_0^t \int_{\mathbf{A}''} \varphi_0(\mathbf{A}, t-t'')\, w(\mathbf{A}(t-t''), \mathbf{A}'')\, \varphi(\mathbf{A}'', \mathbf{U}, t'')\, d\mathbf{A}''\, dt''. \tag{14}$$

Equation (14), together with Eq. (12), gives the general diffusion equation. For practical purposes, Eq. (14) can be transformed to a more suitable form.

6. We transform Eq. (14) into an integro-differential equation in the following way. Setting $t' = t - t''$, we get from Eq. (9)

$$\varphi_0(\mathbf{A}, t-t'') = \varphi_0(\mathbf{A}, t) / \varphi_0(\mathbf{A}(t-t''), t'').$$

Introducing this expression in Eq. (14), we obtain

$$\varphi(\mathbf{A}, \mathbf{U}, t) = \varphi_0(\mathbf{A}, t)\Big\{\Delta(\mathbf{A}(t), \mathbf{U}) + \int_0^t \int_{\mathbf{A}''} \frac{w(\mathbf{A}(t-t''), \mathbf{A}'')}{\varphi_0(\mathbf{A}(t-t''), t'')}\, \varphi(\mathbf{A}'', \mathbf{U}, t'')\, d\mathbf{A}''dt''\Big\}.$$

Differentiating this expression with respect to t, we have

$$\frac{\partial \varphi(\mathbf{A}, \mathbf{U}, t)}{\partial t} = \frac{\partial \ln \varphi_0(\mathbf{A}, t)}{\partial t}\, \varphi(\mathbf{A}, \mathbf{U}, t) + \int_{\mathbf{A}''} \omega(\mathbf{A}, \mathbf{A}'')\, \varphi(\mathbf{A}'', \mathbf{U}, t)\, d\mathbf{A}'' + \left(\frac{\partial I(\tau)}{\partial \tau}\right)_{\tau=0} \varphi_0(\mathbf{A}, t), \tag{15}$$

where

$$I(\tau) = \Delta(\mathbf{A}(t+\tau), \mathbf{U}) + \int_0^t \int_{\mathbf{A}''} \frac{w(\mathbf{A}(t-t''+\tau), \mathbf{A}'')}{\varphi_0(\mathbf{A}(t-t''+\tau), t'')}\, \varphi(\mathbf{A}'', \mathbf{U}'', t'')\, d\mathbf{A}''dt'',$$

and finally

$$I(0) = \varphi(\mathbf{A}, \mathbf{U}, t) / \varphi_0(\mathbf{A}, t).$$

In order to carry out the differentiation, we recall that

$$\frac{\partial}{\partial \tau} f(\mathbf{A}(t+\tau-t'')) = \frac{\partial}{\partial \tau} f[A_1^{(0)} + A_1^{(1)}(t+\tau-t'') + {}^1/_2\, A_1^{(2)}(t+\tau-t'')^2 \ldots$$
$$\ldots A_2^{(0)} + A_2^{(1)}(t+\tau-t'') + {}^1/_2\, A_2^{(2)}(t+\tau-t'')^2 + \ldots]$$

and thus,

$$\left(\frac{\partial}{\partial \tau} f(\mathbf{A}(t+\tau-t''))\right)_{\tau=0} = \sum_{k,l} A_k^{(l+1)} \frac{\partial f(\mathbf{A}(t-t''))}{\partial A_k^{(l)}};$$

consequently,

$$\left(\frac{\partial I(\tau)}{\partial \tau}\right)_{\tau=0} = \sum_{k,l} A_k^{(l+1)} \frac{\partial I(0)}{\partial A_k^{(l)}} + \sum_{k,l} A_k^{(l+1)} \frac{\partial}{\partial A_k^{(l)}} \left(\frac{\varphi(\mathbf{A}, \mathbf{U}, t)}{\varphi_0(\mathbf{A}, t)}\right).$$

Substituting in Eq. (15) we get

$$\frac{\partial \varphi(\mathbf{A}, \mathbf{U}, t)}{\partial t} = \int_{\mathbf{A}''} w(\mathbf{A}, \mathbf{A}'')\, \varphi(\mathbf{A}'', \mathbf{U}, t)\, d\mathbf{A}'' + \sum_{k,l} A_k^{(l+1)} \frac{\partial \varphi(\mathbf{A}, \mathbf{U}, t)}{\partial A_k^{(l)}} + \left(\frac{\partial}{\partial t} - \sum_{k,t} A_k^{(l+1)} \frac{\partial}{\partial A_k^{(l)}}\right) \ln \varphi_0(\mathbf{A}, t)\, \varphi(\mathbf{A}, \mathbf{U}, t).$$

It is easy to see that the last term is equal to $-w(\mathbf{A})\,\varphi(\mathbf{A}, \mathbf{U}, t)$. Finally, the diffusion equation takes the form

$$\left(\frac{\partial}{\partial t} + w(A) - \sum_{k,l} A_k^{(l+1)} \frac{\partial}{\partial A_k^{(l)}}\right) \varphi(\mathbf{A}, \mathbf{U}, t) = \int_{\mathbf{A}''} w(\mathbf{A}, \mathbf{A}'')\, \varphi(\mathbf{A}'', \mathbf{U}, t)\, dA'' \ldots \tag{16}$$

7. As an example of an application of our formula, we consider the scattering of a particle in a homogeneous absorber and, in particular, the distribution of the area between the projection of the trajectory and a straight line (see Fig. 2). Knowledge of the distribution of this quantity can be useful in the determination of the energy of the

particle from its track in the emulsion.

Let us consider a particle which moves at a small angle to the x axis, and only those cases of scattering which do not lead to large departures from this direction. We neglect quantities of order A^2, where A is the projection of the angle of the track on the x, z plane.

Neglecting large angle scattering, we can also neglect the possibility of recurrence of the initial value of x for the moving particle, and therefore we can use x as the independent variable instead of t (see Sec. 2).

The particle is thus characterized by its energy E, the coordinates x, Z, the angle A with the x axis and the area between the trajectory and the x axis (Fig. 2). Physical interest attaches not to S but to the area of the segment s, i.e., (see Fig. 2)

$$s = S - {}^1/_2\,(Z + Z')\,x. \tag{17}$$

It would be more suitable, however, first to determine the distribution of S and then derive the distribution of s.

In order that the notation be the same as used in Eq. (16), we write

$$E = A_1, \quad A_1(x) = A_1^{(0)},$$
$$A = A_2, \quad A_2(x) = A_2^{(0)},$$
$$Z = A_3, \quad A_3(x) = A_3^{(0)} + xA_3^{(1)},$$
$$\text{where} \quad A_3^{(1)} = A_2^{(0)} = A,$$
$$S = A_4, \quad A_4(x) = A_4^{(0)} + xA_4^{(1)} + {}^1/_2\,x^2 A_4^{(2)},$$

where $A_4^{(1)} = A_3^{(0)} = Z$, $A_4^{(2)} = A_2^{(0)} = A$. The diffusion equation then has the form

$$\left(\frac{\partial}{\partial x} + w(\mathbf{A}) - A_3^{(1)}\frac{\partial}{\partial A_3^{(0)}} - A_4^{(1)}\frac{\partial}{\partial A_4^{(0)}} - A_4^{(2)}\frac{\partial}{\partial A_4^{(1)}}\right)\varphi(\mathbf{A}, \mathbf{U}, x) = \int_{\mathbf{A}''} w(\mathbf{A}, \mathbf{A}'')\,\varphi(\mathbf{A}'', \mathbf{U}, x)\,d\mathbf{A}'' \tag{18}$$

with the additional conditions

$$A_4^{(2)} = A_3^{(1)} = A_2^{(0)} = A, \tag{19}$$
$$A_4^{(1)} = A_3^{(0)} = Z. \tag{20}$$

Equation (19) can be substituted directly in Eq. (18), since Eq. (18) does not contain any derivative with respect to $A_4^{(2)}$ or $A_3^{(1)}$. However, direct substitution of Eq. (20) in Eq. (18) is not possible, since the derivatives with respect to $A_4^{(1)}$ and $A_3^{(0)}$ apply to different processes, even though the computed values of these quantities can coincide. We demonstrate that we can eliminate Eq. (20). Let $A_4^{(1)} = Z_1$, $A_3^{(0)} = Z$; then we have in place of Eq. (18):

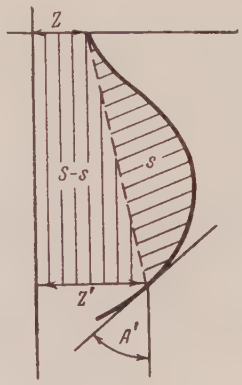

FIG. 2

$$\left(\frac{\partial}{\partial x} + w(\mathbf{A}) - A\frac{\partial}{\partial Z} - Z\frac{\partial}{\partial S} - A\frac{\partial}{\partial Z_1}\right) \times \varphi(\mathbf{A}, \mathbf{U}, x) = \int_{\mathbf{A}''} w(\mathbf{A}, \mathbf{A}'')\,\varphi(\mathbf{A}'', \mathbf{U}, x)\,d\mathbf{A}''.$$

We now set

$$\varphi(\mathbf{A}, \mathbf{U}, x) = \bar{\varphi}(\mathbf{A}, \mathbf{U}, x)\,f(Z - Z_1), \tag{21}$$

where

$$\partial\bar{\varphi}/\partial z_1 = 0, \quad f(Z - Z_1) \neq 0.$$

Substituting Eq. (21) in Eq. (20) and dividing by $f(Z - Z_1)$, we get (under the assumption that $w(\mathbf{A}, \mathbf{A}'')$ clearly does not depend on Z or Z_1):

$$\left(\frac{\partial}{\partial x} + w(\mathbf{A}) - A\frac{\partial}{\partial Z} - Z\frac{\partial}{\partial S}\right)\bar{\varphi}(\mathbf{A}, \mathbf{U}, x) = \int_{\mathbf{A}''} w(\mathbf{A}, \mathbf{A}'')\,\bar{\varphi}(\mathbf{A}'', \mathbf{U}, x)\,d\mathbf{A}'', \tag{22}$$

for $Z = Z_1$ we get $\varphi(\mathbf{A}, \mathbf{U}, x) = f(0)\,\bar{\varphi}(\mathbf{A}, \mathbf{U}, x)$.

We can assume $f(0) = 1$ and, consequently, in the most interesting region, $\varphi = \bar{\varphi}$. For this reason, we omit the bar over φ in Eq. (22). We can therefore remove completely both the condition (19) and condition (20), and solve Eq. (22) without additional conditions.

8. In what follows we introduce approximations for the purpose of simplifying Eq. (22). Thus, we assume that $w(\mathbf{A}, \mathbf{A}'')$ depends only on the energy and the absolute value of the angle of scattering. We then write

$$w(\mathbf{A}, \mathbf{A}'') = \overline{w}(E; E'', |A - A''|)$$
$$\times \delta(Z - Z'')\delta(S - S'');$$

we then get, in place of Eq. (22),

$$\left(\frac{\partial}{\partial x} - A\frac{\partial}{\partial Z} - Z\frac{\partial}{\partial S}\right)\varphi(E, A, Z, S; \mathbf{U}; x)$$
$$= \iint \overline{w}(E; E'', |A - A''|)\{\varphi(E'', A'', Z, S; \mathbf{U}; x)$$
$$- \varphi(E, A, Z, S; \mathbf{U}; x)\}\, dE''dA''.$$

If we assume further that, for $E - E'' \approx 0$ and $A - A'' \approx 0$, the quantity $\overline{w}$ has a sharp maximum, i.e., that both the energy losses and the scattering essentially consist of many components of small value, then the expression under the integral will be

$$\varphi(E'', A'', Z, S; \mathbf{U}; x) - \varphi(E, A, Z, S; \mathbf{U}; x)$$
$$= \left\{(E'' - E)\frac{\partial}{\partial E} + (A'' - A)\frac{\partial}{\partial A} + \frac{1}{2}(E'' - E)^2\frac{\partial^2}{\partial E^2}\right.$$
$$\left. + (E'' - E)(A'' - A)\frac{\partial^2}{\partial E\,\partial A} + \frac{1}{2}(A'' - A)^2\frac{\partial^2}{\partial A^2} + \cdots\right\}\varphi(E, A, Z, S; \mathbf{U}; x).$$

Upon integration, all terms proportional to A-A'' vanish because of symmetry and there is left

$$\iint \cdots dE''dA'' = -a(E)\frac{\partial}{\partial E} + \frac{1}{2}b(E)\frac{\partial^2}{\partial E^2}$$
$$+ \frac{1}{2}\sigma(E)\frac{\partial^2}{\partial A^2} + \cdots,$$

where

$$a(E) = \int (E - E'')\, w(E, E'')\, dE'',$$
$$w(E, E'') = \int w(E, E'', |A - A''|)\, dA'',$$
$$b(E) = \int (E - E'')^2 w(E, E'')\, dE'',$$
$$\sigma(E) = \iint (A - A'')\, w(E, E''|A - A''|)\, dA''dE''.$$

In the latter approximation we have, consequently,

$$\left(\frac{\partial}{\partial x} + a(E)\frac{\partial}{\partial E} - \frac{1}{2}b(E)\frac{\partial^2}{\partial E^2} + \frac{1}{2}\sigma(E)\frac{\partial^2}{\partial A^2}\right.$$
$$\left. - A\frac{\partial}{\partial Z} - Z\frac{\partial}{\partial S}\right)\varphi(E, A, Z, S; \mathbf{U}; x) = 0. \tag{23}$$

Further, we neglect the fluctuations of energy loss, i.e., we set $b(E) \sim 0$. Finally, for convenience in later calculations, we introduce more symmetrical notation, namely, $E = X_0$, $A = X_1$, $Z = X_2$, $S = X_3$ and $\mathbf{X} = X_0, X_1, X_2, X_3$; furthermore, we shall assume that U denotes a narrow interval in the neighborhood of

$$\mathbf{X}' = X_0', X_1', X_2', X_3'.$$

Thus our problem reduces to the solution of the equation

$$\left(\frac{\partial}{\partial x} + a(X_0)\frac{\partial}{\partial X_0} + \frac{1}{2}\sigma(X_0)\frac{\partial^2}{\partial X_1^2}\right.$$
$$\left. - X_1\frac{\partial}{\partial X_3}\right)\varphi(\mathbf{X}, \mathbf{X}', x) \tag{24}$$

under the initial condition

$$\varphi(\mathbf{X}, \mathbf{X}', 0) = \delta(\mathbf{X} - \mathbf{X}')$$
$$= \delta(X_0 - X_0')\delta(X_1 - X_1') \tag{25}$$
$$\times \delta(X_2 - X_2')\delta(\mathbf{X}_3 - \mathbf{X}_3').$$

9. For the solution of Eq. (24) we separate that part of the function which depends on the energy, i.e., we set

$$\varphi(\mathbf{X}, \mathbf{X}', x) = f(X_0, x)\,\overline{\varphi}(\mathbf{X}, x). \tag{26}$$

Substituting Eq. (26) in Eq. (24), we get

$$\frac{\partial f(X_0)}{\partial x} + a(X_0)\frac{\partial f(X_0)}{\partial X_0} = 0.$$

The solution of the equation above, which satisfies the condition (25), has the following form

$$f(X_0, x) = \delta\left(x - \int_{X'}^{X_0}\frac{\partial X_0''}{a(X_0)}\right). \tag{27}$$

Substituting Eq. (26) in Eq. (24), we find that, for all values of the variables for which $f \neq 0$, the function φ must satisfy Eq. (24). It follows from Eq. (27) that $\overline{\varphi}$ must satisfy Eq. (24) only for

$$X_0 = X_0(x), \tag{28}$$

where

$$\int_{X_0'}^{X_0(x)}\frac{dX_0''}{a(X_0'')} = x.$$

Thus we can rewrite Eqs. (24) and (25) in the following form

$$\left(\frac{\partial}{\partial x} + \frac{1}{2}\sigma(x)\frac{\partial^2}{\partial X_1^2} - X_1\frac{\partial}{\partial X_2}\right.$$
$$\left. - X_2\frac{\partial}{\partial X_3}\right)\overline{\varphi}(X, x) = 0, \tag{29}$$

$$\sigma(x) \equiv \sigma(X_0'(x)),$$
$$\bar{\varphi}(X, 0) = \delta(X_1 - X_1')\,\delta(X_2 - X_2')\,\delta(X_3 - X_3')$$

and it is now possible not to consider the components X_0.

10. To obtain a solution of Eq. (29) in clear form we apply a Laplace transformation relative to the three components of X to $\bar{\varphi}$ and Eq. (29). Consequently we introduce the function

$$\psi(\vec{\lambda}, x) \equiv \psi(\lambda_1, \lambda_2, \lambda_3, x) = \int_{-\infty}^{+\infty} e^{\vec{\lambda}X}\,\bar{\varphi}(\mathbf{X}, x)\,d\mathbf{X}, \tag{30}$$

where $\lambda\mathbf{X} = \lambda_1 X_1 + \lambda_2 X_2 + \lambda_3 X_3$;
$d\mathbf{X} = dX_1\,dX_2\,dX_3$.

After the transformation, Eq. (29) takes the form

$$\left(\frac{\partial}{\partial X} + \frac{1}{2}\sigma(x)\lambda_1^2 + \lambda_2\frac{\partial}{\partial\lambda_1} + \lambda_3\frac{\partial}{\partial\lambda_2}\right)\psi(\lambda, x) = 0, \tag{31}$$
$$\psi(\vec{\lambda}, 0) = \exp\{\vec{\lambda}\mathbf{X}'\}.$$

Assuming that (32)

$$\ln\psi(\vec{\lambda}, X) = \sum_{k=1}^{3}\alpha_k\lambda_k + \sum_{i,k=1}^{3}\beta_{ik}\lambda_i\lambda_k;\quad \beta_{ik} = \beta_{ki},$$

we find from Eq. (31)

$$\alpha_1 = A',\ \alpha_2 = Z' - A'x, \tag{33}$$
$$\alpha_3 = S' - Z'x + {}^1/_2 A'x^2;$$
$$\beta_{11} = \sigma_0(x),\quad \beta_{12} = -\sigma_1(x), \tag{34}$$
$$\beta_{13} = {}^1/_2\,\sigma_2(x),$$
$$\beta_{22} = \sigma_2(x),\qquad \beta_{23} = -{}^1/_2\sigma_3(x),$$
$$\beta_{33} = {}^1/_4\,\sigma_4(x),$$

where

$$\sigma_k(x) = \int_0^x (x - x')^k\sigma(x')\,dx'. \tag{35}$$

Substituting Eqs. (33)-(35) in Eq. (32), we obtain the Laplace transform of the solution of Eq. (29). Carrying out the inverse transformation, we find the solution in the following form:

$$\bar{\varphi}(\mathbf{X}, x) = (2\pi\det\beta_{ik})^{-1/2} \times \exp\left\{-\frac{1}{2}\sum_{i,k}\tilde{\beta}_{ik}(X_i - \alpha_i)(X_k - \alpha_k)\right\}, \tag{36}$$

where $\tilde{\beta}_{ik}$ is equal to the minor $\beta_{ik}/\det\beta_{ik}$, i.e., $\tilde{\beta}_{ik}$ are the terms of the inverse matrix for β_{ik} where $\sum_k \tilde{\beta}_{ik}\beta_{kl} = \delta_{ik}$.

11. Equation (36) gives a similar expression for the instantaneous distribution of A', Z', S' at a given depth x, for given initial values of A, Z, S. If we take the theoretical value of $\sigma(x)$, we can compute numerically the values of all the coefficients. By way of an example, we consider in more detail the properties of the distribution (36) under neglect of energy losses, i.e., considering $\sigma(x)$ = const. For simplicity, we take

$${}^1/_2\,\sigma(x) = 1. \tag{37}$$

$\sigma(x)$ has the dimensions of inverse length and therefore Eq. (37) determines the unit of length.

Substituting Eq. (37) in Eq. (35) we find $\sigma_k(x) = x^{k+1}/(k+1)$; further, from Eq. (34) it follows that

$$\beta_{11} = x,\quad \beta_{12} = -{}^1/_2\,x^2,\quad \beta_{13} = {}^1/_6\,x^3,$$
$$\beta_{22} = {}^1/_3\,x^3,\quad \beta_{23} = -{}^1/_8\,x^4,$$
$$\beta_{33} = {}^1/_{20}\,x^5,$$
$$\det\beta_{ik} = x^9/8640,\quad 8640 = 3!4!5!/2.$$

Substituting $\mathbf{X} = 0$ in Eq. (36), i.e., $A = Z = S = 0$, and considering that the particles set out parallel to the X axis from the origin of the coordinates, we find

$$\bar{\varphi}(0, \mathbf{X}', x) = \gamma x^{-9/2}\exp\left\{-\frac{1}{2x}\left(9A'^2 + 72A'\left(\frac{Z'}{x} - A'\right) + 120A'\left(\frac{S'}{x^2} - \frac{Z'}{x} + \frac{1}{2}A'\right) + 192\left(\frac{Z'}{x} - A'\right)^2 + 720\left(\frac{Z'}{x} - A'\right)\left(\frac{S'}{x^2} - \frac{Z'}{x} + \frac{1}{2}A'\right) + 720\left(\frac{S'}{x^2} - \frac{Z'}{x} + \frac{1}{2}A'\right)^2\right)\right\};$$
$$\gamma = (8640/2\pi)^{1/2}.$$

Writing, for brevity, $\varphi(\mathbf{X}', x)$ in place of $\bar{\varphi}(0, \mathbf{X}', x)$, we find, after transformation of the polynomial in the exponent,

$$\varphi(\mathbf{X}', x) = \gamma x^{-9/2} \exp\left\{-\frac{1}{2x}(9A'^2 - 72A'Z'/x + 120A'S'/x^2 + 192\,Z'^2/x^2 - 720\,Z'S'/x^3 + 720\,S'^2/x^4)\right\}. \tag{38}$$

Equation (38) gives in clear form the instantaneous distribution of A', Z', S'; with the help of this formula, it is possible to determine, in the usual fashion, the mean quantities of momentum, correlation coefficient, etc. From Eq. (38) we can also obtain the homogeneous distribution of A', Z' and $s' = S' - {}^1/_2\, xZ'$; we get (see Fig. 2)

$$\varphi(A', Z', s'; x) = \gamma x^{-9/2} \times \exp\left\{-\frac{1}{2x}(9A'^2 - 12A'Z'/x + 12\,Z'^2/x + 120\,A's'/x^2 + 720\,s'^2/x^4)\right\}. \tag{39}$$

We can average over A' or Z' and, consequently, obtain the double distribution:

$$\varphi(A', s'; x) = \int_{-\infty}^{+\infty} \varphi(A', Z', s', x)\, dZ' = \gamma_1 x^{-3} \exp\left\{-\frac{1}{2x}(4A'^2 + 120\,A's'/x^2 + 720\,s'^2/x^4)\right\}. \tag{40}$$

However, the distribution (40) is not of immediate interest. We are interested in the instantaneous distribution of the quantities $a' = A' - Z'/x$ and s'. The importance of these quantities is clear from Fig. 3; a' is the angle between the trajectory of the particle and the straight line connecting the origin of the trajectory with the final point.

The distribution for a', s' has the form

$$\varphi(a', s'; x) = \gamma_2 x^{-3} \times \exp\left\{-\frac{1}{2x}(8a'^2 + 80a's'/x^2 + 320\,s'^2/x^4)\right\}. \tag{41}$$

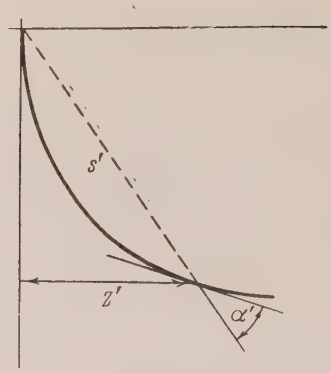

FIG. 3

As is evident from Eq. (41), there is a strong negative correlation between a' and s'; the reason for this negative correlation can be found in a consideration of Fig. 3. In particular, according to Eq. (41), for a fixed value of A', the most probable value of s' is equal to

$$s_0'(a') = -a'x^2/8. \tag{42}$$

Similarly, the most probable angle a', for a fixed value of s', is obtained from Fq. (41):

$$a_0'(s') = -5\,s'/x^2. \tag{43}$$

It is interesting to compare the values of the coefficients in Eqs. (42) and (43). Averaging over a' we can determine the distribution of s'. We obtain, finally,

$$\varphi(s'; x) = \gamma_3 x^{-5/2} \exp\{-60\,s'^2/x^5\}.$$

The distribution is strictly Gaussian, with the most probable value of $s' = 0$.

In the future, we hope to return to the question of the application of the formulas just developed to the problem of the measurement of the energy of particles which undergo scattering in a photographic emulsion.

Translated by R. T. Beyer
61

The Hodoscopic Delayed Coincidence Method and Its Application to the Investigation of Slow Meson Formation in Cosmic Radiation.

G. B. ZHDANOV
P. N. Lebedev Physical Institute, Academy of Sciences, USSR

(Submitted to JETP editor January 27, 1955)
J. Exptl. Theoret. Phys. (U.S.S.R.) 30, 437-449 (March, 1956)

There is presented the basis of the hodoscopic delayed coincidence method of studying the processes of formation of slow $\pi^{\pm}$-mesons by the nuclear-active component of the cosmic radiation. Aside from describing the apparatus, an analysis of the various instrumental effects is carried out. An estimate is made of the effective energy of formation of the particles and also of the instrumental corrections, which must be taken into account in order to determine the energy spectrum and absolute intensity of formation of slow $\pi^{\pm}$-mesons.

FOR the study of the elementary acts of interaction of high energy nucleons ($10^9 - 10^{10}$ ev) with atomic nuclei, the most reliable and detailed information which characterizes this interaction has been obtained by the method of the thick photographic emulsions. However, along with its undoubted values, this method has a set of disadvantages which in certain cases limit considerably the possibilities of the experimenter. The most serious disadvantage is the laborious processing of the material and the difficulty of connecting the observed processes to nuclei with a definite atomic number, and also of determining the signs of charged particles. All of the specified difficulties can be overcome to a considerable degree by working with a controlled Wilson chamber, located in a magnetic field and provided with a plate of a given composition. However the latter method suffers from its own specific disadvantages, which combine with the usual large distortions, and the controlling system introduces errors into the observations of the numbers of particles and the energies and scattering angles of the particles.

We therefore go to indirect methods of investigating nuclear interactions which permit the detection of certain special phenomena which escape direct observation. The clearest example of this type was given by Grigorov[1], where the method was used for an analysis of the latitude and altitude dependence of the primary component of the cosmic rays and it was shown that in the interaction of nucleons of high energy with light nuclei the nucleons retain, on the average, 70% of their original energy. The ionization method can be applied to the investigation of the integral properties of the radiation and may be used in certain cases for direct, although not entirely well-defined, studies of the characteristics of elementary processes. One of the possible methods of this type is offered by the hodoscope, where, under the proper conditions, one is permitted not only to observe the trajectories of individual particles, but also to measure the energy and to identify the nature of the particles, as is given in particular by use of the well known mass spectrometer system of Alikhanov and Alikhanian. In spite of its weaknesses, the hodoscope has advantages over the Wilson chamber or photographic emulsion, combining both a large "luminosity" and a small dead time of the apparatus. The latter permits use of the simplest control system of counters which will essentially only reduce the discrimination and introduces a statistical regularity into the study of the phenomena.

As examples of various successful uses of the method of counters for investigating individual aspects of the elementary acts of nuclear interactions it is possible to cite experiments carried out in the course of a series of flights, on an extensive atmospheric scale, by the group of Zatsepin and Nikol'skov bv the method of the "correlated hodoscope" (see Ref. 2) and also the first experiments on the study of the decay electrons from μ-mesons[3] and the investigation of the spectrum of formation of π-mesons in the mass spectrometer of Alikhanian.[4] In the case of the decay of μ-mesons, a simple application of the method of delayed coincidences (without a hodoscope) permitted one to make a satisfactory reliable identification of the pheno-

[1] N. L. Grigorov, Dokl. Akad. Nauk SSSR 94, 835 (1954).

[2] N. A. Dobrotin, G. T. Zatsepin et al, Usp. Fiz. Nauk 49, 185 (1953).

[3] V. Kamalian and A. Alikhanian, Dokl. Akad. Nauk SSSR 97, 425 (1954).

[4] G. B. Zhdanov and A. A. Khaidarov, Dokl. Akad. Nauk SSSR 65, 287 (1949).

menon above the background of a considerable number of possible instrumental effects.

The decay of μ-mesons is by no means the only phenomenon in the study of which it is possible to use the method of delayed coincidences. Beginning in 1947, this method was used by us to study the processes of formation of slow mesons in the depths of the atmosphere (for example, see Ref. 5). The clarification of the nature of these processes, in particular, the determination of the number and average energy of formation of these particles and also the energy of the mesons in the backwards stream (from below upwards) is of great interest from the point of understanding the mechanism of interaction of fast nucleons and nuclei. So, for example, if they emerge from the interaction of two virtually free nucleons, then, in view of the relatively high speed of the combined center of gravity, the appearance of slow mesons in electron-nuclear showers can be principally the result of secondary processes, depending to a great degree on the atomic number of the nucleus. In order to study directly the processes of formation of slow mesons it is natural to supplement the usual method of delayed coincidences with a special counter hodoscope. Such a hodoscope was constructed in 1950-1951 by Korablev, and was used by us in work done in 1951-1952[6].

Unlike other hodoscopes, which use the combination of the delayed coincidence scheme (see Ref. 7), in the hodoscope system of Korablev (which we call GK-5) the delay of the coincidences is accomplished in every hodoscope cell, whereupon the output of the cell in the form of a single cascade is collected on the negative electrode of the thyratron MTX-90, allowing us to operate the system with a very high "luminosity" and to detect the processes of slow meson formation with a frequency of the order of 10 per hour.

2. DESCRIPTION OF THE APPARATUS

The hodoscope of the type GK-5 makes it possible to investigate the formation of slow π^+-mesons in thick substances from the ensuing π-μ-e decays within the confines of the apparatus. For this purpose the apparatus can be set up in one of two ways: on the one hand, with the help of certain detectors we select nuclear interactions of a definite class (in particular, electron-nuclear showers) where it is possible to determine how often and with what energy or angular distribution slow π^+-mesons are generated in a given interaction; on the other hand, we have a detector which operates only in the presence of any μ-e decay, and it is possible to investigate how often a stopped meson is formed within the confines of the apparatus, and what kinds are characteristic of nuclear interactions which are accompanied by such generation. Consequently, there are two specific problems to be treated and two types of experimental arrangements (GK-5A and GK-5B), characteristic types of which are shown in Fig. 1*a* and 1*b*. In both cases the arrangement consists of the following principle parts: a) a control counter system (row VU and NU) in Fig. 1*a* and 1*b*, designed to detect mesons and other particles which accompany their generation; b) another series of counters, a stratified filter *d*, which, combined with the rows of the GK-5 hodoscope, are so designed as to detect directly the stopping of mesons as well as electronic decays; c) a side group of counters (BG not shown in Fig. 1b) designed for selecting wide angle showers; d) the hodoscope GK-3, which, combined with the control and side counters, is intended to specify the character of the processes of meson formation; e) an electronic amplifier which accomplishes the selection and detection of the necessary delays from the control system and also controls the hodoscope.

The thickness of the filter *d* usually conforms to the range of the decay electron so that the efficiency of any layer of the hodoscope is small and depends on the presence of other filters in the arrangement.

The principle of operation of the apparatus in each of the variations *A* and *B* is easy to explain with the help of the block diagrams shown in Fig. 2a and 2b respectively. The pulse from the control counters (VU and NU) enters the corresponding cell of the hodoscope GK-3 and simultaneously enters the delay block through the preliminary shaping block (arrangement *A*) or cathode follower (arrangement *B*). In the first case, the amplitude of the pulse from the control group is proportional to the number of counters that were fired, which permits one to assign a definite lower limit to the number of particles in the shower being studied. The operation of the delay block involves the formation of three square master-pulses (M_1, M_2, and M_3) whose amplitude and duration determine which hodoscope section is allowed to function. The pulse M_1 (duration $T_1 \sim 0.7\mu$ sec) feeds the upper series of cells of the GK-5 hodoscope which

---

[5] A. Abdullaev, G. Zhdanov et al, J. Exptl. Theoret. Phys. (U.S.S.R.) **20**, 673 (1950).

[6] A. A. Abdullaev, G. B. Zhdanov, L. N. Korablev and A. A. Khidarov, J. Exptl. Theoret. Phys. (U.S.S.R.) **21**, 1078 (1951).

[7] A. O. Vaisenberg, J. Exptl. Theoret. Phys. (U.S.S.R.) **24**, 545 (1953).

serves to detect non-delayed particles, i.e., slow mesons and accompanying particles. The pulse $M_2(T_2 = 1.3\mu$ sec) is formed with a delay ($\Delta t = 1.5$ sec) and goes to the lower series of cells of GK-5, which can detect only particles which are delayed for a time relative to the original meson, comparable to their own lifetime. A sufficiently high resolving power of the neon lamps of the hodoscope is achieved by means of proper shaping of not only the master pulses but also the pulses entering from the counters. The details of the scheme of both (upper and lower) of the cells of the hodoscope GK-5 for detecting either non-delayed or delayed discharges in one of the counters are shown in Fig. 3. Finally the pulse $M_3(T_3 = 3\mu$ sec) goes to the neon lamp hodoscope of the usual type GK-3, having a low resolving power.

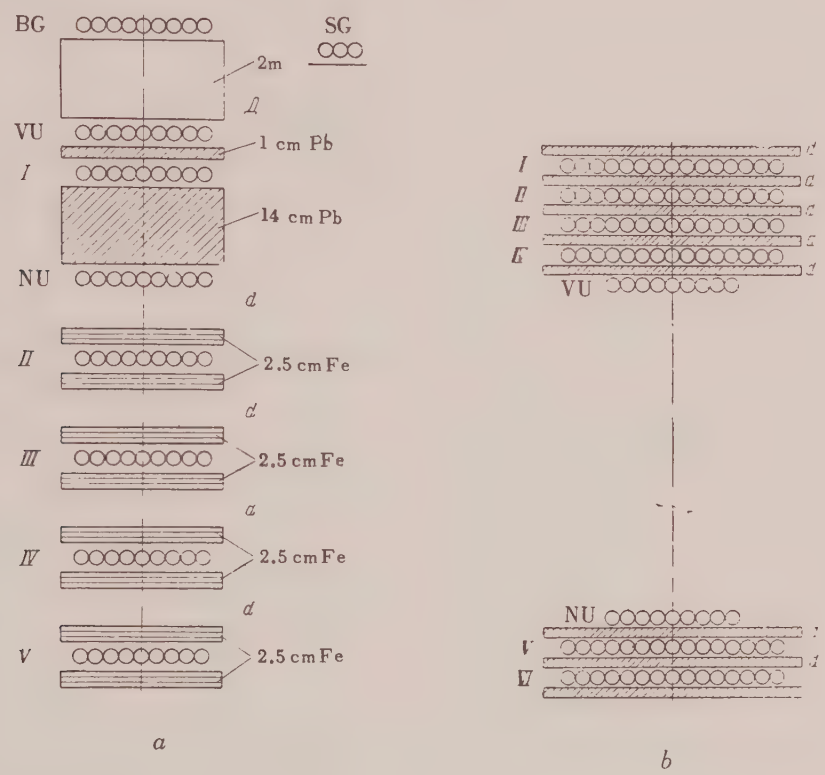

FIG. 1. Two variations of the arrangement of the hodoscope for studying the process of slow meson formation by the delayed coincidence method. a — arrangement of type GK-5A, b — arrangement of type GK-5B; VU and NU — control group of counters (upper and lower), BG and SG — supplementary group of counters (upper and side) for examining the role of air showers, I — VI — series of counters combined with the double cell of the GK-5 hodoscope, d — filter, designed to slow down mesons and act as a source of decay electrons.

Following the master pulse block is the automaton unit whose task it is to start the camera and later to extinguish the neon lamps. In arrangement *B* (Fig. 2b) the automation has a double stage, — it starts the camara and later permits the admission of the auxiliary pulse from any of the lower hodoscope cells of GK-5 i.e., from the delayed discharge of any of the counters of the hodoscope.

In connection with the usual scheme of operating with neon lamps we have the characteristic obstacles to achieving high resolving power, i.e., the lag of the gas discharge and the instability of the lamps, so it is interesting to point out here the main parameter of our apparatus, which characterizes its resolving power and (in part) the stability of operation. The resolving power of the GK-5 hodoscope for non-delayed particles is $\tau_1 = 1$ sec, for delayed particles $\tau_2 = 3$ sec $\pm 10\%$ (we can choose a time interval of 1-4 sec for non-delayed particles).

The resolving power of the GK-3 hodoscope is 30μsec. The range of operation of the cells of GK-5 for feeding the control anodes of the neon lamps is 60-80 volts (i.e., $\pm 15\%$) and for feeding the main anodes ~ 5 volts ($\pm 2.5\%$).

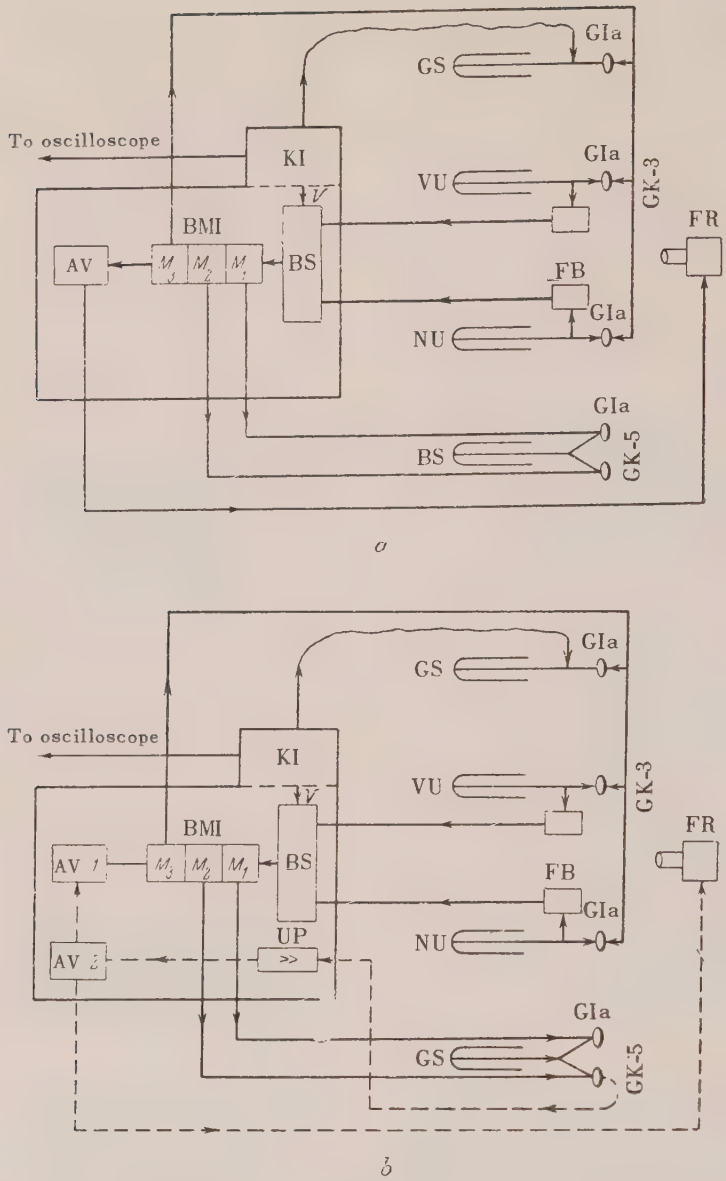

FIG. 2. Block diagram of the electronics of the experimental arrangement: a) GK-5A, b) GK-5B, VU, NU — control counters, GS, GIa — hodoscope counters and cells, FB — shaping block, BS — delay block, BMI — Master pulse block, AV — automaton, FR — camera, KI — control pulser, UP — constant current amplifier.

We will conclude by saying a few words concerning the control and regulation of the resolution of the GK-5 hodoscope. The adjustment of each of the tubes was checked once a day and in case it was necessary, it was changed by means of the special trimmers (see Fig. 3) at the entrance to the condenser which separates the circuit from the master pulses M_1 and M_2. The control of the resolution of the cells of GK-5 was done weekly, for which special pulses from the control pulser K' (which satisfactorily regulated the delay from one unit to the next) were supplied to the coincidence block and the entrance to the appropriate tube of the hodoscope.

3. ANALYSIS OF INSTRUMENTAL EFFECTS AND CORRECTIONS

In order to study the processes of formation of slow π-mesons by the method of the delayed coincidence hodoscope it is necessary to take into account the following instrumental effects and

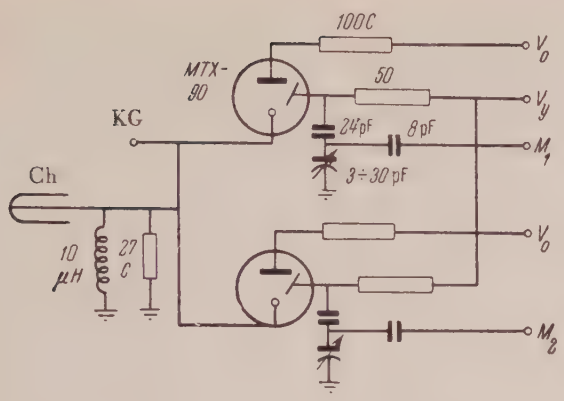

FIG. 3. Principle of the double cell scheme of the GK-5 hodoscope. Ch — counter; V_0, V_y — input supply to the main and control anodes of the lamp MTX-90; input for master pulses: M_1 — delayed; M_2 — non-delayed; KG — control connection

corrections: a) apparent decays, connected with the appearance of delayed coincidences due to accidental particles and delayed discharges of the counters (we will call these events accidentals and false coincidences); b) decay of stopped mesons which are not connected with the formation of these mesons by nuclear action of particles inside the apparatus; c) correction for the efficiency of detection of various processes, connected with the formation, stopping and finally the decay of mesons within the limits of the apparatus; d) errors in determining the point of formation of the mesons, connected with imperfection in the hodoscopic method, in particular, secondary interaction of particles in the electronic-nuclear shower; e) different values for the relation between the range and original energy of π-mesons, connected with the processes of nuclear absorption and scattering of these particles, and the circumstance whereby we detect only the projection of the range onto the plane of the hodoscopic photograph.

The relative importance of accidental coincidences can be estimated with the aid of the relation

$$N_{acc} = (N_{stop} + N'_{stop})\tau_2 N_3, \qquad (1)$$

where N_{stop} is the frequency of events connected with the stopping of the mesons, N'_{stop} is the frequency of events which imitate the stopping events, N_3 is the total of all pulses from counters which surround the stopping point, $\tau_2 = 3 \times 10^{-6}$ sec is the resolving time of the hodoscope for delayed particles, N_{acc} is the frequency of accidental coincidences that is being sought.

We compare the derived frequency N_{acc} with the frequency of true decays that are detected by the apparatus N_{det}:

$$N_{det} = N_{stop}\eta_0, \qquad (2)$$

where η_0 is the efficiency for detecting decays.

As will be shown below, the efficiency under our conditions was usually not less than 0.1. If we take into account the fact that the point at which the meson stops is in the immediate neighborhood of 5-7 counters, each having a cross section* of 100-160 cm^2, then the total load is $N_3 \leq 50$ sec^{-1} and in the absence of the "background" phenomenon, which imitates stopped mesons ($N'_{stop} = 0$), the accidental coincidences constitute a small part of the true decays. Unfortunately, such ideal conditions are practically impossible for two reasons: first, because of the presence in the shower of non-mesonic particles, which are connected with the stopping of particles which do not decay and only increase the "background" of accidental coincidences (this factor applies only in arrangements of class B, which have a sufficiently "soft" control system); second, because of the imperfect geometric conditions of the experiment (particularly in the arrangements of class A), when there are fast particles which are moving laterally (in the direction perpendicular to the plane of the hodoscope photograph); these give the appearance of particles which are stopped between two rows of the hodoscope. Owing to the influence of the factors just mentioned, the total background of accidental coincidences in certain experiments with the arrangements of class B turns out to be comparable to the frequency of the decays being studied. This circumstance deprives us of the possibility of making a simple interpretation of each hodoscope photograph; however, for the statistical treatment of the data (in particular, for the study of the energy spectrum of the mesons) it is sufficient to determine the number of accidental coincidences with the aid of a special controlled experiment. For this purpose we made use of the usual experiment with the additional time displacement of the delayed master-pulse M_2, in which the apparatus did not detect any decays, but detected accidental coincidences at the same rate as in the primary experiment.

In contrast to the accidental coincidences, the dangers of false coincidences (caused by delayed discharges of the counters) did not enter into the work. This is explained by the fact that the experimentally selected displacement of our delayed master-

* Experiment showed that the passage of decay electrons through the more remote counters did not, as a rule, have to be taken into account.

pulse was already sufficiently larger than the time for the delayed discharge of the counters. Actually, if the delayed discharges were essential, then one would need not only the end of the "track", but also the middle, which is practically not observable.

We investigate the effects of processes which may imitate the local formation of slow mesons by nuclear action of particles. Here we are concerned with various types of electromagnetic processes, and also nuclear splittings without emission of mesons. A share of these processes (electron-photon showers, δ-showers, from fast mesons and particles of non-mesonic nature) may imitate the formation and decay of mesons only because of the appearance of accidentally delayed particles, and also when one takes account of the controlled accidental delayed coincidences. In all cases, we have the point of the actual decay of the meson in the apparatus, but this meson either comes into the apparatus from the air (δ-showers from slow mesons, air showers) or is generated by nuclear-inactive particles (photogeneration)**.

An estimate of the possible portion of the mesons which come from the air was made by us by a computation made with the help of a special control experiment. The calculation of this estimate starts with the data on the flux from, on the one hand, slow mesons and mesons from wide air showers of a given density (several particles over the area of the apparatus), and on the other hand, nuclear-active particles with energies that are sufficient for efficient meson formation. The control experiment was designed to determine the role of the δ-showers and was based, first, on the height of passage through the apparatus at which the shower was detected, and second, on the study of the penetrating power and spatial distribution of the shower particles. The role of the air showers was determined both with the use of the special group of side counters, as well as by the method of analyzing the penetrating power of the shower particles.

The result of all of the mentioned estimates and control experiments consisted of the following. The contribution of δ-showers comprised no more than 5% in set-ups of class A (in this case the apparatus can only operate from twofold δ-showers), in set-ups of class B – 10% of the frequency of occurrence of local meson forming showers. The contribution of air showers in arrangements of class A was $\sim$ 10% of the number of showers which generated mesons in the apparatus, whereupon the main part of these processes is dependent on nuclear-active particles, which go along with low density air showers, and they are distinguished from showers of the local type only by the very large average energy of the particles which form slow mesons in the apparatus***. The air showers in the arrangement GK-5B cause 25% of the total number of delayed coincidences that are detected from showers. However the majority of similar events are attributed to accidental coincidences, which is easy to understand. Because of the "softness" of the control system of counters the apparatus separates efficiently nuclear-active particles which have comparatively low energies, and hence may not have much air accompaniment.

The possible contribution of processes of photogeneration of mesons may only be estimated by calculation. We proceed from the flux of photons with energy > 200 mev in the atmosphere where as is well known (from accelerator data) we have the maximum effective coss section for photogeneration, and obtain a value of the order of 5% (in comparison with the frequency of generation by the nuclear-active component) as an upper limit for the relative frequency of photogeneration of mesons in our apparatus.

We pass now to the estimate of the efficiency of detection of slow mesons which are generated in the apparatus. This estimate is of interest from various points of view: for example, it permits one to make a comparison between the true decays and the "background" of accidental events, and also between the intensities of slow meson formation from various nuclei; by means of a comparison of the well known flux and energy spectrum of nuclear-active particles, it permits one to determine the efficiency of formation of the mesons under study over a range of energies. Aside from this, an analysis of the question of the efficiency of detection permits one to go into the corrections that are necessary to determine the true form of the spectrum for meson formation.

The problem of the efficiency of the apparatus, i.e., the relation between the number of generated and detected slow mesons, can be broken down into two independent parts: first, the determination of the probability with which the nuclear-active particles of a fixed energy create in the filter of

** In both cases, the particles which accompany the meson may sometimes imitate local showers and appear as a source of formation and decay of mesons in the apparatus.

*** As was shown in the experiments of Liubimov et al[8], an increase in the energy of the particles which generate electron-nuclear showers, is accompanied by an increase in the probability of concomitant air showers.

[8] N. L. Korablev, A. L. Liubimov and A. T. Nevraev, Dokl. Akad. Nauk SSSR 68, 273 (1949).

the apparatus a π^+-meson of a given range****, which is confined within the limits of the apparatus; second, the probability of detection of electrons, which originate as a result of the decay of a meson which stops in one of the filters of the apparatus. For a single meson, proceeding into the apparatus from the air, only the second possibility remains. This is the simpler part of the problem at which we begin our calculation.

If we denote by d the thickness of the filter between the rows of the counters of the GK-5 hodoscope which detect the decay electrons, and by $F[E(X)]$ – the integral energy spectrum (X is the range of these electrons), then the average efficiency for detecting isotropically emitted decay electrons is to a first approximation of the form:

$$\eta_0 = \left[\exp\left(-\frac{t_1}{\tau_\mu}\right) - \exp\left(-\frac{t_2}{\tau_\mu}\right)\right] \frac{1}{d} \int_0^d dX \int_0^{\theta_{max}(X)} F\left[E\left(\frac{X}{\cos\theta}\right)\right] d(\cos\theta). \quad (3)$$

In this expression t_1 and t_2 are the limits of the time interval in which the hodoscope can detect delayed particles, $\tau_\mu = 2.15\ \mu$ sec – the mean lifetime of the μ-meson and θ_{max} is the limiting angle at which there can emerge from the filter the electrons which originate at a depth X and which possess the maximum possible length. The scattering of the electrons in the layers of the filter and at the ends of the filter (in a direction perpendicular to its thickness) is thereby not taken into account; however, it cannot introduce any essential error into the calculation of η_0.

For a practical calculation of the efficiency it is expeditious not to use the energy spectrum of the decay electrons, which was determined with great precision by use of the Wilson chamber or photographic plates, but to go directly from the integral range spectrum, i. e., the absorption curve, determined for various substances by the method of delayed coincidences from counters (see, for example, Refs. 4 and 9 and 10). The efficiency η_0 calculated from this data for several variations of our apparatus is presented below.

Thickness of filter, d	2 cm Pb	2 cm Fe	2 cm C
Efficiency for detecting decays, η_0	0.14	0.20	0.30

The derived value lacks certain corrections, which are connected with the fact that a part of the counters, which detect decay electrons, may appear to be "busy" with discharges from non-delayed particles. For a single meson, such particles may appear only from the stopping of mesons, and in this case (when only one counter near the point of decay is busy) the average correction for the effect of the busy counters is a constant factor $\eta_i = 0.8$. In order to check experimentally the efficiency for detecting the decay of such mesons, we carried out a special control experiment in an underground installation (i.e., under the conditions when the penetrating particles consist only of mesons). The experiment was arranged so that the control system of the arrangement GK-5A was "adjusted" to select single penetrating particles, going in a narrow solid angle, and arranged under one of the rows of the GK-5 hodoscope which detected all stoppings of these particles as well as the accompanying decay electrons. We determined by this experiment a value of the efficiency which agreed well with the value deduced above (from the calculation of the correction due to the counters being "busy").

For mesons which strike the filter of the hodoscope accompanied by other particles, the correction for the occupied counters is calculated and the average value depends on the scattering from the point of formation of the original local shower to the meson track. In this case the correction to the factor η_i is determined purely experimentally, by means of utilizing the hodoscope pictures and determining the average probability of counters being occupied by various scatterings from the point of formation of the shower +.

After determining the efficiency for detecting

****In order to simplify the problem we will, for the present, assume that the range has a vertical component only.

[9] J. Steinberger, Phys. Rev. 75, 1136 (1949).

[10] E. P. Hincks and B. Pontecorvo, Phys. Rev. 77, 102 (1950).

+ In contrast to the case of the single meson the position of the occupied counters relative to the point of decay is no longer essential and hence the correction factor η_i can be taken as simply equal to the number of occupied counters of the hodoscope.

decays we turn to the calculation of what is called the "luminosity" of the apparatus, i.e., the frequency N_{det}, of detected slow mesons, produced by the nuclear-active component and stopped inside the same apparatus. The expression for the luminosity can be written in the following form:

$$N_{det} = \int_{E_0}^{\infty} \left[1 - \exp\left(-\frac{\Delta R}{\lambda(E)}\right)\right] S(E)\, \overline{W}_p(E)\, \bar{\nu}_{\pi^+}(E)\, dE \tag{4}$$

$$= \frac{1}{l} \sum_{ij} \eta_{i0}\eta_{ii} \frac{d\Phi_{\pi}(r_B)}{dr_B} \Delta_i r \Omega_{ij}(r_B),$$

where E_0 is the threshold energy for generation of slow mesons by nucleons, ΔR is the sum of the thicknesses of all of the filters of the apparatus, whose number is denoted by 1, $\Delta_i r$ is the thickness of each separate filter, $\lambda(E)$ is the average path for generating mesons by nuclear-active particles of energy E, $S(E)$ is the energy spectrum of the nuclear-active component in the atmosphere, $\overline{W}_p(E)$ is the mean probability of detection of showers by the control system of counters, the showers being formed with a fixed energy, $\bar{\nu}_{\pi^+}(E)$ is the average multiplicity of generation of the slow π^+-mesons in such showers, $\eta_{i0}\eta_{ii}$ is the previously determined efficiency for detecting decays and the correction for the occupied counters, $\Phi_{\pi}(r_B)$ is an average over the primary integral energy spectrum of the meson range (actually, the vertical component of the range), $\Omega_{ij}(r_B)$ is called the "geometrical factor", i.e., the correction taking into account the finite size of the hodoscope filters.

We note that in the average over the primary meson energy spectrum (in order to normalize the spectrum, we must determine the energy dependence of the factor $\bar{\nu}_{\pi^+}$) we must take care of the circumstance that the true dependence of the spectrum on the energy E appears in the form of the function under the integral in expression (4) which cannot be calculated compared to such functions as $\lambda(E)$, $S(E)$ and $\overline{W}_p(E)$[++].

There is no possibility of examining in detail all of the quantities which enter into (4), so we limit ourselves here only to some short remarks, after which we will give, for various cases derived by us, the function under the integral, which may be called "the energy generating function" of slow mesons by the nuclear-active component.

The threshold energy "E_0" and the total range of energies for an efficient generation of mesons can be obtained by combining the data, determined with accelerators, on the generation cross section for heavy nuclei and photographic plate data on the probability of "inelastic" nuclear collisions for various energies of the nucleons in the cosmic radiation[+++]. The differential energy spectrum $S(E)$ of the nuclear-active component in the atmosphere, in particular at mountain altitudes (where we carried out our experiments) is known at the present time from a whole series of works, carried out by various methods[8*], and can be represented satisfactorily by a function of the form $p^{-2.5}$ (p is the momentum). The probability of detecting showers $\overline{w}_p(E)$ for an actual system of control counters may be calculated to a satisfactory approximation only in cases when the operation of the system is determined by penetrating shower particles; then we may use the photographic plate data for multiple formation of relativistic particles (see, for example, Refs. 12 and 13). As an average energy spectrum of slow mesons we can use the spectrum of Camerini et al.[12], which was determined with an arrangement in which the average energy of the nuclear-active particles was not too different from the energies at which our apparatus is efficient. The least obvious point appears to be the question of the function $\bar{\nu}_{\pi}(E)$, i.e., the multiplicity of generation of slow mesons. The fairly meager photographic plate

[++] If the multiplicity J_{π^+} is not a monotonically increasing or rapidly decreasing function of the energy E, then the three functions also determine the effective range of primary energies for the given arrangement.

[+++] Suitable data were considered by us in the survey Ref. 11.

[8*] The similarity of the conditions of observation is explained by the energy estimate made below.

[11] G. B. Zhdanov, Usp. Fiz. Nauk 54, 435 (1954).

[12] U. Camerini, P. H. Fowler et al, Phil. Mag. 41, 413 (1950).

[13] U. Camerini, J. H. Davies et al, Phil. Mag. 42, 1241 (1951).

data on the generation of slow mesons (with energies of tens of mev) in the stratosphere[14] shows that this multiplicity, does not apparently increase with the primary energy, and if it decreases, then it does so very weakly. Therefore, in carrying out our calculation, we start from two alternative assumptions about the form of the function $\bar{\nu}_{\pi^+}(E)$: a) $\bar{\nu}_{\pi^+}(E) =$ constant; b) $\bar{\nu}_{\pi^+}(E) \sim 1/n_s$ (for $E > 2$ bev), where n_s is the number of relativistic particles in the shower.

In Fig. 4 are shown the results of our calculation of the energy generation function of slow mesons for three different cases: a) Arrangement GK-5A, $\bar{\nu}_{\pi^+}(E) =$ constant, b) Arrangement GK-5B, $\bar{\nu}_{\pi^+}(E) =$ constant, c) arrangement GK-5B, $\bar{\nu}_{\pi^+}(E) \sim 1/n_s$ with $E > 2$ bev.

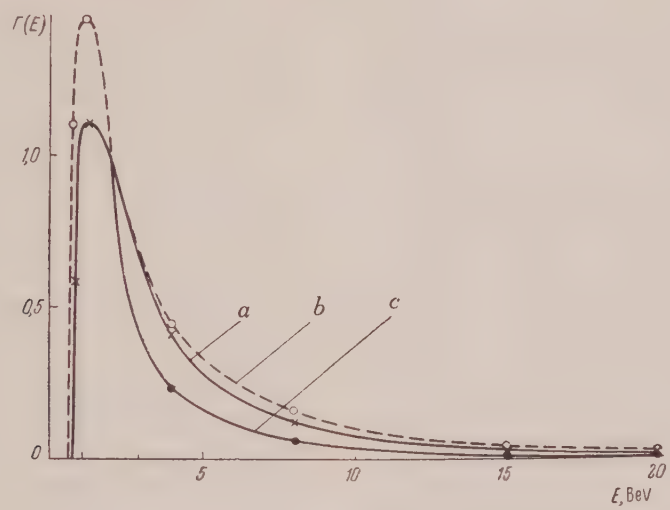

FIG. 4. Dependence of the output of slow mesons $G(E)$ on the energy of the generating particle E for various arrangements and assumptions about the multiplicity of formation: a) arrangement GK-5A, $\bar{\nu}_{\pi^+} =$ const., b) arrangement GK-5B, $\bar{\nu}_{\pi^+} =$ const., c) arrangemnet GK-5B, $\bar{\nu}_{\pi^+} \sim 1/n_s$ (for $E > 2$ bev).

With the help of these curves, it is possible in each case to determine characteristic energies — the threshold energy E_0 and the average energy of the generated component E_{av}. These values can be determined from the energy limits to whose left there is respectively 5 and 50% of the total area, within the limits of the curves of Fig. 4. In this manner we obtain the "thresholds" and average energies (for each of the three cases):

Arrangement and multiplicity of meson generation	GK-5A $\bar{\nu}_{\pi^+} =$ const	GK-5B $\bar{\nu}_{\pi^+} =$ const	GK-5B $\bar{\nu}_{\pi^+} \sim 1/n_s$
Threshold Energy, E_0 in bev	1,1	1,0	0,9
Average Energy E_{av} in bev	2,9	3,0	2,0

By using the expression (4) we determined not only the energy dependence of the "output" of slow mesons, but the overall frequency of detecting decays by the apparatus (the "luminosity" of the apparatus). A comparison of the calculated number with the experimental observations showed that both of the initial assumptions about the dependence of the value of $\bar{\nu}_{\pi^+}$ on the initial energy are in accord with experiment (within the limits of error of the experiments and the calculations), as well as the assumption about the increase of the "output" of slow mesons with the primary energy E, for example according to the law $\nu_{\pi^+} \sim n_s(E)$ which leads directly to an es-

[14] H. Yagoda, Phys. Rev. 85, 891 (1952).

timate of the "luminosity" of the apparatus.

We will consider methodically the question of the connection of the observed spectra and the energy of the mesons. In order to analyze the hodoscope picture of the appropriate shower, the terminus of the meson path is fixed by the appearance of the decay electron, and the average error is determined by measurement. Obviously, half the thickness of the filter separates two rows of the hodoscope counters. Errors in fixing the beginning of the track are connected with two factors: the inaccuracy in determining the point of formation of the initial shower in the filter of the hodoscope, and the possibility of generation of mesons by secondary nuclear-active particles in the shower. To explain the role of the first factor, we plot the distribution curve of the number of fired counters in the rows of the hodoscope, reading off the number of the row each time for the filter in which the shower was supposedly generated (absolute numbers are read off vertically downwards). The character of these curves plotted in Fig. 5 for two concrete arrangements (the hodoscope with graphite and lead filters each 2 cm thick), shows that the average error in determining the point of formation of the shower, apparently does not exceed half the thickness of the filter by virtue of the strong dependence of the number of counters that are fired on the number of the row. As a rule, nothing can be said about the effect of processes of secondary mesons on the shape of the hodoscopic pictures. It is possible, however, to take into account these processes with the aid of the following discussion. As is well known, the average ranges for absorption and interaction of the nuclear-active components in substances λ_{abs} and λ_{int} are connected by a simple relation (see, for example, Ref. 15):

$$\lambda_{int}/\lambda_{abs} = 1 - \bar{\nu}_{sec} \tag{5}$$

where $\bar{\nu}_{sec}$ is the average over the spectrum of the number of secondary nuclear-active particles. Taking into account the fact that, according to the data of Ref. 15, $\lambda_{int}/\lambda_{abs} = 1/3$ (independent of the atomic number of the nucleus), we obtain $\bar{\nu}_{sec} = 2/3$ and, consequently, the probability of forming secondary showers in each of the filters at a depth Δr located under the point of formation of the initial shower, is, on the average, $2/3\,\Delta r/\lambda_{int}$.

In order to go over from the distribution in range to the initial energy spectrum of π^+-mesons it is necessary to introduce corrections of two kinds. First of all it is necessary to take into account the fact that the hodoscope photograph does not permit one to obtain a representation of

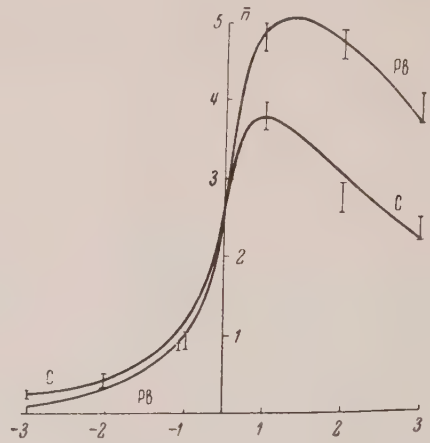

FIG. 5. Average number $\bar{n}$ of fired counters of the hodoscope through various scatterers from the point of supposed formation of the shower. The number of the hodoscope row is read from the vertical-positive downwards and negative upwards. Pb, C — are the curves for the arrangement GK-5B with lead and graphite filters respectively.

the complete meson track in space, and in the best case it is possible to represent only the projection of this track on the plane of the photographic plate. However, if we neglect the effect of the finite size of the hodoscope filters and the scattering of mesons in these filters, then the distribution of the vertical component of the track r_b can be converted into the distribution of the total range without difficulty, and conversely, if we know the angular distribution of the mesons relative to the vertical. Actually, the question in this case can be resolved by the method of generalization of the well known relation of Gross between the vertical absorption curve and the global intensity of cosmic rays. For an angular distribution of the radiation, incident within the limits of a certain plane area, of the form of $\cos^n\theta$ (θ — the angle with the vertical), the relation, which connects the vertical $f_b(X)$ and the global $F_{gl}(X)$ intensity of the radiation at a depth X has the form:

$$F_{gl}(X) = \lim_{\theta_m \to \pi/2} \int_0^{\theta_m} f_B\left(\frac{X}{\cos\theta}\right) \cos^n\theta \, d\cos\theta; \tag{6a}$$

$$f_b(X) = (n+1)\,F_{гл}(X) - X\frac{dF_{гл}}{dX}. \tag{6b}$$

---

[15] S. A. Azimov, N. A. Dobrotin and A. L. Liubimov, Izv. Akad. Nauk SSSR, Ser Fiz. 17, 80 (1953).

For slow mesons we assume $n = 3$ (see 16), whereupon we can calculate the production with the help of the relation (6a) for the function $f_b(X)$, corresponding to the meson spectrum of Camerini[12], and show that the distribution from complete tracks and from the vertical components of the tracks differ very little in this case (considerably less than for isotropic radiation).

The other type of correction to the meson spectrum is connected with the calculation of the nuclear interactions with matter. All nuclear interactions, in which the meson is absorbed, not reaching the end of its ionization range, are taken into account by the simple method of multiplying the ordinate of the range spectrum with an exponential factor of the form $\exp(X/\lambda_{abs})$, where λ_{abs} is the mean range for nuclear absorption. A calculation of the nuclear scattering of π-mesons, inelastic as well as from elastic (at large angles), appears to be a considerably more complicated problem; however, over our range of energies, the effective scattering cross section is not large, and therefore to a first approximation one need take into account only pure absorption. Thus, for example, on the basis of a series of a large number of investigations, using various methods (see, for example, Refs. 17-20), it is proved that for energies up to 150 mev, the cross section for nuclear absorption of π^+-mesons constitutes 60-80% of the total (equal to the geometrical) cross section, and the cross section for processes which are accompanied by a large change of energy and angle does not exceed 15% of the geometrical cross section, although with increasing energy this cross section increases markedly.

CONCLUSIONS

We presented above an analysis of the hodoscope method with delayed coincidences and used this method to study the processes of generating slow mesons, which permits one to settle the following three questions:

1. We determined the range of the energy spectrum of nuclear-active particles, which gives the main contribution to the generation of slow mesons (under the conditions of our experiments this energy is on the average 2-3 bev).
2. We introduced all of the necessary instrumental corrections for determining the intensity of generating slow mesons from various nuclei (in above specified range of energies).
3. We introduced the instrumental corrections necessary to determine the energy spectrum of slow mesons from the point of generation.

The experimental results, which were obtained by us by use of the method considered above, were described in the second part of this paper.

In conclusion the author would like to thank for their great help L. N. Korablev, V. F. Tulinov, A. A. Abdullaev and A. A. Khidarov for adjusting the apparatus and for the time spent in making measurements.

---

[16] W. L. Kraushaar, Phys. Rev. 76, 1045 (1949).

[17] G. Bernardini and F. Levy, Phys. Rev. 84, 610 (1951).

[18] H. Bradner and B. Rankin, Phys. Rev. 87, 547 and 553 (two papers) (1952).

[19] J. F. Tracy, Phys. Rev. 91, 960 (1953).

[20] R. L. Martin, Phys. Rev. 87, 1052 (1952).

Translated by B. Hamermesh
87

Formation of Negative Hydrogen Ions by Collision of Protons with Gas Molecules

IA. M. FOGEL' AND R. V. MITIN
Physical and Technical Institute, Academy of Sciences, Ukrainian SSSR
Kharkov State University

(Submitted to JETP editor February 7, 1955)
J. Exptl. Theoret. Phys. (U.S.S.R.) 30, 450-457 (March, 1956)

Measurements were made of effective cross sections of two electron capture by collisions of protons of energies from 9.5 to 29 kev with molecules of H_2, N_2, O_2, He, Ne and A. The ratio of the number of negative hydrogen ions to the number of protons in the balanced beam formed after the proton beam has passed through the six mentioned gas targets, was determined as a function of energy. The effective cross section of capture of a single electron by collision of a fast hydrogen atom with a fast hydrogen atom with a hydrogen molecule was computed on the basis of the experimental results.

FORMATION of negative ions by single collisions of fast singly charged positive ions with gas molecules results from the exchange of two electrons between the colliding particles. Effective cross sections of two electron capture by positive oxygen ions upon collision with molecules of hydrogen, nitrogen and oxygen were given in the work of Fogel and Krupnik[1]. For protons colliding with hydrogen molecules initial measurements of double exchange of charges were presented in the work of Fogel, Krupnik and Safronov[2].

The process of two electron capture by triply charged ions of argon in neon, argon and nitrogen were studied by Fedorenko[3].

As is evident from this brief review, processes involving double exchanges (unlike atomic collisions involving exchange of single electrons) have been inadequately studied and therefore, in order to understand the mechanism of such processes, it is necessary to make further investigations for different ion-molecule pairs over a widest possible range of ion energies.

METHOD OF MEASUREMENTS

For the study of the process of double exchange of charge of protons we have constructed an experimental equipment basically similar to that used in Ref. 1 and will therefore not describe the equipment here. The basic difference between our experimental arrangement and that previously used was that the analysis of the beam, after it passed through the collision chamber, was performed by an electrostatic and not a magnetic analyzer. Measurements of the I^+ and I^- currents in the Faraday trap of the electrostatic analyzer were made simultaneously by a mirror galvanometer and a string electrometer so that errors caused by accidental fluctuations of the primary proton current were removed.

A liquid air trap was inserted in the collision chamber used in this work. The trap served to freeze out the condensed vapors and resulted in a considerable reduction of the number of negative ions produced by double ionization of the residual gas molecules in the collision chamber.

The electric potentials in the ion source, focusing lens and the accelerating tube were measured by a voltmeter calibrated with a resistance voltmeter similar to the one used in Refs. 1 and 2.

The content of the beam formed as a result of passage of protons through matter is represented by differential equations.

$$dN^+/d(nx) = -(\sigma_{10}+\sigma_{1-1})N^+ + \sigma_{01}N^0 + \sigma_{-11}N^-; \quad (1a)$$

$$dN^0/d(nx) = \sigma_{10}N^+ - (\sigma_{01}+\sigma_{0-1})N^0 + \sigma_{-10}N^-; \quad (1b)$$

$$dN^-/d(nx) = \sigma_{1-1}N^+ + \sigma_{0-1}N^0 - (\sigma_{-11}+\sigma_{-10})N, \quad (1c)$$

where N^+, N^0 and N^- are the number of protons,

[1] Ia. M. Fogel and L. I. Krupnik, J. Exptl. Theoret. Phys. (U.S.S.R.) 29, 209 (1955); Soviet Phys. JETP 2, 252 (1956).

[2] N. V. Fedorenko, J. Tech. Phys. (U.S.S.R.) 24, 769 (1954).

[3] Ia. M. Fogel', L. I. Krupnik and R. G. Safronov, J. Exptl. Theoret. Phys. (U.S.S.R.) 28, 589 (1955). Soviet Phys. JETP 1, 415 (1955).

neutral atoms of nydrogen and negative ions of hydrogen, respectively in the beam; σ_{ik} is the effective cross section of the process, as a result of which a particle with a charge i is converted into a particle with a charge k; n if the number of atoms per cc of the matter, x the length of path in matter.

By Eq. (1c) and by use of the initial conditions $nx = 0$, $N^+ = N_0^+$, $N^0 = 0$, $N^- = 0$, the following formula for determining the cross section for two electron capture by a proton is readily obtained:

$$\sigma_{1-1} = 1.08\times10^{-19}(T/L)\left[\frac{d(I^-/I_0^+)}{dp}\right]_{p=0}, \tag{2}$$

where L is the effective length of the collision chamber, T the temperature of the gas in the chamber, I^- the current of negative hydrogen ions in the beam, I_0^+ the ion beam current entering the collision chamber.

The method of measuring the cross section σ_{1-1}, based on Eq. (2), consists of studying the dependence of the ratio I^-/I_0^+ on the gas pressure p in the collision chamber. The derivative in Eq. (2) is determined from the linear portion of this dependence, the presence of which is conditioned by the formation of negative ions by single collisions of protons with the gas molecules.

The solutions of differential equations (1) have the following form:

$$N^- = a_0 + a_1e^{-r_1nx} + a_2e^{-r_2nx}, \tag{3}$$

$$N^+ = b_0 + b_1e^{-r_1nx} + b_2e^{-r_2nx},$$

$$N^0 = c_0 + c_1e^{-r_1nx} + c_2e^{-r_2nx},$$

where the quantities r_1, r_2, a_0, a_1, a_2, etc. are the functions of the six cross sections entering into the differential equation (1). When $nx \to \infty$, $N^- \to a_0$, $N^+ \to b_0$, $N^0 \to c_0$, i.e., with sufficient increase of the thickness of the gas target, the composition of the beam no longer changes. The content of the beam is said to be in equilibrium. It can be shown that $(N-/N^+)_p$ will have the following form:

$$\left(\frac{N^-}{N^+}\right)_p = \left(\frac{I^-}{I^+}\right)_p = \frac{\sigma_{10}\sigma_{0-1} + \sigma_{1-1}\sigma_{01} + \sigma_{1-1}\sigma_{0-1}}{\sigma_{01}\sigma_{-10} + \sigma_{-11}\sigma_{01} + \sigma_{-11}\sigma_{0-1}}. \tag{4}$$

For sufficiently small values of nx, Eqs. (3) can be expanded into series. By neglecting all powers of nx higher than second we obtain:

$$I^-/I^+ = \sigma_{1-1}nx + {}^1/_2(\sigma_{10}\sigma_{0-1} + \sigma_{1-1}\sigma_{10} + \sigma_{1-1}^2 - \sigma_{1-1}\sigma_{-10} - \sigma_{1-1}\sigma_{-11})(nx)^2 \tag{5}$$

Thus, in the region of gas pressures in the collision chamber when multiple collisions of the beam particles with gas molecules begin to appear and while these pressures are not yet too great, the dependence of the ratio I^-/I^+ on the pressure is expressed by the equation

$$I^-/I^+ = \gamma p + \delta p^2, \tag{6}$$

where

$$\gamma = \sigma_{1-1}L/kT; \tag{7}$$

$$\delta = {}^1/_2(\sigma_{10}\sigma_{0-1} + \sigma_{1-1}\sigma_{10} + \sigma_{1-1}^2 - \sigma_{1-1}\sigma_{-10} - \sigma_{1-1}\sigma_{-11})L^2/k^2T^2.$$

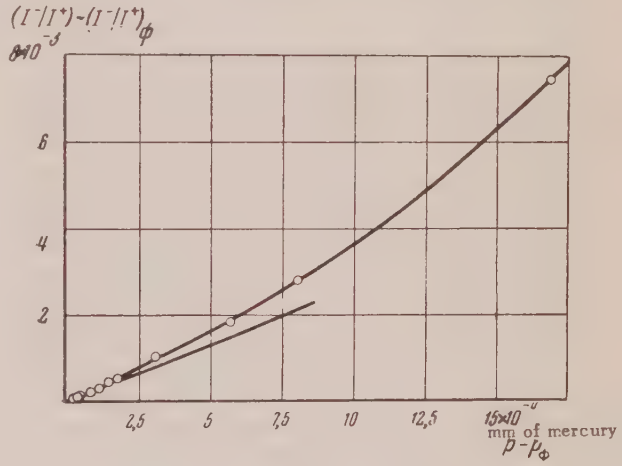

FIG. 1

In Fig. 1 is shown part of the curve of variation of I^-/I^+ with pressure for 29 kev protons passing through hydrogen. In constructing this graph the double charge transfers from the protons to the molecules of the residual gas in the collision chamber, were taken into consideration. This was done by making the values on the axes of abscissas and ordinates to correspond to $p - p_\phi$ and $(I^-/I^+) - (I^-/I^+)_\phi$ respectively, where p_ϕ is the pressure of the residual gas and $(I^-/I^+)_\phi$ the value of the ratio I^-/I^+ at the pressure of the residual gas. The pressure of the residual gas in the chamber was 5×10^{-5} mm of mercury. It should be noted that upon freezing of the condensed vapors in the collision chamber, the value of $(I^-/I^+)_\phi$ decreases from 3×10^{-3} to 2×10^{-4}. As seen from Fig. 1, the dependence of I^-/I^+ on pressure appears linear up to a pressure $\sim 10^{-4}$ mm of mercury. At higher

pressures there is observed a departure from linearity, resulting from the formation of negative hydrogen ions as a result of multiple collisions of the beam particles with the gas molecules.

It follows from the above that the dependence of I^-/I^+ on pressure at not too high pressures should be expressed by Eq. (6). From eleven experimental points in Fig. 1, using the method of least squares, we have determined the values of constants γ and δ in Eq. (6), which turned out to be 2.74 and 1.03×10^3, respectively. Application of the least square method to the 5 points of the linear portion of the curve gives for the value of $\gamma = 2.7$. The values of I^-/I^+ computed according to Eq. (6), with the indicated values of the constants γ and δ, differed from the experimental values by not more than 7.6%. This result indicates that, up to the pressure of 1.7×10^{-3} mm of mercury, the dependence of $I-/I^+$ on the pressure follows Eq. (6).

In the following, for the determination of σ_{1-1}, the quantity γ was determined by the method of least squares from the linear portion of the graph of the dependence of I^-/I^+ on pressure.

The mass spectroscopy method used by us for the measurement of cross sections σ_{1-1} can yield sufficiently accurate values of these cross sections if the following factors which distort the results of measurements are corrected for or removed:

(a) Weakening of the proton beam in the collision chamber resulting from neutralization of protons by collision with gas molecules.*

(b) Unequal distribution of protons and negative hydrogen ions in the collision chamber.

(c) Unequal weakening of the proton and negative hydrogen ion beams in the path from the collision chamber exit to the cylinders of the Faraday analyzer.

The correction for the neutralization of protons can be readily computed if cross section σ_{10} is known. For protons in hydrogen and helium this correction does not exceed several percent and was therefore not introduced by us.

Certain experiments described below indicate that unequal distribution of protons and negative hydrogen ions in the gas of the collision chamber cannot substantially distort the results of measurements.

The correction for the unequal attenuation of the positive and negative beams in the analyzing chamber can only be computed for the case of hydrogen in the collision chamber since for this computation it is necessary to know (besides cross section σ_{10}) the cross section σ_{-10} which was measured in Ref. 4 for negative hydrogen ions in hydrogen. This correction did not exceed 0.2% and is therefore insignificant. Accidental errors in the measurement of cross section σ_{1-1} amounted to 30%. The errors in the measurements of the proton energy was of the order of 3%.

For the determination of the equilibrium value of the ratio I^-/I^+ the curve of I^-/I^+ in its dependence on pressure was plotted up to pressures corresponding to the equilibrium state of the beam. The equilibrium state of the beam is reached for all six gases at pressures of the order of 10^{-2} mm of mercury. Accidental errors in the measurements of $(I^-/I^+)_p$ amounted to 18%.

RESULTS OF MEASUREMENTS

Measurements were made of the effective cross sections of the double exchange of charge process for protons with energy from 9.5 to 29 kev in hydrogen, nitrogen, oxygen, helium, neon and argon. To fill the collision chamber we used hydrogen passed through a palladium filter, spectrally pure helium and neon, oxygen with 0.9% impurities, argon with 0.3% impurities and nitrogen obtained by evaporation of liquid nitrogen and purified from admixtures of oxygen (of the order of 4%) by passage through copper filings heated to 600°. In Fig. 2 is presented the dependence of the effective cross sections σ_{1-1} on the proton energy for all six gases investigated. The value of $\sigma_{1/1}$ for each energy was obtained by averaging two measurements. In the energy range investigated the effective cross section σ_{1-1} for protons in nitrogen, oxygen, argon and neon decreases with increase in energy; for protons in helium there is observed quite a shallow maximum around 14 kev and finally for protons in hydrogen there is a sharp maximum around 17.5 kev. The values of σ_{1-1} fall within the limits from 5×10^{-19} cm^2(neon, 29 kev) to 1.27×10^{-17} cm^2 (hydrogen, 17.5 kev).

Since the measurements of effective cross sections of double exchange of charge for protons are being made for the first time, it is not possible to compare the results with published data. The only comparison could be made with results obtained in the work of Fogel'and Krupnik. In that work measurement was made of the cross section

* The necessity of compensating for this arises from the fact that actually measurement is made of the ratio of currents I^-/I^+ in the Faraday trap of the electrostatic analyzer, while according to Eq. (2) it is necessary to measure the ratio I^-/I^+ where I^+ is the current of protons at the entrance to the collision chamber.

[4] A. C. Whittier, Canad. J. Phys. 32, 275 (1954).

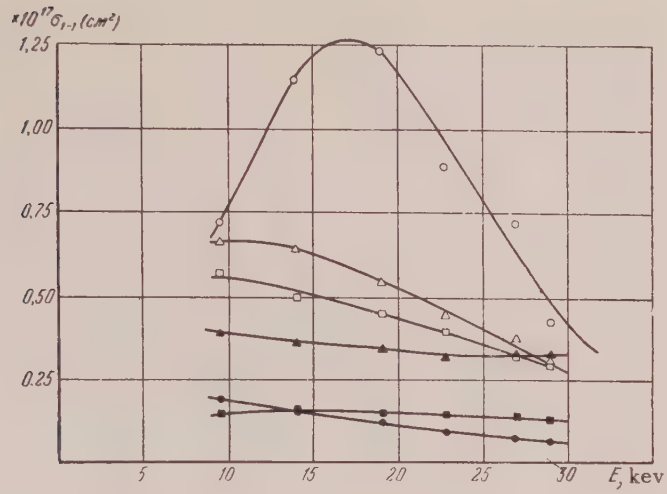

FIG. 2 ○ — H_2, △ — N_2, □ — O_2, ● — Ne, ▲ — A, ■ — He

$\sigma_{1/1}$ for protons in hydrogen for the energy 21 kev and this was given as 1.5×10^{-17} cm^2. According to the results of this present work σ_{1-1} for the mentioned energy is 1.1×10^{-17} cm^2. The difference is within the limits of experimental error.

It is of interest to compare the effective cross sections for the capture by protons of one and two electrons by collision with gas molecules. Such comparison can be made for protons in hydrogen and helium, since only for these two cases reliable measurements were made of the effective cross sections of one electron capture.

For comparison curves of the effective cross section dependence of one electron capture by protons in hydrogen are shown in Fig. 3. The data were taken from the work[5] (solid curve) and[2] (dotted curve), and curves of effective cross section for the capture of two electrons as measured in the present work. As can be seen from this Figure, the effective cross section for one electron capture in the investigated energy interval is 50 to 100 times greater than the effective cross section of two electron capture.

A similar comparison (Fig. 4) for protons in helium made on the basis of data obtained in this work and by Keene[5] shows that in this case the ratio σ_{10}/σ_{1-1} for the investigated energy interval varies from 120 to 250.

The dependence of the equilibrium value of the ratio I^-/I^+ on the energy of protons for the investigated gases is shown in Fig. 5. For nitrogen, oxygen, neon and argon in the interval from 9.5 to 29 kev, there is observed a decrease of $(I^-/I^+)_p$ with increase of energy; for helium this ratio remains approximately the same; in the case of hydrogen for which this ratio is much higher than for the rest of the gases, there is a maximum of 17% (for energies of the order of 8.5 kev). The dependence of $(I^-/I^+)_p$ on energy for protons in hydrogen was investigated by Whittier[4]. His results

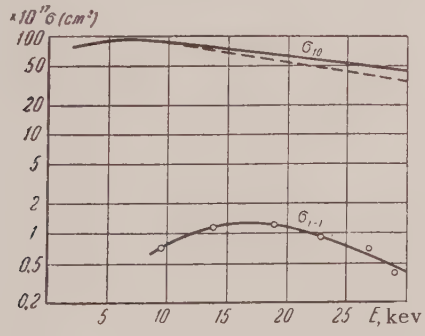

FIG. 3

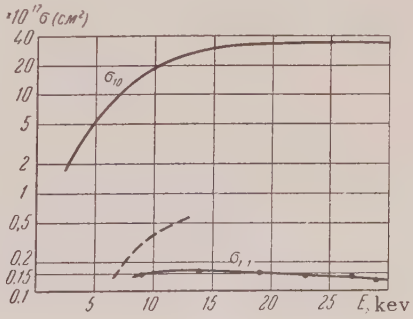

FIG. 4

[5] J. P. Keene, Phil. Mag. **40**, 369 (1949).

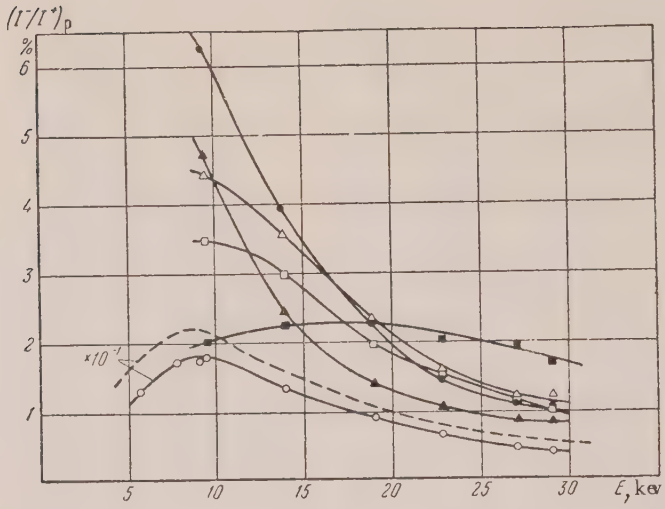

FIG. 5 ○ — H_2, △ — N_2, □ — O_2, ● — Ne, ▲ — A, ■ — He

are shown in Fig. 5 by the dotted line. As seen from this Figure, our values of $(I^-/I^+)_p$ are systematically smaller than those of Whittier, while the differences are beyond the limits of measurement errors.

It should be noted that the collision chamber used in the work of Whittier differed very little in length from our chamber but had an output channel 1 mm in diameter and 75 mm long while the dimensions of the output channel in our camera were 5 and 50 mm respectively. On the assumption that the scattering of protons and negative hydrogen ions in the gas of the collision chamber are not equal, we can conclude that there must exist a systematic error in the determination of $(I^-/I^+)_p$ connected with this unequal scattering. It is easy to understand that this error must be greater in the work of Whittier than in ours since in his chamber the scattered particles are restricted to a much smaller angle than in ours. In order to determine the influence of unequal scattering of protons and negative hydrogen ions on the quantity $(I^-/I^+)_p$ we have placed in the output channel of the collision chamber a 2 mm diameter diaphragm and under these conditions determined the ratio $(I^-/I^+)_p$ for

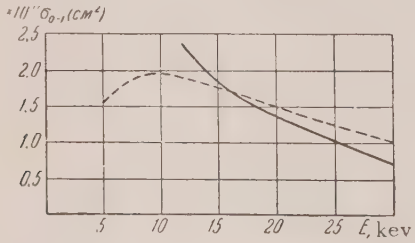

FIG. 6

protons in hydrogen. The results were the same as those obtained without the diaphragm in the output channel. This experiment shows quite conclusively that scattering of the beam particles in the gas of the collision chamber has no effect on the value of $(I^-/I^+)_p$ and therefore cannot be considered as the cause of discrepancy between results of Whittier and the data obtained in this work. The possibility is not excluded that these differences are connected with unequal neutralization of protons and negative hydrogen ions on the walls of the output canal in the collision chamber used by Whittier.

DISCUSSION OF RESULTS

An examination of the shape of the curves of effective cross section dependence on energy in Fig. 2 shows that the energy range studied by us is located in the region of maximum cross section or near it. As is known, the theoretical computation of effective cross sections of inelastic processes is possible for either slow collisions, when $v_u \ll v_0$ (v_u is the relative velocity of the colliding particles, v_0 is the velocity of the electrons in the atom) or for fast collisions, when $v_u \gg v_0$. For collisions accompanied by exchange of electrons, such computations were made only for the simplest ion-molecule pairs (protons and singly charged ions of helium in hydrogen and helium) and for single electron exchanges. For the simplest atomic collision $H_1^+ + He \rightarrow H_1^- + He^{++}$, accompanied by an excnange ot two electrons, computation of effective cross section σ_{1-1} for slow collisions was made by Rosentsveig and Gerasi-

menko[6]. The results obtained by them on the dependence of cross section σ_{1-1} on energy are shown by the dotted lines in Fig. 4. At 9.5 kev, the smallest energy in the energy range investigated by us, the computed theoretical value of σ_{1-1} is approximately three times greater than the experimental value. Such a disagreement is quite understood since at the energy of 9.5 kev the condition of slow collisions is not fulfilled. It would be of considerable interest, to refine, on one hand, the theoretical computation of the effective cross section of σ_{1-1} for collisions of protons with helium atoms and on the other to make experimental investigations in the proton energy range of 100 to 1000 ev where the criterion of slowness of collisions is well fulfilled.

The position of the maximum on the curve of dependence of cross section of nonelastic processes on energy is determined by Massey's[7] criterion:

$$a\,|\Delta\varepsilon|\,/\,hv_u \approx 1, \tag{8}$$

where a is the range of the force of mutual action between the colliding particles, $\Delta\epsilon$ the resonance defect ,i.e., the change in the internal energy of the particles as the result of their interaction, h = Planck's constant.

The resonance defect for the collision of a proton with two atoms of helium which is accompanied by the exchange of two electrons, is equal to the difference between the energy released at the formation of the negative hydrogen ion and the energy spent in the double ionization of the helium atom. In the case under consideration, $|\Delta\epsilon| = 64.4$ ev. If we consider that the maximum cross section σ_{1-1} for the process $H^+_1 + He \rightarrow H^-_1 + He^{++}$ is observed at an energy of 14.0 kev, we have according to Eq. (8), $a \approx 1$ A. Computation shows that the parameter a for collisions between the same particles, but with single electron exchanges, is of the order of $8A$. This result appears reasonable since for the exchange of two electrons the particles must be in closer proximity than for the exchange of single electrons. Similar conditions prevail for collisions of a proton with a hydrogen molecule. For the exchange of two electrons between these particles $\Delta\,\epsilon$=35.5 ev (see Ref. 1), the maximum cross section is observed at 17.5 kev, which yields, according to Eq. (7), $a = 2A$. For the single electron exchange the parameter $a \sim 26A$.

It woukd be interesting, for the understanding of the processes of negative ion foramtion, to study atomic collisions with the capture of one electron by the neutral particle. There are no data on direct experimental measurements of effective cross sections σ_{0-1} for such a process, but it is possible to evaluate this cross section for hydrogen atoms in hydrogen, from the known values of other effective cross sections for collisions of protons, hydrogen atoms and negative hydrogen atoms with molecules of hydrogen.

Assuming that the effective cross section σ_{-11} for the loss of two electrons by a negative hydrogen ion through a single collision with a molecule of hydrogen for the energy range investigated by us is equal to zero, the following expression for the cross section σ_{0-1} can be obtained by making use of Eq. (4):

$$\sigma_{0-1} = \frac{[(I^- + I^+)/I^0]_p}{1 + (I^-/I^+)_p}\{[(\sigma_{-10} - \sigma_{10}) + \sigma_{10}](I^-/I^+)_p - \sigma_{1-1}\} \tag{9}$$

For the computation of σ_{0-1} we have used values of $[(I^- + I^+)/I^0]_p$, obtained in Ref. 8, values of $(I^-/I^+)_p$ and σ_{1-1} as measured in the present work, cross section σ_{10} as measured in Ref. 2. The values of σ_{10} and $(\sigma_{-10} - \sigma_{10})$, were determined by Whittier[4]. We consider the values of the difference $(\sigma_{-10} - \sigma_{10})$, as measured by Whittier more reliable since this value was determined from the tangent of the slope of a semilogarithmic dependence, (see Fig. 8 in Ref. 4) the extrapolation of which to zero pressure gives values of $(I^-/I^+)_p$ not much different from ours. On the other hand the value of σ_{10} obtained by Whittier by subtracting the value $(\sigma_{-10} - \sigma_{10})$ from σ_{-10} is roughly twice smaller than the most reliable values obtained by other authors[2,5,9], which points to a systematic error in the determination of cross section σ_{-10}. For this reason we preferred, in computing cross sections σ_{0-1}, to use Eq. (9), and the values of $(\sigma_{-10} - \sigma_{10})$ from Ref. 4.

Computations of cross section σ_{01} were also made by Whittier, who considered cross sections σ_{-11} and σ_{1-1} equal to zero. In Fig. 6 are given curves of cross section σ_{0-1} dependence on energy, computed by us (solid curve) and by Whittier (dotted curve). It is interesting to note that the magnitude of the effective cross section σ_{0-1} is only 1½ to 2 times greater than the cross section σ_{1-1}

[6] L. N. Rosenzweig and V. I. Gerasimenko, Works (Trudy) of the Phys.-Mat. Dept., Univ. of Kharkov, 6, 87 (1955).

[7] H. S. W. Massey and E. H. Burhop, *Electronic and ionic impact phenomena*, Oxford, 1952.

[8] H. Bartels, Ann. Physik 13, 373 (1932).

but is 40 to 50 times smaller than cross section σ_{10}.

There exists another possible method of computing σ_{0-1} using equation (7) which, taking $\sigma_{-11} = 0$, can be written in the form

$$\sigma_{0-1} = \{2\delta (kT/L)^2 - \sigma_{1-1}[\sigma_{1-1} - (\sigma_{-10} - \sigma_{10})]\}/\sigma_{10}. \quad (10)$$

Substituting here the value $\delta = 1.03 \times 10^3$, obtained from the curve in Fig. 1, and also the values of σ_{1-1}, σ_{10}, $(\sigma_{-10} - \sigma_{10})$ and kT/L we obtain for the energy 29 kev cross section $\sigma_{0-1} = 1.3 \times 10^{-17}$ cm^2. By computing σ_{0-1} according to Eq. (9) we obtain for this energy the value 0.8×10^{-17} cm^2. Considering the large errors in the measurements of the quantities entering into equations (9) and (10) the agreement between the values of σ_{0-1} computed by two different methods must be considered satisfactory.

In conclusion we consider it a pleasant duty to thank Prof. A. K. Val'ter for his constant interest and attention to this work and also V. Z. Surkov for his practical help in the construction and arrangement of the equipment.

Translated by J. L. Herson
88

SOVIET PHYSICS JETP VOLUME 3, NUMBER 2 SEPTEMBER, 1956

Nucleomesodynamics in Strong Coupling. II. The Ground and Isobar States, Nucleon Charge and Spin

V. N. BAIER AND S. I. PEKAR
Institute of Physics, Academy of Sciences, Ukrainian SSR

(Submitted to JETP editor July, 28, 1954)
J. Exptl. Theoret. Phys. (U.S.S.R.) 30, 317-329 (February, 1956)

A nucleon is considered that interacts strongly with a pseudoscalar meson field. The interaction is assumed to be of the symmetric pseudovector type. The eigenvalues of the energy, charge and spin of the nucleon are determined, and also the explicit form of the wave function of the system. The ground and isobar states of the system are obtained.

1. WAVE EQUATION OF THE MESON FIELD IN THE ABSENCE OF THE NUCLEON

IN a previous paper[1] (which appears in this issue of the journal and which shall be referred to later as I), an approximate method is given for the consideration of a nucleon which interacts strongly with the meson field. The Hamiltonian of the system was simplified with the aid of a series of approximations and the spin-charge part of the wave function was determined. As a result the problem of the determination of the stationary quantum states of the system reduces to finding the eigenfunction and eigenvalues of the operator

$$\hat{H} = -G + {}^1/_2 \sum_{\vec{\alpha}\varkappa} \omega_{\vec{\varkappa}} \quad [(q_{\vec{\alpha}\varkappa} - q^v_{\vec{\alpha}\varkappa})^2 - \partial^2/\partial q^2_{\vec{\alpha}\varkappa}]. \quad (1)$$

[1] S. I. Pekar, J. Exptl. Theoret. Phys.(U.S.S.R.) 30, 304 (1956); Soviet Phys. JETP 3, No. 3 (October, 1956).

Here, all the symbols of paper I have been retained. An operator similar to (1) has already been met in earlier works [see Ref. 2, p. 99, and Ref. 3, Sec. 3] and, as was shown therein, the eigenfunctions of this operator must be sought in the form

$$\Phi(q) = V(\vartheta, \beta; \delta) \exp\left\{-\frac{1}{2}\sum_{\alpha\varkappa}\left[(q_{\vec{\alpha\varkappa}} - q^{v}_{\vec{\alpha\varkappa}})^2 + \frac{1}{2}\ln\pi\right]\right\}\prod_{l=1}^{N} q_l \cdot 2^{N/2}. \quad (2)$$

Here q_i is one of the coordinates $q_{\vec{\alpha\varkappa}}$.

The arguments $q_{\vec{\alpha\varkappa}}$ enter directly into Φ, and, moreover, are contained in $v_i(q)$. Let $\partial/\partial^* q_{\vec{\alpha\varkappa}}$ denote differentiation only with respect to the $q_{\vec{\alpha\varkappa}}$ which do not enter into the argument of v_i. Then

$$\frac{\partial}{\partial q_{\vec{\alpha\varkappa}}} = \frac{\partial}{\partial^* q_{\vec{\alpha\varkappa}}} + \sum_{i=1}^{3}\frac{\partial v_i}{\partial q_{\vec{\alpha\varkappa}}}\frac{\partial}{\partial v_i}, \quad (3)$$

$$\sum_{\vec{\alpha\varkappa}}\omega_{\vec{\varkappa}}\frac{\partial^2}{\partial q^2_{\vec{\alpha\varkappa}}} = \sum_{\vec{\alpha\varkappa}}\omega_{\vec{\varkappa}}\frac{\partial^2}{\partial^* q^2_{\vec{\alpha\varkappa}}} + \sum_{\vec{\alpha\varkappa}ij}\omega_{\vec{\varkappa}}\frac{\partial v_i}{\partial q_{\vec{\alpha\varkappa}}}\frac{\partial v_j}{\partial q_{\vec{\alpha\varkappa}}}\frac{\partial^2}{\partial v_i\,\partial v_j}$$
$$+ \sum_{\vec{\alpha\varkappa}ij}\omega_{\vec{\varkappa}}\frac{\partial v_j}{\partial q_{\vec{\alpha\varkappa}}}\left(\frac{\partial}{\partial v_j}\frac{\partial v_i}{\partial q_{\vec{\alpha\varkappa}}}\right)\frac{\partial}{\partial v_i} + 2\sum_{i\vec{\alpha\varkappa}}\omega_{\vec{\varkappa}}\frac{\partial v_i}{\partial q_{\vec{\alpha\varkappa}}}\frac{\partial^2}{\partial v_i\partial^* q_{\vec{\alpha\varkappa}}}. \quad (4)$$

Taking into account Eqs. (59), (64), (67)-(69) of I we obtain

$$\sum_{\vec{\alpha\varkappa}ij}\omega_{\vec{\varkappa}}\frac{\partial v_j}{\partial q_{\vec{\alpha\varkappa}}}\left(\frac{\partial}{\partial v_j}\frac{\partial v_i}{\partial q_{\vec{\alpha\varkappa}}}\right)\frac{\partial}{\partial v_i} = \frac{I^{(2n)}}{(I^{(n)})^2}\operatorname{ctg}\delta\cdot\frac{\partial}{\partial\delta}, \quad (5)$$

$$\sum_{\vec{\alpha\varkappa}ij}\omega_{\vec{\varkappa}}\frac{\partial v_i}{\partial q_{\vec{\alpha\varkappa}}}\frac{\partial v_j}{\partial q_{\vec{\alpha\varkappa}}}\frac{\partial^2}{\partial v_i\,\partial v_j} = \frac{I^{(2n)}}{(I^{(n)})^2}\left[\frac{1}{\sin^2\delta}\left(\frac{\partial^2}{\partial\vartheta^2} + \frac{\partial^2}{\partial\beta^2} + 2\cos\delta\frac{\partial^2}{\partial\vartheta\,\partial\beta}\right) + \frac{\partial^2}{\partial\delta^2}\right] \quad (6)$$

It must be kept in mind that even in the development of Eqs. (67)-(69) in I, it was assumed that $\varphi_\alpha(\mathbf{r})$ differed slightly from $\varphi^v_\alpha(\mathbf{r})$; therefore if the function under the integral contained the factor φ_α and was significant only in the local region where φ^v_α differed appreciably from zero, then φ_α could be replaced by φ^v_α under the integral. On this this basis, we can neglect terms of the form

$$\sum_{\vec{\alpha\varkappa}}\left(q_{\vec{\alpha\varkappa}} - q^v_{\vec{\alpha\varkappa}}\right)\frac{\partial q^v_{\vec{\alpha\varkappa}}}{\partial v_i};\quad \sum_{\vec{\alpha\varkappa}}\left(q_{\vec{\alpha\varkappa}} - q^v_{\vec{\alpha\varkappa}}\right)\frac{\partial^2 q^v_{\vec{\alpha\varkappa}}}{\partial v_i\,\partial v_j} \quad (7)$$

in the calculation of the derivatives of Φ with respect to v_i and $q_{\vec{\alpha\varkappa}}$. We then have

$$\frac{\partial\Phi}{\partial v_i} = \frac{\partial V}{\partial v_i}e^{-s}\prod_{l=1}^{N} q_l\cdot 2^{N/2}, \quad (8)$$

$$s = \frac{1}{2}\sum_{\vec{\alpha\varkappa}}\left[\left(q_{\vec{\alpha\varkappa}} - q^v_{\vec{\alpha\varkappa}}\right)^2 + \frac{1}{2}\ln\pi\right], \quad (9)$$

$$\frac{\partial^2\Phi}{\partial v_i\,\partial v_j} = \frac{\partial^2 V}{\partial v_i\,\partial v_j}e^{-s}\prod_{l=1}^{N} q_l 2^{N/2} - R^{(1)}_{ij}\Phi, \quad (10)$$

$$\frac{\partial^2\Phi}{\partial v_i\,\partial^* q_{\vec{\alpha\varkappa}}} = -\frac{\partial V}{\partial v_i}\left(q_{\vec{\alpha\varkappa}} - q^v_{\vec{\alpha\varkappa}}\right)e^{-s}\prod_{l=1}^{N} q_l\cdot 2^{N/2} + \frac{\partial q^v_{\vec{\alpha\varkappa}}}{\partial v_i}\Phi + \frac{\partial V}{\partial v_i}e^{-s}\Pi^{\vec{\alpha\varkappa}}, \quad (11)$$

$$\Pi^{\vec{\alpha\varkappa}} \equiv \frac{\partial}{\partial q_{\vec{\alpha\varkappa}}}\prod_{l=1}^{N} q_l\cdot 2^{N/2}.$$

Taking into account Eqs. (4)-(6) and also Eqs. (59) and (64) of I, the effect of operator (1) on Φ can

[2] S. I. Pekar, *Investigations on the Electron Theory of Crystals*, Gostekhizdat, 1951.

[3] S. I. Pekar, J.Exptl.Theoret. Phys .(U.S.S.R.) 27, 411 (1954).

be put in the following form:

$$\hat{H}\Phi = \Big\{ -G + \frac{3}{2}\sum_{\vec{\varkappa}} \omega_{\vec{\varkappa}} + \sum_{l=1}^{N} \omega_l - 3\frac{I^{(n+1)}}{I^{(n)}} + \frac{3}{2}\frac{I^{(1)}I^{(2n)}}{(I^{(n)})^2} \Big\}\Phi + (\hat{\mathcal{H}}V)\, e^{-s}\prod_{l=1}^{N} q_l 2^{N/2} + \hat{H}_1\Phi, \tag{12}$$

where

$$\hat{\mathcal{H}} = -\frac{1}{2}\frac{I^{(2n)}}{(I^{(n)})^2}\Big[\frac{1}{\sin^2\delta}\Big(\frac{\partial^2}{\partial\vartheta^2} + \frac{\partial^2}{\partial\beta^2} + 2\cos\delta\frac{\partial^2}{\partial\vartheta\,\partial\beta}\Big) + \frac{\partial^2}{\partial\delta^2} + \operatorname{ctg}\delta\frac{\partial}{\partial\delta}\Big], \tag{13}$$

$$\hat{H}_1\Phi \equiv -\sum_{\vec{\alpha}\vec{\varkappa} i} \omega_{\vec{\varkappa}} \frac{\partial V}{\partial v_i}\frac{\partial v_i}{\partial q_{\vec{\alpha}\vec{\varkappa}}}\, e^{-s}\Pi^{\vec{\alpha}\vec{\varkappa}}. \tag{14}$$

The wave function (2) corresponds to a state of the system in which all the oscillators of the meson field are in the ground state, with the exception of N oscillators which are in singly excited states. In Eq. (12), the term $^3/_2 \sum_{\vec{\varkappa}} \omega_{\vec{\varkappa}}$ represents the energy of the zero point vibrations of all the oscillators and the term $\sum_{l=l}^{N} \omega_l$ the energy of the single excitations of the N oscillators. Physically, this means that there are N free mesons in addition to the nucleon.

In the case of the absence of free mesons, $N = 0$, $\hat{H}_1\Phi = 0$, and if $V(v_i)$ is so chosen that it satisfies the equation

$$\hat{\mathcal{H}}V = \mathcal{H}V, \tag{15}$$

then Φ is an eigenfunction of the operator (1), as is seen from Eq. (12):

$$\hat{H}\Phi = H\Phi. \tag{16}$$

The eigenvalue of the energy of the system is

$$H = -G + \frac{3}{2}\sum_{\vec{\varkappa}} \omega_{\vec{\varkappa}} - 3\frac{I^{(n+1)}}{I^{(n)}} + \frac{3}{2}\frac{I^{(1)}I^{(2n)}}{(I^{(n)})^2} + \mathcal{H}. \tag{17}$$

In the absence of free mesons, Φ does not describe the stationary state of the system. The term $\hat{H}_1\Phi$ determines the scattering of the mesons on the nucleon. This scattering will be considered in a subsequent paper; here we shall limit ourselves to the case of the absence of free mesons ($N = 0$).

2. DETERMINATION OF THE ANGULAR PART OF THE WAVE FUNCTION

We now find the eigenfunctions and the eigenvalues of Eq. (15). Inasmuch as the variables θ and β do not enter explicitly into the operator (13), its eigenfunctions must, as is known, depend on these variables exponentially; therefore we must seek the solution of Eq. (15) in the form

$$V = D(\delta)\, e^{i(s\vartheta + p\beta)}. \tag{18}$$

Substituting (18) in (15) we get an equation for the function $D(\delta)$:

$$\frac{d^2D}{d\delta^2} + \operatorname{ctg}\delta\frac{dD}{d\delta} - \frac{1}{\sin^2\delta}(s^2 + p^2 + 2sp\cos\delta)\,D = -\lambda D, \tag{19}$$

$$\lambda I^{(2n)}/2\,(I^{(n)})^2 = \mathcal{H}.$$

If Eq. (52) or (53) of I is written in explicit form, then it is evident that they are trigonometric equations relative to the angles ϑ, β and δ. The roots of these equations, ϑ and β, for each given configuration of the meson field q are determined only with accuracy to shifts of multiples of 2π. If the given configurations of the meson field q correspond to values of the angles ϑ and β, then these configurations will also correspond to the angles $\vartheta + 2\pi$ and $\beta + 2\pi$. Usually, the requirement in quantum mechanics that the wave function of the whole system be a single valued function of the configuration q leads to the requirement that this function possess a periodicity of 2π in the arguments ϑ and β. Inasmuch as ψ^ν changes sign upon change of ϑ or β by 2π (see Eq. 35, Ref. 1), then, according to Eq. (9)[1], Φ must also change sign. Therefore, the quantum numbers s and p in Eq. (18) must be half integers. The eigenfunctions and the eigenvalues of Eq. (19) will be found by the method of factorization (Ref. 4, part 4). Substitution of

$$Y(\delta) = \sin^{1/2}\delta\, D(\delta) \tag{20}$$

in Eq. (19) leads to the standard form suitable for factorization:

[4] L. Infeld and E. Hull, Revs. Mod. Phys. **23**, 21 (1951); Sec. 4.

$$\frac{d^2Y}{d\delta^2} - \frac{1}{\sin^2\delta}\Big(s^2 + p^2 + 2sp\cos\delta - \frac{1}{4}\Big)Y + \Big(\lambda + \frac{1}{4}\Big)Y = 0. \tag{21}$$

The integral index m, according to which factorization is carried out,[4] is connected with the quantum numbers by the relations

$$1)\ m = s - {}^1/_2 \ \text{ for } \ s \geqslant {}^1/_2, \tag{22}$$

$$2)\ m = {}^1/_2 - s \ \text{ for } \ s < {}^1/_2.$$

In the first case the factorization is carried out by the usual method, with the use of the recurrence form (2.6, Ib) of Ref. 4. In the second case, we take as the initial eigenfunction the function found by the first method with quantum number $s = 1/2$; we then apply the recurrence relation (2.6, Ia) of Ref. 4.

As a result, the eigenvalues λ in the equation (19) are given by

$$\lambda_j = j(j+1), \quad j = {}^1/_2,\ {}^3/_2,\ {}^5/_2,\ {}^7/_2 \ldots \tag{23}$$

For the eigenfunctions of Eq. (21) we get the recurrence relation

$$Y^j_{s-1,\,p} = \Big[\Big(j + \frac{1}{2}\Big)^2 - \Big(s - \frac{1}{2}\Big)^2\Big]^{-1/2} \times \Big[\Big(s - \frac{1}{2}\Big)\operatorname{ctg}\delta + \frac{p}{\sin\delta} + \frac{d}{d\delta}\Big] Y^j_{s,\,p}. \tag{24}$$

The latter enables us to get the totality of eigenfunctions from the initial function

$$Y^j_{j,\,p} = \Big[\frac{\Gamma(2j+2)}{\Gamma(j+p+1)\,\Gamma(j-p+1)}\Big]^{1/2} \times \sin^{j+p+1/2}\frac{\delta}{2}\cos^{j-p+1/2}\frac{\delta}{2}. \tag{25}$$

We can obtain completely analogous recurrence relations with respect to the index p, inasmuch as s and p appear symmetrically in Eq. (21). The half integer quantum numbers s and p change in the following way

$$|s| \leqslant j, \quad |p| \leqslant j. \tag{26}$$

In the ground state

$$j = \frac{1}{2}, \quad \mathscr{H}_{1/2} = \frac{\lambda_{1/2}}{2}\frac{I^{(2n)}}{(I^{(n)})^2} = \frac{3}{8}\frac{I^{(2n)}}{(I^{(n)})^2} \tag{27}$$

there exist 4 eigenfunctions of Eq. (15),

$$V^1_{1,1} = \frac{1}{2\pi}\sin\frac{\delta}{2}e^{i(\vartheta+\beta)/2},$$

$$V^1_{1,-1} = \frac{1}{2\pi}\cos\frac{\delta}{2}e^{i(\vartheta-\beta)/2}; \tag{28}$$

$$V^1_{-1,1} = \frac{1}{2\pi}\cos\frac{\delta}{2}e^{i(\beta-\vartheta)/2},$$

$$V^1_{-1,-1} = -\frac{1}{2\pi}\sin\frac{\delta}{2}e^{-i(\vartheta+\beta)/2}.$$

Here and later we shall write, for brevity, the double of the quantum numbers s, p and j: $V^{2j}_{2s,\,2p}$.

In the first excited state,

$$j = {}^3/_2, \quad \mathscr{H}_{3/2} = 15\,I^{(2n)}/8\,(I^{(n)})^2 \tag{29}$$

there are 16 eigenfunctions:

$$\begin{aligned}
V^3_{3,3} &= -V^{3*}_{-3,-3} = \frac{\sqrt{2}}{2\pi}\sin^3\frac{\delta}{2}e^{i(3\vartheta+3\beta)/2};\\
V^3_{1,3} &= V^{3*}_{-1,-3} = \frac{\sqrt{6}}{2\pi}\sin^2\frac{\delta}{2}\cos\frac{\delta}{2}e^{i(\vartheta+3\beta)/2};\\
V^3_{-1,3} &= -V^{3*}_{1,-3} = \frac{\sqrt{6}}{2\pi}\sin\frac{\delta}{2}\cos^2\frac{\delta}{2}e^{i(-\vartheta+3\beta)/2};\\
V^3_{-3,3} &= V^{3*}_{3,-3} = \frac{\sqrt{2}}{2\pi}\cos^3\frac{\delta}{2}e^{i(-3\vartheta+3\beta)/2};\\
V^3_{3,1} &= V^{3*}_{-3,-1} = \frac{\sqrt{6}}{2\pi}\sin^2\frac{\delta}{2}\cos\frac{\delta}{2}e^{i(3\vartheta+\beta)/2};\\
V^3_{1,1} &= -V^{3*}_{-1,-1} = \frac{\sqrt{2}}{2\pi}\sin\frac{\delta}{2}\Big(3\cos^3\frac{\delta}{2} - 1\Big)e^{i(\vartheta+\beta)/2};\\
V^3_{-1,1} &= V^{3*}_{1,-1} = \frac{\sqrt{2}}{2\pi}\cos\frac{\delta}{2}\Big(1 - 3\sin^2\frac{\delta}{2}\Big)e^{i(-\vartheta+\beta)/2};\\
V^3_{-3,1} &= -V^{3*}_{3,-1} = -\frac{\sqrt{6}}{2\pi}\sin\frac{\delta}{2}\cos^2\frac{\delta}{2}e^{i(-3\vartheta+\beta)/2}.
\end{aligned} \tag{30}$$

For a given j, each of the quantum numbers s and p, being limited by the inequalities (26) have $2j+1$ values; therefore the multiplicity of the degeneracy of the level $\mathcal{H}_j$ will be $(2j+1)^2$.

Thus, in a system which consists of a nucleon that interacts strongly with the meson field, three types of excitation are possible:

1. Excitation of the spin-charge motion, with transition from a state defined by Eq. (28) of I. These excited states are evidently always unstable; they will not be considered in this paper.

2. Excitation of the oscillators of the meson field, i.e., creation of free mesons. The energy of such excitation is given by the term $\sum_{l=1}^{N} \omega_l$ of Eq. (17).

3. Excitation of rotational motion, described by Eqs. (15) and (13). The energy of this motion, in accordance with Eqs. (19) and (23), is given by the equation

$$\mathcal{H}_j = \frac{1}{2}\frac{I^{(2)}}{(I^{(1)})^2} j(j+1). \tag{31}$$

The wave equation of this motion coincides in form with the equation of motion of a symmetric rotator. However, in the latter case, s, p, and j are integers, while in Eqs. (18), (19) and (31) they are half integers. Such states, excited in the quantum number j, are appropriately called isobars.

Comparison of the energy (17) with the corresponding energies calculated by Pauli and Dancoff [see Ref. 5, Eq. (76)], shows that the term G, proportional to g^2, agrees exactly with the corresponding term of Pauli and Dancoff (in the comparison it should be noted that our g is equal to $2^{-1/2}g$ in Ref. 5). The energy of excitation of the isobars of $\mathcal{H}_j$, determined by Eq. (31), agrees exactly with Eq. (80) of Ref. 5, if we set $n=0$, i.e., if the parameters $v_i(q)$ are chosen by approximating φ_α by the functions φ_α^v by the method of least squares (see Ref. 1, Sec. 5). In obtaining Eq. (76) of Ref. 5, Pauli and Dancoff evidently made an approximation. Without this approximation in their work, the energy of excitation of the isobars would have been obtained that would have agreed with that obtained by us in the case $n=2$, i.e., in the case of most accurate energy approximation. Comparison of the remaining terms of the energy (17) is difficult, since they are not explicitly calculated in Ref. 5.

Equations (17) and (31) determine the energy of the system only in the zero approximation. Below we have also calculated the corrections to the energy in higher approximations.

[5] W. Pauli and S. M. Dancoff, Phys. Rev. 62, 85 (1942).

3. THE BASIS OF THE ADIABATIC APPROXIMATION AND ACCOUNT OF NONADIABATICITY

It was assumed in I that the spin-charge motion took place adiabatically because of the comparatively slow vibrations of the meson field. We shall now consider nonadiabaticity as a small perturbation and criteria will also be given for the adiabatic approximation.

We begin with the exact wave equation

$$\hat{H}\Psi \equiv (\hat{H}_0 + \hat{H}')\Psi = H\Psi. \tag{32}$$

We now introduce a complete set of orthogonal functions $\psi_s(q)$, which satisfy the equation

$$\hat{H}'(q)\psi_s(q) = H_s'(q)\psi_s(q), \quad \psi_s = \begin{vmatrix} C_{1s} \\ C_{2s} \\ C_{3s} \\ C_{4s} \end{vmatrix}, \tag{33}$$

in which the q appear as parameters. We expand the wave function of the system in the orthogonal functions $\psi_s(q)$:

$$\Psi(q) = \sum_{s=1}^{4} \Phi_s(q)\psi_s(q). \tag{34}$$

Substitution of this expansion in Eq. (32) leads to the following equations for the expansion coefficients $\Phi_s(q)$:

$$[\hat{H}_0 + H_s'(q)]\Phi_s - \sum_{s'\alpha\vec{\varkappa}} \omega_{\vec{\varkappa}} \left\{\psi_s^*, \frac{\partial\psi_{s'}}{\partial q_{\alpha\vec{\varkappa}}}\right\} \frac{\partial\Phi_{s'}}{\partial q_{\alpha\vec{\varkappa}}} \tag{35}$$

$$-\frac{1}{2}\sum_{s'\alpha\vec{\varkappa}} \omega_{\vec{\varkappa}} \left\{\psi_s^*, \frac{\partial^2\psi_{s'}}{\partial q^2_{\alpha\vec{\varkappa}}}\right\}\Phi_{s'} = H\Phi_s; \quad s = 1, 2, 3, 4.$$

The second and third terms of the left hand side represent the nonadiabatic perturbation. In order to be able to use standard perturbation theory, we must put the system of equations (35) into form of the usual operator equation. For this purpose, we introduce the four vector $\Phi(q)$, whose components are the $\Phi_s(q)$. Furthermore, we introduce the matrices

$$A_{ss'}^{\alpha\vec{\varkappa}}(q) = -\omega_{\vec{\varkappa}} \left\{\psi_s^*, \frac{\partial\psi_{s'}}{\partial q_{\alpha\vec{\varkappa}}}\right\}; \tag{36}$$

$$B_{ss'} = -\frac{1}{2}\sum_{\alpha\vec{\varkappa}} \omega_{\vec{\varkappa}} \left\{\psi_s^*, \frac{\partial^2\psi_{s'}}{\partial q^2_{\alpha\vec{\varkappa}}}\right\};$$

$$O_{ss'} = H_s'(q)\delta_{ss'}.$$

Then we can write the system of equations (35) in the form of a single vector equation of the operator type:

$$\left[\hat{H}_0 + O(q) + \sum_{\vec{\alpha\varkappa}} A^{\vec{\alpha\varkappa}} \frac{\partial}{\partial q_{\vec{\alpha\varkappa}}} + B\right]\Phi = H\Phi. \tag{37}$$

Here $O\Phi$, $A^{\vec{\alpha\varkappa}}\,\partial\Phi/\partial q_{\vec{\alpha\varkappa}}$ and $B\Phi$ are to be understood as the usual multiplications of matrices and vectors.

The nonadiabatic perturbation

$$\hat{\Omega} = \hat{M} + \hat{B},\ \hat{M} \equiv \sum_{\vec{\alpha\varkappa}} A^{\vec{\alpha\varkappa}}\,\partial/\partial q_{\vec{\alpha\varkappa}} \tag{38}$$

is omitted in zeroth approximation. Then the vector equation (37) breaks up into a series of independent equations for the different components of the vector Φ; these equations have the form:

$$[\hat{H}_0 + H_s'(q)]\,\Phi_s = H\Phi_s. \tag{39}$$

Since, in the different equations (39) (with different s), there enter different functions $H_s'(q)$, the spectra of the eigenvalues for these equations will in general be different. Therefore, the entire series of equations (39) can be satisfied only by such a vector Φ for which all the components are different from zero except the single component Φ_s; the latter must satisfy the corresponding Eq. (39). If we number the solutions of Eq. (39) by the quantum number m in the order of increasing H, then the solutions of the zeroth approximation will be denoted by Φ_{sm} and H_{sm}, where s is the number of the only component of the vector Φ different from zero.

In the zeroth approximation in the decomposition (34), there is only one term. Consequently, we can consider that the nucleon is found in the state $\psi_s(q)$, defined by Eq. (33), and possesses the energy $H'_s(q)$. In this case the index s takes on the sense of a quantum number of the nucleon.

The zeroth approximation described above coincides exactly with the adiabatic approximation used in the previous research (Eq. (11) of I). We now introduce the previously discarded terms $\hat{\Omega}$ as a small perturbation and compute the correction of the next order. In this case, we can replace ψ_s by ψ_s^v [see Eqs. (33) and (42) of I], inasmuch as (in addition to the adiabatic approximation) it has also been assumed that $\varphi_\alpha(\mathbf{r})$ differs only slightly from $\varphi_\alpha^v(\mathbf{r})$. With the help of Eq. (29) of I, we get

$$A_{11}^{\vec{\alpha\varkappa}} = -\omega_{\vec{\varkappa}} \frac{\partial}{\partial q_{\vec{\alpha\varkappa}}}[\,|c_1|^2 + |c_2|^2] = 0. \tag{40}$$

In accordance with Eqs. (4)-(6) and (13), the operator $-\frac{1}{2}\sum_{\vec{\alpha\varkappa}} \omega_{\vec{\varkappa}} \frac{\partial^2}{\partial q^2_{\vec{\alpha\varkappa}}}$ in application to the function of v_i is equivalent to the operator $\hat{\mathfrak{N}}$. Further, we can represent the function ψ_1^v in the form

$$\psi_1^v = \frac{\pi}{\sqrt{2}} \begin{vmatrix} iV_{11}^1 + V_{1,-1}^1 + V_{-1,1}^1 - iV_{-1,-1}^1 \\ -V_{11}^1 + iV_{1-1}^1 - iV_{-1,1}^1 - V_{-1,-1}^1 \\ -V_{11}^1 - iV_{1,-1}^1 + iV_{-1,1}^1 - V_{-1,1}^1 \\ -iV_{11}^1 + V_{1,-1}^1 + V_{-1,1}^1 + iV_{-1,1}^1 \end{vmatrix} \tag{41}$$

It is evident from this that each of the four components ψ_1^v is an eigenfunction of $\hat{\mathfrak{N}}$ and corresponds to the eigenvalue

$$\mathscr{H}_{1/2} = \frac{3}{8}\frac{I^{(2n)}}{(I^{(n)})^2}.$$

Therefore

$$B_{11} = +\{\psi_1^{v*},\ \hat{\mathscr{H}}\,\psi_1^v\} = \frac{3}{8}\frac{I^{(2n)}}{(I^{(n)})^2}. \tag{42}$$

Taking into account Eqs. (49) and (42), we find the correction due to nonadiabaticity of first order in the energy to be

$$\Delta_1 H = \int \Phi_{1,m}^* \hat{\Omega}\Phi_{1,m}\,dq\,dv = \frac{3}{8}\frac{I^{(2n)}}{(I^{(n)})^2}; \tag{43}$$

$$dv = \sin\delta\,d\vartheta\,d\beta\,d\delta.$$

It must be emphasized that the correction to the energy (43) is the same for all states of the system which are not excited by the spin-charge motion. Consequently, this correction does not change the energy of excitation of the isobar states and free mesons.

Here it should be clear why the integration in Eq. (43) was carried out over the variables $q_{\alpha\vec{\varkappa}}$ and also over v_i, in spite of the fact that v_i and $q_{\alpha\vec{\varkappa}}$ are not independent variables. In Eq. (37), only the variables $q_{\alpha\vec{\varkappa}}$ appear at first. Expressing $A_{ss'}^{\vec{\alpha\varkappa}}$ and $B_{ss'}$ in Eq. (36) by ψ_s^v, and also representing Φ in the form of Eq. (2), we introduce into Eq. (43) the arguments v_i which are definite functions of $q_{\alpha\vec{\varkappa}}$ (see Sec. 5 of I). Simultaneously, differentiation with respect to $q_{\alpha\vec{\varkappa}}$ leads to the form (3) and the operator $\hat{H}$ takes the form (12), (13). For this reason, Eq. (43) must be treated as a more general problem in which the variables v_i and $q_{\alpha\vec{\varkappa}}$ are considered as independent. If, in the solution

of this generalized problem, we replace v_i by the above mentioned functions $v_i(q)$, then we obtain the solution of the original equation (43). Because of technical advantages, we introduce the nonadiabatic perturbation at that stage of the calculation when v_i and $q_{\alpha\vec{\varkappa}}$ are considered as independent variables. In connection with this, the eigenfunctions obtained above for the unperturbed problem are orthonormal for integration over $dvdq$; therefore, we can integrate in Eq. (43) over $dvdq$, considering v_i and $q_{\alpha\vec{\varkappa}}$ to be independent.

For a calculation of the correction to the energy of second order of smallness, we must consider the perturbation $\hat{M}$ in Eq. (38) and ignore $\hat{B}$, since, in the adiabatic approximation, as is well known, $\hat{B}$ is a quantity of second order of smallness in comparison with $\hat{M}$. The perturbation operator has the form:

$$\hat{M}_{1s} = \sum_{\alpha\vec{\varkappa}} A_{1s}^{\alpha\vec{\varkappa}} \frac{\partial}{\partial q_{\alpha\vec{\varkappa}}} \tag{44}$$

$$= -\sum_{ij=1}^{3} Q_{ij}^{(1)} \left\{\psi_1^{*v}, \frac{\partial\psi_s^v}{\partial v_i}\right\} \frac{\partial}{\partial v_j}$$

$$-\sum_{i\alpha\vec{\varkappa}} \omega_{\vec{\varkappa}} \left\{\psi_1^{*v}, \frac{\partial\psi_s^v}{\partial v_i}\right\} \frac{\partial v_i}{\partial q_{\alpha\vec{\varkappa}}} \frac{\partial}{\partial^* q_{\alpha\vec{\varkappa}}},$$

where

$$Q_{ij}^{(\nu)} = \sum_{\alpha\vec{\varkappa}} \omega_{\vec{\varkappa}}^{\nu} \frac{\partial v_i}{\partial q_{\alpha\vec{\varkappa}}} \frac{\partial v_j}{\partial q_{\alpha\vec{\varkappa}}}. \tag{45}$$

With the help of Eqs. (67)-(69), (59) and (64) of Ref. 1, we obtain

$$Q_{11}^{(\nu)} = Q_{22}^{(\nu)} = \frac{I^{(2n+\nu-1)}}{(I^{(n)})^2 \sin^2\delta}, \quad Q_{33}^{(\nu)} = \frac{I^{(2n+\nu-1)}}{(I^{(n)})^2}; \tag{46}$$

$$Q_{12}^{(\nu)} = Q_{21}^{(\nu)} = \frac{I^{(2n+\nu-1)}\cos\delta}{(I^{(n)})^2 \sin^2\delta},$$

$$Q_{13}^{(\nu)} = Q_{31}^{(\nu)} = Q_{23}^{(\nu)} = Q_{32}^{(\nu)} = 0.$$

In (44) there appear the eigenfunctions of Eq. (40) of I—ψ_s^v, which represent the perturbed spin-charge state of the nucleon in the fixed selfconsistent field configuration of the meson field $q_{\alpha\vec{\varkappa}}^v$ in the ground state. These ψ_s^v are put in the following form, with the aid of Eqs. (32)-(33), (42) of I:

$$\psi_2^v = \| T \| \cdot \| S \| \psi_2^0 e^{-i\gamma}, \tag{47}$$

$$\psi_3^v = \| T \| \cdot \| S \| \psi_3^0 e^{i\gamma},$$

$$\psi_4^v = \| T \| \cdot \| S \| \psi_4^0$$

Here we have multiplied ψ_s^v on the right by an arbitrary factor of modulus unity. This factor ($e^{\pm i\gamma}$) does not depend on the spin-charge degrees of freedom. As a result, the ψ_s^v are functions not of the four angles ϑ, φ β, γ, but of only three angles ϑ, β, δ. Making use of Eq. (47), and taking the orthonormality of the φ_s^v into account, we obtain:

$$\left\{\psi_1^{v*}, \frac{\partial\psi_2^v}{\partial\vartheta}\right\} = \frac{1}{2\sqrt{2}} e^{-i\delta}, \qquad \left\{\psi_1^{v*}, \frac{\partial\psi_3^v}{\partial\vartheta}\right\} = -\frac{1}{2\sqrt{2}} e^{i\delta};$$

$$\left\{\psi_1^{v*}, \frac{\partial\psi_3^v}{\partial\beta}\right\} = -\left\{\psi_1^{v*}, \frac{\partial\psi_2^v}{\partial\beta}\right\} = \frac{1}{2\sqrt{2}} \left\{\psi_1^{v*}, \frac{\partial\psi_4^v}{\partial\delta}\right\} = -\frac{i}{2} \tag{48}$$

$$\left\{\psi_1^{v*}, \frac{\partial\psi_4^v}{\partial\vartheta}\right\} = \left\{\psi_1^{v*}, \frac{\partial\psi_4^v}{\partial\beta}\right\} = \left\{\psi_1^{v*}, \frac{\partial\psi_2^v}{\partial\delta}\right\} = \left\{\psi_1^{v*}, \frac{\partial\psi_3^v}{\partial\delta}\right\} = 0.$$

In going on to the calculation of the second order energy correction, defined by the perturbation M, it should be noted that the perturbed ground state of the system is fourfold degenerate [see Eq. (28)], but the matrix elements of all transitions between these degenerate states are equal to zero, inasmuch as $A_{11}^{\alpha\vec{\varkappa}} = 0$. In this case the second order correction to the energy is determined by setting the determinant equal to zero:[6]

$$\left| \sum_{s,m_1}{}' \frac{(1m \mid M \mid sm_1)(sm_1 \mid \hat{M} \mid 1\hat{m}')}{H_{1m} - H_{sm_1}} - \Delta_2 H \delta_{mm'} \right| = 0. \tag{49}$$

Here the energy difference which appears in the denominator is basically the energy of excitation of spin-charge motion, and is approximately equal to $-(2/3)G$. Carrying out the averaging of the energy difference before the summation sign, we can treat the sum as a matrix element of $\hat{M}^2$ $[(1m \mid \hat{M} \mid 1m) = 0]$. It is equal to

[6] L. D. Landau and E. M. Lifshitz, *Quantum Mechanics*, Gostekhizdat, 1948, p. 165.

$$(1m\,|\,\hat{M}^2\,|\,1m') = \delta_{mm'}\left\{\frac{3}{16}\left[\frac{I^{(2n)}}{(I^{(n)})^2}\right]^2 + \frac{3}{4}I^{(1)}\left[\frac{I^{(2n)}}{(I^{(n)})^2}\right]^2 + \frac{3}{8}\frac{I^{(2n+1)}}{(I^{(n)})^2}\right\}. \tag{50}$$

Here Φ_{1m} and $\Phi_{1m'}$ are two degenerate states of the ground level of the system.

The determinant (49) is diagonal. Inasmuch as the matrix elements (50) do not depend on m, the same correction to the energy is obtained in all degenerate states of the ground level of the system, namely

$$\Delta_2 H = -3\,(1m\,|\,\hat{M}^2\,|\,1m)/2G. \tag{51}$$

The nonadiabaticity can be considered as a small perturbation if $\Delta_2 H$ is significantly less than the difference G between the levels of the unperturbed problem:

$$(1m\,|\,\hat{M}^2\,|\,1m)/G^2 \ll 1. \tag{52}$$

This same inequality guarantees the smallness of the energy correction of first order $\Delta_1 H$ [see (43)] in comparison with G. If we assume a simple and monotonic path of the form factor $u(r)$ and characterize its effective radius by $a(\mu a \lessapprox 1)$, then the inequality (52) means

$$g/\mu a \gg 1. \tag{53}$$

In completely analogous fashion, as was done in Ref. 7, it can be shown that the use in Ref. 1 of an assumption on the smallness of $\varphi'_\alpha(\mathbf{r})$ in comparison with $\varphi^v_\alpha(\mathbf{r})$ is correct for satisfaction of the inequality (53).

4. SPIN AND ISOTOPIC SPIN OF A SYSTEM

The momentum operator of a system

$$L_{ik} = -\sum_{\alpha=1}^{3}\int\left[x_i\frac{\partial\varphi_\alpha}{\partial x_k} - x_k\frac{\partial\varphi_\alpha}{\partial x_i}\right]\pi_\alpha dV + \frac{1}{2}\sigma_{ik};\quad \sigma_{12} = \sigma_3 \ldots \tag{54}$$

commutes with the energy operator of the system, i.e., the momentum is an integral of motion. With the help of Eq. 1[1], and also (3), we obtain

$$\begin{aligned} L_{ik} &= L^q_{ik} + L^v_{ik} + \frac{1}{2}\sigma_{ik};\\ L^q_{ik} &= i\sum_{\alpha\vec{\varkappa}}\int\left[x_i\frac{\partial\varphi_\alpha}{\partial x_k} - x_k\frac{\partial\varphi_\alpha}{\partial x_i}\right]\chi_{\vec{\varkappa}}(\mathbf{r})\,dV\sqrt{\omega_{\vec{\varkappa}}}\,\frac{\partial}{\partial^* q_{\alpha\vec{\varkappa}}};\\ L^v_{ik} &= i\sum_{\alpha\vec{\varkappa}}\int\left[x_i\frac{\partial\varphi_\alpha}{\partial x_k} - x_k\frac{\partial\varphi_\alpha}{\partial x_i}\right]\chi_{\vec{\varkappa}}(\mathbf{r})\,dV\sqrt{\omega_{\vec{\varkappa}}}\sum_{j=1}^{3}\frac{\partial v_j}{\partial q_{\alpha\vec{\varkappa}}}\frac{\partial}{\partial v_j}. \end{aligned} \tag{55}$$

In the calculation of L^v_{ik} the expressions $\partial v_j/\partial q_{\alpha\vec{\varkappa}}$ are put in the form of Eqs. (67)-(69)[1], and as a result of the use of Eq. (1), expressions are obtained which contain integrals of the form

$$\int\left[x_i\frac{\partial\varphi_\alpha}{\partial x_k} - x_k\frac{\partial\varphi_\alpha}{\partial x_i}\right]\hat{\omega}^n\frac{\partial\varphi^v_\alpha}{\partial v_j}\,dV. \tag{56}$$

In the calculation of these integrals, φ_α is replaced by φ^v_α. For the latter, the expressions (60) and (38) are used[1]. It is convenient to express the operator $x_i\,\partial/\partial x_k - x_k\partial/\partial x_i$ in spherical coordinates as the derivative withrespect to the corresponding angle. One should also note that the unit vector $\mathbf{r}/r$ is an eigenfunction of the operator $\hat{\omega}$. As a result, we obtain

$$L^v_1 \equiv L^v_{23} \equiv -L^v_{32} = -i\left(\operatorname{ctg}\delta\cos\vartheta\frac{\partial}{\partial\vartheta} + \frac{\cos\vartheta}{\sin\delta}\frac{\partial}{\partial\beta} + \sin\vartheta\frac{\partial}{\partial\delta}\right); \tag{57}$$

$$L^v_2 \equiv L^v_{31} \equiv -L^v_{13} = i\frac{\partial}{\partial\vartheta}; \tag{58}$$

$$L^v_3 \equiv L^v_{12} \equiv -L^v_{21} = -i\left(\operatorname{ctg}\delta\sin\vartheta\frac{\partial}{\partial\vartheta} + \frac{\sin\vartheta}{\sin\delta}\frac{\partial}{\partial\beta} - \cos\vartheta\frac{\partial}{\partial\delta}\right). \tag{59}$$

Only one of these three expressions need be obtained by calculation; the other two can be obtained from

[7] S. I. Pekar, J. Exptl. Theoret. Phys. (U.S.S.R.) 27, 579 (1954).

the three commuting relations

$$L_1^v L_2^v - L_2^v L_1^v = iL_3^v; \tag{60}$$

$$L_2^v L_3^v - L_3^v L_2^v = iL_1^v;\ L_3^v L_1^v - L_1^v L_3^v = iL_2^v.$$

One can prove the relations (60) without resorting to concrete expressions for the operators (57)-(59), if we first prove the analogous relations for L_{ik}^q:

$$L_1^q L_2^q - L_2^q L_1^q = iL_3^q; \tag{61}$$

$$L_2^q L_3^q - L_3^q L_2^q = iL_1^q;\ L_3^q L_1^q - L_1^q L_3^q = iL_2^q.$$

The latter are proved by means of simple substitution in Eq. (61) of L_{ik}^q in the form (55) and division into products of integrals of sums of the form $\sum_{\vec{\varkappa}} \chi_{\vec{\varkappa}}(\mathbf{r})\chi_{\vec{\varkappa}}(\mathbf{r}')\quad \delta(\mathbf{r}-\mathbf{r}')$. Inasmuch as the commutation relations of the form (61), as is known, are valid even for L_i and $^1/_2\,\sigma_i$, Eqs. (60) follow at once, since L_i, L_i^q and σ_i commute amongst themselves.

The operator of the isotopic spin of the system

$$T_{\alpha\beta} = \int [\varphi_\alpha \pi_\beta - \varphi_\beta \pi_\alpha]\, dV + \frac{1}{2}\tau_{\alpha\beta};\ \tau_{12} \equiv \tau_3 \ldots \tag{62}$$

commutes with the operator of the energy of the system and with the operators L_{ik}. Consequently, the isotopic spin is an integral of the motion. With the help of Eq. (1) of I, and also Eq. (3), we get

$$T_{\alpha\beta} = T_{\alpha\beta}^q + T_{\alpha\beta}^v + \frac{1}{2}\tau_{\alpha\beta};$$

$$T_{\alpha\beta}^q = -i\sum_{\vec{\varkappa}}\left(q_{\alpha\vec{\varkappa}}\frac{\partial}{\partial^* q_{\beta\vec{\varkappa}}} - q_{\beta\vec{\varkappa}}\frac{\partial}{\partial^* q_{\alpha\vec{\varkappa}}}\right); \tag{63}$$

$$T_{\alpha\beta}^v = -i\sum_{\vec{\varkappa}j}\left[q_{\alpha\vec{\varkappa}}\frac{\partial v_j}{\partial q_{\beta\vec{\varkappa}}} - q_{\beta\vec{\varkappa}}\frac{\partial v_j}{\partial q_{\alpha\vec{\varkappa}}}\right]\frac{\partial}{\partial v_j}.$$

In the calculation of $T_{\alpha\beta}^v$, the expressions $\partial v_j / \partial q_{\alpha\vec{\varkappa}}$ are put in the form of Eqs. (67) - (69) of I. As a result of the use of Eq. (1) of I, we obtain the expression in the form

$$\int\left[\varphi_\alpha \hat{\omega}^n \frac{\partial \varphi_\beta^v}{\partial v_i} - \varphi_\beta \hat{\omega}^n \frac{\partial \varphi_\alpha^v}{\partial v_i}\right] dV. \tag{64}$$

In the calculation of these integrals, φ_α is replaced by φ_α^v, and for the latter, use is made of Eqs. (60) and (38) of I. With the aid of Eqs. (63), the integrals (64) reduce to expressions of the form:

$$\frac{I^{(n)}}{2}\sum_\nu\left[\overline{\tau_\alpha\sigma_\nu}^{\psi^v}\frac{\partial}{\partial v_i}\overline{\tau_\beta\sigma_\nu}^{\psi^v} - \overline{\tau_\beta\sigma_\nu}^{\psi^v}\frac{\partial}{\partial v_i}\overline{\tau_\alpha\sigma_\nu}^{\psi^v}\right], \tag{65}$$

which are calculated directly. As a result, we obtain

$$T_1^v \equiv T_{23}^v \equiv -T_{32}^v = -i\left(\operatorname{ctg}\delta\cos\beta\frac{\partial}{\partial\beta} + \frac{\cos\beta}{\sin\delta}\frac{\partial}{\partial\vartheta} + \sin\beta\frac{\partial}{\partial\delta}\right); \tag{66}$$

$$T_2^v \equiv T_{31}^v \equiv -T_{13}^v = i\partial/\partial\beta; \tag{67}$$

$$T_3^v \equiv T_{12}^v \equiv -T_{21}^v = -i\left(\operatorname{ctg}\delta\sin\beta\frac{\partial}{\partial\beta} + \frac{\sin\beta}{\sin\delta}\frac{\partial}{\partial\vartheta} - \cos\beta\frac{\partial}{\partial\delta}\right). \tag{68}$$

The components of the operators T_i, T_i^q, T_i^v and $(1/2)\tau_i$ satisfy the general commutation relations of the form (60).

Comparison of L_i^v and T_i^v shows that they interchange with one another upon substitution of $\vartheta \rightleftarrows \beta$. This means that the eigenfunctions of these operators are identical, and their eigenfunctions are obtained from one another by exchange of the angles $\vartheta \rightleftarrows \beta$. Direct calculation shows that

$$L^{v^2} \equiv \sum_{i=1}^{3} L_i^{v^2} = T^{v^2} \equiv \sum_{i=1}^{3} T_i^{v^2} = \frac{2(I^{(n)})^2}{I^{(2n)}}\hat{\mathcal{H}}, \tag{69}$$

where $\hat{\mathcal{H}}$ is the operator of the energy of rotational motion, determined by Eq. (13).

It is interesting to note that the operators L_i^v and T_i^v coincide with the operators of infinitely small rotations in three dimensional space, while the Euler angles of these rotations are identified

with the angles ϑ, β and δ. These operators of infinitely small rotations have been suitably investigated in the theory of the representation of three dimensional rotation groups (see Ref. 8). The eigenfunctions of these operators were investigated and a series of interesting relations among them were established.

It should be emphasized that the operators L_{ik} $T_{\alpha\beta}$ represent operators of infinitely small rotations, respectively, of ordinary and isotopic space, and therefore commute. The operators L^v_{ik} and $T^v_{\alpha\beta}$ are operators of infinitely small rotations of the same three dimensional space, in which the Euler angle belongs to ordinary space, the Euler angle β to isotopic space, and the σ angle $\delta = \varphi + \gamma$ is related to both spaces. Nontheless, L^v_{ik} and $T^v_{\alpha\beta}$ also commute. The operators L^v_{ik} and $T^v_{\alpha\beta}$ differ from those operators of the zero field introduced by Pauli and Dancoff[5], because the latter are operators of rotation corresponding to ordinary and isotopic spaces. However, the operators L^0_{ik} and $T^0_{\alpha\beta}$ also satisfy a condition analogous to Eq. (69).

We now proceed to the determination of such eigenfunctions of the energy operator which are related to the lowest level ($j = 1/2$), which would simultaneously be eigenfunctions of the operators L_{12} and T_{12}. The latter is related to the charge operator of the system $\hat{e}$ by the expression

$$\hat{\varepsilon} = T_{12} + {}^1/_2. \tag{70}$$

First, let us consider the result of the action of the operators L_{12} and T_{12}, which are defined by Eqs. (55) and (63), on the wave function of the ground state of the system:

$$\Psi^1_{2s,2p} = \psi^v V^1_{2s.2p}(\vartheta\beta\delta) \exp\left\{-\frac{1}{2}\sum_{\vec{\alpha}\vec{\varkappa}}\left[(q_{\vec{\alpha}\vec{\varkappa}} - q^v_{\vec{\alpha}\vec{\varkappa}})^2 + \frac{1}{2}\ln\pi\right]\right\}, \tag{71}$$

where $V^1_{2s,2p}$ is defined by Eq. (28) and ψ^v by Eq. (41). In the application of the operators L^q_{12} and T^q_{12} to $\Psi^1_{2s,2p}$, we are obliged to differentiate only the exponential factor in Eq. (71). We can neglect the result of this differentiation, inasmuch as we have previously neglected terms of the form

$$\sum_{\vec{\varkappa}}(q_{\vec{\alpha}\vec{\varkappa}} - q^v_{\vec{\alpha}\vec{\varkappa}})\, q^v_{\vec{\beta}\vec{\varkappa}} = \int(\varphi_\alpha - \varphi^v_\alpha)\,\hat{\omega}\,\varphi^v_\beta\, dV. \tag{72}$$

The result of the action of operators L^v_{12} and T^v_{12} on the function $V^1_{2s.2p}$ has the following form:

$$\begin{aligned}
L^v_{12}V^1_{11} &= \frac{i}{2}V^1_{-11}; & T^v_{12}V^1_{11} &= \frac{i}{2}V^1_{1-1};\\
L^v_{12}V^1_{1-1} &= \frac{i}{2}V^1_{-1-1}; & T^v_{12}V^1_{-11} &= \frac{i}{2}V^1_{-1-1};\\
L^v_{12}V^1_{-11} &= -\frac{i}{2}V^1_{11}; & T^v_{12}V^1_{1-1} &= -\frac{i}{2}V^1_{11};\\
L^v_{12}V^1_{-1-1} &= -\frac{i}{2}V^1_{1-1}; & T^v_{12}V^1_{-1-1} &= -\frac{i}{2}V^1_{-11}.
\end{aligned} \tag{73}$$

With the help of these formulas, and keeping in mind Eq. (8) of I and Eq. (41), we get

$$L^v_{12}\psi^v = -\frac{1}{2}\sigma_{12}\psi^v; \quad T^v_{12}\psi^v = -\frac{1}{2}\tau_{12}\psi^v. \tag{74}$$

From this it is evident that the action of the operators L_{12} and T_{12} on $\Psi^1_{2s,2p}$ reduces to the action of L^v_{12} and T^v_{12} on the factor $V^1_{2s,2p}$ in Eq. (71).

The problem consists in looking for such linear combinations of the four functions $V^1_{2s,2p}$, which would simultaneously be eigenfunctions of the operators L^v_{12} and T^v_{12}. These linear combinations, fortunately, exactly coincide with the components ψ^v [see Eq. (41)], because Eqs. (74) show that each of the four components ψ^v are eigenfunctions of the operators L^v_{12} and T^v_{12}, inasmuch as σ_{12} and τ_{12} are diagonal.

Thus the eigenfunctions of the charge and spin operators of the system are given by an expression of the form (71), in which we must put the appropriate linear combination in place of the function $V^1_{2s,2p}$. This combination can be taken from the table below:

---

[8] I. M. Gel'fand and Z. Ia. Shapiro, Usp. matemat. nauk 7, 1 (1952).

Projection of the spin of the system L_{12}	Charge of the system $(T_{12}+{}^1/_2)$	
	0 (neutron)	1 (proton)
$-{}^1/_2$	$\frac{1}{\pi\sqrt{2}}C_1^v$	$\frac{1}{\pi\sqrt{2}}C_3^v$
$+{}^1/_2$	$\frac{1}{\pi\sqrt{2}}C_2^v$	$\frac{1}{\pi\sqrt{2}}C_4^v$

The C_k^v are defined by Eq. (35) of I.

The calculated eigenvalues of the charge and spin projections of the system consisting of a nucleon that strongly interacts with the vacuum vibrations of the meson field, coincide with the observed values.

In subsequent papers we shall consider, on the basis of the theory developed above, the scattering of π mesons on nucleons, the magnetic moments of nucleons, quasi-statistic nuclear forces and other phenomena.

Translated by R. T. Beyer
57

SOVIET PHYSICS JETP VOLUME 3, NUMBER 3 OCTOBER, 1956

Meson Component of the Cosmic Radiation at an Altitude of 3200 m Above Sea Level

N. M. KOCHARIAN, M. T. AIVAZIAN, Z. A. KIRAKOSIAN AND A. S. ALEKSANIAN
Institute of Physics, Academy of Sciences, Armenian SSR

(Submitted to JETP editor, Dec. 1, 1954)
J. Exptl. Theoret. Phys. (U.S.S.R.) 30, 243-247 (February, 1956)

The momentum spectrum of μ-mesons was measured in the momentum range $0.4 \leq p \leq 14$ bev/c at an altitude of 3200 m above sea level. The ratio of the number of protons to μ-mesons at this altitude was determined. The ratio of positive to negative μ-mesons was found as a function of momentum.

In 1951 we began an investigation of the proton and meson components of the cosmic radiation at an altitude of 3200 m above sea level. For this purpose there was constructed a special magnetic spectrometer, a description of which was given in Ref. 1. The proton component was determined as a result of the investigation. The actual shape of the spectrum was determined for the meson component. By using a series of improvements, the momentum of the particles in the magnetic field was determined with great precision.[1] The relative error in determining the momentum of the particles is equal to

$$\sigma = [(0.035\,p)^2 + (0.018/\beta)^2]^{1/2}. \qquad (1)$$

Here and everywhere below the momentum p of the particles is measured in units of bev/c; β is the velocity of the particles, measured in units of the velocity of light.

1. Protons in the Hard Component

In a second variation of the determination of Ref. 1, in which there was no lead above the magnet and under the magnet was located $x_1 = 45.2$ gm/cm^2 of lead and $x_2 = 139$ gm/cm^2 of copper, then simultaneously with particles which were stopped in the absorbers, we also detected those particles which had gone through the complete system of absorbers. In contrast with the former particles the latter are called the "hard" component. The hard component consists principally of μ-mesons with momenta greater than 0.370 bev/c (i.e., kinetic energy $E \geq 260$ mev), and a certain

[1] N. M. Kocharian, J. Exptl. Theoret. Phys. (U.S.S.R.) 28, 160 (1955); Soviet Phys. JETP 1, 128 (1955).

number of protons(here we have in mind the components of the hard component at the entrance to the system of absorbers, i.e. in the air; following the passage through the absorbers the constitution of the hard component changes; in the flux of these particles there appear π-mesons, nuclear fragments and electrons.). In very great absorber thicknesses (approximately 21 radiation units long) we can conclude that the hard component is practically free of electrons. The relative number of protons in the hard component is not very small, and in order to determine the differential μ-meson spectrum, it is necessary to take it into account. Protons with momentum $p \geq 1.11$ ($E > 500$ mev) have an ionization range greater than the overall absorber thickness and may emerge from it. As a result of the work in Ref.1, we can determine the number of protons in the hard component. In 267 hours there passed through the magnetic field of the apparatus 680 protons with momenta $1.11 \leq p \leq 2.33$, which stopped in the absorbers and were removed from the hard component. The number of protons with $p > 2.33$ may be determined from the power law for the integral spectrum

$$n(p) = 1{,}46 \cdot 10^{-3} / 1{,}65 \cdot p^{1{,}35} \qquad (2)$$

given in Ref. 1. We determine from Eq. (2) that the number of protons with $p > 2.33$ is equal to 300.

Hence the number of protons with momentum $p > 1.11$ equals 970. Of this number 450 protons were detected as having stopped in the absorbers. At the same time 19, 150 hard component particles were detected. Consequently, the protons constitute (970-450) / 19150 = 2.7% of the total number of particles found in the hard component, and the hard component consists principally of μ-mesons. We have compared the relative number of protons with $p > 1.1$ and μ-mesons with $p > 0.37$ in the hard component. If we compare the number of protons and mesons in the hard component with $p > 1.1$ then the number of protons is greater, consisting (see Table 1) of about 8% of the number of μ-mesons.

TABLE 1

Momentum Spectrum of Hard μ-Mesons

Interval	Average Momentum	Number of Hard Particles		Luminosity of Spectrometer	Number of Particles Corrected for Luminosity		Number of Protons Among Hard Particles	Number of μ-Meons Following Subtraction of Proton Background	Total Number of Mesons	Number of Mesons in the Momentum Interval $\times 10^3$
		+	−		+	−				
	2	3	4	5	6	7	8	9	10	11
19—15	0,411	414	402	0,825	501	488	0	501	989	8,0
15—13	0,500	336	306	0,890	378	344	0	378	722	7,5
13—11	0,583	475	427	0,929	512	460	0	512	972	7,4
11—9	0,778	618	545	0,952	649	572	0	649	1221	6,48
9—8	0,823	410	344	0,965	425	356	0	425	781	6,01
8—7	0,933	509	363	0,975	522	372	0	522	894	5,33
7—6	1,075	625	458	0,982	635	466	94	541	1007	4,52
6—5	1,271	854	637	0,987	864	645	128	736	1381	4,45
5—4	1,552	1037	689	0,995	1040	692	112	928	1620	3,48
4—3	2,000	1336	855	1,0	1336	855	78	1258	2113	2,75
3—2	2,800	1537	1158	1,0	1537	1158	77	1460	2618	1,73
2—1	4,660	1575	1066	1,0	1575	1066	83	1492	2558	0,611
1—0	14,000	993	725	1,0	993	725	41	952	1677	0,0446

2. Momentum Spectrum of μ-Mesons

In Table 1 are presented the results of studying the trajectories of the particles which make up the hard component. In the first column are given intervals of range $\delta = 7/p$ where p, as elsewhere, is measured in bev/c. In the second column is given the average momentum, corresponding to the interval δ in the first column. In the third and fourth columns are given the number of positive and negative particles. In the sixth and seventh columns are given the numbers of these particles corrected

for the luminosity of the apparatus. The number of protons in the hard component (column 8) is calculated from the results given in Ref. 1. As was already stated above, only protons with $p > 1.1$ can get into the hard component, hence the hard component particles with $p < 1.1$ are only mesons. The number of protons with momentum $1.1 \leq p \leq 2.33$ entering with the hard component is taken from Ref. 1. For $p > 2.33$ the number of protons is calculated from the formula

$$(1.46 \cdot 10^{-3} / 1.65)(p_1^{-1.65} - p_2^{-1.65}) - \Delta n, \quad (3)$$

where n is the number of protons with $p_1 < p < p_2$, stopped in the absorbers. This number was taken from the result given in Ref. 1. Subsequently, we subtract the proton background in the ninth and tenth columns and give the number of positively charged and the total number of mesons. In the eleventh column we calculate the ordinates of the differential meson spectrum, i.e., the number of mesons arriving in a momentum range equal to 1 bev/c. The numbers in this column are obtained by dividing the numbers in the preceding column by the value of $ks\omega t = 1.344 \times 10^6$ cm^2 ster. sec.[1]

In Fig. 1 there is represented the differential momentum spectrum of μ-mesons on a log log scale. On the axis of abscissas is plotted the logarithm of the momentum in bev/c and on the ordinate axis is plotted the logarithm of the number of mesons (number in column 11).

In Table 2 there is shown the calculated intensity of mesons with momenta greater than a given p (p in units of bev/c, $n(p)$ in units of cm^{-2} sec^{-1} ster^{-1}).

TABLE 2.

Intensity of the Vertical Flux of μ-Mesons with Momentum Greater than p

p	$10^3 n(p)$	p	$10^3 n(p)$
0,370	13,8	1,165	8,90
0,466	13,09	1,40	7,87
0,539	12,53	1,75	6,67
0,636	11,80	2,33	5,1
0,777	10,90	3,50	3,15
0,875	10,32	7,00	1,25
1,00	9,65		

Rossi[2] gives for the intensity of mesons with an ionization range greater than 167 gm/cm^2 of Pb (i.e. with momentum $p \geq 0.305$) at the same altitude, a value of $n(0.3) = 15.2 \times 10^{-3}$ particles/cm^2 sec ster. It is difficult to find any agreement with this value from the corresponding momentum deduced from Table 2.

As can be seen from Fig. 1 the differential momentum spectrum of μ-mesons is determined up to the momentum $p=14$. In other work [3,4] the μ-meson spectrum at mountain altitudes was determined up to a momentum of $p=7$. In this range of momentum, within the limits of experimental error, our results agree with the work cited.

We can now derive a comparison of the intensity of the vertical flux of protons and μ-mesons. The result of this comparison is shown in Fig. 2. The upper curve in this figure represents the relative number of protons and μ-mesons at a definite momentum. The lower of these curves represents the relative number of protons and μ-mesons with momenta greater than that which is designated on the axis of abscissas. At the beginning, the ratio of the differential spectra increases rapidly with the value of the momentum. For momentum $p \approx 0.9$ this ratio reaches its maximum value and, for further increases in the momentum of the particles, decreases rapidly. At the peak ($p \approx 0.9$) the number of protons constitute $\sim 20\%$ of the number of mesons at this momentum. The ratio of the ordi-

[2] B. Rossi, Revs. Mod. Phys. 20, 537 (1948).

[3] J. G. Wilson and others, Progress in Cosmic Ray Physics, Amsterdam, 1952, pp. 358 and 360.

[4] W. L. Whittemore and R. P. Shutt, Phys. Rev. 86, 940 (1952).

nates of the integral spectra of protons and μ-mesons decreases monotonically with increasing momentum of the particles. For $p > 0.4$ the protons constitute $\sim$ 12% of the number of mesons, for $p > 1 \sim 9\%$ and for $p > 8$ about 2.7%.

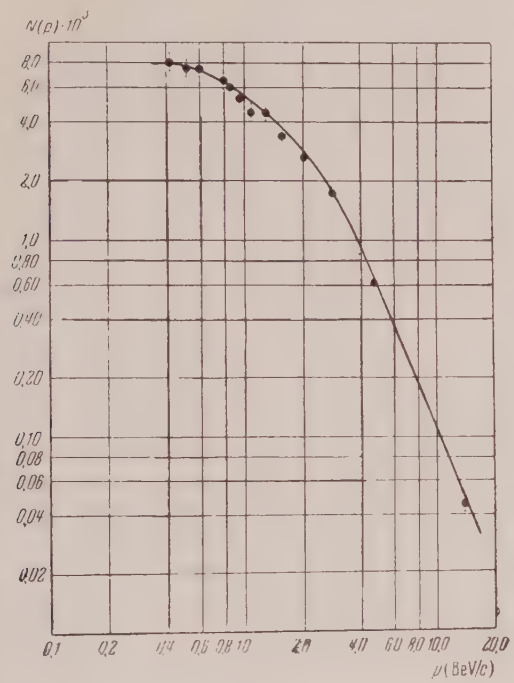

FIG. 1.

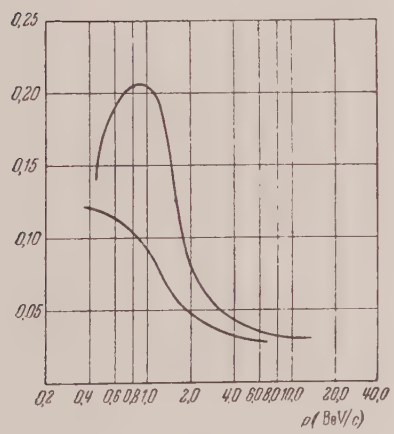

FIG. 2.

Whittemore and Shutt[4] found that at an altitude of 3400 m above sea level the number of protons with momentum $p > 0.3$ constitute $19 \pm 2\%$ of the number of μ-mesons of the same momentum. If we take into account the difference in altitude and recalculate for an altitude of 3200 m, then we obtain a value of 17%. This result does not agree with ours, where for this momentum the number of protons is $\sim$ 12% of the number of μ-mesons. The difference that is found is beyond the limits of the experimental errors.

We found more serious differences between the cited work and our own work. The relative numbers of protons and μ-mesonswith momenta in the range given in Whittemore and Shutt increases monotonically with decreasing momentum of the particles down to $p = 0.3$, whereas our curve of this ratio has a sharp maximum at $p \approx 0.9$.

However, our results are in accord with those of Miller et al.[5] In this work it was found that protons of momentum $\sim$ 0.6 constitute approximately 20% of the number of μ-mesons of this momentum. In a later work of these authors[6] there is deduced the result concerning the relative numbers of μ-mesons which agrees with ours.

3. The Positive Excess

The magnetic spectrometer also allows one to determine the charge of the particles which are present in the hard component. Hence we have the possibility of determining the dependence of the ratio of the number of positive and negative mesons on their momenta: $k(p) = N_+(p)/N_-(p)$, where $N_+(p)$ and $N_-(p)$ are respectively the ordinates of the curves of the differential spectra of + and –mesons. These ordinates are presented in the ninth and seventh columns of Table 1.

The function k is shown in Fig. 3. The logarithm of the momentum is plotted along the absicssa, and the relative number of + and – mesons at the

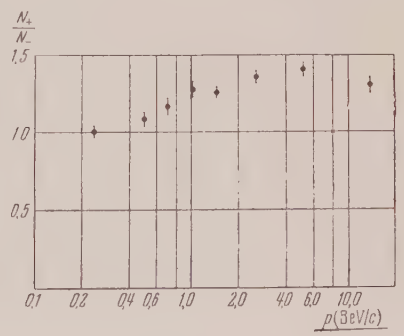

FIG. 3.

[5] C. E. Miller, J. E. Henderson, D. S. Potter, J. Todd Jr., and W. Wotring, Phys. Rev. 79, 459 (1950).

[6] C. E. Miller, J. E. Henderson, G. R. Garrison, D. S. Potter, W. M. Sandstorm and J. Todd Jr., Phys. Rev. 94, 167 (1954).

given momentum is plotted along the ordinate. From this figure it is seen thatin the limit of smallmomentum $p \approx 0.2$ the numbers of mesons of opposite sign are equal (this point was made in Ref. 7). The ratio $k(p)$ increases with increasing momentum and at first proceeds at a relatively rapid rate up to the value of $p \approx 1$, then the rate decreases and apparently, for very large momenta, the ratio $k(p)$ begins to decrease.

The origin of the positive excess, as already noted in the literature, is closely linked to the nature of the primary particles of cosmic radiation. In fact, starting from the known spectrum of μ-mesons which are generated at different depths of the atmosphere[8,9] it is not difficult to show that mesons with $p > 0.2$ originate on the average at a depth of ~ 400 gm/ cm^2, and 50% of these particles are generated at depths from 400 to 700 gm/ cm^2, i.e., not far from the location of the points of observation. At these depths the numbers of protons and neutrons capable of generating fast μ-mesons are approximately equal, and hence, on the average, generate the same number of mesons of both signs. For momentum $p > 1$, the mesons generated at an average depth of 260 gm / cm^2 are 25% of the total number produced at the depths from 0 to 100 gm / cm^2, where the number of protons is considerably in excess of the number of neutrons. Hence for this part of the μ-meson spectrum we may observe a positive excess.

A comparison of our work on the positive excess and the work of other authors performed at sea level[10,11] seems to indicate that the value of $k(p)$ at sea level is smaller than at the altitude of Aragats (700 gm/ cm^2). This circumstance determines the nature of their explanation that the mesons at sea level are on the average generated at greater depths of the atmosphere than those mesons that are observed at mountain altitudes.

As may be seen from Fig. 3, for $p \approx 14$, the ratio of the number of positive to negative mesons is equal to 1.30 ± 0.04. Clearly, these mesons are generated at the expense of nucleons with energy considerably in excess of 14 bev / c. As is well known, at these energies we have the place of multiple meson production[12-15]. However for multiple meson production the mesons of both signs that are produced should be of nearly equal numbers, i.e., $k(p) = 1$. Hence it follows that our experiment rejects the mechanism of multiple meson production. The larger values of $k(p)$ may be explained qualitatively, if we assume that the main number of μ-mesons with $p \approx 14$ are formed in nuclear collisions in which the number of secondary particles that is generated is comparatively small. In regard to those μ-mesons, which appear as products of nuclear collisions with large numbers of secondary particles, most of these appear with low energies, and hence they disintegrate in the upper part of the atmosphere and do not reach us.

---

[7] N. M. Kocharian, M. T. Aivazian, Z. A. Kirakosian and S. D. Kaitmazov, J. Exptl. Theoret. Phys. (U.S.S.R.) 25, 364 (1953).

[8] G. M. Garibian and I. I. Gol'dman, J. Exptl. Theoret. Phys. (U.S.S.R.) 26, 257 (1954).

[9] M. Sands, Phys. Rev. 77, 180 (1950).

[10] B. G. Owen and J. G. Wilson, Proc. Phys. Soc. (London) 64A, 417 (1951).

[11] D. E. Caro, J. K. Parry and H. D. Rathgeber, Nature 165, 688 (1950).

[12] E. Fermi, Progress Theor. Phys. 5, 570 (1950)

[13] E. Fermi, Phys. Rev. 81, 683 (1951).

[14] L. D. Landau, Izv. Akad. Nauk SSSR, Fiz. Series, 7, 51 (1953).

[15] E. L. Feinberg and D. S. Chernavskii, Dokl. Akad. Nauk SSSR 81, 795 (1951).

Translated by B. Hamermesh
45

Predischarge Phenomena in Liquids

I. E. BALYGIN

(Submitted to JETP editor March 30, 1955)
J. Exptl. Theoret. Phys. (U.S.S.R.) 30, 464-470 (March, 1956)

The results of an investigation of prebreakdown phenomena in transformer oil, castor oil, xylene and distilled water are presented. At voltages sufficient for breakdown, it is shown that ionization by collision occurs during the statistical delay period, resulting, in a time of approximately 10^{-8} sec, in the production of electron avalanches and small streamers. The latter do not always lead to cumulative breakdown, but are a preparatory stage. It has been established that breakdown can occur when the streamer current is greater than $5 - 8 \times 10^{-5}$ amp.

It is also shown that in distilled water with highly inhomogeneous fields the breakdown mechanism depends on the polarity of the point. If the latter is positive, then during the statistical delay period a positively charged column of very small radius is formed in about 5×10^{-6} sec.

IT is well known that both a definite voltage and sufficient time are required before a discharge can occur in a dielectric. The time interval between the application of a voltage, adequate for breakdown, to the electrodes and the appearance of a free electron, capable of initiating a cumulative discharge, is usually called the statistical delay time. It is virtually impossible to determine experimentally the moment at which such an electron appears, and consequently, for experimental purposes, the end of the statistical delay period is taken to be the moment at which there occurs either a noticeable voltage drop across the electrodes or a cumulative increase in the electrode current.

The question of what occurs in a dielectric during the statistical delay time is of great interest. To shed light on these phenomena we have performed a number of experiments in liquids. The results of these experiments are reported below.

In solid or liquid dielectrics, it is well known that the energy of free electrons, moving under the influence of an applied field, is dissipated in excitation of oscillations in nearby atoms and molecules, electronic excitation in these atoms and molecules, molecular dissociation, and collisions of the second kind[1,2]. The dielectric, as it were, hinders the development of discharges at low field intensities. Another barrier to the development of a discharge is the capture of free electrons by molecules of the material[3]. It is reasonable to believe that these processes depend on the physico-chemical properties of the dielectric. If ionization takes place during the statistical delay period, but a cumulative discharge does not occur, these physico-chemical properties should have some effect on the character of the predischarge phenomena. The experiments reported here indicate that such is the case, at least in certain liquid dielectrics.

According to present-day ideas of the structure of the amorphous phase, a liquid consists of separate crystallite aggregates comprising several tens of molecules in a group[4]. These groups, as might be supposed, do not consist of rigidly bound molecules but are constantly being dissolved and reformed. In certain liquids at least, there is some justification for the assumption that ions of opposite sign are contained in these crystallite groups. This assumption is based on the experimental finding that the electrical conductivity σ of heptane is very small at low field intensities. With increasing intensities, however, there is a pronounced rise in σ. It is believed[5] that this increase results from the destruction of electrically neutral ion pairs by the externally applied field. It is also possible to explain the increase in σ on the basis of crystallite ion groups.

It is well known that a wave function has a strong maximum at any defect of a perfect crystal, including those close to the surface of the crystal.[6] Consequently, it may be expected that extensive trapping takes place at the boundary surfaces of a crystal. In this connection it may be assumed that the size of the crystallite aggregates, the stability of the bonds, the nature of the levels, and various other characteristics, pertinent to the formation and

---

[1] A. von Hippel and G. Lee, Phys. Rev. 59, 824 (1941).
[2] G. Hurd, Gen. Elec. Rev. 51, 26 (1948).
[3] A. Von. Hippel, J. Appl. Phys. 8, 815 (1937).
[4] P. P. Kobeko, *Amorphous Materials*, Academy of Sciences Press (USSR), 1952, p. 17.
[5] K. A. Reiss, Ann. Physik 28, 325 (1937).
[6] I. E. Tamm, Z. Physik Sowjetunion 1, 733 (1932).

maintenance of an electric discharge, should also depend on the physico-chemical constitution of the liquid.

The experiments were performed using the apparatus shown in Fig. 1. The voltage from a pulse

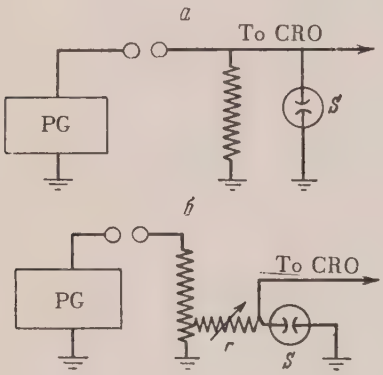

FIG. 1. Experimental set-up

generator *PG* was applied directly to the sample under observation *S* (diagram *a*). This voltage was also applied, through a capacity divider, to the plates of a high-voltage oscilloscope which had been calibrated for the measurements. Certain of the experiments were performed using the scheme shown in diagram *b*. In these cases an ohmic resistance *r* was connected in series with the discharge gap in order to limit the discharge current.

It has been stated in the literature that relatively small variations of the voltage across the spark gap are to be associated with the onset of stepped leaders or streamers[7,8] and that the production of streamers causes a sharp drop in the voltage[9] even within so short time as 4×10^{-9} sec. Hence impact ionization and the resulting production of avalanches and streamers can be observed through changes in the pulse amplitude as seen on the oscillographs.

In Fig. 2 are presented oscillographs recorded with scheme *a* (I-III) and scheme *b* (IV-VI) of Fig. 1. The period of the reference sinusoidal oscillations along the abscissa axis in Oscillographs I-III is 5×10^{-7} sec. Explanatory data for these oscillographs are given in Table 1.

Inspection of Oscillograph I reveals that the statistical delay time in transformer oil was greater than 30 μsec. During this period there was intense ionization by impact with resulting avalanche production; this can be seen from the nicks (1, 2, 3, 4) in the top of the pulse. Similar results were obtained in the tests performed in castor oil (Oscillograph II). In the latter case it is worthy of note that a small avalanche was formed immediately after the application of the voltage (1). During the statistical delay time, which lasted for 50μsec, three partial discharges were recorded; as in the transformer-oil test, two of these occurred immediately prior to the terminal discharge of the gap.

In the transformer-oil test, as can be seen from Oscillograph I, the avalanches appeared within small time intervals (1-3.5 μsec) and the cumulative discharge was initiated within 3 μsec after the the last avalanche. It would seem that the avalanches prepare the way for the formation of the discharge.

In the castor-oil test the avalanches appeared at considerably longer time intervals (3.5-28 μsec), but again the cumulative discharge appeared within 3.5 μsec after the last avalanche.

For strongly inhomogeneous fields, it appears that ionization processes occur during the so-called statistical delay time; these do not cause direct breakdown but constitute a preparatory stage in that ionization processes in the discharge gap lead to the production of volume charges. From a knowledge of the prebreakdown time (statistical delay time) for strongly inhomogeneous fields it is possible to ascertain the time during which impact ionization occurs with the resulting production of avalanches and small streamers. The latter processes do not initiate a breakdown but act to set the stage for it. It should be remembered that at the same time there are processes taking place in the dielectric which tend to inhibit the development of a discharge. In the main, these same results were found in the tests with homogeneous fields; a typical case (transformer oil) is shown in Oscillograph III of Fig. 2. At intensities of 315-350 kv/cm, breakdown did not occur in spite of the fact that the prebreakdown phenomena were relatively strong. Almost immediately after the pulse reached its highest amplitude (0.5 μsec) 350 kv, nicks can be seen in the top of the pulse; these are similar to those which were observed in the tests with inhomogeneous fields. In certain cases the nicks appeared somewhat later (2). A large number of rather weak lines – short-term fluctuations in the voltage which are indicated by arrows – can be seen in Oscillograph III. These all appeared within a time interval

---

[7] T. E. Allibone and J. M. Meek, Proc. Roy. Soc. (London) 169A, 246 (1938); 166A, 97 (1938).

[8] N. A. Kaptsov, *Electrical Phenomena in Gases and Vacuum*, GITL, 1950, p. 582.

[9] F. Dunnington and H. J. White, Phys. Rev. **46**, 99, (1934).

less than a microsecond. These small voltage fluctuations are undoubtedly caused by electron avalanches which result from impact ionization in the oil. Small streamers, which are formed at the very beginning, ionize the interelectrode gap and produce a number of relatively low-intensity avalanches with lifetimes less than 10^{-8} sec. Because of the various electron-energy loss mechanisms and electron capture in the potential within the crystallites, a discharge did not occur.

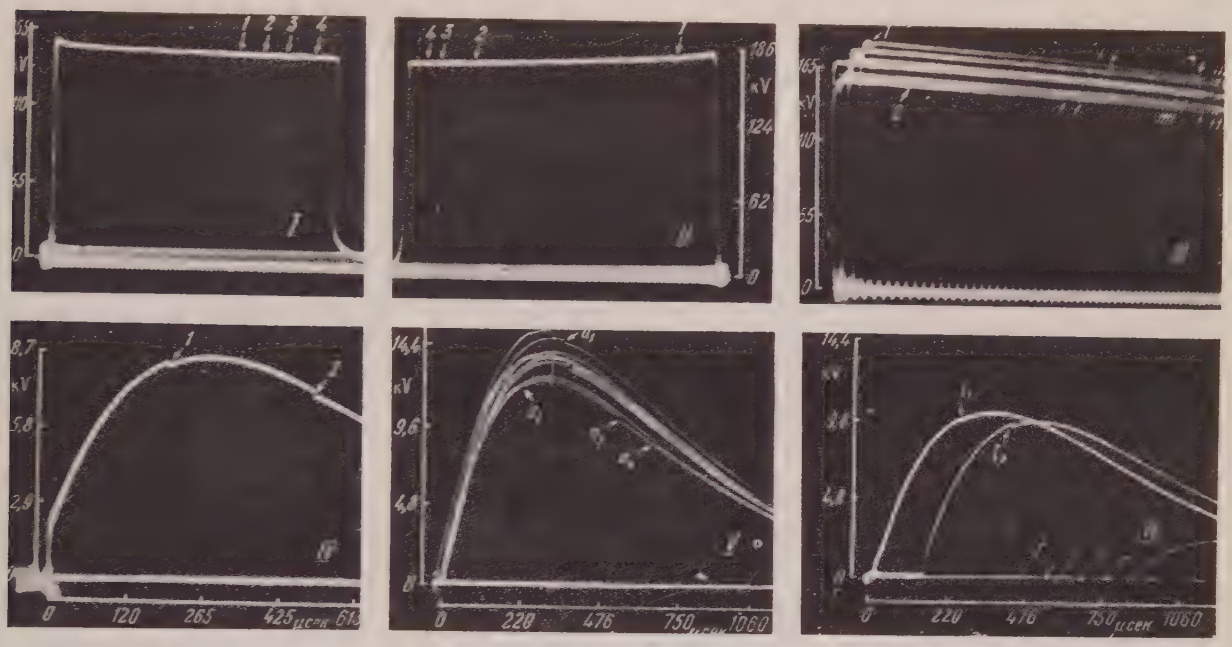

FIG. 2. Oscillographs of the voltage behavior at breakdown and during the prebreakdown period in transformer oil, castor oil, xylene, and paper impregnated with transformer oil.

It has been shown experimentally that small electron avalanches in CCl_4, mineral oil and certain other liquids can also be produced in an almost uniform ac field at very low field intensities (several kilovolts per millimeter)[10].

Oscillographs IV-VI of Fig. 2 were also made with uniform electric fields but using small spark gaps and limiting of the discharge current. For comparison purposes, tests were carried out on condenser paper saturated under vacuum with transformer (condenser) oil(Oscillograph IV). This oscillograph was made using a limiting resistance (see *b*, Fig. 1) of 3×10^6 ohms. The partial discharges could not be seen when smaller values of *r* were used. Two well-defined incipient discharges (1 and 2) can be seen. In both cases these were limited to partial discharges because the formation of a complete discharge was inhibited. It may be noted that this type of oscillograph could not always be reproduced in subsequent experiments.

In the formation of a breakdown and the increase of the current in the discharge gap, a definite voltage appears across the resistance *r*. Since the dominant resistance in the circuit is that of the resistance *r*, the major part of the voltage drop appears across this resistance when a breakdown occurs. For a drop of 180 volts and $r = 3 \times 10^6$ ohms the current at the instant of discharge was approximately 6×10^{-5} amp. With this current and the given intensity of the applied field, a cumulative breakdown can be cut off by inhibitory processes.

Oscillographs V in Fig. 2 were obtained in experiments with xylene from which the volatile component had been distilled off at a temperature of 110-129°. These experiments were carried out with steel spheres 11 mm in diameter, a gap of 0.2 mm and a limiting resistance of 5×10^6 ohms. The pulse voltage was increased gradually to the value at which breakdown occurred, which was 7×10^5 kv/cm; at smaller intensities, however,

[10] S. Yamanka and T. Suita, J. Phys. Soc. Japan 8, 277 (1953).

numerous breakdowns were observed even before the time at which maximum amplitude of the pulse was reached. The current for partial breakdowns $a_1 \ldots a_4$ was roughly 5×10^{-5} amp. This type of partial breakdown was not observed in subsequent experiments if r was less than 3×10^6 ohms. When the current is limited, a highly conducting bridge is not always formed when the gap breaks down. After some deionization of the discharge column, the latter continues to break down but at considerably lower voltages.

The appearance of partial discharges $a_1 \ldots a_4$ is an indication that impact ionization, with the production of electron avalanches and possibly streamers, takes place up to the moment of breakdown. Complete breakdown of the gap, however, occurs only at a definite intensity of the applied field.

TABLE 1

Reference data for oscillographs in Fig. 2.

Oscillograph no.	Liquid	Electrodes	Distance between electrodes in mm	Size of resistance used to limit discharge current.	Time in μsec required for first avalanche to appear after pulse reached greatest amplitude.
I	Transformer (condenser) oil	Negative (steel) point and brass plane	50	—	19.5
II	Castor oil	Positive point and plane	150	—	6.5
III	Transformer (condenser) oil	Brass spheres (nickel-plated) $d = 62.5$ mm	10	—	0.5—3
IV	Four layers of condenser paper-total thickness 40μ. Saturated under vacuum with condenser oil.	Steel sphere $d = 11$ mm and brass plane in transformer oil	4×10^{-2}	3×10^6	at maximum amplitude
V	Xylene with volatile fraction distilled off at 110-129°.	Steel spheres $d = 11$ mm	0.2	5×10^3	,,
VI	Vacuum dried castor oil.	,,	0.2	5×10^6	,,

In Fig. 2 VI are shown oscillographs obtained in tests with vacuum-dried castor oil. The limiting resistance was 5×10^6 ohms. Inspection of these oscillographs reveals that breakdown of a gap with $l = 0.2$ mm occurred at about 480 kv/cm, but that with a constant pulse the discharge began to form at somewhat lower intensities (points l_1 and l_2). In these partial discharges the current was $4 - 6 \times 10^{-5}$ amp.

The data on current strengths in partial breakdown given here indicate that total breakdown can occur for currents greater than $5 - 8 \times 10^{-5}$ amp.

Several other predischarge processes were observed in the distilled water experiments. For a voltage pulse this liquid may be assumed to be an insulator. The oscillographs in question were made using the arrangement shown in Fig. 1 (scheme *a*) and are shown in Fig. 3, while the explanatory data are given in Table 2. The period of the reference sinusoidal oscillations in Oscillographs V and VI was also 5×10^{-7} sec. The reproducibility of these oscillographs was found to be excellent.

The lower two oscillographs in I of Fig. 3 are for cases in which breakdown did not occur. These give an indication of the length of the applied pulse (343 μsec from maximum to half amplitude). In the other pulses, in which breakdown did take place, the length of the pulse is found to be shortened. This results from the fact that during the predischarge period there is an uninterrupted flow

of the ever-increasing prebreakdown currents which prepare the gap, so to speak, for breakdown. Since the form of the pulse remains the same, the duration of all these pulses in I of Fig. 3 should also be the same. These prebreakdown processes in distilled water have also been observed with homogeneous fields[11]. It is evident from examination of the oscillographs in Fig. 3 that a more rapid decay of the pulse is to be associated with higher amplitudes, i.e., a greater current flows across the spark gap during the prebreakdown time. In a paper which has been published earlier, the assumption has been made that electrons which move from the negative point into the region of smaller field intensity are captured by water molecules and form volume charges during the formative lag period; these charges lead to an increase in the field intensity and are responsible for the cumulative breakdown[12].

In addition to the ionization processes, the point,

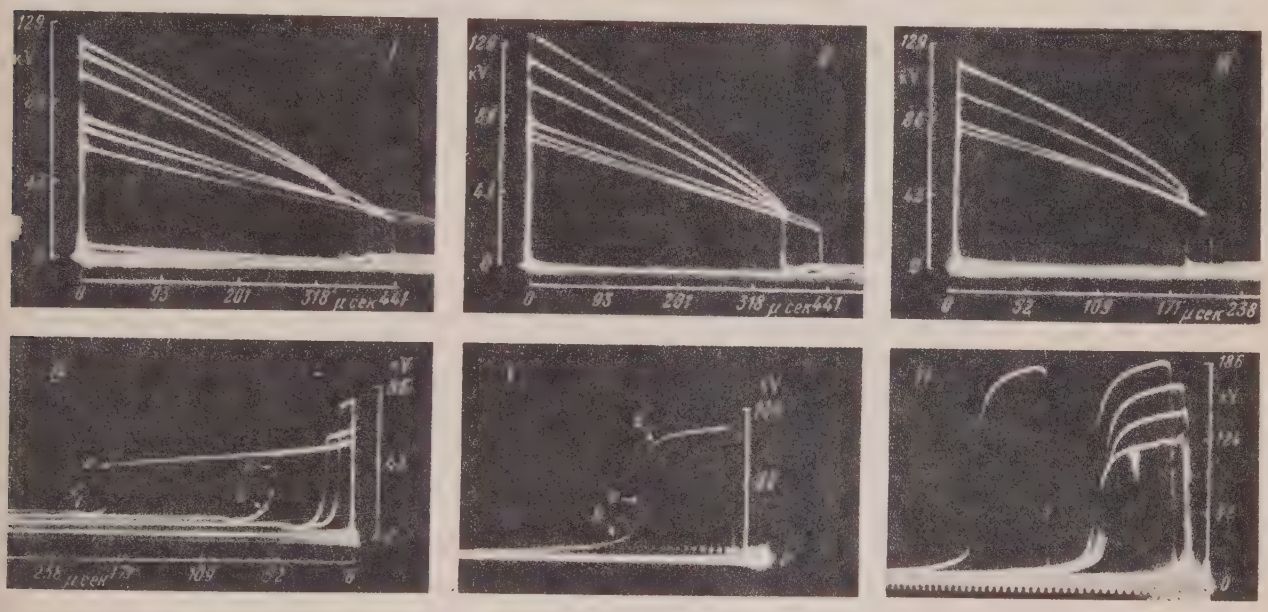

FIG. 3. Oscillographs of the voltage behavior at breakdown and during the prebreakdown period in distilled water.

itself, can act as an electron source[13-15]. It follows from Oscillographs I -III of Fig. 3 that the magnitude of the overvoltage plays a relatively small role in the general dynamics of the cumulative discharge. The length of the formative lag period, however, is strongly affected by the length of the spark gap; this lag is decreased in a pronounced way when the gap is reduced. For example, with a gap spacing of 100 mm and maximum amplitude $U = 77$ kv for the applied pulse, the formative lag period before breakdown occurs is 202 μsec; with a gap of 150 mm, however, and the same value of U, the time lag is 423 μsec. This large difference may be attributed to the length of time required for electrons and negative ions to travel to the positive electrode.

With a high intensity field, it may be assumed that impact ionization occurs within a region of radius R_1 during the prebreakdown period. This process leads to the production of electron avalanches; simultaneously, however, electron capture is taking place, especially in the region $R_2 > R_1$. Thus avalanche production should occur in accordance with the well-known relation

$$n = n_0 \exp\left\{\int_0^{R_1} (\alpha - \alpha_1)\, dx\right\} \quad \text{for} \quad x < R_1,$$

[11] I. E. Balygin, J. Exptl. Theoret. Phys. (U.S.S.R.) 25, 738 (1953).

[12] I. E. Balygin, J. Tech. Phys. (U.S.S.R.) 24, 338 (1954).

[13] D. W. Goodwin and K. A. Macfadyen, Proc. Phys. Soc. (London) B66, 85 (1953).

[14] T. J. Lewis, Proc. Phys. Soc. (London) B66, 425 (1953).

[15] Bragg, Sharbaugh and Crowe, J. Appl. Phys. 25, 382 (1954).

where, as usual, α is the number of ionization events per centimeter of path length due to one electron and α_1 is the number of electron attachments in the path length. In the region $R_2 > R_1$, electrons due to incipient avalanches will be captured by water molecules or at the surfaces of the crystallites. The rate at which this process proceeds is proportional to the average number of capture centers K and the number of electrons n' in an avalanche. Thus we can write

$$dn'/dx = -\mu n' k \text{ and}$$

$$n' = ne^{-\mu k(x-R_1)} \text{ for } x > R_1,$$

since $n' = n$ when $x = R_1$. Hence, the avalanche is attenuated; on the other hand, the negative ions with captured electrons, moving toward the anode, form an ever-increasing field up to the moment at which breakdown occurs.

In the case of a positive point and plane, an altogether different kind of effect is observed in distilled water. At threshold voltages, it can be seen from Oscillographs IV of Fig. 3 that the drop in the amplitude of the pulse does not occur. The decay of the voltage becomes noticeable only in strongly overvolted gaps (*d*, Oscillograph V).

This decay may be called the initial (prebreakdown) stage in the development of the breakdown. Immediately afterwards there is a second stage — a sharp drop in the voltage (*a*, Oscillograph IV and V). The third stage is characterized by a relatively slow drop in the voltage (*b*, Oscillograph IV) and the fourth by a slight increase (*c*, Oscillograph IV). It is assumed that in the first stage a positive streamer column is formed which propagates from the anode to the cathode. In the effective short-circuiting of the electrodes due to this column, the current increases and the voltage "collapse" occurs. It is evident that the magnitude of this "collapse" depends on the amplitude of the applied pulse; this is apparent on inspection of the curves in Fig. 4 ($U_1 \ldots U_6$) which have been drawn from Oscillographs IV-VI of Fig. 3. After a time, which is taken as zero in Fig. 4, there is a pronounced drop in the amplitude of the pulse (beginning of breakdown). In the absence of an overvoltage, the first stage of the development of the discharge remains invisible because of the low intensity of the process and the "collapse" seems to occur suddenly. It would seem that the formation of a positively charged column occurs during the predischarge period, which as we have indicated, is called the statistical delay. In oscillographs IV, this time is 184 and 52 μsec. Judging from the size of the "collapse", which is very small, it appears that the radius of the column is also very small. When the amplitude of the applied pulse is increased, this radius increases and there is a corresponding growth in the "collapse" $U_1 \ldots U_6$ of Fig. 4. In the third stage the radius of the column grows slowly because of photoioniza-

TABLE 2

Reference data for oscillographs in Fig. 3

Oscillograph No.	Electrodes	Distance between electrodes in mm	Maximum pulse amplitude in kv	Voltage at which voltage "collapse" occurred in kv.	Formative lag period in μ sec	Statistical delay time in μsec
I and *II*	Negative steel point and brass plane	150	60—132	25,5—34.0	423—348	—
III	"	100	77—115	30—43	202—180	—
IV—*VI*	Positive steel point and brass plane	150	53—185	39—125	0—10	184—0

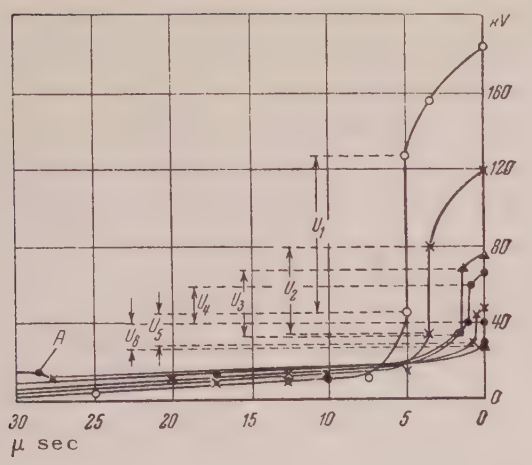

FIG. 4. Curves showing the decay of the voltage in the formation of a discharge in distilled water (positive point and plane); $U_1 = 84$; $U_2 = 44$; $U_3 = 34$; $U_4 = 22$; $U_5 = 16$; $U_6 = 12$ kV

tion and thermal ionization. During this stage the temperature of the column increases and gas is produced; this process is terminated with an "explosion" and the ejection of liquid[11]. At this point molecules of non-ionized liquid penetrate the column, the current diminishes, and there is a corresponding increase in the voltage (fourth stage; *A* of Fig. 4 and *C* of Oscillograph IV, Fig. 3).

It is evident from Oscillographs V and VI of Fig. 3 that even in the case of a very large overvoltage (3.5 times) a relatively long time (about 5 μsec) is reguired for the formation of the positive column which short-circuits the electrodes. During this period, as may be seen from the nicks in the front of the pulses in Oscillographs VI, small streamers are formed; these do not start breakdown but cause a certain amount of ionization in the gap. The development of the filamentary positive column from the positive point also depends on random factors. This is seen in Oscillographs IV of Fig .3 in which breakdown occurs after a lag of 184 μsec in one case and 52 μsec in the other although the amplitude of the applied pulse was the same in both cases.

Translated by H. Lashinsky
90

SOVIET PHYSICS JETP VOLUME 3, NUMBER 3 OCTOBER, 1956

Energy Spectrum of the Penetrating Particles of Extensive Cosmic Ray Showers

I. I. SAKVARELIDZE
Physics Institute, Georgian Academy of Sciences, USSR

(Submitted to JETP editor March 18, 1955)
J. Exptl. Theoret. Phys. (U.S.S.R.) 30, 458-463 (March, 1956)

The depth-intensity curve of penetrating shower particles absorbed in lead and rock of water equivalent of 3.7, 5.9, 27, 65.5 and 148 meters has been measured. The studies are carried out at an elevation of 400 meters above sea level. On the basis of the resulting path lengths, the integral energy spectrum of penetrating shower particles is found in the form of a power function. This function has the form $E^{-\gamma}$, where $\gamma = 0.62 \pm 0.05$ (for the energy interval from 5×10^8 to 3×10^{10} ev).

INVESTIGATION of the characteristics of penetrating shower particles is essential in connection with the mechanism of generation of extensive cosmic ray showers that is proposed by a group of Soviet students working under the guidance of Skobel'tsyn[1-4]. According to their idea, the formation of an extensive atmospheric shower appears to be the result of a nuclear-cascade process in which the main role is played by nuclear-active and penetrating components. The latter carry the major part of the energy of the whole shower, and determine the significant characteristics of the shower, its spatial structure, and the energy balance among its different components.

To this day, studies of the nature of extensive cosmic ray showers furnish the only key to understanding the interactions of high energy (of the order of 10^{15} - 10^{18} ev) particles with matter, and those physical processes which accompany these interactions. From this point of view, investiga-

[1] D. V. Skobel'tsyn, G. T. Zatsepin and V. V. Miller, Phys. Rev. 71, 315 (1947).

[2] D. V. Skobel'tsyn, Dokl. Akad. Nauk SSSR 67, 45 (1949).

[3] D. V. Skobel'tsyn, Dokl. Akad. Nauk SSSR 67, 225 (1949).

[4] G. T. Zatsepin, Dokl. Akad. Nauk SSSR 67, 993 (1949).

tion of the nuclear active and penetrating components of extensive showers holds the most interest. Nevertheless, these components of extensive cosmic ray showers remain relatively little studied. In particular, the mass spectrum of these components has not been investigated, nor has the spatial distribution of high energy penetrating particles along the radius of the shower. The goal of the present work is the investigation of the energy spectrum of penetrating particles of extensive cosmic ray showers.

1. EXPERIMENTAL ARRANGEMENT

In order to investigate the integral energy spectrum of penetrating shower particles, the attenuation of the intensity of these particles was studied by means of absorbers of various thicknesses. Lead and iron filters of a total thickness of 3.7 meters water equivalent were used in one series of experiments. Absorbing layers composed mainly of rocky soil of thicknesses 5.9, 27, 65.5 and 148 meters water equivalent were used in another series.

The measurements were carried out at an elevation of 400 meters above sea level. The intensity versus depth curve is dependent upon the energy spectrum of the penetrating components[5]. To obtain the one relationship from the other, it is necessary to use the relation between the energy and path length of penetrating particles. Let us deduce this relationship for μ-mesons, since at present it is generally accepted that the major part of the penetrating component of cosmic radiation underground consists of μ-mesons.[6,7] The loss of energy by fast μ-mesons can be represented, according to Wilson[7], by

$$dE/dx = a + bE + c\ln(E\cdot 10^{-3}). \qquad (1)$$

where E is expressed in mev. The first term on the right of Eq. (1) represents the magnitude of the energy lost by the fast μ-mesons in ionizing processes, the second term comprises radiation loss and the loss through nuclear interactions, and the third term gives the energy lost by the μ-mesons through Cerenkov radiation.

TABLE 1

Values of dE/dx (mev g/cm^2)

Energy in bev	a		bE		$c\ln(E\cdot 10^{-3})$	
	earth	lead	earth	lead	earth	lead
1	2.2	1.3	0.005	0.019	0	0
10	2.2	1.3	0.05	0.19	0.2	0.1
100	2.2	1.3	0.5	1.9	0.45	0.2
1000	2.2	1.3	5	19	0.7	0.3

From Table 1 it can be seen that at about 100 bev the term which is proportional to E becomes comparable in magnitude to the term representing the ionization losses.

For smaller energies, the ionization losses far exceed the other losses. In particular, in our case, where the maximum measurable energy of the particles does not exceed 3×10^{10} ev one needs to consider only the ionization losses. In this case, the energy loss versus path length relationship takes the form:

$$dE/dx = 2.2 \text{ mev g/cm}^2 \text{ for rock;}$$

$$dE/dx = 1.3 \text{ mev g/cm}^2 \text{ for lead.} \qquad (2)$$

Knowing the relationship between the energy and the path length of particles, and using the dependence of the intensity of the penetrating shower particles on the absorber thickness, one can obtain the integral energy spectrum by means of a well-known relationship[5].

2. MEASUREMENT TECHNIQUE

The measurement of the intensity of the penetrating shower particles under absorbers was carried out by means of Geiger-Mueller counters set up in an arrangement providing for two, three, and fourfold coincidences. The counters were connected

[5] L. Janossy, *Cosmic Rays*, p. 214 Sec. 11L 285 (Russian translation) 1949.

[6] C. A. Randall, Phys. Rev. 87, 241 (1952).

[7] G. Wilson, *Physics of Cosmic Rays*, p. 331 IIL, Moscow, Leningrad, (Russian translation) (1954).

in parallel, and were joined in rows in such a manner that the total effective area of each row equalled one square meter. In all, there were five such rows, three of which were arranged on top of the ground at the vertices of a right-angle triangle, with legs equal to 30 meters. The other two rows were placed one atop the other underground. Figure 1 shows the schematic arrangement of the rows.

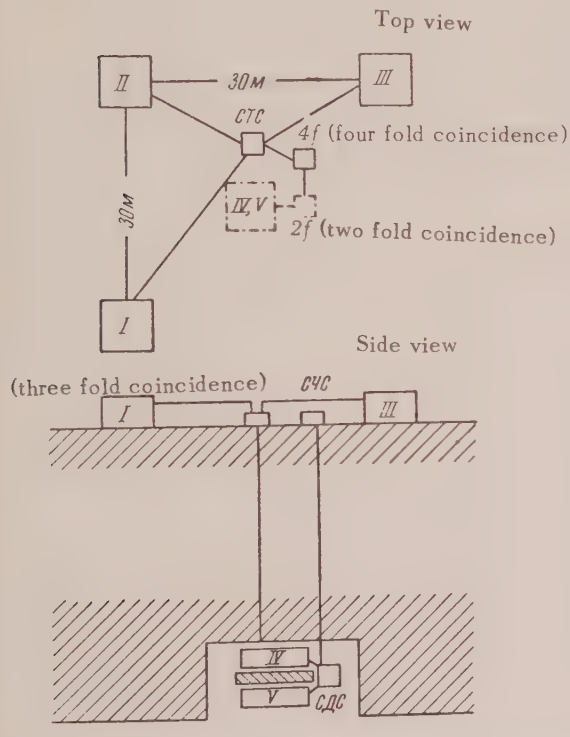

FIG. 1. *I, II, III, IV* and *V* rows of counters; *3f, 4f, 2f* scheme of 3, 4 and 2 fold coincidence.

The arrangement of rows I, II and III was not changed during the course of the entire experiment. Rows IV and V were moved in depth after each series of measurements. The impulses from counter rows I, II and III were channeled for three-fold coincidences. Each functioning of the three-fold coincidence system was caused by the passage of an extensive cosmic ray shower through the rows of counters. By this means, a three-fold coincidence of the impulses from the upper rows registered an extensive cosmic ray shower. The penetrating component of this shower was registered with the aid of the underground row of counters, whose impulse was channeled for coincidence with the master signal received from the three-fold coincidence of the upper counters. The underground part of the arrangement consisted of two rows. These two rows were of identical construction, were placed one above the other, and were connected for two-fold coincidence. This duplication of the rows registering underground particles was used to eliminate accidental coincidences between impulses from the upper and lower portions of the arrangement, which were not caused by shower particles. In several series of measurements eight centimeters of lead were placed between the two underground rows of counters.

The resolving time of the three and four-fold coincidence systems was 3.5×10^{-6} sec. For the two-fold coincidence systems it was 1.5×10^{-6} sec. Such a system of registering shower particles completely eliminated all possible false coincidences arising in separate parts of the arrangement. By means of this arrangement, the frequency of three-fold coincidences in the upper rows and the frequency of four-fold coincidences between impulses from the upper and lower rows was measured during the entire series of experiments. From the experimental values of three and four-fold coincidences per unit time with different absorber thicknesses, there were determined the intensities of penetrating shower particles at these depths (see Sec. 4 below).

3. RESULTS OF MEASUREMENTS

In Table 2 are given the pertinent properties of the absorbers which were used in the course of the work. In the first three cases, 8 cm of lead was placed between the underground counter rows IV and V (Fig. 1). In addition, measurements were made at a depth of 27 meters water equivalent of the increase in the number of coincidences upon removal of the lead absorber from between rows IV and V. During this trial no change was observed in the number of four-fold coincidences recorded. The remaining two series of measurements were carried out without any lead absorber between rows IV and V.

The resulting measurements of the frequency of three and four-fold coincidences are reported in Table 3.

4. COMPUTATION AND DISCUSSION OF RESULTS

The experimental results given in Table 3 furnish the means for establishing the relationship governing the decrease of the intensity of penetrating particles with increasing absorber thickness. We shall first ascertain the relationship between the intensity of penetrating shower particles at a given depth and the frequency of four-fold coincidences at that depth. The frequency of four-fold coincidences, produced by the passage of shower particles through four rows of counters, is equal to

TABLE 2

Absorbing material	Thickness	Density in gm/cm^3	Thickness in meters water equivalent.
Pb, Fe, Al	18 см Pb+ +8 см Fe+ +10 см Al+ +8 см Pb	11 7,3 2,7	3,7
Brick Masonry	2,7 м+ +8 см Pb	1,85	5,9
Rock	11,0 м	2,55	27,0
Rock	28,5 м	2,3	65,5
Rock	55,0 м	2,7	148,0

TABLE 3

Depth in meters water equivalent	Duration of measurements in hours	No. of 3-fold coinc.	No. of 4-fold coinc.	3-fold coinc. per hr.	4-fold coinc. per hr.	100 α
3,7	97	1360	107	13,9±0,7	1,1 ±0,1	3
5,9	118	1615	108	13,5±0,6	0,85±0,07	2,4
27	416	5720	120	13,6±0,4	0,29±0,03	0,75
65,5	554	7625	105	13,7±0,3	0,19±0,02	0,46
148	852	11 180	106	13,9±0,2	0,13±0,01	0,3

$$C_4 = A\int_0^\infty \rho^{-(\varkappa+1)} \prod_{i=1}^{4} (1 - e^{-\rho_i \sigma})\, d\rho. \qquad (3)$$

Here $A\rho^{-(\varkappa+1)}$ is the differential spectrum of the density of extensive cosmic ray showers, ρ_i is the density of shower particles falling on the ith row of counters, σ is the effective area of each row of counters.

To evaluate the integral (3), we must determine ρ_i with the aid of the spatial distribution function of the shower particles, taking into account the geometry of the experimental arrangement. However, considering the unwieldiness of the resulting expression and the fact that the spatial distribution function of the shower particles is not known with sufficient accuracy at large distances, such an evaluation cannot be justified. Instead, for a first approximation, we can assume that for recorded showers the densities ρ_i of particles falling on rows I, II and III respectively of the above-ground portion of the arrangement ($i = 1, 2, 3$), are identical and are equal to ρ. Furthermore, the density of penetrating particles ρ_4 will be equal to $\alpha\rho$, where α is the fraction of particles that consists of penetrating particles. Thus integral (3) takes the form

$$C_4 = A\int_0^\infty \rho^{-(\varkappa+1)} (1 - e^{-\rho})^3 (1 - e^{-\alpha\rho})\, d\rho. \qquad (4)$$

This takes into account that for our arrangement $\sigma = 1$. Similar integrals are investigated in detail in the works of Daudin[8] and Zatsepin[9], where the method of solution can be found.

Integral (4) can be broken up into two integrals: $C_4 = I_1 - I_2$ where

$$I_1 = A\int_0^\infty (1 - e^{-\rho})^3 \rho^{-(\varkappa+1)}\, d\rho; \qquad (5)$$

$$I_2 = A\int_0^\infty (1 - e^{-\rho})^3 e^{-\alpha\rho} \rho^{-(\varkappa+1)}\, d\rho.$$

Using the method shown in the latter reference[8] we obtain

$$I_1 = \frac{A\Gamma(3-\varkappa)}{\varkappa(\varkappa-1)(\varkappa-2)}[3 - 3\cdot 2^\varkappa + 3^\varkappa], \qquad (6)$$

$$I_2 = \frac{A\Gamma(3-\varkappa)}{\varkappa(\varkappa-1)(\varkappa-2)} \qquad (7)$$

$$\times\ [\alpha^\varkappa - 3(1+\alpha)^\varkappa + 3(2+\alpha)^\varkappa - (3+\alpha)^\varkappa].$$

[8] J. Daudin, J. Phys. Radium 8, 301 (1947).

[9] G. T. Zatsepin, Dissertation, FIAN, (1950).

Inserting the numerical value $x = 1.4$, we finally obtain

$$C_4 = \frac{A\Gamma(1.6)}{1.4 \cdot 0.4 \cdot 0.6}\,[0.262 + \alpha^{1.4} - 3\,(1+\alpha)^{1.4} + 3\,(2+\alpha)^{1.4} - (3+\alpha)^{1.4}]. \quad (8)$$

Knowing the number of four-fold coincidences per unit time C_4 at a given depth, it is possible to determine the fraction of penetrating particles α at this depth. To do this it would be necessary to insert a numerical value for A in equation (8). However, it is more convenient to compute α from the relationship between the frequency of four-fold coincidences and the frequency of three-fold coincidences. The frequency of the three-fold coincidence is:

$$C_3 = A \int_0^\infty (1 - e^{-\rho})^3 \rho^{-(x+1)}\, d\rho. \quad (9)$$

Equation (9) coincides with (6). For the ratio C_4/C_3 we obtain

$$\frac{C_4}{C_3} = 1 - \frac{\alpha^{1.4}}{0.262} - \frac{3}{0.262}(1+\alpha)^{1.4} + \frac{3}{0.262}(2+\alpha)^{1.4} - \frac{1}{0.262}(3+\alpha)^{1.4}. \quad (10)$$

The third, fourth and fifth terms of right side of equation (8) can be expanded in powers of α. Furthermore ,bearing in mind the small magnitude of α (a few percent), it is possible to disregard the terms containing α^2. Therefore

$$C_4 / C_3 = 3\,2\alpha\,(1 - 1.2\,\alpha^{0.4}). \quad (11)$$

Substituting experimental values of C_4 and C_3 into the left side of this expression from the fifth and sixth columns of Table 3, we obtain values for α which are given in the last column of Table 3.

Figure 2 shows the dependence of intensity on depth according to the data given in the first and last columns of Table 3. The ordinate is the logarithm of the intensity, and the abscissa is the logarithm of the effective depth expressed in meters of water. Within the limits of error, all experimental points lie on a straight line. Therefore the dependence of the intensity of penetrating particles on the depth can be expressed as a power function of the form

$$I = c_1 x^{-\gamma}. \quad (12)$$

The value of the exponent, as determined from the experimental results, is 0.62 ± 0.05.

Given the above, it is possible to construct the integral energy spectrum of the penetrating par-

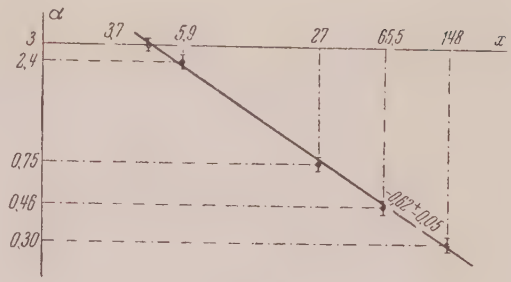

FIG. 2

ticles from the change of the intensity with depth. For this purpose we substitute the value of x obtained from expression (2) into (12); as a result we obtain:

$$N(>E) = c_2 E^{-\gamma}. \quad (13)$$

This is the expression for the energy spectrum of penetrating particles of extensive cosmic ray showers. Here N is the number of penetrating particles which have an energy greater than E. The constant C_2 represents the total number of penetrating particles in the entire shower at an elevation of 400 meters above sea level. The differential energy spectrum has the form:

$$NdN = c_3 E^{-(\gamma+1)}\, dE, \quad (14)$$

where NdN is the number of penetrating shower particles with energy lying between E and $E + dE$. With the aid of this spectrum, it is possible to find the lower limit of the mean energy of penetrating shower particles. For the limits of integration employed in finding the mean value, one must use the limiting values of the measurable energy, namely, 5×10^8 and 3×10^{10} ev. By carrying out the integration we obtain the value $\bar{E}_{min} = 1.7 \times 10^9$ ev for the lower limit of the mean energy of penetrating particles.

Comparing the energy spectrum of the penetrating particles of the vertical component of a cosmic shower at sea level[10] with the energy spectrum of the penetrating particles of extensive atmospheric showers, we come to the conclusion that shower particles are absorbed significantly more slowly than are the particles of the vertical component. This fact confirms the work of George[11]. George, comparing his results for measurements of extensive shower underground with the results of Greisen, was able to advance the hypothesis that the depth dependence of the intensity of penetrating shower particles must be a power relationship, with an ex-

[10] J. G. Wilson, Nature 158, 414 (1946).

[11] E. P. George, J. W. Mac Anuff and W. Sturgess, Proc. Phys. Soc A66, 346 (1953).

ponent equal to 0.66, down to depths of 1600 meters water equivalent.

The results of our direct measurements definitely confirm George's hypothesis. However, in spite of George's assertion, one must expect the curve of the energy spectrum to start falling sharply at certain depths significantly less than 1600 meters water equivalent in the contrary case, where the mean energy of penetrating shower particles becomes more like that reported by Eidus and co-workers[12]. For this reason, further investigation of the intensity of the penetrating components of extensive cosmic ray showers at significantly greater depths is of definite interest.

In conclusion, I wish to express my thanks to Professor E. L. Andronikashvili for proposing the problem and guiding the work; to Professors C. H. Vernov and G. T. Zatsepin for valuable discussions, and to M. F. Bibilashvili, G. N. Muskhelishvili, G. E. Chikovan and G. R. Khutsishvili for assistance rendered.

[12] L. Kh. Eidus, M. P. Adamovich, I. L. Ivanovskaia, V. S. Nikolaev and M. S. Tuliankina, J. Exptl. Theoret. Phys. (U.S.S.R.) 22, 440 (1942).

Translated by D. A Kellogg
89

SOVIET PHYSICS JETP VOLUME 3, NUMBER 3 OCTOBER, 1956

The Electromagnetic Field of a Linear Emitter Located inside an Ideally Conducting Parabolic Screen

G. G. GRINBERG, N. N. LEBEDEV, I. P. SKAL'SKAIA AND IA. S. UFLIAND
Leningrad Physico-technical Institute, Academy of Sciences, USSR

(Submitted to JETP editor, November 15, 1954)
J. Exptl. Theoret. Phys. (U.S.S.R.) 30, 528-543 (March, 1956)

On the basis of a critical examination of researches previously published, the inadequate basis of the results obtained in them is pointed out. A rigorous solution of the problem is given. It is also shown that the solution takes the form corresponding to the approximation of geometrical optics in the limiting case of very high frequencies.

AT first glance, the problem under consideration appears to be almost trivial, since the variables are separated in the basic equation of the problem. However, the desired choice of partial solutions, which can serve for the construction of the solution of the problem which satisfies all requirements, included the appropriate radiation principle at infinity, and the correct behavior at the focus of the cylinder, and the actual obtaining of such a solution is not so simple, as could be shown. In particular, nowhere, to our knowledge, in the series of researches[1-4] on the wave problem for a parabolic region, is any fundamental solution of the problem under consideration given in the desired form.* Such a problem is taken up in the present work. It is shown further that the solution, in the limiting case of very high frequencies, takes the form which corresponds to the ray approximation of optics.

1. STATEMENT OF THE PROBLEM

We consider the problem of the reflection of electromagnetic waves from a conducting screen which has the form of a parabolic cylinder. We assume a linear vibration source placed inside the cylinder along its focal line.** The current strength of the source is $I = I_0 e^{i\omega t}$, where I_0 = const = amplitude of the current, ω = angular frequency.

We set up a cartesian coordinate system (x, y, z) so that the axis Ox lies in the plane of symmetry of the parabolic cylinder, and the axis Oz coincides with the exciting current. In addition, we introduce the parabolic coordinates (α, β) with the help of the relations

*For more detail, see Sec. 1 of Ref. 5.

[1] Encyklopädie Math. Wissensch. 5, 3, 511.

[2] P. S. Epstein, Dissertation, Munich, 1914.

[3] W. Magnus, Jahresber. deut. Math. Verein. 50, 140 (1940).

[4] W. Magnus, Z. Physik 118, 343 (1941).

[5] G. A. Grinberg, N. N. Lebedev, I. P. Skal'skaia and Ia. S. Ufliand, Dokl. Akad. Nauk SSSR 95, 961 (1954).

*The case of arbitrary disposition of the source is considered in Sec. 8.

$$x + iy = {}^1/_2(\alpha + i\beta)^2, \tag{1.1}$$

$$-\infty < \alpha < +\infty, \quad 0 \leqslant \beta < \infty,$$

from which follow

$$x = {}^1/_2(\alpha^2 - \beta^2), \quad y = \alpha\beta. \tag{1.2}$$

Then the equation of the surface of the cylinder will be $\beta=\beta_0$ (Fig. 1), where β_0 is some constant.

The electric field vector E has in this case only the single component E_z of the form

$$E_z = E(x, y)\, e^{i\omega t} = Ee^{i\omega t} \tag{1.3}$$

To separate the field of the source, we write

$$E = E_0 + u, \tag{1.4}$$

where

$$E_0 = -\pi\omega I c^{-2} H_0^{(2)}(kr); \quad r = \sqrt{x^2 + y^2} = {}^1/_2(\alpha^2 + \beta^2), \tag{1.5}$$

$k = \omega/c$, c= velocity of light in a vacuum, $H_0^{(2)}(z)$ is the Hankel function of the second kind, u is the secondary electric field.

Since the electric field E must satisfy the Helm-Hotz equation $\Delta E + k^2 E = 0$, the radiation principle, and must vanish on the surface of the conducting screen, we can give the following mathematical formulation of the problem: to find the solution $E(\alpha, \beta)$ of the equation

$$(\partial^2 E / \partial\alpha^2) + (\partial^2 E / \partial\beta^2) + k^2(\alpha^2 + \beta^2) E = 0, \tag{1.6}$$

which is regular within the parabolic cylinder, except for the line $\alpha=\beta=0$, in the vicinity of which

$$E = -\frac{\pi\omega I}{c^2} H_0^{(2)}\left(k\,\frac{\alpha^2 + \beta^2}{2}\right) + u \tag{1.7}$$

(where u is a regular function), which satisfies the boundary condition

$$E|_{\beta=\beta_0} = 0 \tag{1.8}$$

and the radiation principle*

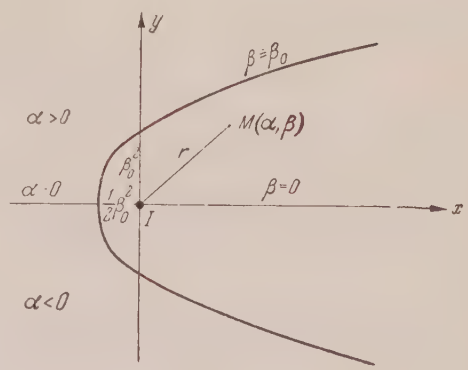

FIG. 1.

$$E|_{|\alpha|\to\infty} = O(|\alpha|^{-1/2}); \tag{1.9}$$

$$\left(\frac{1}{\alpha}\frac{\partial E}{\partial\alpha} + ikE\right)_{|\alpha|\to\infty} = o(|\alpha|^{-1/2})$$

(uniformly, relative to β).

It will be shown below (see Sec. 6) that the problem has a unique solution when stated in this way.

2. CONSTRUCTION OF A FORMAL SOLUTION OF THE PROBLEM

In order to separate variables in the wave equation

$$(\partial^2 u / \partial\alpha^2) + (\partial^2 u / \partial\beta^2) + k^2(\alpha^2 + \beta^2) u = 0 \tag{2.1}$$

we set

$$u = A(\alpha) B(\beta). \tag{2.2}$$

We then get for the factors A and B the ordinary differential equations

$$A'' + (k^2\alpha^2 + \lambda) A = 0; \tag{2.3}$$

$$B'' + (k^2\beta^2 - \lambda) B = 0,$$

where λ is the separation parameter.

Making the substitution

$$A(\alpha) = \exp\{-ik\alpha^2/2\}\, v(\xi); \quad \xi = \sqrt{ik}\,\alpha, \tag{2.4}$$

in the first of these equations, and setting

$$\lambda = ik(2\nu + 1), \tag{2.5}$$

we get an equation for the function $v(\xi)$:

$$v'' - 2\xi v' + 2\nu v = 0, \tag{2.6}$$

the general solution of which has the form

*Equations (1.9) follow in the usual way from the condition that the same amount of energy is radiated outwards (by the wave) across an arbitrary cross section α= const per unit time, if the waves returning from infinity, are absent.

$$v(\xi) = MF\left(-\frac{\nu}{2},\ \frac{1}{2},\ \xi^2\right) + N\xi F\left(\frac{1-\nu}{2},\ \frac{3}{2},\ \xi^2\right), \tag{2.7}$$

where M and N are constants;

$$F(a, b, z) = \frac{\Gamma(b)}{\Gamma(a)} \sum_{n=0}^{\infty} \frac{\Gamma(a+n)}{\Gamma(b+n)} \frac{z^n}{n!} \tag{2.8}$$

is the degenerate hypogeometric function.

Since the solution in our case must be an even function of the variable α, we must set $N=0$, so that*

$$A(\alpha) \equiv A_\nu^{(1)}(\alpha) = \exp\{-ik\alpha^2/2\} F(-\nu/2,\ {}^1/_2,\ ik\alpha^2) = (ika^2)^{-1/4} M_{\nu/2+1/4}(ik\alpha^2). \tag{2.9}$$

In this case we can limit ourselves to the interval $0 < \alpha < \infty$, which is done in what follows.

If we make use of the asymptotic expression for the function $A_\nu^{(1)}(\alpha)$ as $\alpha \to \infty$.**

$$A_\nu^{(1)}(\alpha)|_{\alpha\to\infty} \approx \varphi(\nu, \alpha) \exp\{ik\alpha^2/2\} \alpha^{-(\nu+1)} + \psi(\nu, \alpha) \exp\{-ik\alpha^2/2\} \alpha^\nu, \tag{2.10}$$

where φ and ψ are functions which approach finite limits as $\alpha \to \infty$, and if we require that the desired partial solutions have the character of waves going off to infinity, and indefinitely decreasing in amplitude, then we get the condition for the parameter ν:

$$-{}^1/_2 < \mathrm{Re}\{\nu\} < 0. \tag{2.11}$$

The general integral of the second of Eqs. (2.3) (for a given value of the parameter λ) will be

$$B = B_\nu(\beta) = \exp\{-ik\beta^2/2\} \times \left[PF\left(\frac{1+\nu}{2},\ \frac{1}{2},\ ik\beta^2\right) + Q\sqrt{ik}\,\beta F\left(1+\frac{\nu}{2},\ \frac{3}{2},\ ik\beta^2\right)\right], \tag{2.12}$$

where P and Q are constants.

From the condition of boundedness of grad u at the focus it follows that $Q=0$ *, so that

$$B_\nu(\beta) \equiv B_\nu^{(1)}(\beta) = \exp\{-ik\beta^2/2\} F\left(\frac{1+\nu}{2},\ \frac{1}{2},\ ik\beta^2\right) \tag{2.13}$$

Thus the chosen partial solutions of the wave equation (2.1) have the form

$$u_\nu = A_\nu^{(1)}(\alpha) B_\nu^{(1)}(\beta);\ -{}^1/_2 < R\{\nu\} < 0, \tag{2.14}$$

and the general solution of the problem can be hypothetically represented in the form of the following complex integral:

$$u(\alpha, \beta) = \int_{-\delta-i\infty}^{-\delta+i\infty} C(\nu) A_\nu^{(1)}(\alpha) B_\nu^{(1)}(\beta)\, d\nu; \quad 0 < \delta < {}^1/_2. \tag{2.15}$$

The unknown function $C(\nu)$ must be found from the boundary condition (1.8) i.e., from the equality

$$\int_{-\delta-i\infty}^{-\delta+i\infty} C(\nu) A_\nu^{(1)}(\alpha) B_\nu^{(1)}(\beta_0)\, d\nu = \frac{\pi\omega I}{c^2} H_0^{(2)}\left(k\,\frac{\alpha^2+\beta_0^2}{2}\right) (-\infty < \alpha < +\infty). \tag{2.16}$$

The problem is thus reduced to an expansion of the field of the source in an integral over the functions $A_\nu^{(1)}(\alpha)$. Such an expansion can be obtained with the aid of the expansion theorem of Magnus.[3]:

$$f(\alpha) = \int_{-\delta-i\infty}^{-\delta+i\infty} F(\nu) A_\nu^{(1)}(\alpha)\, d\nu; \tag{2.17}$$

$$F(\nu) = \frac{\sqrt{k}e^{-i\pi/4}}{2\pi^2} \Gamma\left(-\frac{\nu}{2}\right) \times \Gamma\left(\frac{\nu+1}{2}\right) e^{i\pi\nu/2} \int_0^\infty f(\alpha) A_\nu^{(1)}(\alpha)\, d\alpha$$

$(0 < \delta < 1)$, from which it follows that

$$C(\nu) = \frac{\omega\sqrt{k}\, I e^{-i\pi/4} \Gamma\left(-\frac{\nu}{2}\right) \Gamma\left(\frac{\nu+1}{2}\right) e^{i\pi\nu/2}}{2\pi c^2 B_\nu^{(1)}(\beta_0)} \times \int_0^\infty H_0^{(2)}\left(k\,\frac{\alpha^2+\beta^2}{2}\right) A_\nu^{(1)}(\alpha)\, d\alpha. \tag{2.18}$$

Making use of the value of the integral

*See, for example, Refs. 6,7.

**See Appendix A, Eq. (A-1), and also Ref. 8.

[6] W. Magnus and F. Oberheffinger, *Formeln und Satze f. d. spez. Funktionen der mathemat. Physik*, Berlin, Gottingen, Heidelberg.

[7] I. M. Ryzhik and I. S. Gradshtein, *Tables of integrals, sums, series and products*, GTTI, 1951.

[8] H. Jeffreys, *Methods of Mathematical Physics*, Cambridge, 1950.

*This result is obtained by means of a substitution of the partial solutions under consideration in Eq. (3.5) below.

$$\int_0^\infty H_0^{(2)}\left(k\,\frac{\alpha^2+\beta^2}{2}\right) A_\nu^{(1)}(\alpha)\,d\alpha \tag{2.19}$$
$$= (\pi k)^{-1/2} e^{i\pi/4} B_\nu^{(3)}(\beta),$$

where*

$$B_\nu^{(3)}(\beta) = (ik\beta^2)^{-1/4}\,\Gamma\left(\frac{\nu+1}{2}\right) W_{-1/4-\nu/2,\,1/4}(ik\beta^2) \tag{2.20}$$

($W_{\lambda,\mu}(z)$ is the Whittaker function[9]), we obtain the final solution of the problem:

$$u(\alpha,\ \beta) = \frac{\omega I}{2\pi\sqrt{\pi}\,c^2}\int_{-\delta-i\infty}^{-\delta+i\infty} \Gamma\left(-\frac{\nu}{2}\right) \tag{2.21}$$
$$\times\ \Gamma\left(\frac{\nu+1}{2}\right) e^{i\pi\nu/2}\,\frac{B_\nu^{(3)}(\beta_0)}{B_\nu^{(1)}(\beta_0)}\,B_\nu^{(1)}(\beta)\,A_\nu^{(1)}(\alpha)\,d\nu$$
$$\times\ (0<\delta<1/2).$$

It is obvious that the formal solution thus obtained needs detailed proof. Such proof is carried out in Sec. 5.

3. INVESTIGATION OF THE CONVERGENCE OF THE INTEGRAL WHICH REPRESENTS THE SECONDARY FIELD, AND PROOF OF THE REGULARITY OF THE RESULTANT SOLUTION

1. The functions under the integral in Eq. (2.21) are entire, and therefore continuous, functions of the variable ν. Since the function $B_\nu^{(1)}(\beta_0)$ does not vanish anywhere in the path of integration (see Appendix B), the existence of the integral over arbitrary finite limits is assured.

For the proof of the convergence of the integral over infinite limits, we make use of the asymptotic representations of the functions $A_\nu^{(1)}(\alpha)$, $B_\nu^{(1)}(\beta)$ and $B_\nu^{(3)}(\beta)$ for fixed α and β ($\alpha<A$, $0\leq\beta<\infty$), $|\nu|\to\infty$, $R\{\nu\}\geq-\delta>-1/2$*. Setting $\nu=-\delta+i\tau$, we have, for $\tau\to-\infty$:

$$|A_\nu^{(1)}(\alpha)| = O(1); \tag{3.1}$$
$$|B_\nu^{(1)}(\beta)| = O(\exp\{\sqrt{2k|\tau|}\,\beta\});$$
$$|B_\nu^{(3)}(\beta)| = O(|\tau|^{-1/2}\exp\{-\sqrt{2k|\tau|}\,\beta\}).$$

Since

$$\left|\Gamma\left(-\frac{\nu}{2}\right)\Gamma\left(\frac{\nu+1}{2}\right)e^{i\pi\nu/2}\right| = O(|\tau|^{-1/2}), \tag{3.2}$$

$$\left|\int_{-\delta-iT}^{-\delta-i\infty}\Gamma\left(-\frac{\nu}{2}\right)\Gamma\left(\frac{\nu+1}{2}\right)e^{i\pi\nu/2}\right.$$
$$\left.\times\frac{B_\nu^{(3)}(\beta_0)}{B_\nu^{(1)}(\beta_0)}B_\nu^{(1)}(\beta)\,A_\nu^{(1)}(\alpha)\,d\nu\right|$$
$$\leq M\int_T^\infty \exp\{-\sqrt{2k|\tau|}\,\beta_0\}\,\frac{d|\tau|}{|\tau|},$$

the uniform convergence of the integral (2.2) at the lower limit follows directly.

In precisely the same way, we find for $\tau\to+\infty$:

$$|A_\nu^{(1)}(\alpha)| = O(\exp\{\sqrt{2k\tau}\,\alpha\}); \tag{3.3}$$
$$|B_\nu^{(1)}(\beta)| = O(\tau^{-1/2});$$
$$|B_\nu^{(3)}(\beta)| = O\left(\frac{1}{\sqrt{\tau}}\right);$$
$$\left|\Gamma\left(-\frac{\nu}{2}\right)\Gamma\left(\frac{\nu+1}{2}\right)e^{i\pi\nu/2}\right| = O(\tau^{-1/2}e^{-\pi\tau}),$$

whence

$$\left|\int_{-\delta+iT}^{-\delta+i\infty}\Gamma\left(-\frac{\nu}{2}\right)\Gamma\left(\frac{\nu+1}{2}\right)e^{i\pi\nu/2}\right. \tag{3.4}$$
$$\left.\times\frac{B_\nu^{(3)}(\beta_0)}{B_\nu^{(1)}(\beta_0)}B_\nu^{(1)}(\beta)\,A_\nu^{(1)}(\alpha)\,d\nu\right|$$
$$\leq M\int_T^\infty e^{-\pi\tau}e^{\sqrt{2k\tau}}\,\frac{d\tau}{\sqrt{\tau}}$$

so that the integral (2.21) converges uniformly at the upper limit also.

It follows from the uniform convergence of the

---

*$B_\nu^{(3)}(\beta) = \Gamma\left(\frac{1}{2}\right)\frac{\Gamma\left(\frac{\nu+1}{2}\right)}{\Gamma(\nu/2)}B_\nu^{(1)}(\beta) + \Gamma(-1/2)\,B_\nu^{(2)}(\beta)$,

where

$$B_\nu^{(2)}(\beta) = e^{-ik\beta^2/2}\sqrt{ik}\,\beta F\left(1+\frac{\nu}{2},\ \frac{3}{2},\ ik\beta^2\right)$$

is the odd solution of the second of Eqs. (2.3)

*Equations (A-3) (A-4), (A-5).

[9] E. T. Whittaker and G. N. Watson, *Modern Analysis*.

integral (2.21) that u is a continuous function of the variables α and β in the region under consideration.

2. For proof of the regularity of the function u, we must satisfy ourselves of the existence and continuity of its first and second derivatives with respect to x and y, for which it is sufficient to show the unifrom convergence of the integrals which are obtained after carrying out differentiation under the integral sign.

From the estimate as $\tau \to -\infty$,

$$|A_\nu^{(1)\prime}(\alpha)| = O(|\tau|);$$

$$|B_\nu^{(1)\prime}(\beta)| = O(|\tau| \exp\{\sqrt{2k|\tau|}\beta\})$$

there follows the uniform convergence at the lower limit of the integrals obtained from Eq. (2.21) by differentiation with respect to α and β under the integral sign. In exactly the same way, there follows from $\tau \to +\infty$,

$$|A_\nu^{(1)\prime}(\alpha)| = O(\tau \exp\{\sqrt{2k\tau}\,\alpha\});$$

$$|B_\nu^{(1)\prime}(\beta)| = O(\tau)$$

the uniform convergence of these integrals at the upper limit. In a similar way, the existence and continuity of the derivatives of u of arbitrary order with respect to α and β can be demonstrated.

We now consider the derivatives of u with respect to x and y, which are given by the expressions

$$\frac{\partial u}{\partial x} = \frac{\alpha}{\alpha^2+\beta^2}\frac{\partial u}{\partial \alpha} - \frac{\beta}{\alpha^2+\beta^2}\frac{\partial u}{\partial \beta}; \tag{3.5}$$

$$\frac{\partial u}{\partial y} = \frac{\alpha}{\alpha^2+\beta^2}\frac{\partial u}{\partial \beta} + \frac{\beta}{\alpha^2+\beta^2}\frac{\partial u}{\partial \alpha}.$$

It follows from these equations that $\partial u/\partial x$ and $\partial u/\partial y$ are continuous everywhere in the region under consideration, with the exception, perhaps, of the point $\alpha=\beta=0$, in the vicinity of which an additional investigation is necessary. We set

$$\alpha = r\cos\theta;\ \beta = r\sin\theta\ (0 \leqslant \theta \leqslant \pi) \tag{3.6}$$

and consider the expression

$$\frac{\partial u}{\partial x} = \frac{\omega I}{2\pi\sqrt{\pi}\,c^2}\int_{-\delta-i\infty}^{-\delta+i\infty}\Gamma\left(-\frac{\nu}{2}\right)\Gamma\left(\frac{\nu+1}{2}\right)e^{i\pi\nu/2}\frac{B_\nu^{(3)}(\beta_0)}{B_\nu^{(1)}(\beta_0)}\chi_\nu(r)\,d\nu, \tag{3.7}$$

where

$$\chi_\nu(r) = \frac{1}{r}[\cos\theta\, B_\nu^{(1)}(r\sin\theta)\, A_\nu^{(1)\prime}(r\cos\theta) - \sin\theta\, A_\nu^{(1)}(r\cos\theta)\, B_\nu^{(1)\prime}(r\sin\theta)]. \tag{3.8}$$

Since the quantity $\chi_\nu(r)$ approaches a finite limit as $r \to 0$, equal to $-ik(2\nu+1)$, and uniform convergence of the integral (3.7) in the region $r \leqq r_0$ follows from the estimate

$$|\chi_\nu(r)|_{|\tau|\to\infty} = O(|\tau| \exp\{\sqrt{2k|\tau|}\,r_0\}),$$

we can allow a transition to the limit under the integral sign. Then

$$\lim_{r\to 0}\frac{\partial u}{\partial x} = -\frac{ik\omega I}{2\pi\sqrt{\pi}\,c^2}\int_{-\delta-i\infty}^{-\delta+i\infty}\Gamma\left(-\frac{\nu}{2}\right)\Gamma\left(\frac{\nu+1}{2}\right)e^{i\pi\nu/2}(2\nu+1)\frac{B_\nu^{(3)}(\beta_0)}{B_\nu^{(1)}(\beta_0)}\,d\nu.$$

This integral does not depend on θ, which also proves the continuity of the derivative $\partial u/\partial x$ in the vicinity of the point $\alpha=\beta=0$.

As regards the limit of the derivative $\partial u/\partial y$ for

$r \to 0$, the analogous expressions show that $\lim_{r \to 0} \partial u/\partial y = 0$, i.e., the derivative is also continuous in the vicinity of the point. In similar fashion we can establish the continuity of the second derivatives of u with respect to x and y.

Hence it has been shown that $u(\alpha, \beta)$ is a regular function in the entire region $\alpha < A$, $0 \leq \beta < \beta_0$.

4. TRANSFORMATION OF THE SOLUTION TO DIFFERENT FORMS

For subsequent examination of the formal solution that has been obtained, it is expedient first to transform it to other forms.

1. In order to obtain the first of these representations, we complete the contour of integration in the formula (2.21) on the right by another circle of radius $R \to \infty$, drawn from the point $\nu = -1/2$. and apply the theorem of residues. The asymptotic expressions for the functions of a parabolic cylinder* show that the integral over the path, under fulfillment of the condition

$$\alpha < 2\beta_0 - \beta \tag{4.1}$$

in every case tends to zero.

If the inequality (4.1) holds then u, after calculation of the residues at the poles $\nu = 2n$, has the form of the following series:

$$u = \frac{2\omega i I}{c^2 \sqrt{\pi}} \sum_{n=0}^{\infty} \frac{\Gamma(n + 1/2)}{\Gamma(n+1)} \frac{B_{2n}^{(3)}(\beta_0)}{B_{2n}^{(1)}(\beta_0)} B_{2n}^{(1)}(\beta) A_{2n}^{(1)}(\alpha). \tag{4.2}$$

The corresponding transformation of the contour integral (2.16)-(2.18) for the primary field reduces to the analogous expression

$$H_0^{(2)}\left(k \frac{\alpha^2 + \beta^2}{\alpha}\right) = \frac{2i}{\pi^{3/2}} \sum_{n=0}^{\infty} \frac{\Gamma(n + 1/2)}{\Gamma(n+1)} B_{2n}^{(3)}(\beta) A_{2n}^{(1)}(\alpha), \tag{4.3}$$

which is valid under the condition that

$$\alpha < \beta. \tag{4.4}$$

We note that the functions $A_{2n}^{(1)}(\alpha)$ are simply related to the Hermite polynomials:

$$A_{2n}^{(1)}(\alpha) = (-1)^n \frac{n!}{(2n)!} \exp\{-ik\alpha^2/2\} H_{2n}(\sqrt{ik}\,\alpha). \tag{4.5}$$

Thus, our solutions for the case $\alpha < \beta$ can always be represented in the form of a series in the Hermite polynomials $H_{2n}((\sqrt{ik}\,\alpha).)/.$: In regard to the region $\alpha > \beta$, we can demonstrate, by direct investigation of the convergence of the series (4.3) that it converges for $\alpha > \beta$. Similarly, the series (4.2) is convergent* for $\alpha > 2\beta_0 - \beta$. Summing up, we can say that the decomposition of the total field into a series of Hermite polynomials is valid only in those parts of the region which are determined by the inequality $\alpha < \beta$. Thus, there does not exist a single analytical representation of the desired solution in the form of a series of Hermite polynomials.**

2. A solution of the problem has been given by Magnus[4] in the form

$$u = \frac{\omega I}{2\pi c^2} \int_{-\delta - i\infty}^{-\delta + i\infty} \frac{B_\nu^{(3)}(\beta_0)}{B_\nu^{(1)}(\beta_0)} B_\nu^{(1)}(\beta) A_\nu^{(3)}(|\alpha|)\, d\nu \quad (0 < \delta < 1/2), \tag{4.6}$$

where

$$A_\nu^{(3)}(\alpha) = B_{-\nu-1}^{(3)}(\beta). \tag{4.7}$$

Inasmuch as Magnus did not establish the regularity of his solution for an arbitrary point within the region of interest, it is not possible, without further investigation, to draw any conclusions as to the correctness of his solution. A detailed investigation is all the more necessary in that the partial solutions $A_\nu^{(3)}(|\alpha|)\beta_\nu^{(1)}(\beta)$ given by Magnus do not possess the property of regularity in the vicinity of the point $\alpha = \beta = 0$.

Coincidence of the solution of Magnus (4.6) with our solution (2.21) in there common region of regularity can be established by means of the addition of an integration contour in (4.6) on the right of another circle of radius $R \to \infty$ (which is permissible for $\alpha < 2\beta_0 - \beta$) and computation of the residues at the poles $\nu = 2n$. In this case, since the

*See Eqs. (A-3) - (A-5).

*The convergence of these series has been investigated with the help of the asymptotic expressions for the Hermite polynomials for $n \to \infty$.

*This circumstance has evidently not been noted properly in the literature.

previous formula (4.2) is obtained, then, by virtue of the known properties of the solution of equations of the elliptic type, the identity of the solutions (4.6) and (4.2) takes place wherever the two solutions are regular.

We also note that the field of the source can also be decomposed into integrals of the functions $A_\nu^{(3)}(|\alpha|)$:

$$H_0^{(2)}\left(k\,\frac{\alpha^2+\beta^2}{2}\right)=\frac{1}{2\pi^2}\int\limits_{-\delta-i\infty}^{-\delta+i\infty} B_\nu^{(3)}(\beta)\,A_\nu^{(3)}(|\alpha|)\,d\nu \qquad (0<\delta<1), \tag{4.8}$$

this decomposition is valid in all regions, with the exception of the line $\beta=0$.*

3. On the basis of the results obtained in Sec. 2, the complete solution E can be represented by the following integral**

$$E=\frac{\omega I}{2\pi c^2}\int\limits_{-\delta-i\infty}^{-\delta+i\infty}[B_\nu^{(1)}(\beta_0)\,B_\nu^{(2)}(\beta) - B_\nu^{(2)}(\beta_0)\,B_\nu^{(1)}(\beta)]\,\frac{A_\nu^{(3)}(|\alpha|)}{B_\nu^{(1)}(\beta_0)}\,d\nu \quad (\beta>0), \tag{4.9}$$

which allows us to obtain still another form of the solution, which is extremely useful for what follows.

We complete the contour of integration with another circle $R\to\infty$ at the left, and make use of the theorem of residues. Since the poles of the integrand are the roots of equation

$$B_{\nu_n}^{(1)}(\beta_0)=0 \qquad (n=1,\ 2,\ 3,\ \ldots), \tag{4.10}$$

located, as shown in Appendix B, to the right of $Re\{\nu\}=-1/2$, where $\mathrm{Im}\{\nu_1\}<\mathrm{Im}\{\nu_2\}<\ldots$, and the integral along the path approaches zero, we obtain

$$E=-\frac{2\sqrt{\pi}\,ik\,I}{c}\sum_{n=1}^{\infty}\frac{B_{\nu_n}^{(2)}(\beta_0)\,B_{\nu_n}^{(1)}(\beta)}{[dB_\nu^{(1)}(\beta_0)/d\nu]_{\nu=\nu_n}}\,A_{\nu_n}^{(3)}(|\alpha|). \tag{4.11}$$

Calculation of the derivative in the square brackets leads to the following decomposition of E in a series of functions $B_{\nu n}^{(1)}(\beta)$:

$$E(\alpha,\ \beta)=-\frac{I\sqrt{\pi}\,ik}{c}\times\sum_{n=1}^{\infty}B_{\nu_n}^{(1)}(\beta)\,A_{\nu_n}^{(3)}(|\alpha|)\Big/\int\limits_0^{\beta_0}B_{\nu_n}^{(1)2}(\beta)\,d\beta. \tag{4.12}$$

Such a form of the solution will be used in the following Section for proof of the fact that the solution of the problem satisfies the boundary condition and the radiation principle.

We also note that the decomposition (4.12) can be obtained directly by integration of the wave equation

$$(\partial^2E/\partial\alpha^2)+(\partial^2E/\partial\beta^2)+k^2(\alpha^2+\beta^2)\,E=4\pi i\omega c^{-2}(\alpha^2+\beta^2)\,j, \tag{4.13}$$

if we consider the current density to be uniformly distributed over a small region about the focus:

$$j(\alpha,\ \beta)=\begin{cases} I/2(\alpha^2+\beta^2)\,\alpha_1\beta_1 & \text{for } |\alpha|<\alpha_1,\quad 0\leqslant\beta<\beta_1,\\ 0 & \text{for other values of } \alpha \text{ and } \beta,\end{cases}$$

while, in what follows, α, β, approach zero.

5. PROOF OF THE EQUATION OBTAINED FORMALLY

It follows from the results of Sec. 3 that the function u constructed above, which is defined by Eq. (2.21), is a regular solution of the Helmhotz equation at every point of the region under examination. As far as the complete solution E is concerned, this, being the sum of the field of the linear radiator which proceeds across the focus, and the function u, it evidently satisfies the Helmhotz equation at all points of the region except the focus, where it has a singularity of the required type.

It is then left to prove that the solution $E(\alpha,\beta)$ satisfies the boundary condition and the radiation

*See Ref. 4.

*Here we make use of the relation $B_\nu^{(3)}(\beta_0)\,B_\nu^{(1)}(\beta) - B_\nu^{(1)}(\beta_0)\,B_\nu^{(3)}(\beta)=2\sqrt{\pi}\,[B_\nu^{(1)}(\beta_0)\,B_\nu^{(2)}(\beta) - B_\nu^{(2)}(\beta_0)\,B_\nu^{(1)}(\beta)]$

principle. Such a proof can be carried out with the help of the form of Equation (4.12).

1. Since the eigenfunctions $B_{\nu n}^{(1)}(\beta)$ satisfy the boundary condition $B_{\nu n}^{(1)}(\beta_0)=0$, to prove that the boundary condition $E(\alpha,\beta_0)=0$ is satisfied, it suffices to establish the uniform convergence of the series (4.12) in the interval $0<\beta\leqq\beta_0$.

Making use of the asymptotic expressions for the functions $B_\nu^{(1)}(\beta)$ and $A_\nu^{(3)}$ for $\nu_n=-1/2+i\tau_n$ ($\tau_n\to\infty$):

$$B_{\nu_n}^{(1)}(\beta)\approx\cos\sqrt{2ki\tau_n}\,\beta; \tag{5.1}$$

$$A_{\nu_n}^{(3)}(\alpha)\approx 2\sqrt{2\pi i/\tau_n}\exp\{-\sqrt{2k\tau_n}\,\alpha\},$$

and also Eq. (B-2)

$$\tau_n\Big|_{n\to\infty}\approx\frac{1}{2k\beta_0^2}\left(\frac{2n-1}{2}\pi\right)^2, \tag{5.2}$$

we find that the terms of the series (4.12) will be of the order

$$n^{-1}\exp\left\{-\frac{2n-1}{2\beta_0}\pi\alpha\right\},$$

from which follows the uniform convergence of the series in the region of interest. At the same time, satisfaction of the boundary condition is proved.

2. In order to demonstrate that the solution we have obtained satisfies the radiation principle (1.9), it suffices to show that the following two equations are satisfied:

$$|u|_{\alpha\to\infty}=O(\alpha^{-1/2}); \tag{5.3}$$

$$\left|\frac{1}{\alpha}\frac{\partial u}{\partial\alpha}+iku\right|_{\alpha\to\infty}=o(\alpha^{-1/2}).$$

From the estimate for $n\to\infty$,

$$\left|\frac{B_{\nu_n}^{(1)}(\beta)}{\int_0^{\beta_0}B_{\nu_n}^{(1)2}(\beta)\,d\beta}\right|=O(1),\quad |A_{\nu_n}^{(3)}(\alpha)|=\alpha^{-1/2}O(n^{-5/2}), \tag{5.4}$$

the correctness of the first part of the radiation principle follows at once.

Differentiating the series (4.12) and making use of the estimate

$$\left|\frac{1}{\alpha}A_{\nu_n}^{(3)\prime}(\alpha)+ikA_{\nu_n}^{(3)}(\alpha)\right|_{n\to\infty} \tag{5.5}$$

$$=\alpha^{-5/2}O(n^{-5/2}),$$

investigated in Appendix C, which is valid for arbitrary α, we have the equality

$$\left|\frac{1}{\alpha}\frac{\partial u}{\partial\alpha}+iku\right|_{\alpha\to\infty}=O(\alpha^{-5/2}),$$

whereby the second part of the radiation principle is established.

Thus the solution of the problem obtained formally in Sec. 2 satisfies all the conditions set forth in Sec. 1 in its mathematical formulation.

6. UNIQUENESS THEOREM

The solution of the Helmholtz equation

$$\Delta v+k^2v=0, \tag{6.1}$$

is regular in the region (D), bounded by the branch of the parabola $\beta=\beta_0$ and the abscissa, satisfies the boundary conditions

$$v|_{\beta=\beta_0}=0,\quad \partial v/\partial y|_{y=0}=0 \tag{6.2}$$

and the radiation principle**

$$v\Big|_{\alpha\to\infty}=O(\alpha^{-1/2}); \tag{6.3}$$

$$\frac{1}{\alpha}\frac{\partial v}{\partial\alpha}+ikv\Big|_{\alpha\to\infty}=o(\alpha^{-1/2}),$$

is identically equal to zero.

For proof, we consider the region (D'), bounded by the x axis, the branch of the parabola $\beta=\beta_0$ and the branch of the parabola $\alpha=A$ orthogonal to it. Multiplying Eq. (6.1) by the conjugate function $\bar{v}$, and the conjugate function by v, calculating the one from the other and integrating over the area (D'), we obtain [making use of Green's theorem and the condition (6.2)]:

*The second estimate of (5.4), which is investigated in Appendix C, is uniform relative to α.

**And similarly for the variable β.

$$\int_0^{\beta_0}\left(\bar{v}\frac{\partial v}{\partial\alpha}-v\frac{\partial\bar{v}}{\partial\alpha}\right)_{\alpha=A}d\beta=0. \tag{6.4}$$

Making use of the relation

$$\frac{1}{\alpha}\left(\bar{v}\frac{\partial v}{\partial\alpha}-v\frac{\partial\bar{v}}{\partial\alpha}\right) \tag{6.5}$$

$$=-2ik|v|^2+\bar{v}o(\alpha^{-1/2})-vo(\alpha^{-1/2})$$

which follows from the radiation principle, and taking into consideration the fact that as $\alpha\to\infty$ the products $\alpha^{1/2}v$ and $\alpha^{1/2}\ v$ are bounded quantities, we obtain the following equality from Eq. (6.4):

$$\lim_{\alpha\to\infty}\int_0^{\beta_0}\alpha|v|^2d\beta=0. \tag{6.6}$$

In order to show that the identity $v=0$ follows from Eq. (6.6), we consider the following partial solution of the Helmholtz equation:

$$u_n=A^{(3)}_{\nu_n}(\alpha)B^{(1)}_{\nu_n}(\beta), \tag{6.7}$$

where ν_n are the roots of the equation $B^{(1)}_{\nu n}(\beta_0)=0$. These solutions are regular in the region (D''), which is bounded by the parabola $\beta=\beta_0$, $\alpha=\epsilon>0$, $\alpha=A$ and the x axis, and satisfy the boundary conditions

$$u_n|_{\beta=\beta_0}=0;\ \partial u_n/\partial\beta|_{\beta=0}=0 \tag{6.8}$$

and the radiation principle (6.3).

Applying Green's formula to the region (D'') for the pair of functions (v, u_n), we get

$$\int_0^{\beta_0}\left(u_n\frac{\partial v}{\partial\alpha}-v\frac{\partial u_n}{\partial\alpha}\right)_{\alpha=\varepsilon}d\beta \tag{6.9}$$

$$=\int_0^{\beta_0}\left(u_n\frac{\partial v}{\partial\alpha}-v\frac{\partial u_n}{\partial\alpha}\right)_{\alpha=A}d\beta.$$

From this it follows that the value of the integral

$$\int_0^{\beta_0}\left(u_n\frac{\partial v}{\partial\alpha}-v\frac{\partial u_n}{\partial\alpha}\right)d\beta$$

does not depend on α, and, since as $\alpha\to\infty$ this integral approaches zero (on the basis of the radiation principle), then

$$\int_0^{\beta_0}\left(u_n\frac{\partial v}{\partial\alpha}-v\frac{\partial u_n}{\partial\alpha}\right)d\beta=0 \text{ for arbitrary } \alpha. \tag{6.10}$$

Substituting here the value of u_n, and assuming

$$v_n=\int_0^{\beta_0}vB^{(1)}_{\nu_n}d\beta\Big/\int_0^{\beta_0}B^{(1)^2}_{\nu_n}d\beta\quad(n=1,\ 2,\ 3,\ \ldots), \tag{6.11}$$

we find

$$A^{(3)}_{\nu_n}(\alpha)\frac{dv_n}{d\alpha}=v_n\frac{dA^{(3)}_{\nu_n}(\alpha)}{d\alpha},$$

whence

$$v_n=c_nA^{(3)}_{\nu_n}(\alpha), \tag{6.12}$$

where c_n is a constant.

Since the system of functions $B_{\nu n}(\beta)$ is closed*, i.e.,

$$\sum_{n=1}^{\infty}|v_n|^2\int_0^{\beta_0}B^{(1)^2}_{\nu_n}d\beta=\int_0^{\beta_0}|v|^2d\beta, \tag{6.13}$$

then it follows from Eq. (6.6) that $\lim_{\alpha\to\infty}\alpha|v_n|^2=0$ or, on the basis of Eq. (6.12),

$$|c_n|^2\lim_{\alpha\to\infty}\alpha|A^{(3)}_{\nu_n}|^2=0. \tag{6.14}$$

But the asymptotic expression for the function $A^{(3)}_{\nu n}(\alpha)$ as $\alpha\to\infty$** shows that the product $\alpha|A^{(3)}_{\nu n}(\alpha)|^2$ does not approach zero as $\alpha\to\infty$, so that $c_n=0$, i.e.,

$$v_n=0;\ n=1,\ 2,\ 3,\ \ldots \tag{6.15}$$

By virtue of the closure condition (6.13), we have $\nu=0$ for arbitrary $\alpha>0$ and $0\leq\beta\leq\beta_0$, which also was to be proved.

7. INVESTIGATION OF THE SOLUTION FOR LARGE VALUES OF THE WAVE NUMBER k. TRANSITION TO GEOMETRIC OPTICS

We shall investigate the behavior of the solu-

*This follows from the general theory of eigenfunctions associated with differential equations of second order.

**See Eq. (A-2).

tion obtained in Sec. 2 as $k \to \infty$, which should correspond to the case of geometric optics. To investigate the behavior as $k \to \infty$ of the secondary field, we make use of the following asymptotic formulas:

$$B_\nu^{(1)}(\beta)|_{k\to\infty} \approx \frac{\sqrt{\pi}}{\Gamma((\nu+1)/2)}(ik\beta^2)^{\nu/2}e^{ik\beta^2/2}; \tag{7.1}$$

$$B_\nu^{(3)}(\beta)|_{k\to\infty} \approx \Gamma\left(\frac{\nu+1}{2}\right)(ik\beta^2)^{-(1+\nu)/2}e^{-ik\beta^2/2}, \quad R\{\nu\} > -{}^1/_2,$$

which were obtained from Eqs. (A-1) and (A-2) by replacing ν by $-\nu-1$, taking the relation $A_\nu(\alpha) = B_{-\nu-1}(\alpha)$ into account.

Substitution of (7.1) into (2.21) leads to the expression:

$$u(\alpha, \beta)|_{k\to\infty} \approx \frac{I\sqrt{k}\,e^{-i\pi/4}}{2\pi\sqrt{\pi}\,c\beta_0}\exp\left\{\frac{ik}{2}(\beta^2-2\beta_0^2)\right\}I_1; \tag{7.2}$$

$$I_1 = \int_{-\delta-i\infty}^{-\delta+i\infty}\Gamma\left(-\frac{\nu}{2}\right)\Gamma^2\left(\frac{\nu+1}{2}\right)k^{-\nu/2}\left(\frac{\beta_0^2}{\beta}\right)^{-\nu}e^{i\pi\nu/4}A_\nu^{(1)}(\alpha)\,d\nu.$$

In calculating the integral I_1 we make use of the integral representation (A-6) which, when substituted in Eq. (7.2), yields

$$I_1 = \frac{\sqrt{2k}}{c\beta_0}\exp\left\{-\frac{i\pi}{4}-\frac{ik}{2}(\beta^2-2\beta_0^2)\right\}\int_{-\infty}^{\infty}\exp\left\{\frac{\theta}{2}-\frac{ik\alpha^2}{2}\operatorname{th}\theta\right\}\frac{I_2 d\theta}{\sqrt{\operatorname{ch}\theta}}; \tag{7.3}$$

$$I_2 = \frac{1}{2\pi i}\int_{-\delta-i\infty}^{-\delta+i\infty}\Gamma\left(\frac{\nu+1}{2}\right)e^{\nu\theta}k^{-\nu/2}\left(\frac{\beta_0^2}{\beta}\right)^{-\nu}e^{i\pi\nu/4}d\nu.$$

We make the substitution $\nu = 2\mu - 1$ in the complex integral. Denoting $2\delta' = 1 - \delta$, we have

$$I_2 = \frac{2\beta_0^2}{\sqrt{k}\beta}\exp\left(-\frac{i\pi}{4}-\theta\right)\frac{1}{2\pi i}\int_{\delta'-i\infty}^{\delta'+i\infty}\Gamma(\mu)\left(-ike^{-2\theta}\frac{\beta_0^4}{\beta^2}\right)^{-\mu}d\mu,$$

whence*

$$I_2 = 2\sqrt{k}\left(\frac{\beta_0^2}{\beta}\right)\exp\left\{-\frac{i\pi}{4}-\theta+ik\frac{\beta_0^4}{\beta^2}e^{-2\theta}\right\}. \tag{7.4}$$

Substituting (7.4) in (7.3), and carrying out the substitution $e^{-\theta} = x$ in the integral I_1, we get

$$u|_{k\to\infty} \approx \frac{4kI\beta_0}{c\beta}\exp\left\{\frac{ik}{2}(\beta^2-2\beta_0^2)\right\}\int_0^\infty \times \exp\left\{-\frac{ik\alpha^2}{2}\frac{1-x^2}{1+x^2}+ik\frac{\beta_0^4}{\beta^2}x^2\right\}\frac{dx}{\sqrt{1+x^2}}. \tag{7.5}$$

As $k \to \infty$ the principal contribution to the latter integral comes from the neighborhood of the point $x = 0$. Therefore

$$u|_{k\to\infty} = \frac{1}{\sqrt{c}}2I(\pi k)^{1/2}[\beta_0^2+(\alpha\beta/\beta_0)^2]^{-1/2} \times \exp\left\{\frac{i\pi}{4}-ik\beta_0^2-\frac{ik}{2}(\alpha^2-\beta^2)\right\}. \tag{7.6}$$

Transforming to cartesian coordinates, and taking into account the relation $s = OA + AM = 1/2(\alpha^2+\beta^2)+\beta_0^2$ (Fig. 2), we can transform Eq. (7.6) to the form

$$u|_{k\to\infty} \approx \frac{2I}{c\beta_0}\left(\frac{\pi k}{1+(y/\beta_0)^2}\right)^{1/2}e^{i\pi/4-iks}. \tag{7.7}$$

It is immediately evident that the index s, which appears in the phase factor, represents the path OAM which that ray would follow which sets out

*Here we make use of the relation

$$e^{-x} = \frac{1}{2\pi i}\int_{\delta'-i\infty}^{\delta'+i\infty}\Gamma(\mu)\,x^{-\mu}\,d\mu.$$

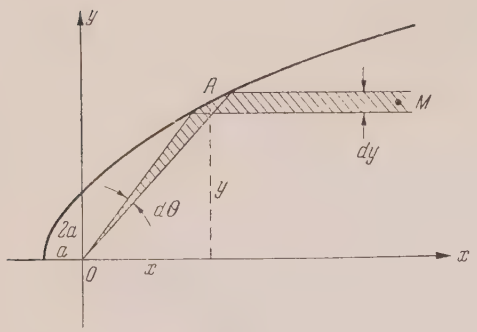

FIG. 2.

from the focus O and falls on the point M as a result of reflection (according to the laws of geometric optics) from the surface of the parabolic cylinder.

So far as the amplitude factor in Eq. (7.7) is concerned, we can demonstrate that it also corresponds to the approximation of geometric optics. In fact, computing the mean over a period, of the density p of energy flow incident at a certain point M^{**} :

$$p = (c/16\pi)(u^* H_y - u H_y^*), \tag{7.8}$$

and using the asymptotic representations for H_y [coincident with Eq. (7.7)], we get

$$p|_{k\to\infty} \approx (kI^2/2c\beta_0^2)/[1+(y/\beta_0^2)^2], \tag{7.9}$$

On the other hand, we can get this same expression by starting out with the laws of geometric optics, if we calculate the electromagnetic energy $\frac{W}{2\pi}d\theta = \frac{W}{2\pi|dy/d\theta|}|dy| = p|dy|$, which is transmitted per unit time across an area of height dy in the vicinity of the point M (Fig. 2); here, $W = \pi k I^2/2c$ denotes the time average of the amount of energy radiated by the source per unit length. From the geometric relations $\tan\theta = y/x$, $y^2 = 2\beta_0^2(x+\beta_0^2/2)$, we find that

$$y = \beta_0^2 \operatorname{ctg}\frac{\theta}{2};\quad \frac{dy}{d\theta} = -\frac{\beta_0^2}{2}\left[1+\left(\frac{y}{\beta_0}\right)^2\right],$$

whence the above expression (7.9) is obtained for the quantity p.

Thus the solution of the problem in the limiting case k transforms us to the approximation of geometric optics.

**Here we neglect the component H_x of the secondary magnetic field, since it is of the order of $1/k$ in comparison with H_y.

8. GENERAL SOLUTION IN THE CASE OF AN ARBITRARY LOCATION OF THE SOURCE ON THE AXIS OF THE CYLINDER

When the source of vibrations is not placed at the focus, the method of solution of the problem set forth in Sec. 2 leads to complicated calculations, which are concerned with the decomposition of the source field in the integral into parabolic cylindrical functions. In such problems, it is expedient to proceed otherwise, namely, by investigating the total field at once.

Let us first consider the case in which the source is located at an arbitrary point $\alpha=\alpha^*$, $\beta=0$ on the positive part of the abscissa. Replacing the linear current I by a current which is equal to it but uniformly distributed over a small area, we can write down the following inhomogeneous equation:

$$\frac{\partial^2 E}{\partial\alpha^2} + \frac{\partial^2 E}{\partial\beta^2} + k^2(\alpha^2+\beta^2)E = \frac{4\pi i\omega}{c^2}(\alpha^2+\beta^2)\,j(\alpha,\beta)$$

$$(0<\alpha<\infty,\ 0<\beta<\beta_0);$$

$$j(\alpha,\beta) = \begin{cases} I/[4(\alpha^2+\beta^2)\varepsilon\gamma] & \text{for } \alpha^*-\varepsilon<\alpha<\alpha^*+\varepsilon,\ 0<\beta<\gamma, \\ 0 & \text{for other } \alpha \text{ and } \beta, \end{cases} \tag{8.1}$$

and the boundary conditions

$$E|_{\beta=\beta_0} = 0,\ \partial E/\partial\alpha|_{\alpha=0} = 0, \tag{8.2}$$

$$\partial E/\partial\beta|_{\beta=0} = 0.$$

If we seek the function $E(\alpha,\beta)$ in the form of an expansion

$$E = \frac{\sqrt{k}\,e^{-i\pi/4}}{2\pi^2}\int_{-\delta-i\infty}^{-\delta+i\infty} E_\nu(\beta)\,\Gamma\left(-\frac{\nu}{2}\right) \tag{8.3}$$

$$\times\ \Gamma\left(\frac{\nu+1}{2}\right)e^{i\pi\nu/2}A_\nu^{(1)}(\alpha)\,d\nu,\quad 0<\delta<1/2,$$

where

$$E_\nu(\beta) = \int_0^\infty E A_\nu^{(1)}(\alpha)\,d\alpha, \tag{8.4}$$

then, multiplying (8.1) by $A_\nu^{(1)}(\alpha)$, and integrating* over α from zero to infinity, we get the usual differential equation for $E_\nu(\beta)$. Solving it under the conditions $E_\nu(\beta_0)=0$, $E_\nu'(0)=0$, we are led to the expression

$$E_\nu(\beta) = \frac{IV\sqrt{\pi i k}}{c}B_\nu^{(1)}(\beta)B_\nu^{(3)}(\beta_0) \tag{8.5}$$

$$-B_\nu^{(3)}(\beta)B_\nu^{(1)}(\beta_0)\frac{A_\nu^{(1)}(\alpha^*)}{B_\nu^{(1)}(\beta_0)}.$$

*Here we also make use of the radiation principle.

as $\epsilon, \gamma, \to 0$. Substituting (8.5) in (8.3), we obtain the final solution of the problem:

$$E(\alpha, \beta) = \frac{Ik}{2\pi\sqrt{\pi}\, c} \int_{-\delta-i\infty}^{-\delta+i\infty} \Gamma\left(-\frac{\nu}{2}\right)\Gamma\left(\frac{\nu+1}{2}\right) e^{i\pi\nu/2} [B_\nu^{(1)}(\beta) B_\nu^{(3)}(\beta_0) - B_\nu^{(3)}(\beta) B_\nu^{(1)}(\beta_0)] \frac{A_\nu^{(1)}(\alpha^*)}{B_\nu^{(1)}(\beta_0)} A_\nu^{(1)}(\alpha)\, d\nu. \tag{8.6}$$

In a similar fashion, we can consider the case in which the source is located to the left of the focus at an arbitrary point on the negative abscissa.

We have limited ourselves here to the consideration of the case in which the source lies on the axis of the cylinder. Similarly, it would be possible to investigate the general case of an arbitrary location of the source within the cylinder. In such a case, we would have to take into consideration (along with the four functions $A_\nu^{(1)}(\alpha)$ odd functions, for which one would have to introduce the corresponding expansion formula.

APPENDIX A
SOME PROPERTIES OF PARABOLIC CYLINDRICAL FUNCTIONS ASYMPTOTIC BEHAVIOR FOR LARGE VALUES OF THE ARGUMENT:

$$A_\nu^{(1)}(\alpha)\big|_{|\alpha|\to\infty} = e^{ik\alpha^2/2} \frac{\Gamma(1/2)}{\Gamma(-\nu/2)} (ik\alpha^2)^{-(\nu+1)/2}\left[1 + O\left(\frac{1}{k\alpha^2}\right)\right] + \exp\left\{-\frac{ik\alpha^2}{2} - \frac{i\pi\nu}{2}\right\} \frac{\Gamma(1/2)}{\Gamma[(\nu+1)/2]} (ik\alpha^2)^{\nu/2}\left[1 + O\left(\frac{1}{k\alpha^2}\right)\right]; \tag{A-1}$$

$$A_\nu^{(3)}(\alpha)\big|_{|\alpha|\to\infty} = (ik\alpha)^{\nu/2}\Gamma\left(-\frac{\nu}{2}\right) e^{-ik\alpha^2/2}\left[1 + O\left(\frac{1}{k\alpha^2}\right)\right]. \tag{A-2}$$

Asymptotic representation for $|\nu| \to \infty$:

$$A_\nu^{(1)}(\alpha) = \cos\sqrt{ik(2\nu+1)}\,\alpha\left[1 + O\left(\frac{1}{\sqrt{2\nu+1}}\right)\right]; \tag{A-3}$$

$$B_\nu^{(1)}(\beta) = \operatorname{ch}\sqrt{ik(2\nu+1)}\,\beta\left[1 + O\left(\frac{1}{\sqrt{2\nu+1}}\right)\right]; \tag{A-4}$$

$$B_\nu^{(3)}(\beta) = \mp\frac{2\sqrt{\pi}}{\sqrt{2\nu+1}} \exp\{\pm\sqrt{ik(2\nu+1)}\beta\}. \tag{A-5}**$$

Integral representations

$$A_\nu^{(1)}(\alpha) = \frac{\sqrt{2\pi}}{\Gamma(-\nu/2)\Gamma((\nu+1)/2)} \int_{-\infty}^{\infty} \exp\left\{\left(\nu + \frac{1}{2}\right)\theta - \frac{ik\alpha^2}{2}\operatorname{th}\theta\right\} \frac{d\theta}{\sqrt{\operatorname{ch}\theta}} \quad (-1 < \operatorname{Re}\nu < 0); \tag{A-6},***$$

$$A_\nu^{(3)}(\alpha) = \frac{2^{\nu+1}\sqrt{\pi}}{\Gamma((1-\nu)/2)} (k\alpha^2)^{\nu/2} \exp\left\{\frac{i\pi\nu}{4} - \frac{ik\alpha^2}{2}\right\} \int_0^\infty \exp\left\{\frac{ix^2}{4k\alpha^2} - x\right\} x^{-\nu-1}\, dx \quad (\operatorname{Re}\nu < 0), \tag{A-7}$$

APPENDIX B. THE DISTRIBUTION OF THE ROOTS OF B

In order to locate the roots of the equation

$$B_\nu^{(1)}(\beta) = 0 \quad (\nu = \sigma + i\tau), \tag{B-1}$$

we make use of the relation

$$\overline{B}_{-\nu}^{(1)}(\beta) B_\nu^{(1)\prime}(\beta) - \overline{B}_{-\nu}^{(1)\prime}(\beta) B_\nu^{(1)}(\beta) = 2ik(1 + 2\sigma) \int_0^\beta |B_\nu^{(1)}|^2\, d\beta,$$

**Here the upper sign refers to the region Re $\{\nu\} < -1/2$, the lower to the region Re $\{\nu\} > -1/2$.

***This formula was obtained from the well-known integral representation[10]

$$F(a, b, z) = \frac{\Gamma(b)}{\Gamma(a)\Gamma(b-a)} \int_0^1 t^{a-1}(1-t)^{b-a-1} e^{tz}\, dt; \quad (\operatorname{Re} b > \operatorname{Re} a > 0)$$

by the change of variables $(1-t)/t = e^{2\sigma}$,

[10] N. N. Lebedev, *Special Functions and their application*, GTTI, 1953.

which is easily obtained from the differential equations and initial conditions for the functions under consideration. If we assume that, for given β, the value of ν is such that $\beta_\nu^{(1)}(\beta)=0$ then $\bar{\beta}_{-\nu}^{(1)}(\beta)=0$ also, and consequently, $\mathrm{Re}\{\nu\}=\sigma=-1/2$, i.e., all the roots ν_n of the function $\beta_\nu^{(1)}$ $\beta_\nu^{(1)}(\beta)$ are located to the right of $\mathrm{Re}\{\nu\}=-1/2$.

As a more detailed investigation shows, the imaginary parts of these roots take the following asymptotic forms for $|\tau_n|\to\infty$:

$$\tau_n \approx \frac{1}{2k\beta^2}\left(\frac{2n-1}{2}\pi\right)^2. \qquad \text{(B-2)}$$

One can also show that the number τ_n is bounded below.

APPENDIX C. DERIVATION OF AN ESTIMATE FOR THE FUNCTION

The purpose of this appendix – to establish some estimate for functions of the third type $A_\nu^{(3)}(\alpha)$, uniformly valid in α for $-\tau < Im\{\nu\} < \infty$ (T an arbitrarily large positive number).

Integrating Eq. (A-7) by parts, we find

$$A_\nu^{(3)}(\alpha) = \frac{2^{\nu+1}\sqrt{\pi}}{\Gamma(1-\nu/2)}(k\alpha^2)^{\nu/2}\exp\left\{\frac{i\pi\nu}{4}-\frac{ik\alpha^2}{2}\right\}$$
$$\times\frac{1}{\nu}\int_0^\infty x^{-\nu}\exp\left\{\frac{ix^2}{4\alpha^2k}-x\right\}\left(\frac{ix}{2k\alpha^2}-1\right)dx;$$
$$\nu=-\delta+i\tau;\quad \delta>0.$$

Estimating the modulus of the latter integral, and taking into account the behavior of gamma functions for large τ, we get

$$|A_\nu^{(3)}(\alpha)| = \alpha^{-\delta}\varphi(\tau)\ (\delta>0), \qquad \text{(C-1)}$$

where

$$\varphi(\tau)=\begin{cases} O(1) & \text{for } -T\leqslant\tau\leqslant T,\\ O(\tau^{-1-\delta/2}) & \text{for } T<\tau<\infty.\end{cases} \qquad \text{(C-2)}$$

Making use further of the integral representations for the linear combination $\alpha^{-1}A_\nu^{(3)'}(\alpha)+ikA_\nu^{(3)}(\alpha)$ [easily obtained from Eq. (A-7)], we find, as above,

$$\left|\frac{1}{\alpha}A_\nu^{(3)'}(\alpha)+ikA_\nu^{(3)}(\alpha)\right| = \alpha^{-2-\delta}\psi(\tau), \qquad \text{(C-3)}$$

where

$$\psi(\tau)=\begin{cases} O(1) & \text{for } -T\leqslant\tau\leqslant T,\\ O(\tau^{-1-\delta/2}) & \text{for } T<\tau<\infty.\end{cases} \qquad \text{(C-4)}$$

Translated by R. T. Beyer
97

Scattering of High-Energy Electrons and Positrons by Electrons

A. A. ABRIKOSOV
Institute of Physical Problems, Acad, Sci. USSR

(Submitted to JETP editor, November 21, 1954)
J. Exptl. Theoret. Phys. (U.S.S.R.) 30, 544-550 (March, 1956)

The scattering of charged particles is considered in the energy region $V(\pi)/e \ll \ln(E/m) \ll \pi/e^2$. It is shown that the cross section for electron-electron scattering with arbitrary radiation dees not differ from that given by zero-order approximation. For the positron-electron scattering the cross section is changed in the region of small angles. This change is determined by solving an integral equation.

IN two previous papers[1,2] we have discussed the scattering of an electron by an external field and the Compton scattering at energies in the region $\sqrt{\pi}/e \ll \ln(E/m) \ll \pi/e^2$. This revealed the following situation. The alteration in the cross section for the scattering by the external field and for Compton scattering is such that the reduction in the cross section for the basic process, without the emission of additional quanta, is compensated by an increase in the cross section for processes with multiple emission of additional hard quanta. The total cross section for processes with arbitrary emission is still given by the zero-order approximation. In the case of the Compton effect[2] however, it was discovered that, in addition to the effect just described, there is a change in the angular distribution for small angles, which is not compensated by the inclusion of processes with additional radiation. The angular region in which this happens is so small that the change does not affect the total cross section; however, the forward scattering may change appreciably.

In the present paper we examine the scattering of charged particles by each other. We shall not be interested in the amount of radiation emitted in the course of the scattering, i.e., we shall determine in practice the sum of the cross sections for the processes involving the emission of one, two, &c, real quanta. As we know from the previous papers[1,2], such emission processes are compensated in a generalized graph by integrals over the momenta of the virtual quanta, taken over the region $k^2 = 0$, Here we consider only the possible change in the cross section not relating to any real emission.

1. BASIC DIAGRAMS

The basic diagrams for single electron-electron scattering in zero approximation are shown in Fig. 1. Consider first the question of virtual quanta with $k^2 = 0$. We shall show that these are compensated by the effect of corresponding real quanta. For this purpose we consider one of the generalized diagrams for the process in question, e.g., the one shown in Fig. 2, *a*. In Fig. 2, *b* we show the different types of virtual lines, and the real ones which cancel them. Each type is labeled by a number, and the corresponding real line by the same number with a prime. The proof of this cancellation to order e^2, i.e., for only one line, is extremely simple. For the general case the proof does not differ materially from that given in Ref. 2.

There is only one point worth noting. The electron-electron scattering differs from the Compton effect in particular by the presence of two fermions, and this can, in general, affect the calculation of the spinor numerators. (An example of this will occur below). However, here this fact makes no difference at all. Indeed, consider, for example, line 2 in Fig. 2, *b*. Its spinor numerator (multiplied on the left by $\hat{p}_1\hat{p}_2$ and on the right by $\hat{q}_1\hat{q}_2$, where $\hat{p}_1$ and $\hat{q}_1$ relate to the first, and $\hat{p}_2$ and $\hat{q}_2$ to the second electron, i.e., $\hat{p}_1$, $\hat{q}_1$ commute with $\hat{p}_2$, $\hat{q}_2$) is of the form

$$(\hat{p}_1\gamma_\mu(\hat{p}_1 - \hat{k})\gamma_\nu\hat{q}_1)(\hat{p}_2\gamma_\mu(\hat{p}_2 + \hat{k})\gamma_\nu\hat{q}_2)$$
$$\approx (\hat{p}_1\gamma_\mu\hat{p}_1\gamma_\nu\hat{q}_1)(\hat{p}_2\gamma_\mu\hat{p}_2\gamma_\nu\hat{q}_2)$$
$$\approx 2(p_1p_2)(\hat{p}_1\gamma_\nu\hat{q}_1)(\hat{p}_2\gamma_\nu\hat{q}_2),$$

i.e., of the same form as in zero-order approximation. The same can be shown for any number of virtual lines with $k^2 = 0$.

Now consider the possibility of a change in the cross section which is not compensated by the emission of real quanta. From Ref. 2 it is evident that such a contribution can come only from lines of type 2 or 3 (Fig. 2, *b*). Assume there is one virtual line of type 2. In that case we have in the denominator of the matrix element the expression

[1] A. A. Abrikosov, J. Exptl. Theoret. Phys. (U.S.S.R.) 30, 96, (1956); Soviet Phys JETP 3, 71,(1956).

[2] A. A. Abrikosov, J. Exptl. Theoret. Phys. (U.S.S.R.) 30, 386 (1956);

$(p_1 - k)^2 (p_2 + k)^2 k^2 (l - k)^2$. In the numerator, on the other hand, we have the spinors $\hat{p}_1 - \hat{k}$ and $\hat{p}_2 + \hat{k}$. By comparison with Ref. 2 we conclude that the appearance of the terms for which we are looking requires that $|(p_1, q_1)| >> |(p_1, p_2)|$. It is easy to see that this is impossible. Indeed, consider the scattering in the centre-of-mass system (Fig. 3). We see that

$$(p_1 p_2) = E^2 + \mathbf{p}^2 \approx 2E^2,$$

$$(p_1 q_1) = E^2 - \mathbf{p}^2 \cos\theta \ll E^2 + \mathbf{p}^2.$$

Now assume there is one line of type 3. Then we require that $|(p_1 q_1)| \gg |(p_1 q_2)|$. This may happen, since in the center-of-mass system $(p_1 q_2) = E^2 - \mathbf{p}^2 \cos\theta'$, which may be much less than $p_1 \cdot q_1$, if the angle θ' is small enough, i.e., if in the center-of-mass system the scattering is backward, Nevertheless this effect is not observable. Indeed, besides the diagram 1, *a* which we have considered, there is also a contribution from diagram 1, b. In view of the fact that the contribution from any diagram is essentially of the order l^{-2}, where l is the momentum of the photon which is transmitted from one electron to the other, the diagram 1, *b* gives the dominant contribution when $|(p_1 q_2)| \ll |(p_1 q_1)|$, and this diagram does not give the term we require. It would do so in the opposite case, but then the diagram 1, *a* is dominant. We conclude, therefore, that owing to the possibility of electron exchange the expression for the electron-electron cross section is given correctly by zero-order approximation in the approximation considered here.

The situation is different in the case of positron-electron scattering. There there is no exchange, because the two particles are distinguishable, and the effect we are looking for may take place.

The basic diagrams for this process are shown in Fig. 4. In this case, as in the previous one, a term of the required kind will appear in Fig. 4 from a virtual line of type 3 (Fig. 2, *b*) if $p_1 \cdot q_1 >> p_1 \cdot q_2$. But, contrary to the previous situation, diagram 4, *b* cannot mask this effect, since, according to Fig. 3, $\hat{p}_1$, $\hat{p}_2$ is the largest of all the scalar products of momenta. Therefore diagram 4, *b* will, first, be of the same order as 4, *a*, and second, will itself give a contribution of the required kind.

The conservation of four-momentum requires that

$$p_1 - q_1 = q_2 - p_2. \tag{1}$$

Hence, we may obtain the following equality for the scalar products (remembering that the squares of all vectors p and q are negligible)

$$\begin{aligned}(p_1 q_1) = (p_2 q_2) = (p_2 p_1) - (p_2 q_1) \\ = (p_2 p_1) - (p_1 q_2).\end{aligned} \tag{2}$$

It follows from this that if $(p_1 q_2) \ll (p_1 q_1)$ $(p_1 q_1) \approx (p_1 p_2)$, i.e., $l^2 \approx -l'^2$.

It should be pointed out here that in the diagram 4, *b* it is possible, in principle, to find a contribution of the required type from a line of type 2, provided $p_1 \cdot q_1 << p_1 \cdot q_2$. However, in that case diagram 4, *a* will dominate, and this does not give any such contribution. Thus an interesting contribution can come only from virtual lines of type 3. With the help of this result we shall now determine the matrix element for positron-electron scattering.

2. THE MATRIX ELEMENT FOR POSITRON-ELECTRON SCATTERING

In analogy with Ref. 2, we can determine the matrix element by setting up an equation which gives the sum of all diagrams shown in Fig. 5. Whereas in the previous case[2] the equation could immediately be replaced by a direct summation, here it gives much the simplest way of finding the matrix element. This is connected with the fact that we are now dealing with two electrons. Consider first the diagrams derived from 4,*a*. Taking account of the results of the preceding section, we find the equation for the matrix element in the form

$$\begin{aligned}M^{ab,\,cd}(p_1,\ p_2;\ q_1,\ q_2;\ l) = \gamma_\mu^{ab}\gamma_\mu^{cd} l^{-2} \\ + \frac{e^2}{\pi i}\int\left[\gamma_\mu \frac{1}{\hat{p}_1 - \hat{k} - m}\right]^{ax} M^{xb,\,yd}(p_1 - k,\ p_2; \\ q_2,\ q_1 - k;\ l - k)\left[\gamma_\mu \frac{1}{\hat{k} - \hat{q}_2 - m}\right]^{cy} \frac{d^4k}{k^2}.\end{aligned} \tag{3}$$

In this formula *a* and *b* refer to the initial and final states of the electron, and *d*, *c*, the initial and final states of the positron. (For the latter we take the four-momentum with the opposite sign, and the lines have to be followed in the reverse direction).

Since the behavior of the matrix element M is in zero order given essentially by the factor l^{-2}, we assume that $M = M' l^{-2}$, where M' is some slowly

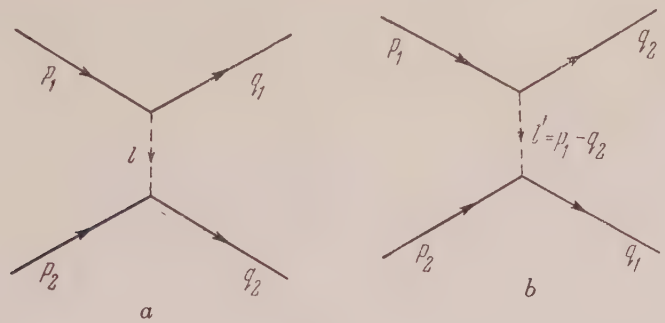

FIG. 1

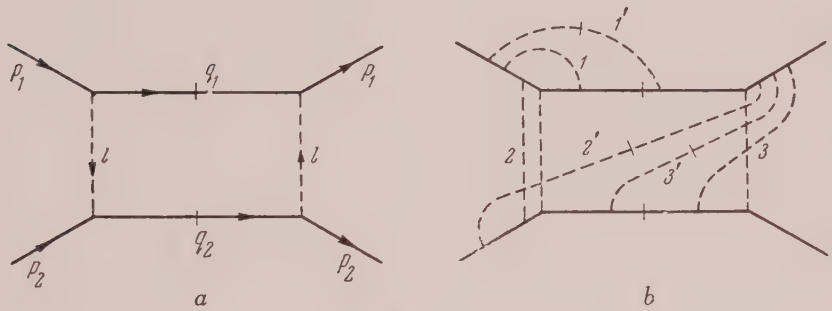

FIG. 2

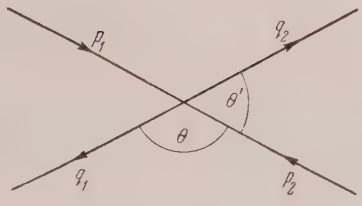

FIG. 3

varying spinor. In addition we carry out a transformation similar to the one used for the corresponding lines in reference[2]. For this purpose we replace $\hat{p}_1 - \hat{k}$ by $\hat{k}$, average the quantities $\hat{k}_{k\text{trans}} \cdots \hat{k}_{k\text{trans}}$ in the numerator over the polarizations, and cancel $\hat{k}^2_{k\text{trans}}$ in the numerator against the same factor in the denominator, remembering the region $l^2 uv \gg (p_1 - q_2)^2$, in which this is permissible. In the end, the equation takes the form

$$M'^{ab,\,cd} = \gamma_\mu^{ab}\gamma_\mu^{cd} + \frac{e^2}{2\pi i}[\gamma_\mu\gamma_\nu]^{ax}\int \frac{M'^{xb,\,yd}(k,\,p_2;\,q_1,q_2 - p_1 + k + q_2;\,-q_1 + k)\,d^4k}{(k^2 - m^2)(p_1 - k)^2(q_1 - k)^2}[\gamma_\mu\gamma_\nu]^{cy}. \tag{4}$$

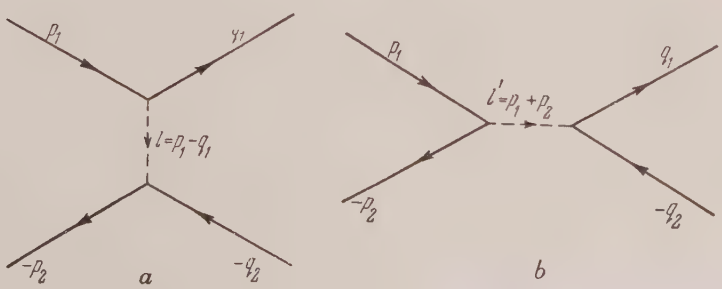

FIG. 4

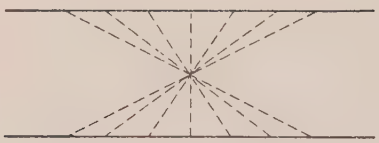

FIG. 5

From this equation it is evident that M' must be a scalar product of two tensors, of which one relates to the electron and the other to the positron. These tensors are products of the γ_μ; their rank therefore cannot exceed four. This means that any tensor of rank higher than four can be expressed in terms of tensors of lower rank, Since the only tensor which can in this case dispose of surplus subscripts is $\delta_{\mu\nu}$, the reduction in rank must always go in even steps. Examination of Eq. (4) shows then that M' may contain scalar products of tensors of first and third rank. Indeed, the tensors of fifth rank in the term with the integral can be expressed in terms of tensors of first and third rank.

We therefore write

$$M'^{ab,\,cd} = \gamma_\mu^{ab} \cdot \gamma_\mu^{cd} f_1 + T_{\mu\tau\nu}^{ab} \cdot T_{\mu\tau\nu}^{cd} f_3, \qquad (5)$$

where f_1 and f_3 are scalar functions and $T_{\mu\tau\nu}$ an antisymmetric tensor of rank 3, formed from the γ_μ:

$$T_{\mu\tau\nu} = {}^1/_6\,(\gamma_\mu\gamma_\tau\gamma_\nu - \gamma_\mu\gamma_\nu\gamma_\tau - \gamma_\tau\gamma_\mu\gamma_\nu + \gamma_\nu\gamma_\mu\gamma_\tau + \gamma_\tau\gamma_\nu\gamma_\mu - \gamma_\nu\gamma_\tau\gamma_\mu). \qquad (6)$$

To find f_1 and f_3 we must, first of all, express the tensors $\gamma_\mu\gamma_\nu\gamma_\tau$ and $\gamma_\xi\gamma_\eta T_{\mu\tau\nu}$ which arise from the integral term in Eq. (4), in terms of γ_μ and $T_{\mu\tau\nu}$. Bringing γ_μ to the left in each term of the expression (6), we see that

$$\gamma_\mu\gamma_\tau\gamma_\nu = T_{\mu\tau\nu} + \gamma_\nu\delta_{\mu\tau} + \gamma_\mu\delta_{\nu\tau} - \gamma_\tau\delta_{\mu\nu}. \qquad (7)$$

As regards the second combination, it is easy to see that, the most general form it can have is

$$\begin{aligned}\gamma_\xi\gamma_\eta T_{\mu\tau\nu} = {} & A\,(\delta_{\eta\mu}T_{\xi\tau\nu} - \gamma_{\eta\tau}T_{\xi\mu\nu} + \delta_{\eta\nu}T_{\xi\mu\tau} \qquad (8)\\ & - \delta_{\xi\mu}T_{\eta\tau\nu} + \delta_{\xi\tau}T_{\eta\mu\nu} - \delta_{\xi\nu}T_{\eta\mu\tau})\\ & \times B\delta_{\xi\eta}T_{\mu\tau\nu} + C\,[(\delta_{\xi\mu}\delta_{\eta\tau} - \delta_{\xi\tau}\delta_{\eta\mu})\,\gamma_\nu\\ & + (\delta_{\xi\nu}\delta_{\eta\mu} - \delta_{\xi\mu}\delta_{\eta\nu})\,\gamma_\tau + (\delta_{\xi\tau}\delta_{\eta\nu} - \delta_{\xi\nu}\delta_{\eta\tau})\,\gamma_\mu].\end{aligned}$$

To determine the coefficient B interchange γ_ξ and γ_η on the left-hand side. This leaves

$$\gamma_\eta\gamma_\xi T_{\mu\tau\nu} = -\gamma_\xi\gamma_\eta T_{\mu\tau\nu} + 2\delta_{\xi\eta}T_{\mu\tau\nu}.$$

On the right -hand side the terms with A and C then change sign, whereas the term with B remains unchanged. Hence $B = 1$. To find A and C we take the special case $\xi = \mu$. and use Eq. (7) on the left-hand side. Displacing γ_μ and equating the coefficients of $T_{\eta\tau\nu}$ and of the combination $2\,(\gamma_\tau\delta_{\nu\eta} - \gamma_\nu\delta_{\tau\eta})$, we conclude that $A = 1$, $C = -1$. The next step is to multiply the expressions which we have obtained. With the help of (7) we see that

$$(\gamma_\mu\gamma_\tau\gamma_\nu)^{ab}\,(\gamma_\mu\gamma_\tau\gamma_\nu)^{cd} = T_{\mu\tau\nu}^{ab}T_{\mu\tau\nu}^{cd} + 10\gamma_\mu^{ab}\gamma_\mu^{cd}. \qquad (9)'$$

Using (8) and the values of the coefficients A, B, and C, we find

$$\begin{aligned}(\gamma_\xi\gamma_\eta T_{\mu\tau\nu})^{ab}\,(\gamma_\xi\gamma_\eta T_{\mu\tau\nu})^{cd} \qquad (10)\\ = 10T_{\mu\tau\nu}^{ab}T_{\mu\tau\nu}^{cd} + 36\gamma_\mu^{ab}\gamma_\mu^{cd}.\end{aligned}$$

We now substitute this result, as well as (5), in Eq. (4). If we assume, as in Ref. 2, that f_1 and f_3 depend only on $a = \ln[l^2/(p_1 - q_2)^2]$, and remembering the region of integration, we obtain the following equations:

$$\begin{aligned}f_1(a^2) &= 1 + \frac{10e^2}{16\pi}\int_0^{a^2} f_1(x)\,dx + \frac{36e^2}{16\pi}\int_0^{a^2} f_3(x)\,dx, \qquad (11)\\ f_3(a^2) &= \frac{e^2}{16\pi}\int_0^{a^2} f_1(x)\,dx + \frac{10e^2}{16\pi}\int_0^{a^2} f_3(x)\,dx.\end{aligned}$$

If we now differentiate with respect to a^2, we obtain two differential equations of first order. The boundary condtions are, according to (11), $f_1(0) = 1$, $f_3(0) = 0$. The solution of the pair of equations with this boundary condition gives f_1 and f_3: (12)

$$f_1 = \frac{1}{2}\left[\exp\left(\frac{e^2}{4\pi}\ln^2\frac{l^2}{p^2}\right) + \exp\left(\frac{e^2}{\pi}\ln^2\frac{l^2}{p^2}\right)\right],$$

$$f_3 = \frac{1}{12}\left[-\exp\left(\frac{e^2}{4\pi}\ln^2\frac{l^2}{p^2}\right) + \exp\left(\frac{e^2}{\pi}\ln^2\frac{l^2}{p^2}\right)\right],$$

where $p = p_1 - q_2$.

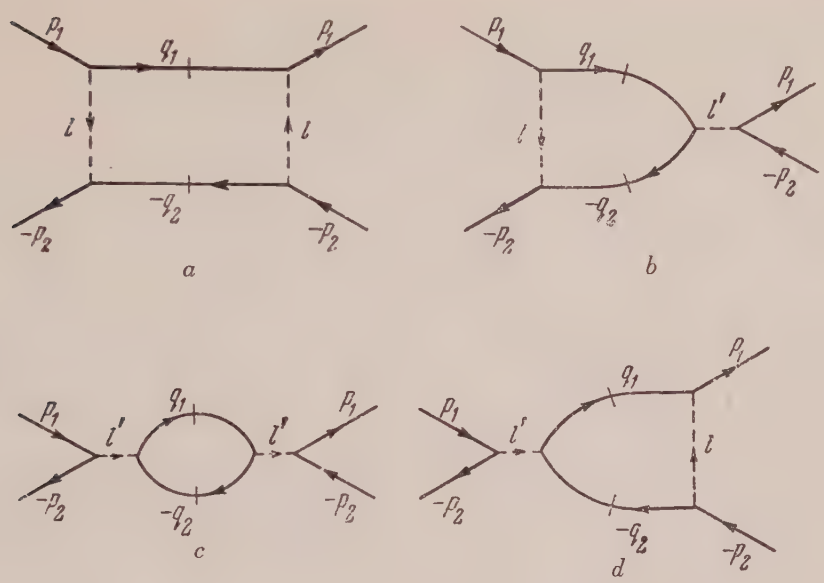

FIG. 6

If we insert these values for f_1 and f_3 in (5) we have the required expression for the sum of all graphs of the type 4, *a*.

Now we would have to find an analogous expression for the diagrams of type 4,*b*. However, this is unnecessary since the diagrams 4, *b* give exactly the same as 4, *a*. The minus sign in the denominator which comes from $l'^2 = -l^2$ is cancelled by the fact that the contribution of the diagram 4, *b* has to be taken with the opposite sign. The only difference is that, in the diagram 4, *b* the states *ab*, *cd*, are replaced by the states *ad*, *cb*.

3. THE CROSS SECTION

We now turn to the calculation of the cross section. The combined diagrams for this (giving as examples only the zero-order ones) are shown in Fig. 6. If we are not interested in the initial or final spin states of electron or positron, then the expression corresponding to the diagram 6, *a* is, apart from small terms (we omit factors which are common to all diagrams):

$$
\begin{aligned}
&{}^1/_4 f_1^2 \,\mathrm{Sp}\,[\hat{p}_1\gamma_\mu\hat{q}_1\gamma_\nu]\,\mathrm{Sp}\,[(-\hat{p}_2)\gamma_\nu(-\hat{q}_2)\gamma_\mu] \\
&+{}^1/_4 f_1 f_3 \,\mathrm{Sp}\,[\hat{p}_1 T_{\mu\tau\nu}\hat{q}_1\gamma_\xi]\,\mathrm{Sp}\,[(-\hat{p}_2)\gamma_\xi(-\hat{q}_2)T_{\mu\tau\nu}] \\
&+{}^1/_4 f_1 f_3 \,\mathrm{Sp}\,[\hat{p}_1\gamma_\xi\hat{q}_1 T_{\mu\tau\nu}]\,\mathrm{Sp}\,[(-\hat{p}_2)T_{\mu\tau\nu}(-\hat{q}_2)\gamma_\xi] \\
&+{}^1/_4 f_3^2 \,\mathrm{Sp}\,[\hat{p}_1 T_{\mu\tau\nu}\hat{q}_1 T_{\xi\eta\lambda}]\,\mathrm{Sp}\,[(-\hat{p}_2)T_{\xi\eta\lambda}(-\hat{q}_2)T_{\mu\tau\nu}].
\end{aligned}
\tag{13}
$$

To evaluate this expression we first find the basic spurs. One easily finds directly:

$$
{}^1/_4\mathrm{Sp}\,[\hat{p}_1\gamma_\mu\hat{q}_1\gamma_\nu] = p_{1\mu}q_{1\nu} + p_{1\nu}q_{1\mu} - (p_1q_1)\,\delta_{\mu\nu}. \tag{14}
$$

The next spur is $\mathrm{Sp}\,[\hat{p}_1 T_{\mu\tau\nu}\hat{q}_1\gamma_\xi]$. By means of equation (7), we can write this expression in the form $\mathrm{Sp}\,[\,T_{\mu\tau\nu}T_{\eta\xi\lambda}]\;p_{1\lambda}q_{1\eta}$. This can be explained by the fact that $\mathrm{Sp}\,[T_{\mu\tau\nu}\gamma_\xi] = 0$, since it is impossible to represent this expression in any other way in terms of δ-functions. If we make use of the symmetry properties of the expression in question, we can write it as a corresponding sum of tensors, which contain $p_{1\mu}$, $q_{1\mu}$ and $\delta_{\mu\nu}$ with unknown coefficients. Combining terms on both sides, and comparing coefficients, we find

$$
{}^1/_4\mathrm{Sp}\,[\hat{p}_1 T_{\mu\tau\nu}\hat{q}_1\gamma_\xi] = (p_{1\nu}q_{1\tau} - p_{1\tau}q_{1\nu})\,\delta_{\mu\xi} + (p_{1\mu}q_{1\nu} - p_{1\nu}q_{1\mu})\,\delta_{\tau\xi} + (p_{1\tau}q_{1\mu} - p_{1\mu}q_{1\tau})\,\delta_{\nu\xi}. \tag{15}
$$

The last spur, $\mathrm{Sp}\,[\hat{p}_1 T_{\mu\tau\nu}\hat{q}_1 T_{\xi\eta\lambda}]$ is

dealt with in the same way. As a result of this calculation we find

$$
\begin{aligned}
{}^1/_4\mathrm{Sp}\,[\hat{p}_1 T_{\mu\tau\nu}\hat{q}_1 T_{\xi\eta\lambda}] = {} & (p_1q_1)(\delta_{\mu\xi}\delta_{\tau\eta}\delta_{\nu\lambda} - \delta_{\tau\xi}\delta_{\mu\eta}\delta_{\nu\lambda} - \delta_{\mu\xi}\delta_{\tau\lambda}\delta_{\nu\eta} + \delta_{\tau\xi}\delta_{\nu\eta}\delta_{\mu\lambda} \\
& + \delta_{\nu\xi}\delta_{\tau\lambda}\delta_{\mu\eta} - \delta_{\nu\xi}\delta_{\mu\lambda}\delta_{\tau\eta}) + (p_{1\mu}q_{1\xi} + p_{1\xi}q_{1\mu})(\delta_{\nu\eta}\delta_{\tau\lambda} - \delta_{\nu\lambda}\delta_{\tau\eta}) + \\
& + (p_{1\nu}q_{1\xi} + p_{1\xi}q_{1\nu})(\delta_{\tau\eta}\delta_{\mu\lambda} - \delta_{\mu\eta}\delta_{\tau\lambda}) + (p_{1\tau}q_{1\xi} + p_{1\xi}q_{1\tau})(\delta_{\nu\lambda}\delta_{\mu\eta} - \delta_{\nu\eta}\delta_{\mu\lambda}) \\
& + (p_{1\mu}q_{1\eta} + p_{1\eta}q_{1\mu})(\delta_{\nu\lambda}\delta_{\tau\xi} - \delta_{\nu\xi}\delta_{\tau\lambda}) + (p_{1\nu}q_{1\eta} + p_{1\eta}q_{1\nu})(\delta_{\mu\xi}\delta_{\tau\lambda} - \delta_{\tau\xi}\delta_{\mu\lambda}) \\
& + (p_{1\tau}q_{1\eta} + p_{1\eta}q_{1\tau})(\delta_{\nu\xi}\delta_{\mu\lambda} - \delta_{\nu\lambda}\delta_{\mu\xi}) + (p_{1\mu}q_{1\lambda} + p_{1\lambda}q_{1\mu})(\delta_{\nu\xi}\delta_{\tau\eta} - \delta_{\nu\eta}\delta_{\tau\xi}) \\
& + (p_{1\nu}q_{1\lambda} + p_{1\lambda}q_{1\nu})(\delta_{\tau\xi}\delta_{\mu\eta} - \delta_{\mu\xi}\delta_{\tau\eta}) + (p_{1\tau}q_{1\lambda} + p_{1\lambda}q_{1\tau})(\delta_{\nu\eta}\delta_{\mu\xi} - \delta_{\nu\xi}\delta_{\mu\eta}).
\end{aligned}
\tag{16}
$$

Now substitute (14) to (16) in (13). After some simple calculation we obtain the expression

$$8\,(f_1^2 - 12 f_1 f_3 + 36 f_3^2)\,(p_1q_1)^2.$$

Here we have used the fact that $p_1q_1 \approx p_2q_2 \approx p_1p_2 >> p_1q_2$, so that we may replace p_2 by q_1 and q_2 by p_1.

Inserting now from (12), we have

$$8\exp\left(\frac{e^2}{2\pi}\ln^2\frac{l^2}{p^2}\right)(p_1q_1)^2. \tag{17}$$

We now proceed to consider the other diagrams of Fig. 6. Although the quantity l'^2, which enters into the denominator of part of the matrix element, equals $-l^2$, there is a minus sign in front of this part. We may therefore regard the matrices in all cases as differing only in the order of factors, and in the way the spurs are taken, but not in their signs or their denominators. Consider diagram 6, *b*. It is easy to see that this differs from 6, *a* only by an interchange between q_1 and $-p_2$, so that it also contributes the expression (17). On the other hand, the diagrams 6, *c* and *d* give only small contributions, as one easily verifies directly. E. g.

$$
\begin{aligned}
{}^1/_4\mathrm{Sp}\,[\hat{p}_1\gamma_\mu\hat{p}_2\gamma_\nu\hat{q}_2\gamma_\mu\hat{q}_1\gamma_\nu] &= -{}^1/_2\,[\hat{p}_1\hat{q}_2\gamma_\nu\hat{p}_2\hat{q}_1\gamma_\nu] \\
&= -8\,(p_1q_2)(p_2q_1).
\end{aligned}
$$

We now obtain the expression for the angular distribution at small angles. It is easy to see that all deviations from the well-known results are contained in the exponential factor. In the centre-of-mass system we have

$$d\sigma = \frac{e^4 d\Omega}{4E^2}\exp\left[\frac{2e^2}{\pi}\ln^2\frac{2}{(\pi-\theta)}\right] \tag{19}$$

if $m/E \ll \pi - \theta \ll \pi/2$,

and

$$d\sigma = \frac{e^4 d\Omega}{4E^2}\exp\left[\frac{2e^2}{\pi}\ln^2\frac{E}{m}\right] \tag{20}$$

if $\pi - \theta \ll m/E$.

In the second case the correction is connected with the fact that, for $(p_1 - q_2)^2 << m^2$ occurs in place of (p_1q_2). It is interesting that these results are very similar to those which were obtained in the investigation of the Compton effect.[2]

In conclusion I wish to express my gratitude to Academician L. L. Landau for discussions about this work.

Translated by R. Peierls
98

Meson Formation in Pb, Cu and C Nuclei by Cosmic Rays in the Stratosphere

D. KAIPOV AND ZH. TAKIBAEV
Institute of Technical Physics, Kazakh Academy of Sciences
(Submitted to JETP editor April 18, 1955)
J. Exptl. Theoret. Phys. (U.S.S.R.) 30, 471-476 (March, 1956)

We have studied the cross section for meson formation in varoius nuclei. It was found that the cross section increases differently at high and low energies.

INTRODUCTION

THE cross section for meson production by low energy protons (~ 400 mev) in various nuclei has been studied in the laboratory[1,2]. These experiments showed that the nuclear cross section for meson formation in various nuclei is proportional to $A^{2/3}$, while the cross section per nucleon decreases with increasing atomic weight of the target nucleus. This behavior of the cross section shows that, at a given energy, not all the nucleons in the nucleus are effective in forming mesons, but only those on the surface of the target nucleus. The decrease in "meson-producing effectiveness" with increasing atomic weight was explained by assuming that the energy of the incident proton is rapidly dissipated in nuclear matter, so that mesons are formed in only the first few collisions with the nucleons of the nucleus. It turns out that this picture does, indeed, lead, at low energies, to the observed dependence of the cross section on atomic weight[3].

At heights in the stratosphere of 25-28 km, we deal with particle energies of order 10^9 ev and higher. When the incident particles have such high energies, one would expect the cross section for formation of slow mesons to be approximately proportional to A, the atomic weight of the target nucleus. Hence it would appear that an investigation of the cross section for meson production in various nuclei at different heights in the stratosphere would lead to the dependence of this cross section both on A and on the energy of the incident particles. This dependence can also be obtained by comparing the cross sections for meson production by cosmic rays at mountain heights in the stratosphere.

Up to now, the cross section for meson production by cosmic rays at mountain altitudes has been studied using thick absorbers[4]. The chief disadvantage of thick (5-17 cm) targets is that, through decay and electromagnetic or nuclear interactions, the mesons formed can again be absorbed in the target, and this must be corrected for in computing the cross section for meson production. This correction is difficult to make because the spectrum of the emitted mesons, for various absorbers at a definite height, is not well known. Some experimental data[5,6] seem to indicate that the spectrum of the emitted mesons depends on height. These difficulties can be bypassed by using thin targets. For sufficiently thin targets, the corrections for decay and for electromagnetic and nuclear interactions can, presumably, be neglected. There is, of course, another difficulty – the incident cosmic rays will produce only a small number of mesons in a thin target. However, the statistical weight of the result can be increased by repeating the experiment.

On the basis of the preceding, we used thin absorbers to investigate the production of mesons in various nuclei.

EXPERIMENTAL METHOD AND RESULTS

In the present work we report our experimental results on the production of mesons by cosmic rays in Pb, Cu and C at heights of 24-28 km. Electron-sensitive photo-emulsions 300 and 340μ thick were exposed to cosmic rays at heights of 24-28 km during two flights in 1953 and one in 1954. The apparatus used in the first two flights is shown in Fig. 1; Fig. 2 shows the height as a function of time for the flights.

The photo-emulsions were surrounded by thin layers of lead, copper, graphite and paraffin; the thickness of the layers is shown in Table 1.

[1] M. Block, S. Passman and W. Havens, Phys. Rev. 88, 1239 (1952).

[2] R. Sagane and W. Dudziak, Phys. Rev. 92, 212 (1953).

[3] S. Gasiarowicz, Phys. Rev. 93, 843 (1954).

[4] N. Dallaporta, M. Merlin, O. Pieruccie and A. Rostagni, Nuovo Cimento 9, 202 (1952).

[5] V. Kamalian and A. Alikhanian, Dokl. Akad. Nauk SSSR 47, 425 (1954).

[6] U. Camerini, P. Fowler, W. Lock and H. Muirhead, Phil. Mag. 41, 413 (1950).

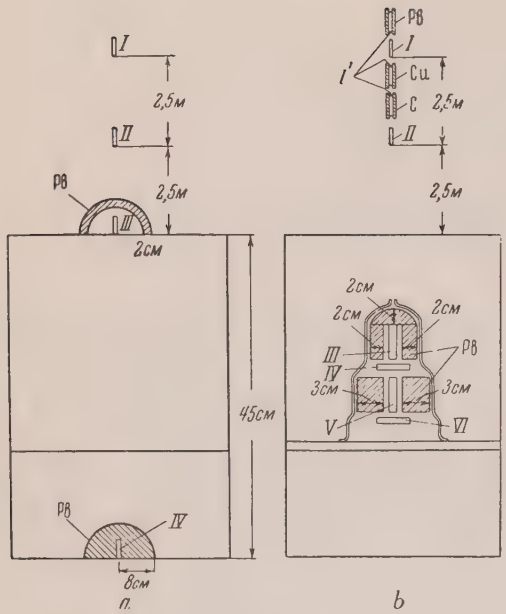

FIG. 1.

Both the shielded photo-emulsions and the air plates were 5 m from the rest of the equipment to avoid side effects due to other dense absorbers. After the flight, all the emulsions were developed and fixed under identical conditions. The emulsions were scanned using a microscope with a 20× objective and 15× eyepiece. The various events were identified by $\pi \to \mu$ decays, σ-capture and also by scattering and grain density measurements.

The experimental results are shown in Table 1. The same table also gives details of the flights and the emulsion thicknesses used. From Table 1, one can see the following:

1) In all three flights, the number of π mesons stopping per gm/cm^2 – hr increases as the atomic weight of the target nucleus increases.

2) The number of ρ mesons does not depend on the atomic weight of the absorber. A small increase in the number of ρ* mesons with increasing A could be due to negative π mesons which do not produce stars; it is known[7] that 27% of the total number of π^- mesons do not produce stars. In our method of analysis, such negative π mesons would be included in the number of ρ mesons.

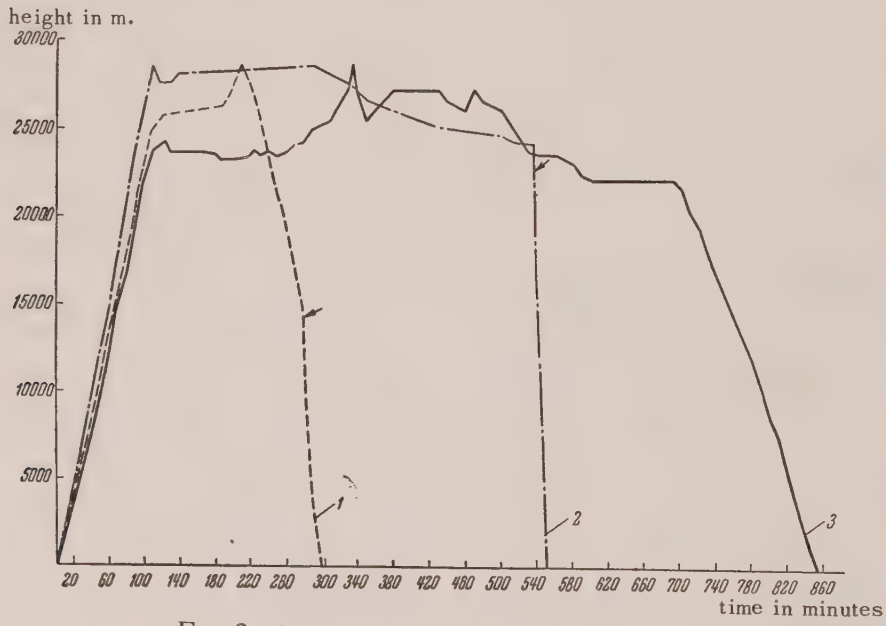

FIG. 2. Arrows indicate the moment of release.

DISCUSSION

Formation of slow π mesons in air:

Surrounding the photoemulsions by a thin absorber increased the number of slow π mesons;

[7] F. Adelman and S. Jones, Phys. Rev. 75, 1468 (1949).

* Translator's note: The original appears to be in error, having π instead of ρ.

TABLE 1

Flight number	Mean height above sea level in km.	length in min.		Time of drift in min.	Emulsion Thickness in μ	Area scanned in cm^2	Absorber	Absorber thickness in gm/cm^2	Number of events		Number of mesons produced per gm/cm^2 – hr.	Energy in mev of mesons produced in the absorber and stopping in the emulsion.
		ascent	descent						π	ρ		
I	26	110	67	123	300	21	air	—	8	60		
						21	paraffin	4	14	62	0.77 ± 0.30	<28
						21	C	4	17	66	1.13 ± 0.37	<28
						21	Cu	3.4	20	68	1.50 ± 0.43	<19
						21	Pb	3.4	28	80	2.6 ± 0.5	<17
II	27	110	18	425	300	20	air	—	6	50		
						20	Cu	1.7	16	60	0.84 ± 0.27	<12
						20	Pb	1.7	23	61	1.6 ± 0.30	<11
III	23.5	110	160	580	340	20	air	—	14	27		
						20	C	2.7	36	20	0.88 ± 0.18	<21
						20	Pb	2.3	62	42	2.16 ± 0.31	<13

this cannot be due to a slowing down in the absorber of π's formed in air, because π's with energy < 100 mev travel ~ 6m, before decaying, while in 6m at 24-25 km in the stratosphere there is about 0.06 gm/cm^2 of matter. This is about 10 times less than the amount of matter in the packing around the plates and in the glass backing. Hence we can say that the π mesons observed in the plate which was suspended in air are formed in the packing material, and in the glass backing, while some of the stars were formed before the ascent to the stratosphere during storage in the laboratory.

Upon comparing the number of events in the control plate with that in the plate suspended in air, we see that almost no slow π mesons are formed in air (in the stratosphere). Hence to find the number of π mesons produced in matter one need only subtract the number of π mesons in the air plate from the number of π mesons underneath the absorber. The number of mesons produced per gm/cm^2 – hr is shown in Table 1.

THE CROSS SECTION FOR π MESON PRODUCTION

From Table 1 we easily obtain the relative cross sections for production of slow π mesons. The second and third columns of Table 2 show the relative cross sections for meson production per nucleon and per nucleus, as calculated from the experimental data.

Table 2 shows that the meson production cross section (relative to lead) increases with increasing atomic weight of the target nucleus; however, the increase differs from that observed at low energies with accelerators (column 4 of Table 2). We can calculate the relative meson production on the basis of various assumptions about the process by which mesons are formed when the incident particles interact with the nucleus. The number of mesons produced per gm/cm^2 – hr is

$$N_\pi = \sigma n S \overline{m}, \tag{1}$$

where $\sigma = kA^{2/3}$ is the nucleus-incident particle interaction cross section, n is the number of nuclei per gm/cm^2, $S = \int F(E)\, dE$ is the current of incident particles per cm^2 – hr, and $\overline{m}$ is the mean number of mesons produced per interaction.

According to (1), if we have two elements of atomic weights A_1 and A_2, the relative meson production cross section per nucleus will be

$$N_{1\pi} A_1 / N_{2\pi} A_2 = \sigma_1 \overline{m}_1 / \sigma_2 \overline{m}_2, \tag{2}$$

We can call $\sigma\overline{m}$ the meson production cross section

TABLE 2

Target nucleus	Meson production cross section relative to lead					
	per nucleon experimental	per nucleus				
		experimental	$A^{2/3}$ law	formula (3)	formula (3′)	formula (3″)
Paraffin	0.30±0.17					
C	0.42±0.12	0.024	0.15	0.06	0 027	0.07
Cu	0.55±0.18	0.16	0.46	0.3	0.18	0.34
Pb	1	1	1	1	1	1

$$\sigma_{1\text{prod}}/\sigma_{2\text{prod}} = \sigma_1 \overline{m}_1/\sigma_2 \overline{m}_2, \qquad (2')$$

$m_1/\overline{m}_2$ depends on the interaction between the incident particles and the nucleus. If we assume that, with a certain probability, mesons are produced only in collisions between the primary particle and individual nucleons in the nucleus, so that δ-nucleons do not take part in the formation of mesons, then the number of mesons produced will be proportional to the number of collisions of the primary particle with the nucleons of the nucleus.

The number of collisions can be found from the following simple considerations. The primary particle cuts out a cylinder upon traversing the nucleus. If r is the radius of nuclear forces, and R_A the radius of a nucleus of atomic weight A, then the volume of the cylinder will be $V = 2\pi r^2 a$, where a is the path length of the primary particle in the nucleus. its value depends on how the primary particle traverses the nucleus ,but on the average will be $\overline{a} = k_0 A^{1/3}$, i.e., proportional to the nuclear radius. The number of collisions (interactions) on the average will be

$$N_{\text{coll}} = \overline{V}\rho = Cr^2 A^{1/3},$$

where ρ is the density of nucleons in the nucleus, and C is a constant, independent of A. Evidently in this case $\overline{m}_1/\overline{m}_2 = (A_1/A_2)^{1/3}$ and formula (2) becomes

$$\frac{\sigma_{1\text{prod}}}{\sigma_{2\text{prod}}} = \frac{\sigma_1}{\sigma_2}\left(\frac{A_1}{A_2}\right)^{1/3}. \qquad (3)$$

If we assume that mesons are formed not only by the primary particles, but also by δ-nucleons, produced in internal cascade processes, then similar considerations show

$$\frac{\sigma_{1\text{prod}}}{\sigma_{2\text{prod}}} = \frac{\sigma_1}{\sigma_2} 2^{-\left(A_2^{1/3} - A_1^{1/3}\right)/k_1}, \qquad (3')$$

where $k_1 = 1.5$ is a geometric factor.

It should be noted that in the above, the interaction of the primary particle with the nucleus was considered to be a succession of independent nucleon-primary interactions. As remarked in Ref. 8 such a picture is valid when the time between interactions is significantly larger than the duration of an interaction. The hydrodynamical theory of Landau[9] gives a different formula for the production cross section

$$\frac{\sigma_{1\text{prod}}}{\sigma_{2\text{prod}}} = \frac{\sigma_1}{\sigma_2}\left(\frac{A_1}{A_2}\right)^{1/4}. \qquad (3'')$$

Equations (3) and (3′) and (3″) can be used to calculate the relative meson production cross sections, and the results compared with the experimental data.

Table 2 gives the results of calculations with Eqs. (3), (3′) and (3″), and also, in column 4, the relative cross section according to the $A^{2/3}$ law. Comparison with the experimental data shows that formula (3′) agrees best with the data which indicates, apparently, that internal cascade processes are important in meson production. We note that our data refers to mesons with energies less than 28 mev, and hence should not be compared with the predictions of theories[9,10] applicable at high energies, as confirmed by Table 2.

Our data can be compared, to some extent, with the results of Refs .11 and 12, in which a cloud

---

[8] I. Rosental and D. Cherniavskii, Usp. Phys. Nauk 52, 185 (1954).

[9] L. D. Landau, Izv. Akad. Nauk SSSR, Ser Fiz. 17, 51 (1953).

[10] E. Fermi, Progr. Theor. Phys. 5, 570 (1950).

[11] B. Gregory and I. Tinlot, Phys. Rev. 81, 667 (1951).

[12] A. Lovati, A. Mura, G. Salvinia C. Tagliaferri, Phys. Rev. 77, 284 (1950).

chamber containing alternate plates of lead and light elements (carbon and aluminum) was used to investigate the dependence of the nuclear cross section on atomic weight. By subtracting out the number of nuclear events with 1,2 etc. end particles, the authors of Refs. 11 and 12 were able to show that the probability of a nuclear interaction (per g/cm^2 of material) with a large number of end products increases considerably with increasing atomic weight. As noted by Rossi[13] this is to be expected if the process goes essentially by successive collisions between the primary particle and the nucleons in the nucleus.

We can apparently draw the following conclusions from our data:

1) As A increases, the meson production cross section increases differently at high energies than it does at low energies (in accelerators).
2) When the primary particle has high energy, then not only the surface nucleons, but also the nucleons inside the nucleus play a role in the production of mesons.
3) At high energies, internal cascade processes are important in meson production.

In conclusion, it is our pleasant duty to thank S. N. Vernov and Prof. N. A. Dobrotin for useful discussions of the results, and our co-workers M. G. Antonov and P. A. Ysik for help in preparing the stratosphere flights.

[13] B. Rossi, *High Energy Particles*, Moscow, 1955 p. 586 (Russian translation).

Translated by R. Krotkov
91

The Investigation of Trapping Centers in Crystals by the Method of Thermal Bleaching

CH. B. LUSHCHIK

Institute of Physics and Astronomy, Academy of Sciences, Estonian SSR

(Submitted to JETP editor December 6, 1954)

(J. Exptl. Theoret. Phys. (U.S.S.R.) 30, 488-500 (March, 1956)

A method of investigating trapping centers in crystals is discussed which consists of measuring the temperature dependence of the absorption coefficient at the maximum of an absorption band of a color center as the excited crystal is warmed up at a constant rate (the method of thermal bleaching). The theory of the method is given for both the case of a single kind of trapping center and for the case of several types of traps of appreciably different depth. The possibilities of the method are illustrated with data obtained in thermal bleaching of single crystals of KCl, $KCl \cdot CaCl_2$, and $KCl \cdot SrCl_2$

INTRODUCTION

At the present time the method of thermal luminescence is widely used in the study of trapping centers in crystals. This method consists of measuring the luminescence intensity I from an excited phosphor as it is warmed up at a constant rate. In the past ten years a series of significant results on trapping centers in different crystal phosphors has been obtained with this method. However, at the same time some unsatisfactory features of this method have also been found. Because this method is essentially connected with observing light intensity, it cannot be applied in the investigation of trapping centers of nonluminescent crystals. Temperature quenching of the luminescence often does not permit the use of this method for the study of deep traps in typical crystal phosphors.[1] Thus it is necessary in many cases to measure some quantity other than the intensity of the emitted light. In several investigations[2] attempts were made to measure the amount of conductivity i as the temperature is raised at a constant rate in excited crystals. However, obtaining the dependence of i on T involves a number of experimental difficulties and the theoretical dependence is not yet known so that the method of thermal release of trapped charge has not received widespread application.

It therefore seems most suitable to use the well-known phenomenon of thermal bleaching to study traps in nonluminescent crystals. This bleaching is caused by the thermal release of electrons or holes from the traps. If the absorption coefficient $\Delta\varkappa$ for traps of a given type is measured as a function of temperature on uniform warming, then the curve $\Delta\varkappa\ (T)$ will have a rapid drop in some rather narrow temperature interval. This temperature will characterize the depth of the corresponding trapping level. A suitable method based on the temperature dependence of $\Delta\varkappa$ will be called in the following the method of thermal bleaching.*

THEORY OF THE METHOD

Since the coefficient of the additional absorption produced by exciting the crystal is proportional to the number n_i of electrons trapped at centers of a given type, then determining the theoretical dependence of $\Delta\varkappa(T)$ leads directly to $n_i(T)$. The latter may easily be determined analogously to the determination of $I(T)$ by Randall[3] and Antonov-Romanovskii.[4] It will be seen that $n_i\ (T)$ is in many cases much simpler than $I\ (T)$.

If the phosphor contains traps of one depth only and if the kinetics are of bimolecular character, then the decrease per unit time in the number of trapped electrons is given by the expression

$$-\frac{dn_i}{dt} = p_i n_i \frac{\sigma_r n}{\sigma_r n + \sigma_t (N_i - n_i)}. \qquad (1)$$

[1] I. A. Farfianovich, J. Exptl. Theoret. Phys. (U.S.S.R.) 21, 314 (1951). M. Schön, Naturwiss. 38, 235 (1951).

[2] G. Garlick and F. Gibson, Proc. Roy. Soc. (London) 188A, 485 (1947). R. Bube, Phys. Rev. 83, 393 (1951). N. P. Kalabuchov, Izv. Akad. Nauk SSSR, Fiz. Ser. 16, 130 (1952). D. Dutton and R. Maurer, Phys. Rev. 90, 126 (1953).

*The absorption associated with trapping centers in many cases, if not in all, lies in the visible region and leads to a coloring of the crystal. A decrease of $\Delta\varkappa$ corresponds to bleaching of the crystal.

[3] J. Randal and M. Wilkins, Proc. Roy. Soc. (London) 184A, 366 (1945).

[4] V. V. Antonov-Romanovskii, Izv. Akad. Nauk SSSR, Fiz. Ser. 10, 477 (1946).

σ_r is the effective recombination cross section; σ_t is the effective capture cross section; N_i, the number of absorption centers; n, the number of ionized luminescence centers; p_i, the probability of thermal release of the electrons. According to Ref. 5,

$$p_i = p_{i0} \exp(-E_T / kT). \qquad (2)$$

The quantity E_T will be called the thermal ionization energy of the absorption center.

Since the lifetime of an electron in a conduction band is much smaller than the lifetime of an electron in a level of the trap, then we may consider that n_i is equal to n. In most practical cases the excitation does not produce a complete filling of the traps [6] so that $n_i << N_i$ Eq. (1) can be rewritten in the form

$$-\frac{dn_i}{dt} = p_i n_i \frac{\sigma_r n_i}{\sigma_r n_i + \sigma_t N_i}. \qquad (3)$$

If the probability of retrapping A_t is significantly larger than the probability of recombination A_r, then

$$-dn_i / dt = p_i n_i^2 \sigma_r / \sigma_t N_i. \qquad (4)$$

Using the fact that, experimentally, the temperature is raised at a constant rate, $dT/dt = \beta_0$, Eq. (4) becomes

$$-dn_i / dT = p_i n_i^2 \sigma_r / \sigma_t N_i \beta_0. \qquad (5)$$

Integrating this expression with the condition $N = n_{i0}$ for $T = T_0$ gives

$$n_i = n_{i0} \left\{ 1 + \frac{\sigma_r n_{i0} p_0}{\sigma_t N_i \beta_0} \int_{T_0}^{T} [\exp(-E_T / kT)]\, dT \right\}^{-1}. \qquad (6)$$

If the probability of retrapping is much smaller than the recombination probability, then

$$-dn_i / dt = p_i n_i \qquad (7)$$

whereupon

$$n_i = n_{i0} \exp\left\{ -\frac{p_0}{\beta_0} \int_{T_0}^{T} [\exp(-E_T / kT)]\, dT \right\}. \qquad (8)$$

The theoretical dependence $n_i(T)$ has a much more complicated character if $A_t \approx A_r$.

Figures 1 and 2 show the theoretical dependence calculated from Eqs. (6) and (8) for trapping levels of different depths. In the calculations, it was assumed that $p_0 = 10^{10}$ sec^{-1}; $\beta_0 = 0.15°$ K/sec. In addition for the case $A_t >> A_r$ we took $\sigma_r n_{i0} / \sigma_t N_i = 10^{-2}$. The characteristic parameter of the curves $n_i(T)$ is the temperature T_k at which $n_i = 0.5\, n_{i0}$. From Figures 1 and 2 it follows that the following relationship holds with considerable accuracy:

$$E_T = \alpha T_k. \qquad (9)$$

The coefficient α depends essentially on the quantities p_0 and β_0 and for the case $A_t >> A_r$ also on n_{i0} / N_i. In Fig. 3 it is seen that upon decreasing β_0 the region of rapid fall-off of $n_i(T)$ is displaced toward lower temperatures. We notice that the form of Eq. (8) does not depend upon the number of trapped electrons, but that the form of Eq. (6) is significantly affected by it. Fig. 4 shows two curves of $n_i(T)$ for the case $A_t >> A_r$, calculated for different numbers of trapped electrons, $\sigma_r n_{i0} / \sigma_t N_i = 10^{-2}$ and 10^{-3}. It is seen that decreasing n_{i0} displaces the region of rapid fall-off toward higher temperatures. As is seen in Fig. 4, $\Delta T_k \approx 30°$ K, which means that this effect can easily be detected experimentally. For the case $A_t << A_r$ the form of $n_i(T)$ does not depend on the number of trapped electrons. Consequently, studying the dependence of the curves $n_i(T)$ on the number of trapped electrons may provide a suitable criterion for the character of the kinetics of the decay. Analogous criteria permitting distinguishing between the cases $A_t >> A_r$ and $A_t << A_r$ by the variation of $I(T)$ with n_{i0} were proposed by Antonov-Romanovskii.

We note that

$$-dn_i / dt = \eta I. \qquad (10)$$

---

[5] R. Kubo, Phys. Rev. 86, 929 (1952). M. A. Krivolgaz, J. Exptl. Theoret. Phys. (U.S.S.R.) 25, 191 (1953).

[6] V. V. Antonov-Romanovskii, Izv. Akad. Nauk SSSR Fiz. Ser. 15, 637 (1951).

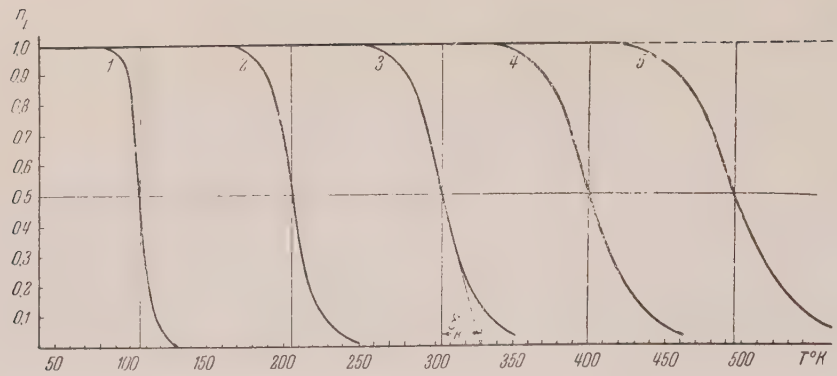

FIG. 1. Theoretical thermal bleaching curves for the case of large retrapping probability.

$p_0 = 10^{10}\ \mathrm{sec}^{-1}$; $\beta_0 = 0.15\ ^\circ\mathrm{K/sec}$; $\sigma_r n_{i0}/\sigma_t N_i = 10^{-2}$; Curve *1*, $E_T = 0.2$; Curve 2, $E_T = 0.4$; Curve *3*, $E_T = 0.6$; Curve *4*, $E_T = 0.8$; Curve *5*, $E_T = 1.0$ ev.

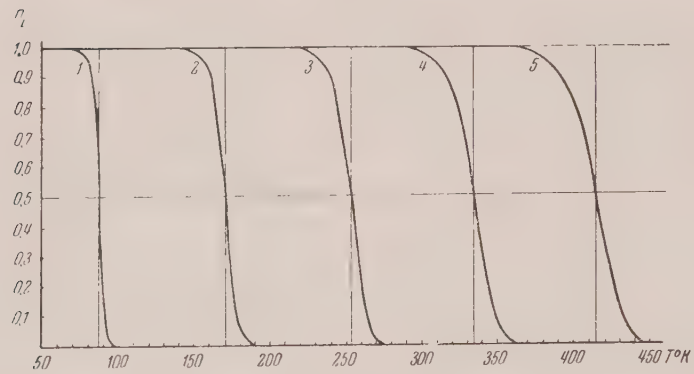

FIG. 2. Theoretical thermal bleaching curves for the case of small retrapping probability.

$p_0 = 10^{10}\ \mathrm{sec}^{-1}$; $\beta_0 = 0.15^\circ\ \mathrm{K/sec}$; E_T values same as in Fig. 1.

In the absence of any temperature quenching, n is a constant and the derivative of $n_i(T)$ should give a curve which has the same form as the thermal luminescence curve of the given phosphor. If there is temperature quenching then a comparison of $n_i(T)$ and $I(T)$ may give the temperature dependence of the "quantum efficiency of the phosphorescence", n. If there are traps of several different sorts in the phosphor with significantly different depths, then in that temperature region in which the electrons are being released from levels i

$$-\frac{dn_i}{dt} = p_i n_i \frac{\sigma_r n + \sum_{j>i} \sigma_{tj}(N_j - n_j)}{\sigma_r n + \sigma_{ti}(N_i - n_i) + \sum_{j>i} \sigma_{tj}(N_j - n_j)}. \quad (11)$$

Again considering that the lifetime of the electrons in the conduction band is short and that n_i is much less than N_i we have

$$-\frac{dn_i}{dt} = p_i n_i \frac{\sigma_r n + \sum_{j>i} \sigma_{tj} N_j}{\sigma_r n + \sigma_{ti} N_i + \sum_{j>i} \sigma_{tj} N_j}. \quad (12)$$

For the deepest levels, $\sum_{j>i} \sigma_{tj} N_j = 0$, and Eq. (12) is equivalent to Eq. (3), i.e., for the deepest traps relations hold which correspond to those found for a single level only. For shallower traps, $\sum_{j>i} \sigma_{tj} N_j \neq 0$. If $A_t >> A_r$ then

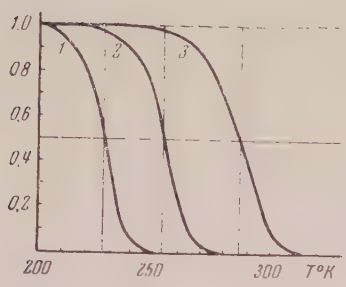

FIG. 3

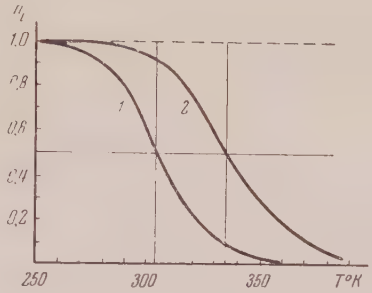

FIG. 4

FIG. 3. Theoretical dependence of the thermal bleaching curves on rate of warm-up for the case of small retrapping probability $E_T = 0.6$ ev; $p_0 = 10^{10}$ sec^{-1}; Curve *1*, $\beta_0 = 0.005$, Curve *2*, $\beta_0 = 0.15$, Curve *3*, $\beta = 4.5°$ K/sec.

FIG. 4. Theoretical dependence of the thermal bleaching curves on the number of trapped electrons for the use of large retrapping probability. $E_T = 0.6$ ev; $p_0 = 10^{10}$ sec^{-1}; $\beta_0 = 0.15°$ K/sec; Curve *1*, $\sigma_r N_{i0}/\sigma_t N_i = 10^{-2}$; Curve *2*, $\sigma_r N_{i0}/\sigma_t N_i = 10^{-3}$.

$$-\frac{dn_i}{dt} = p_i n_i \frac{\sum_{j>i} \sigma_{tj} N_j}{\sigma_{ti} N_i + \sum_{j>i} \sigma_{tj} N_j} = C p_i n_i . \tag{13}$$

From this we get

$$n_i = n_{i0} \exp\left\{ - C \frac{p_0}{\beta_0} \int_{T_0}^{T} [\exp(-E_T/kT)]\, dT \right\}. \tag{14}$$

If $A_t << A_r$ then

$$-dn_i/dt = p_i n_i \tag{15}$$

and

$$n_i = n_{i0} \exp\left\{ - \frac{p_0}{\beta_0} \int_{T_0}^{T} [\exp(-E_T/kT)]\, dT \right\}. \tag{16}$$

Thus for shallow traps, both cases $A_t >> A_r$ and $A_t << A_r$ give identical behaviors for $n_i(T)$. The only difference is the presence of the coefficient C in Eq. (14). We note that for all trapping levels other than the deepest in both limiting cases the form of $n_i(T)$ does not depend on the trapped light sum. Thus

$$I = -\frac{dn}{dt} = p_i n_i \frac{\sigma_r n}{\sigma_r n + \sigma_{ti} N_i + \sum_{j>i} \sigma_{tj} N_j}, \tag{17}$$

so that the curve determined by differentiating $n_i(T)$ will be similar to $I(T)$ only in the case of small probability of retrapping, in which case

$$I = p_i n_i . \tag{18}$$

If the probability of a retrapping is large, then

$$I = \frac{\sigma_r}{\sigma_{ri} N_i + \sum_{j>i} \sigma_{tj} N_j} p_i n_i n \tag{19}$$

and $-dn_i/dt$ will not coincide in general with I. Only if $n_i << n$ and consequently a release of electrons from levels i does not change the light sum n very much,

$$I = B p_i n_i \tag{20}$$

and $-dn_i/dt$ coincide in form with I in the absence of temperature quenching.

Therefore for other than the deepest traps, the theoretical dependence of $n_i(T)$ is much simpler than that of $I(T)$. The variation of $n_i(T)$ is also appreciably simpler than that of $i(T)$.

We now consider some methods for determining the thermal ionization energy of trapping centers from the parameters of the thermal quenching curves. Some such parameters are: 1) the temperature T_k of which $n_i = 0.5\, n_{i0}$; the "halfwidth of the fall-off" $\delta_k = -n_{ik}/(dn_i/dT)\, T_k$; δ_k is shown graphically in Fig. 1.

The relation between E_T and p_0 of the traps with the above parameters and with the warming rate

β_0 also may easily be found. For the case where

$$-\frac{dn_i}{dT} = \frac{p_0}{\beta_0}\left[\exp\left(-\frac{E_T}{kT}\right)\right]\frac{\sigma_r n_i^2}{\sigma_r n_i + \sigma_{ti} N_i}, \quad (21)$$

then for $T = T_k$

$$-\left(\frac{dn_i}{dT}\right)_{T_k} = \frac{p_0}{\beta_0}\left[\exp\left(-\frac{E_T}{kT}\right)\right]\frac{\sigma_r n_{ik}^2}{\sigma_r n_{ik} + \sigma_{ti} N_i}. \quad (22)$$

from which

$$E_T = kT_k \ln\left[\frac{p_0}{\beta_0}\delta_k\left(1 + \frac{2\sigma_{ti}N_i}{\sigma_r n_{i0}}\right)^{-1}\right]. \quad (23)$$

If $A_t >> A_r$, Eq. (23) becomes

$$E_T = kT_k \ln\left[\frac{p_0}{\beta_0}\delta_k \frac{\sigma_r n_{i0}}{2\sigma_{ti}N_i}\right]. \quad (24)$$

If $A_t << A_r$, then

$$E_T = kT_k \ln\left[\frac{p_0}{\beta_0}\delta_k\right]. \quad (25)$$

On the other hand, from the condition $n_i|_{T=T_k} = 0.5\, n_{i0}$, we get for the case $A_t >> A_r$

$$E_T = kT_k \ln\left[\frac{p_0 \sigma_r n_{i0} k T_k^2}{\beta_0 \sigma_{ti} N_i E_T}\right]; \quad (26)$$

and for the case $A_t << A_r$

$$E_T = kT_k \ln\left[\frac{p_0 k T_k^2}{\beta_0 E_T}\right]. \quad (27)$$

[Eqs. (26) and (27) come from an approximate integration of the exponential in (6) using the approximation, $1/T - 1/T_k \simeq (T_k - T)/(T_k^2)$, in the region where the integrand is not very small.) From (24) and (26), for $A_t >> A_r$,

$$E_T = 2kT_k^2/\delta_k. \quad (28)$$

Similarly for $A_t << A_r$, from (25) and (27),

$$E_T = kT_k^2/\delta_k \ln 2. \quad (29)$$

From what has been said before, it is evident that relations similar to (25) and (29) hold for other than the deepest traps. For this case a factor $C \lesssim 1$ must be inserted in (25). In Tables 1 and 2 are given the quantities T_k and δ_k determined from the data in Figs. 1 and 2 respectively. Also given are E_T calculated using (28) and (29). Comparing the first and fourth columns shows that (28) and (29) give somewhat too high values of E_T. The error never exceeds 7 per cent. Thus the expressions obtained above may be used to determine E_T for trapping centers. We note that the derivative curve $n'_i(T)$ also provides parameters (such as the position of the maximum T_m and the halfwidth of the peak δ) depending on E_T and p_0 and from which the latter may be calculated.[7,8] However, the graphical differentiation can be difficult and the determination of E_T using (23)-(29) seems more convenient to us.

TABLE I

E_T, ev	T_k, °K	δ_k, °K	E_T from Eq. (28)
0.2	106	9	0.215
0.4	206	17	0.430
0.6	304	26	0.620
0.8	400	33	0.830
1.0	496	41	1.060

TABLE II

E_T, ev	T_k, °K	δ_k, °K	E_T from Eq. (29)
0.2	88	4.5	0.217
0.4	171	8.5	0.425
0.6	254	12.5	0.635
0.8	335	17	0.820
1.0	415	20	1.070

It is easy to show that T_k differs little from T_m. If $A_t >> A_r$, T_k is a few degrees higher than T_m; if $A_T << A_r$, T_k is a few degrees lower than T_m. In the latter case

$$T_k - T_m \approx T_m \ln\ln 2 / \ln\left[\frac{p_0}{\beta_0}\delta_k\right]. \quad (30)$$

If the kinetics of the afterglow are monomolecular[9] then for the deepest as well as for the shallower traps,

$$n_i = n_{i0} \exp\left\{-C\,\frac{p_0}{\beta_0}\int_{T_0}^{T}\left[\exp\left(-\frac{E_T}{kT}\right)\right]dT\right\}. \quad (31)$$

[7] Ch. B. Lushchik, Dokl. Akad. Nauk SSSR, 101, 641 (1955).

[8] I. A. Farfianovich, J. Exptl. Theoret. Phys. (U.S.S.R.) 26, 696 (1954).

[9] V. V. Antonov-Romanovskii, Works (Trudy) of the Physical Institute, Academy of Sciences USSR, 24, 430 (1939).

For the case $A_t << A_r$, $C < 1$ and for $A_t \gg A$ $C = 1$. The form of $n_i(T)$ does not now depend on the number of trapped electrons. The thermal ionization energies of the traps may be determined using (25) and (29).

Until now we have been assuming that the number of electrons in certain trapping levels decreases as a result of releasing them to the conduction band where they subsequently recombine with holes in empty trapping centers or sometimes with ionized luminescence centers. However, it can also proceed through thermal ionization of the holes in "empty" trapping centers which recombine with trapped electrons. In this case $n_i(T)$ will be determined by the thermal ionization energy of the "empty" trapping centers. The theory developed above may be generalized to the case where both holes and electrons can be released thermally.

We consider a crystal containing electron traps of depth E_T and hole traps of depth Q_T. We will devote all quantities pertaining to electrons with the index "e" and those pertaining to holes with "h". Assuming that the lifetimes of electrons in the conduction band and of holes in the filled band are small compared with p_e^{-1} and p_h^{-1} and also that $n_e << N_e$, $n_h << N_h$, we may write

$$-\frac{dn_i}{dt} = p_e n_i \frac{\sigma_{re}\, n_i}{\sigma_{re} n_i + \sigma_{te} N_e} + p_h n_i \frac{\sigma_{rh}\, n_i}{\sigma_{rh} n_i + \sigma_{rh}\, N_h}. \tag{32}$$

(The number of recombinations of free holes with free electrons will be significantly smaller, because of their small concentrations, than the recombinations with trapped charges and is therefore neglected.) If $Q_T > E_T$ then $p_e >> p_h$ and

$$-\frac{dn_i}{dt} = p_e n_i \frac{\sigma_{re}\, n_i}{\sigma_{re} n_i + \sigma_{te} N_e}. \tag{33}$$

If $Q_T < E_T$ then $p_e << p_h$ and

$$-\frac{dn_i}{dt} = p_h n_i \frac{\sigma_{rh}\, n_i}{\sigma_{rh} n_i + \sigma_{th} N_h}. \tag{34}$$

We emphasize that the law of variation of the number of electron traps and of hole traps are identical. However, for $Q_T > E_T$, $n_i(T)$ leads to a determination of the thermal ionization energy of electron traps and for $Q_T < E_T$ – hole traps. Thus only the smaller of E_T and Q_T can be determined from $n_i(T)$ and not the larger.

The case $Q_T < E_T$ corresponds to the presence of high temperature quenching.[9a] Equation (32) represents a generalization of a relation found by Antonov-Romanovskii for the decay of a bimolecular afterglow process with a monomolecular quenching[9a] (see also Ref. 10). We note that the lower temperature quenching (which occurs after recombination of an electron with a luminescence center) does not affect the behavior of $n_i(T)$ but may greatly change $I(T)$.

Consequently, even for luminescent crystals, the thermal-bleach method has wider applicability than the thermal luminescence method.

EXPERIMENTAL DETERMINATION OF THERMAL BLEACHING CURVES

To determine $n_i(T)$ it is necessary to measure some quantity proportional to n_i while the crystal is being warmed up at a constant rate. One such quantity is the absorption coefficient in the maximum of the band of the additional absorption $\Delta\varkappa_{mi}$

$$\Delta\varkappa_{mi} = Bn_i.$$

It should be remarked that even for the case n_i = const. there is some dependence of $\Delta\varkappa_{mi}$ on temperature because of the change in shape of the absorption band, so that strictly speaking $B = B(T)$. However, as has been shown in a number of experimental investigations and as follows also from the calculations of Pekar[11] when n_i = const $\Delta\varkappa_{mi} \sim T^{-1/2}$ so that the coefficient B depends very weakly on temperature. The dependence $B(T)$ may be entirely neglected in comparison with the extremely rapid variation of $n_i(T)$. For this reason in the following, we will assume that

$$\Delta\varkappa_{mi} = Bn_i \text{ and } B \neq B(T). \tag{35}$$

We note that the increase in dielectric constant of a crystal with excitation $\Delta\epsilon$ is also proportional to n

[10] N. A. Tolstoi, Dokl. Akad. Nauk SSSR 95, 249 (1954).

[11] S. I. Pekar, *Investigations of the Electron Theory of Crystals*, GTTI, 1951 (Translated into German, Academie Verlag, Berlin, 1954).

$$\Delta\epsilon = B'n$$

However in this case, as has been observed by Garlick[12] the coefficient B' is extremely sensitive (exponentially) to temperature. Thus $\Delta\epsilon(T)$ does not permit a determination of $n_i(T)$. Consequently, the measurement of $\Delta\varkappa_{mi}(T)$ seems most suitable for the determination of $n_i(T)$.

In order that the process of measuring $\Delta\varkappa_{mi}$ does not decrease the number of trapped electrons through optical excitation it is necessary to work with weak light intensity. It is evident that this restriction is determined only by the sensitivity of the radiation detector being used and may always be satisfied. For the crystals studied by us using a SF-4 spectrophotometer the number of optically released electrons was determined to be not greater than 1% of the number of electrons thermally released during the measurement.

The most suitable objects for measurement are single crystals which permit precision determinations of the absorption coefficient. Since the determination of the curve $\Delta\varkappa_{mi}(T)$ is made using a single wavelength, the method may also be used with thin polycrystalline layers in which light scattering takes place. For this the most suitable material is evidently the so-called sublimate phosphors.[13]

We have tested the thermal bleach method on single crystals of alkali halides of highest purity. The $\Delta\varkappa_{mi}(T)$ curves were determined using a special adaptation for this purpose of a SF-4 spectrophotometer. The rate of warmup was 0.15°K per second, i.e., the same magnitude that was used in the previous calculations. Since the crystals that were investigated emit a weak thermal luminescence upon being warmed up, we put a filter before the window of the photo element which passed only the "operating wavelength" corresponding to the maximum of the band of the additional absorption.

It should be remarked that the sensitivity of the thermal bleach method is significantly less than that of the method of thermal luminescence. The latter method permits the investigation of traps in phosphors which do not have sufficient absorption to be detected.

APPLICATION OF THE METHOD TO THE STUDY OF TRAPPING CENTERS

The method of thermal bleach has been applied by us to the study of several trapping centers in alkali halide crystals. We studied single crystals KCl with small additions of bivalent ions of metals in the second group. The single crystals were grown by the method of Kyropulous. The concentration of the additive corresponds to the amount introduced in the melt.

The single crystals which were grown from KCl marked cp were very weakly colored by a condensed aluminum spark. Irradiation with x-rays produced an intense violet color. The spectrum of the additional absorption in an x-irradiated single crystal of KCl which was measured on the SF-4 spectrophotometer is shown in Fig. 5 (curve a). It

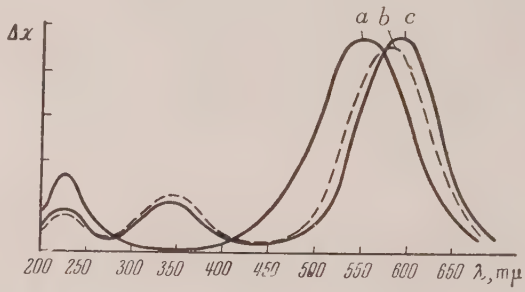

FIG. 5. Spectra of the additional absorption: *a*-KCl, x-rayed; *b*-KCl · $SrCl_2$ · 0.5 mol%, excited by spark; *c*-KCl · $CaCl_2$ · 0.5 mol%, excited by spark.

consists of two widely separated bands at 555 and 225 $m\mu$. The first band corresponds to the so-called F-color centers (electrons), the second to V-color centers (holes). Single crystal KCl containing a small quantity (0.5 mole per cent) $CaCl_2$ and $SrCl_2$ are colored very much more easily than the single crystals of pure KCl. Illumination by an aluminum spark for a period of one hour produced about 10^{16} color centers per cm.^{3} *. The spectra of the additional absorption produced by the aluminum arc in the crystals of KCl · $CaCl_2$ and KCl · $SrCl_2$ are shown in Fig. 5 (curves *b* and *c*).

[12] G. Garlick, *Luminescent Materials*, Oxford, 1949.

[13] F. D. Klement, Izv. Akad. Nauk SSSR, Fiz. Ser. 9, 411 (1945).

*The number of Ca^{++} and Sr^{++} ions present in the crystal and acting as electron traps is not less than $5 \cdot 10^{17}$ per cm.^{3} Thus the relationship $n_i << N_i$ is very well satisfied in our case.

For $KCl \cdot CaCl_2$ there are bands at 580, 350, and 225 mμ. For $KCl \cdot SrCl_2$ there are bands at 590, 350, and 225 $m\mu$. The bands at 580 and 590 $m\mu$ coincide well with the so-called Z_1-bands in additively colored crystals of $KCl \cdot CaCl_2$ and $KCl \cdot SrCl_2$ studied by Pick.[14]

Similar bands have been found by Etzel[15] in x-irradiated crystals of $NaCl_2$ -$CaCl_2$. According to the hypothesis of Seitz[16] these bands correspond to electrons that are trapped at bivalent alkaline earth ions. The bands at 225 $m\mu$, which are present also in pure KCl as well as in KCl containing Ca^{++} and Sr^{++}, Seitz attributes to a complex of vacancies which has trapped holes.[17]

It is of interest to study the 350 $m\mu$ band which is present in $KCl \cdot CaCl_2$ and $KCl \cdot SrCl_2$ but which is absent in pure KCl. As is known[18] in pure KCl at 78° K there is a band of additional absorption at 335 mμ which disappears at room temperature and which Seitz attributes to holes trapped at single cation vacancy sites.[17] Since in crystals containing bivalent positive ions there must also be an equal number of cation vacancy sites, it is not surprising that similar bands appear in crystals of $KCl \cdot CaCl_2$ and $KCl \cdot SrCl_2$.

We note that in correspondence with the data of Etzel for $NaCl \cdot CaCl_2$[15] we have also found that the addition of $CdCl_2$ to KCl does not lead to strong coloring. Apparently the Cd^{++} ions form complexes with the cation vacancy at room temperature in contrast to Ca^{++} and Sr^{++} . This is not surprising since it is more electropositive than Ca^{++} and Sr^{++} because of the special electronic shell structure of Cd^{++}.*

From Fig. 5 it follows that the optical activation energy E_λ of the trapping centers in the impure crystals is less than E_λ for F-centers and that E_λ for Sr^{++} is less than for Ca^{++}. It is of interest to see whether there is a correspondingly similar behavior for the thermal ionization energies also. In order to determine E_T we used the method of thermal bleaching. The curve of $\Delta\varkappa_{mi}(T)$ so obtained for the electron traps is given in Fig. 6. From the figure it is immediately clear that the thermal ionization energies of the traps in the impure crystals is less than E_T for F-centers and that E_T for Sr^{++} is less than for Ca^{++}.

In order to obtain quantitative data about E_T of the corresponding traps it was necessary first to consider the question of the applicability to the present case of the different formulas introduced earlier. Since we experimented with crystals in which there were practically only traps of a single depth, then by studying the dependence of the shape of the curve $\Delta\varkappa_{mi}(T)$ on the number of trapped electrons it was possible to give a direct experimental answer to the question of which one of the various formulas derived earlier is applicable to the present case. We measured the curves $\Delta\varkappa_{mi}(T)$ for two values of the trapped light sum (n_{01}: n_{02} = 8.1). As is seen in Fig. 7, the shape of $\Delta\varkappa_{mi}(T)$ is practically independent of n_{i0} (in particular T_k does not depend on n_{i0}). The data presented justify the conclusion that there is small probability of retrapping in phosphors of this type which was made by us in an earlier work.[7]

In Fig.8 are given curves of thermal bleaching of the phosphor $KCl \cdot TlCl$ which were obtained under the same conditions as the curve $\Delta\varkappa_{mi}(T)$ for KCl.* Comparing T_k of the curve $\Delta\varkappa_{mi}(T)$ for F-centers in KCl and T_m of the corresponding thermal luminescence peak shows that $T_m > T_k$. This also affirms the conclusions of the theory which assumes small probability of retrapping. We note that graphical differentiation of the curve $\Delta\varkappa_{mi}(T)$ gives a curve which almost coincides in form with the curve $I(T)$ (Fig. 8, curves 2 and 3).

On the basis of these experiments we used formulas (25) and (29) to calculate the thermal ionization energy. In using (25) we assumed in accordance with the result of earlier work[20] that $p_0 = 10^{10}$ sec.$^{-1}$ The quantities obtained by the different methods differed from each other by no more than

*Shamovskii and Gosteva[19] have given another interpretation to this observation.

[14] H. Pick, Ann. d. Phys. 5, 35 (1939).

[15] H. Etzel, Phys. Rev. 87, 906 (1952).

[16] F. Seitz, Phys. Rev. 83, 134 (1951).

[17] F. Seitz, Phys. Rev. 79, 529 (1950).

[18] P. Pringsheim, R. Casler, P. Yuster, J. Chem. Phys. 18, 1564 (1950).

[19] L. M. Shamovskii and M. I. Gosteva, Zh. Fiz. Khim. 28, 1266 (1954).

*The curve $I(T)$ was obtained after a preliminary warming to 380° K and subsequent cooling to room temperature.

[20] Ch. B. Lushchik, Dokl. Akad. Nauk SSSR 101, 833 (1955).

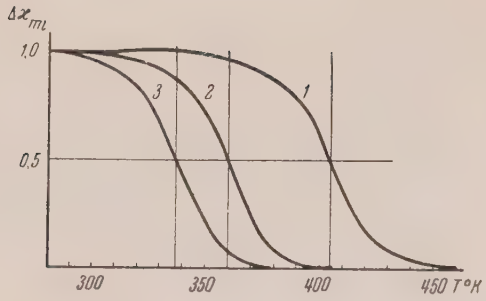

FIG. 6

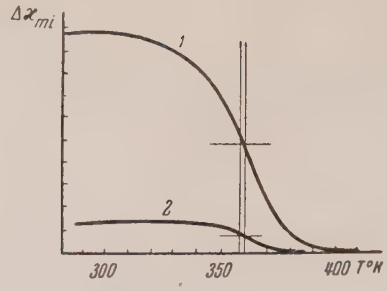

FIG. 7

FIG. 6. Thermal bleaching curves for electron traps: *1*-KCL, λ_m=555 mμ, β_0= 0.15 ° K/sec; *2*-KCl· $CaCl_2$, λ_m= 580 m μ, β_0= 0.15 ° K/sec; *3*-KCL · $SrCl_2$, λ_m= 590 mμ, β_0= 0.15 ° K/sec.

FIG. 7. Dependence of the thermal quenching curves on the number of trapped electrons. λ_m = 580 m μ, β_0 = 0.15 ° K/sec; *2*-KCl· $CaCl_2$ spark excited 3 hours; *2*-KC · $CaCl_2$ spark excited 15 minutes.

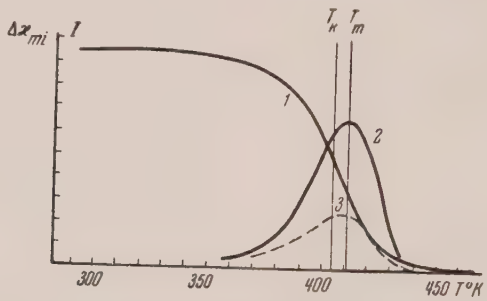

FIG. 8. Comparison of the thermal bleaching and thermal luminescence curves. β_0=0.15 ° K/sec; *1*-$\Delta\varkappa_{mi}(T)$ for the *F*-band of *x*-irradiated KCl; *2*-$I(T)$ for spark excited KCl · TlCl 0.01 mol %; *3*-the graphical differentiation of $\Delta\varkappa_{mi}(T)$.

5%. The calculated values of E_T are given in Table 3. The values of E_λ are given also for comparison. From the values in the table it follows that E_T and E_λ are larger for *F*-centers than for the centers which are produced by adding Ca^{++} and that E_λ and E_T are larger for the impurity centers in KCL · $CaCl_2$ than for the traps in KCl · $SrCl_2$. This agrees with the fact that the ionization potentials of a hydrogen atom (analog of an *F*-center) is greater than the ionization potential of Ca^+ but that the latter is greater than the ionization potential of Sr^+.

We also measured the curves of thermal bleaching of the trapping centers for holes (λ_m = 350 mμ) in KCl · $CaCl_2$ and KCl · $SrCl_2$. Comparing $\Delta\varkappa_{mi}(T)$ for the hole traps (Fig. 9) and $\Delta\varkappa_{mi}(T)$ for the electron traps (Fig. 6) shows that the de-

TABLE III

	E_λ in ev	E_T from Eq. (25) in ev	E_T from Eq. (29) in ev
KCl	2.22	0.97	1.02
KCl·$CaCl_2$	2.12	0.85	0.86
KCl·$SrCl_2$	2.08	0.80	0.80

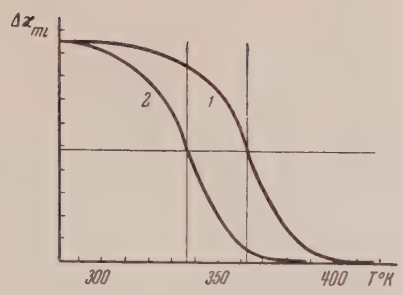

FIG. 9. The thermal bleaching curves for hole traps. *1*-KCl · $CaCl_2$ $\lambda_m = 350$ m μ, $\beta_0 = 0.15$ °K/sec; *2*-KCl · $SRCl_2$, $\lambda_m = 350$ mμ, $\beta_0 = 0.15$ ° K/sec.

crease in the number of electrons and in the number of holes follows the same law just as one should expect. In connection with this result the question arises: Which are freed by the warming up, electrons or holes? We assume that the electrons are released. This assumption is based on the following facts:

1. The peak of the thermal luminescence in the phosphor KCl · TlCl which is associated with recombination of electrons (!) with ionized luminescence centers agrees well with the region of rapid fall-off of the curve $\Delta\varkappa_{mi}(T)$ (see Fig. 8).

2. For electron traps E_λ depends on the type of impurity, for hole traps it is independent of the impurity. Since the data from the thermal quenching shows clearly a dependence of E_T on the type of impurity it is natural to consider that warming the crystal releases electrons. Then the temperature dependence of the absorption coefficient associated with the hole traps is determined by the thermal ionization energy of the trapped electrons.

The data given here, notwithstanding its illustrative character, serve in our opinion as evidence for the potential usefulness of the method of thermal quenching for the investigation of trapping centers in crystals. The application of this method in conjunction with the thermal luminescence method and the method of additional absorption will permit extending our knowledge of trapping centers in crystalline materials.

The present work was carried out in the laboratory of luminescence under the guidance of Prof. F. D. Klement to whom the author offers his deep thanks for the interpretation of the results. An author is very much indebted also to N. Lushchik and E. Vil'per for their help in this work.

Translated by B. Goodman
93

Nuclear Shells and the Classification of Atomic Nuclei*

A. V. SAVICH

J. Exptl. Theoret. Phys. (U.S.S.R.) 30, 501-510 (March, 1956)

A nuclear shell model in proposed, on the basis of which classification is carried out of the spins and magnetic moments of the ground and metastable levels of nuclei with odd mass number. Classification is also made of the masses and of data on β-decay of nuclei with odd mass number.

1. CONSTRUCTION OF A SHELL SYSTEM IN ATOMIC NUCLEI

N the research of Mayer,[1] the three dimensional harmonic oscillator was used as a model for the construction of nuclear shells. The number of states N_v of a three dimensional oscillator with vibration quantum number v for particles of spin ½ is given by the formula

$$N_v = (v+1)(v+2) \quad (v = 0, 1, 2, \ldots)$$

(the number of the shell is designated as $v+1$). In the successive filling of such shells, the following numbers are obtained for closed "magic" configurations: 2,8,20,40,60,112. Absent from this list is a series of "magic" numbers that are well known from the experiment: 28, 50, 82, 126.

We assume that both successive and non-successive filling of shells are possible in atomic nuclei; the latter is the case when one internal shell is entirely unfilled with nuclei (for example, the filling of shells 1, 2, 4 with a skipping of shell 3 gives the "magic" number 28 = 2 + 6 + 20, etc.). We begin with the assumption that in certain atomic nuclei the process of non-successive filling of nuclear shells can be energetically more favorable than the process of their successive filling. For example, one can expect that in nuclei which have a number of nucleons of a particular kind close or equal to 28, non-successive filling of the levels will be more likely than successive filling, in which there are about 8 nucleons outside of the closed shell of 20 nucleons.

All the "magic" numbers which are obtained both in successive filling of the nuclear shells, and in the skipping of one of the interior shells are shown in Table 1. In each square of the table, there is placed, along with the magic number, the list of filled levels which correspond to this magic number. The entire set of magic numbers of Table 1 can be characterized by two integers n_+ and n_- (laid out in the table along the vertical and horizontal axes). The number n_+ denotes the number of levels filled successively before the break, the number n_- denotes the number of levels filled successively after a single interior skipping (unfilled level).

We referred earlier to "subshells", i.e., to energetically less favorable configurations, all capable of filling, for which $n_- > n_+$. In such configurations, relatively low energy levels are left unfilled. Below, we shall give additional arguments for the usefulness of such a subdivision. After separation of the "subshells," there remain 15 "magic" numbers on the left side of Table 1. Of these, 6 correspond to successive filling ($n_- = 0$): 2, 8, 20, 40, 70, 112; 5 correspond to an unfilled penultimate shell ($n_- = 1$) : 14, 28, 50, 82, 126; 3 correspond to $n_- = 2$: 58, 92, 138; and, finally, one — 148 — corresponds to $n_- = 3$. Experimental data show that 7 magic numbers (2, 8, 20, 28, 50, 82, 126) stand out clearly.

There have been reports on the literature in the existence of four more shells: 40, 70, 14, 58[2-3]; there is some indication of the existence of the shells 112, 92, 138. However, there has been very little experimental data in the region of heavy nuclei; it is possible that the existence of the shells 112, 92, 138 and 148 will receive further confirmation. That some of the shells stand out less clearly than the others can be explained in part in the following manner.

The closed properties are most prominent in nuclei with shells that are filled both for protons and for neutrons (double magic numbers). Making use of the list of shells and subshells in Table 1, we can find 19 stable nuclei of this type. In ten of them ($_2He_2^4$, $_8O_8^{16}$, $_{14}S_{14}^{28}$, $_{20}Ca_{20}^{40}$, $_{20}Ca_{28}^{48}$, $_{40}Zr_{50}^{90}$, $_{50}Sn_{70}^{120}$, $_{58}Ce_{82}^{140}$, $_{82}Pb_{126}^{208}$,

*In December, 1955, a supplementary paper was submitted which takes into consideration new data on nuclear masses and levels.

[1] M. G. Mayer, Phys. Rev. 78, 16 (1950).

[2] H. E. Duckworth et al., Phys. Rev. 83, 1114 (1951).

[3] G. P. Dubex and S. Iha, Phys. Rev. 85, 1042 (1952).

TABLE 1.

"Magic numbers"

n_+ \ n_-	0	1	2	3	4	5
0		2 6	2, 3 18	2, 3, 4 38	2, 3, 4, 5 68	2, 3, 4, 5, 6 110
	1 **2**	1, 3 **14**	1, 3, 4 34	1, 3, 4, 5 64	1, 3, 4, 5, 6 106	
2	1, 2 **8**	1, 2, 4 **28**	1 2, 4, 5 58	1, 2, 4, 5, 6 100		
3	1, 2, 3 **20**	1, 2, 3, 5 **50**	1, 2, 3, 5, 5.6 92	1, 2, 3, 5, 6, 7 **148**		
4	1, 2, 3, 4 **40**	1, 2, 3, 4, 6 **82**	1, 2, 3, 4, 6, 7 138			
5	1, 2, 3, 4, 5 **70**	1, 2, 3, 4, 5, 7 **126**				
6	1, 2, 3, 4, 5, 6 **112**					
7						

$_{92}U^{230}_{138}$) both filled shells are ground shells; they ought then to be more clearly delineated in comparison with the others. These are shells with $N = 2, 8, 14, 20, 28, 50, 70, 82, 126, 138$ and $Z = 2, 8, 14, 20, 40, 50, 58, 82, 92$. The remaining shells ought to be less clearly marked— these are the shells with $Z = 28, 70$ and $N = 40, 58, 92, 112, 148$. Seven of the double magic nuclei ($_{28}Ni^{62}_{34}$, $_{34}Se^{74}_{40}$, $_{50}Sn^{114}_{64}$, $_{50}Sn^{118}_{68}$, $_{64}Gd^{156}_{92}$, $_{70}Yb^{170}_{100}$, $_{70}Yb^{176}_{106}$) have a filled ground shell and one subshell; finally, in two nuclei ($_{6}C^{12}_{6}$ and $_{64}Er^{168}_{100}$) both the filled shells are subshells. Therefore, one should expect that the most clearly evident subshells will be $Z = 6, 34, 68$ and $N = 6, 34, 64, 68, 100, 106$. It is interesting to note that in tin, the element with the largest number of β-stable isotopes, there is the largest number of β-stable double magic isotopes: $_{50}Sn^{114}_{64}$, $_{50}Sn^{118}_{68}$, $_{50}Sn^{120}_{70}$.

It is more appropriate to compare the vibrational levels under consideration with the vibrational levels of polyatomic molecules, rather than with single particle levels, as is done in the quasi-atomic model of the nucleus. However, thereexists a definite connection between these two models. Post[4] has shown that the Schrödinger equation for

[4] H. R. Post, Proc. Phys .Soc. (London) 66A, 649 (1 953).

a system of vibrating particles, interacting with each other in pairs according to Hooke's law, can lead to the Schrödinger equation for noninteracting particles located in the field of some effective oscillation potential.

3. CLASSIFICATION OF SPINS AND MAGNETIC MOMENTS OF NUCLEI WITH ODD A: NUCLEAR ISOMERS

In our model, a given atomic nucleus can have different configurations of filled levels, one of which (the energetically more favorable) corresponds to the ground level, the others to definite excited levels. It is appropriate to distinguish the different nuclear configurations with the numbers n_- and n_+ introduced above.

The spin and magnetic moment of a nucleus with odd mass number A is determined, as usual, by the configuration of shells with odd numbers of nucleons. The shell of a given nucleus with different configurations will correspond to different values of nuclear spin I and magnetic moment μ. If the two lowest energy levels of different configuration (one of which is the ground level) are close together in energy, then the phenomenon of isomerism will be observed for the large spin difference of these levels. In our treatment, isomeric transitions are accompanied by a rearrangement of the shells, which leads to additional prohibition rules in addition to those concerning spin and parity. In this connection, attention should be turned to the region of existence of even-even isomers; this is the region of rare earths with $A \approx$ 160-170, where double magic configurations exist with filled subshells. The closeness of the levels corresponding to such configurations, and to configurations with successive filling of shells, also leads to the existence of even-even isomers. Furthermore, it has been repeatedly noted in the literature[5,6] that systems of nuclear levels are observed in the decay schemes of certain radioactive isotopes between which no β-transitions occur, in spite of the fact that such transitions are in general not forbidden. We ascribe such systems of levels to the different shell configurations. It is of interest to note that they are connected with β-transitions and with various isomeric levels of the parent nucleus.

We shall denote the magnetic moments of nuclei with odd A by μ^+ and μ^- for nuclei belonging to the Schmidt groups ($l+1/2$ and $l-1/2$, respectively (or simply by the sign + or – along with the value of the spin). In our treatment, nuclei with magnetic moment μ^+ correspond to configurations in which an odd number of weakly interacting nucleons lie outside of the closed shell; nuclei of the type μ^- correspond to configurations in which a sufficiently large number of nucleons, which are very strongly coupled, lie outside the closed shell, and in which only a small number of nucleons is needed to fill the shell.

Experimental data permit the establishment of the following empirical dependence of the spins of the lowest states of the nuclei (of a definite configuration) on n_- and n_+:

$$I = (n_+ - n_-) + {}^1/_2 \text{ for nuclei of type } \mu^+, \quad (1a)$$

$$I = (n_+ - n_-) - {}^1/_2 \text{ for nuclei of type } \mu^-. \quad (1b)$$

The classification of spins and magnetic moments of the ground and metastable levels of nuclei with odd A which corresponds to these rules is given in Table 2. The Table is divided into four groups, corresponding to the four values of n_-: 0, 1, 2, 3; each group begins with the magic number for which $n_- = n_+$, i. e., the numbers 0, 14, 58, 148, respectively. Each group consists of two parts, which correspond to neutron and proton configurations. Within the limits of a single group, the spins of the nuclei, in accordance with the rules (1 a) and (1b), change regularly, undergoing successive unit increases after the filling of a new shell. A given value of the spin and magnetic moment of the nucleus can arise in the lowest state of a certain configuration for a wide interval of odd N or Z, whereupon configurations of the type μ^+ ought to arise in the initial filling of the shell, and configurations of the type μ^- in the closing of the shell. The regions of possible appearance of nuclear isomers are immediately evident from the Table. These are the regions in which the lowest state of the nuclei of different configurations differ strongly in spin value; N, Z= 41-49, where the configurations $9/2^+$, 0 and $1/2^-$, 1 (the first number denotes the value of n) , can compete with each other. Similar groupings are formed by the region of configuration $11/2^+$, 0, $3/2^-$, 1 and $1/2^+$, 2 for N, Z= 71-81, and the region $13/2^+$, 0, $5/2^-$, 1; $3/2^+$, 2 and $1/2^-$, 2 for N= 113-125.

As is seen from Table 2, the experimental data on spins and magnetic moments of nuclei with odd

[5] L. K. Pekar, L. A. Sliv and A. V. Zolotavin, Dokl. Akad. Nauk SSSR 88, 781 (1953).

[6] L. A. Sliv and L. K. Pekar, Dokl. Akad. Nauk SSSR 92, 277 (1953).

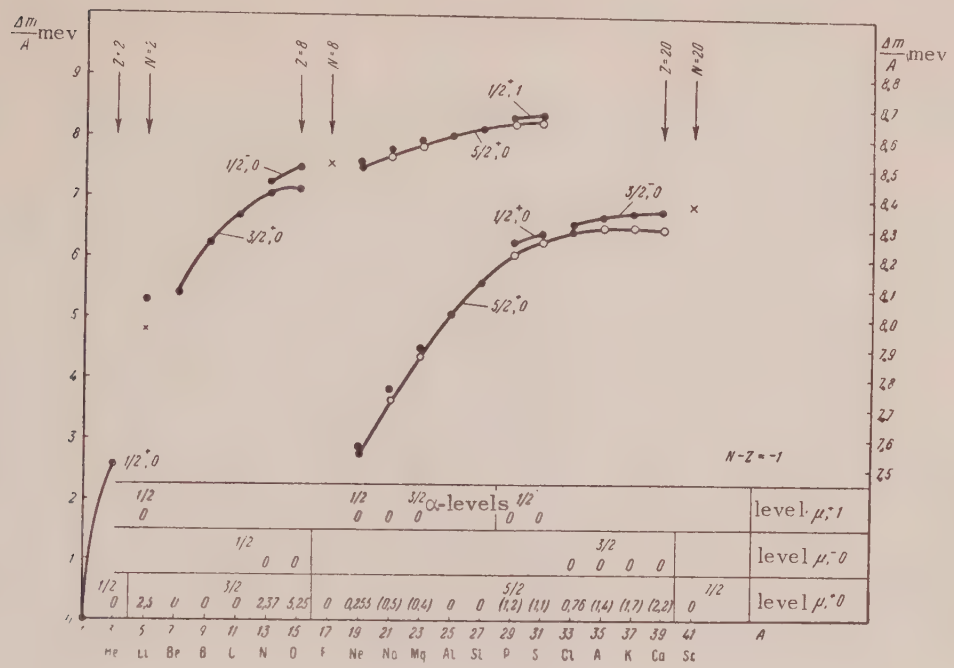

FIG. 1. Curves for the dependence of the packing fractions on the mass number for light nuclei with odd a and $N-Z=-1$. The upper part of the curves is given at the right on the increased mass scale.

NOTATION: O—nucleus with known mass, energy level; O—nucleus with unknown mass or undiscovered level; X—intermediate nucleus with different configurations for neutron and proton shells.

A) on the mass number[9,10]. Let us first consider Fig. 2 ($N-Z=+1$), where the data are most complete. The basic curve in this Figure links up the lowest level of configuration of consecutive filling of shells with the magnetic moment μ^+. It consists of four smooth parts, which correspond to consecutive filling of $l=1/2$, 3/2, 5/2 and 7/2. The following values of spin are attached to the excited levels of the series of nuclei: 3/2 – levels 3.09 C^{13}, 5.28 N^{15}; 5/2 – levels 0.197 F^{19}, 0.347 Ne^{21}, 0.439 Na^{23}, 1.28 Si^{29}, 1.03 P^{31}, 0.85S^{33}, 1.1 Cl^{35}, 1.46 A^{37} (all levels in mev). Such a value of the spin does not contradict the experimental data. In K^{39}, in accordance with the data curve, one must expect the levels $5/2^+$, 0 with energies of the order of 3 mev. The ground levels of the nuclei C^{13}, N^{15}, S^{33}, Cl^{35}, A^{37}, K^{39} correspond to the configurations μ^-, 0 and possess larger binding energies than the excited levels μ^+, 0; the latter are treated as weakly bound configurations. The levels of He^5 (2.6 mev), to which is assigned the spin $3/2^+$, $0^{17}(0)$ $5/2^+$ and Ca^{41} (0) $7/2^+$ lie in the transition region and are not included in the curves (μ^+, 0) and (μ^-,0). They occupy an intermediate position, since they have a closed neutron shell (which corresponds in mass to the configuration μ^-, 0), and a proton shell with the configuration μ^+, 0.

Here we must emphasize the essential difference between the suggested order of the levels and those accepted in the single particle model of Mayer. In accordance with the latter, in a shell with certain orbital quantum number l, the levels with $j=l+\frac{1}{2}$ are filled first, and then $j=lx-\frac{1}{2}$. For example, in the nucleus 0^{17}, for which an odd neutron is found in the shell $d_{5/2}$ in the ground state, there ought to be a low excited level in which the odd neutron would be found in the shell

[9] A. H. Wapstra, Physica 21, 367, 385 (1955); P. M. Endt and J. C. Kluyver, Revs. Mod. Phys. 26, 95 (1955); G. F. Pieper, G. S. Stanford and P. V. Herrman, Phys. Rev. 98, 1185 (1955); H. J. Gerber, M. G. Munoz and D. Maeder, Helv. Phys. Acta 28, 478 (1955); H. Daniel, Z. Naturforsch. 9a, 974 (1954).

[10] F. Ajzenberg and L. Dauritsen, Revs. Mod. Phys. 27, 77 (1955).

TABLE 2 [2]

Systematics of the spins and magnetic moments of stable and metastable levels of nuclei with odd A.

NOTATION: + or − on I conform to the proposed classification respectively for $\mu+$ or $\mu-$ The signs (+) or (-) for the excited levels of the isomers are given in parentheses. The figure in the parentheses denotes the number of nuclei with given (odd) N or Z for which the given value of I is measured (if it is greater than one). When the assumed classification does not agree with experiment, the experimental value of I is given in the table.

N,Z odd	$n_- = 0$			$n_- = 1$		
	I_{theor}	I_{exp} for N	I_{exp} for Z	I_{theor}	I_{exp} for N	I_{exp} for Z
0						
1	$^1/_2{}^+$	+(2)	+(2)			
2						
3	$^3/_2{}^+$	+	+			
5		+	+			
7	$^1/_2{}^-$	—	—			
8						
9	$^5/_2{}^+$	+	$^1/_2$			
11			$^3/_2$			
13		+	+			
14						
15					+	+
17	$^3/_2{}^-$	—	—(2)			
19		—	—(2)			
20				$^1/_2{}^+$		
21			+			
23	$^7/_2{}^+$	+	+			
25		$^5/_2$	$^5/_2$			
27		+	+(2)			
28						
29				$^3/_2{}^+$	+	+(2)
31						+(2)
33						+
35						+(2)
37		—	—			+
39	$^5/_2{}^-$					
4						—

$n_- = 0$	$n_- = 1$	$n_- = 2$

N odd	I_{theor}	I_{exp}	I_{theor}	I_{exp}	I_{theor}	I_{exp}
41		$+, {}^{5}/_{2}$	+			
43	$^{9}/_{2}+$		+	—	(—)	
45		$^{7}/_{2}$			—	
47		+	(+) (2)	(—)	—(3)	
49		+	+ (2)	$^{1}/_{2}-$ (—)	(—) (2)	
50						
51			—	+	+	
53			—(2)	+	+	
55			—(2)	+		
57			—	$^{5}/_{2}+$ +		
59				+	+	
61						
63		(—)	—	(+)	+(2)	
65				(+)	—	
67	$^{7}/_{2}-$		—	(—)		
69				(—)		
70						
71		(+)	$^{7}/_{2}$	(—)		
73	$^{11}/_{2}+$	(+)	$^{7}/_{2}$	(—)		
75		(+)		(—)	+(2)	
77		(+)		—	—(2)	
79		(+)	(+)	$^{3}/_{2}-$ —	(+) —	
81						
82						
83			—	+		
85				$^{7}/_{2}+$ +(2)		
87				+		
89						
91				+		
93				+		
95				+		
97				+		
99	$^{9}/_{2}-$			+		
101						

$n_- = 2$		
I_{theor}	I_{exp} for N	I_{exp} for Z
58		
	+	
$^{1}/_{2}+$	+	
	+	
	+	
	+	
	+	
	(+)	
		(+)
		+(2)
92		
		+
$^{3}/_{2}+$		$^{5}/_{2}$
		—

N odd	I_{theor}	I_{exp}	I_{theor}	I_{exp}	I_{theor}	I_{exp}
97			$^{7}/_{2}+$	+	$^{3}/_{2}+$	
99				+		
101						—
103				—		
105						
107						—
109						
111	$^{9}/_{2}-$					
112						
113	$^{13}/_{2}+$					
115						
117						
119		(+)		(—)		—, (+)
121		(+)		(—)		—, (+)
123			$^{5}/_{2}-$			+
125		(+)		(—)		
126						
127						
129			$^{9}/_{2}+$			
131						
133						
135					$^{1}/_{2}-$	
137						
138						
139						
141					$^{5}/_{2}+$	+
143						+
145						$^{1}/_{2}$
147						
149	$^{11}/_{2}-$		$^{7}/_{2}-$			+
151						

$n_- = 3$	
I_{theor}	I_{exp}
148	
$^{1}/_{2}+$	

[7] E. F. Kiol'ts, V. V. Kuntz and V. G. Khartman, Usp. Fiz. 55, 537 (1955).

A, and also on isomeric atomic nuclei, with few exceptions, agree excellently with the proposed classification.

We emphasize here that:

1) the experimental data verify that nuclei of the type μ^+ originate in the ground state at the beginning of filling of a shell, and nuclei of type μ^- at the end of filling of the shell;

2) the ground state of the nuclei always correspond to small numbers of nucleons outside the closed shell or to an insufficient number for closing. This rule is conspicuously violated among heavy nuclei;

3) Shells of successive filling ($n_- = 0$) appear mainly among nuclei with small A; shells of non-successive filling with $n_- = 1$ predominate in the lower states of nuclei with medium values of A, and, finally, in heavy nuclei, the lower states correspond chiefly to configurations of the type $n_- = 2$. This indicates that the spin of the nuclei is strongly dependent on its binding energy. Configurations with nucleons on the lower levels (successive filling) and even with a small number of nucleons outside of the closed shell, but with high spin (11/2, 13/2) are energetically less favorable than configurations with non-successive and less closed filling of shells, but with small spin (1/2, 3/2).

The possibility of a mutual effect of the proton and neutron shells on the order of nuclear levels can be shown in an example of a nucleus for which $N = 40\text{-}50$, $Z = 30\text{-}40$, and the ground and metastable levels correspond to the configurations $9/2^+$, 0 and $1/2^-$, 1 for neutrons, and $3/2^+$, 1, $5/2^-$, 0 for protons. This is the region of nuclear isomers with odd A and with transitions of the type $M4$. The question can be raised as to what combination of configuratons of neutron and proton shells is energetically most favorable. Frequently it can be solved from a consideration of β-transitions. For example, it is evident from the decay scheme of ${}_{38}Kr^{85}_{49}$ (Ref. 8, p. 193) that β-decay proceeds from the level $1/2^- Kr^{85m}$ to the level $3/2^+$ ${}_{37}Rb^{85}_{48}$ (excited) and from the level $9/2^+$ of the ground state of Kr^{85} to the level $5/2^-$ (ground) of Rb^{85}. One can draw the conclusion from this that the neutron configuration $1/2^-$, 1 exists together with the proton configuration $3/2^+$, 1, and the neutron configuration $9/2^+$, 0 along with the proton $5/2^-$, 0. An addition forbiddenness is superposed on a β-decay between other pairs of levels, by virtue of the configuration change.*

The spin of the ground level of the second isotope of rubidium ${}_{37}Rb^{87}_{50}$ is equal to 3/2. In this nucleus, the neutron configuration $n = 1$ is closed ($N = 50$) and the additional gain in binding energy leads to a change in the order of the levels — the configuration with neutron shell $n_- = 1$ and the proton configuration $3/2^+$, 1 correspond to the ground level. By considering the intercoupling of neutron and proton shells, it is possible to explain why certain configurations out of the number of those possible in the lowest state (that are in accord with the proposed model) are not observed experimentally. Continuing with this same line of argument, we can explain the absence of isomeric transitions for nuclei with $Z = 47\text{-}49$. In this range, for two possible proton configurations $n_- = 0$ and $n_- = 1$, there do not exist two corresponding pairs of neutron configurations which are energetically nearly equally favorable; therefore, the isomeric levels are widely separated.

The assumed model does not correspond to the experimental data in the range of light and medium nuclei for ${}_{9}F^{19}_{10}$ ($I = 1/2$) ${}_{11}Na^{23}_{12}$ (3/2), ${}_{22}Ti^{47}_{25}$ (5/2), ${}_{25}Mn^{55}_{30}$(5/2), ${}_{34}Se^{75}_{41}$(5/2), ${}_{34}Se^{79}_{45}$ (7/2). Further lack of correspondence is observed in the region of rare earths: ${}_{71}Lu^{175}_{104}$ (7/2), ${}_{73}Ta^{181}_{108}$ (7/2) and in the regions near uranium: ${}_{89}Ac^{227}_{138}$(3/2), ${}_{31}Pa^{231}_{140}$(3/2), ${}_{94}Pu^{239}_{145}$ (1/2), ${}_{95}Am^{241}_{146}$ (5/2). A possible explanation of this lack of correspondence in the region of light nuclei will be given below. In the region of rare earths and uranium these noncorrespondences can be connected with the appearance in the nuclei of α-particles — structures which go beyond the framework of the shell model.

3. MASSES OF LIGHT NUCLEI WITH ODD A AND β DECAY

Curves are shown in Figs. 1-3 of the dependence of the packing fraction (binding energy divided by

[8] M. Goldhaber and R. D. Hill, Revs. Mod. Phys. 24, 179 (1952).

*We note that in our treatment the change of spin ΔI coincides, as a rule, with the theory of Mayer, both for β and for γ-transitions; however, the change of parity frequently does not coincide, and together with this, new prohibition rules are introduced, due to the change of configurations, i.e., in Δn. Therefore the classification of β-transitions and nuclear isomers in the given treatment ought to be entirely different.

TABLE 3

lg ft for β-transitions of the type $\Delta I=0$. parity does not change, $\Delta n_{-}=0$, between configurations μ^{+}, 0 and μ^{-}, 0 for light nuclei with odd A(data taken from Refs. 11-13.

Configuration	spin	$N-Z$ original and final	number of nucleons outside of closed shell						
			1	3	5	7	9	11	13
μ^{+}, 0	1/2	−1, +1	n^{1} 3,21	H^{3} 3,06					
	3/2	−1, +1		Be^{7} 3,36		C^{11} 3,59			
	5/2	−1, +1 1,3		O^{19} 5,55*		Ne^{23} ~ 5,2*	Al^{25} 3,47 Na^{25} 5,2	Si^{27} 3,55	Al^{29} 5,21*
	7/2	−1, +1 1,3 3,5	Sc^{41} 3,40	Ti^{43} 3.40 Sc^{43} 5,31	Ti^{45} 4,6 Ca^{45} 5,85	V^{47} 4,7	Cr^{49} 5,0	Mn^{51} 5,4	
μ^{-}, 0	1/2	−1, +1	O^{15} 3,57	N^{13} 3,67					
	3/2	−1, +1 1,3	Ca^{39} 3,49	K^{37} 3,51 A^{37} 4,9	A^{35} 3,53 S^{35} 5,07	Cl^{33} 3.60 P^{33} 5,1			
			number of nucleons lacking to complete shell						
			−1	−3	−5	−7			

*Decay occurs in the excited level, the energy of which is given in Fig. 2.

[11] J. M. Hollander, I. Perlman and G. T. Seaborg, Revs. Mod. Phys. 25, 469 (1953).

[12] A. M. Feingold, Revs. Mod. Phys. 23, 10 (1951).

[13] R. W. King, Revs. Mod. Phys. 26, 327 (1954).

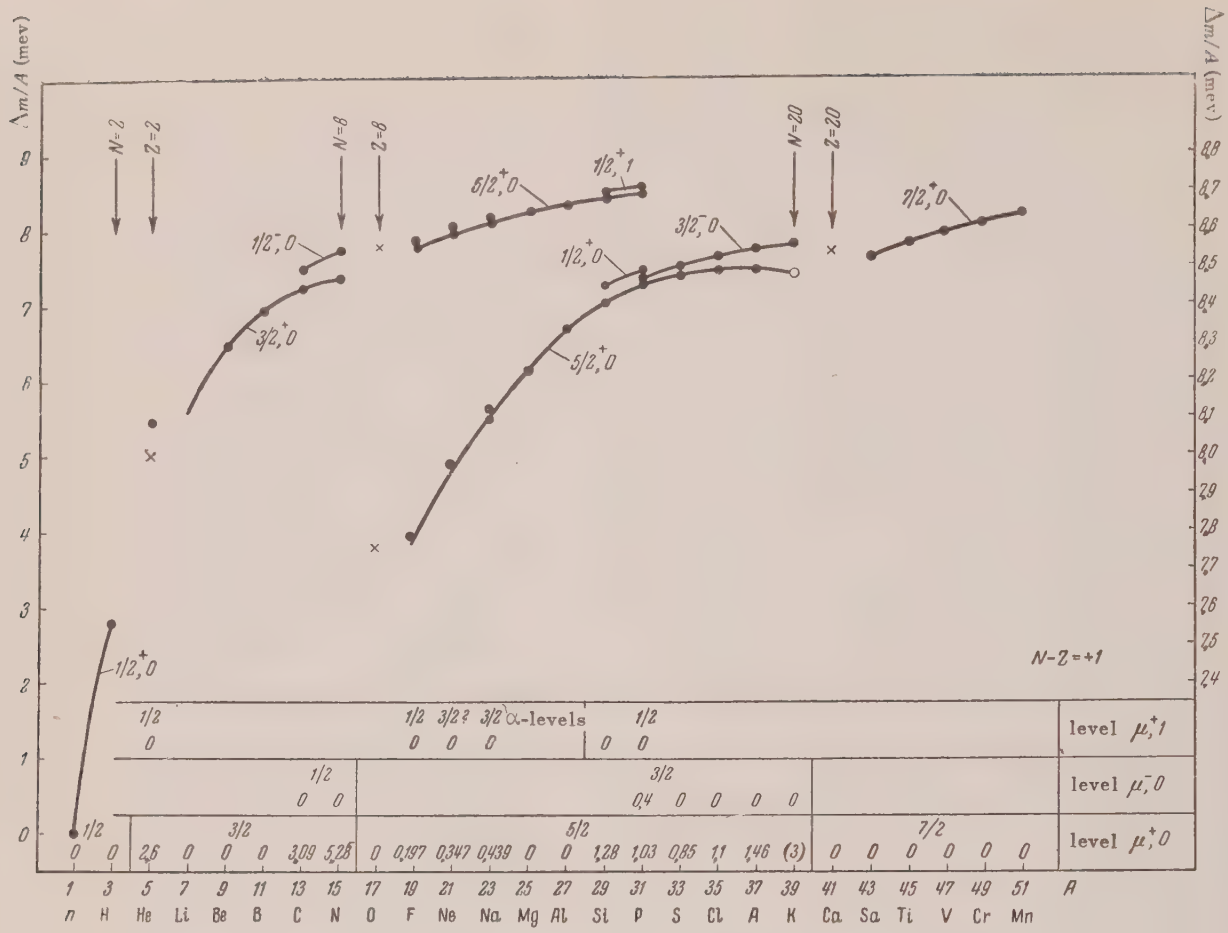

FIG. 2. Curves of the dependence of the packing fractions on the mass number for light nuclei with odd A, with $N - Z = -1$. Upper part of the curve is given at the right with increased mass scale. Notation same as Fig. 1.

$d_{3/2}$. In our treatment, these levels are classified as $5/2^+$, 0 and $3/2^-$, 0 and the level $3/2^-$, 0 cannot be observed in the O^{17} nucleus, since configurations of the type μ^- exist only when the shell is close to being filled (in the given case, for N, $Z = 17$, 19). Furthermore, in our treatment, for nuclei with a ground state μ^- (for example, with $3/2^-$, 0), one should expect a neighboring excited level μ^+ (for example, $5/2^+$, 0). In Mayer's model on the other hand, when an odd nucleon is found in the $d_{3/2}$ shell in the ground state of the nucleus, it cannot undergo transition to the $d_{5/2}$ shell in the excited state, since the latter is already filled.

We turn our attention to a consideration of Fig.2. The packing fractions of the ground state of the nuclei ${}_{14}Si^{29}_{15}$ and ${}_{15}P^{31}_{16}$ are separated on the curve since they correspond to a new configuration μ^+, 1, which is in the region $N, Z = 14$. In a series of nuclei where the rules, which connect the spins and configurations of nuclei (1a) and (1b), are not observed (F^{19}, Ne^{21}, Na^{23}), the ground levels must be related to α-configurations on the possibility of which in light nuclei has never been shown. These levels are drawn in the form of separate points under the curve μ^+, 0. The lower states of He^5 must also be related to α-configurations, which is confirmed by the method of obtaining this level — resonance scattering of neutrons by α-particles. The level 2.6 mev, which lies close to the curve μ^+, 0, is obtained from the reaction Li (d,α) He^5, i.e., from the "shell" nucleus Li^7 [10]. The curves of the packing fractions for nuclei with $N - Z = -1$ (Fig. 1) are analogous to the curves of Fig. 2. The levels of these nuclei are known much worse (the unknown levels are denoted by an open

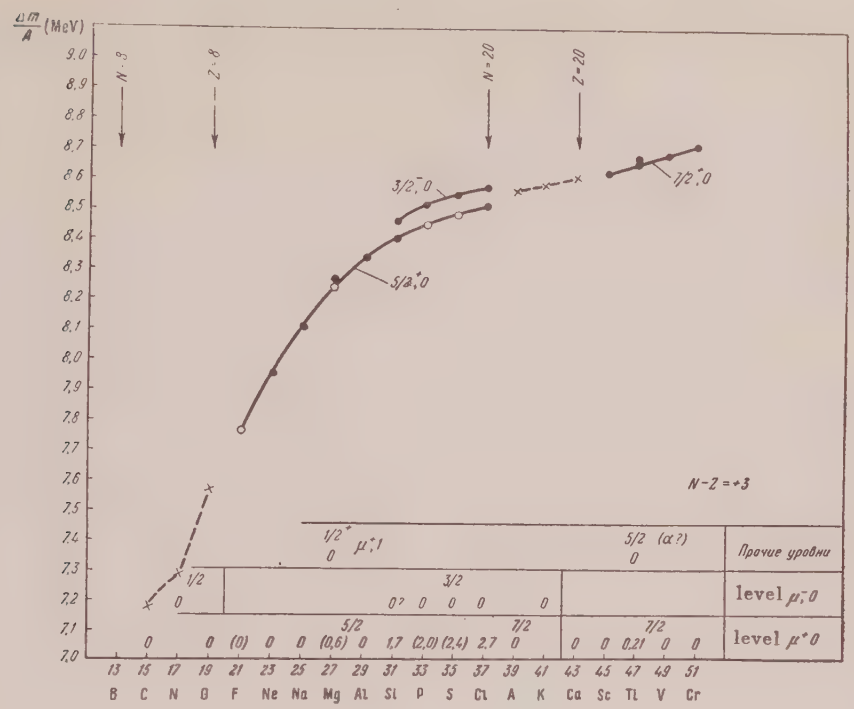

FIG. 3. The same as in Figs. 1 and 2 for nuclei with $N - Z=3$.

circle). It is difficult to doubt the existence of the assumed levels, since "similar" levels are always observed in mirror nuclei. The assumed energies of these levels are indicated in Fig. 1 in parentheses. For nuclei with $N - Z=3$, the packing fractions curve (Fig. 3) is similar to the curves of Figs. 1 and 2. We must regard the level treatment here less hopefully in view of the insufficiency of the experimental data. Thus the assumed classification of the levels makes it possible to systematize the masses and energies of the lowest levels of light nuclei with odd A.

For the systematics of the data on β-decay, we consider transitions between similar nuclear configuration μ^+, 0 or μ^-, 0 of the type $\Delta I=0$, $\Delta M=0$, with no change in the parity . Transitions in which the levels of other configurations enter in, are excluded from consideration.* The values of lg ft for the transitions under consideration are given in Table 3, from which the following regularities are seen;:

1) for nuclei of the type μ^+, 0, lg ft increases systematically with increase in the number of nucleons outside of the closed shell (with increase in A). The nuclei 0^{19} + Se^{43} are excluded;

2) for nuclei of the type μ^-, 0, lg ft increases systematically with increase in the number of nucleons needed to close the shell (with decreasing a).

Such a behavior of lg ft confirms the treatment of nuclei of the types μ^+ and μ^- as subshells and "holes" and indicates the dependence of the probability of transitions, above all, on the degree of closed-ness of the nuclear configurations between which this transition takes place.

Translated by R. T. Beyer
94

*For β-transitions with lg $ft\sim5$, the quantities ΔI cannot be determined unambiguously from β decay alone. The value $\Delta I=0$ is based on theoretical aasumptions, and is confirmed by the location of the corresponding levels on the curves for the packing fractions (see Figs. 2 and 3)

Motion of a Charged Particle in an Optically Active Anisotropic Medium, I

A. G. SITENKO AND A. A. KOLOMENSKII

Physics and Engineering Institute, Academy of Sciences of Ukrainian SSR

P. N. Lebedev Physics Institute, Academy of Sciences, USSR

(Submitted to JETP editor July 8, 1954)

J. Exptl. Theoret. Phys.(U.S.S.R.) 30, 511-517, (March, 1956)

The Fourier method is used to obtain expressions for the components of the electromagnetic field and for the total energy losses of a charged particle moving in an optically-active anisotropic medium.

1. THE passage of a charged particle through an optically-active anisotropic medium is characterized by many features. First, to satisfy the conditions for the Cerenkov radiation the moving charge need have a considerably lower velocity in an anisotropic medium than in an isotropic medium, because the index of refraction of the waves becomes large at certain definite frequencies. Second, if a charge moves in an active anisotropic medium with a uniform velocity greater than the phase velocity of light in the same medium, the light emitted by the charge is more complicated in nature as compared with the isotropic case. Instead of the single circular cone of rays observed for the isotropic body, we have in the active anisotropic case two noncircular cones of rays, with the radiation intensity varying on different generatrices of these conical surfaces.

The electrodynamics of anisotropic media was developed in the investigations of Ginzburg[1] who examined in particular the emission from an electron moving in a uniaxial crystal and from an oscillator placed in such a crystal. The problem of the energy losses of a charged particle moving in an anisotropic medium was subsequently treated in several investigations[2-5]. The work of Ref. 1 was generalized by one of the authors for the case when the medium is optically-active (gyrotropic) in addition to being anisotropic.

This article employs a method different from that used in Ref. 3 to determine the components of the electromagnetic field and the total energy losses of a charged particle moving in an optically-active anisotropic medium. The question of the singularities of the expressions obtained in Refs. 1-5 for the losses is discussed, and a computation method that does not lead to singularities is given.

2. The electromagnetic field produced in a medium in which a point charge q moves at a velocity $\mathbf{v}$ is given by Maxwell's equations:

$$\operatorname{rot}\mathbf{E} = -\frac{1}{c}\frac{\partial \mathbf{H}}{\partial t}; \tag{1}$$

$$\operatorname{rot}\mathbf{H} = \frac{1}{c}\frac{\partial \mathbf{D}}{\partial t} + \frac{4\pi}{c} q\,\mathbf{v}\,\delta(\mathbf{r}-\mathbf{v}t);$$

$$\operatorname{div}\mathbf{H} = 0; \qquad \operatorname{div}\mathbf{D} = 4\pi q\delta(\mathbf{r}-\mathbf{v}t).$$

We shall solve this system using the Fourier method

$$\mathbf{E}(\mathbf{r},t) = \iint \mathbf{E}(\mathbf{k},\omega)\, e^{i\mathbf{k}\mathbf{r}-i\omega t} d\mathbf{k}\, d\omega \tag{2}$$

etc. Using the connection between the Fourier components of the induction and of the field intensity

$$D_i(\mathbf{k},\omega) = \varepsilon_{ik}(\omega) E_k(\mathbf{k},\omega); \quad (\varepsilon_{ik} = \varepsilon_{ki}^*), \tag{3}$$

we obtain the following equation for the Fourier components of the electric field intensity $E(\mathbf{k},\omega)$

$$T_{ik}E_k = -i\frac{q}{2\pi^2}\frac{v_i}{\omega^2}\delta\left(\frac{n}{c}\varkappa_j v_j - 1\right), \tag{4}$$

where

$$T_{ik} = n^2(\varkappa_i\varkappa_k - \delta_{ik}) + \varepsilon_{ik}; \tag{5}$$

$$n^2 = k^2c^2/\omega^2; \quad \varkappa_i = k_i/k.$$

Using the inverse tensor T_{ik}^{-1}, we can represent the solution of Eq. (4) in the following form:

---

[1] V. L. Ginzburg, J. Exptl. Theoret. Phys. (U.S.S.R.) 10, 601, 608 (1940).

[2] A. A. Kolomenskii, Dokl. Akad. Nauk SSSR 86, 1097 (1952).

[3] A. A. Kolomenskii, J. Exptl. Theoret. Phys. (U.S.S.R.) 24, 167 (1953).

[4] M. I. Kaganov, J. Tech. Phys. (U.S.S.R.) 23, 507 (1953).

[5] K. Tanaka, Phys. Rev. 93, 459 (1954).

$$E_k = -i\frac{q}{2\pi^2\omega^2}T_{ki}^{-1}v_i\delta\left(\frac{n}{c}\varkappa_j v_j - 1\right). \tag{6}$$

To calculate the energy losses of a moving charge we employ the relationship

$$-d\mathscr{E}/dl = -(q/v)(\mathbf{vE})_{\mathbf{r}=\mathbf{v}t}, \tag{7}$$

where the value of the field is taken at the point where the charge is located. Using (6) and (2) we obtain the following value per unit path for the total energy losses due to the remote collisions:

$$-\frac{d\mathscr{E}}{dl} = i\frac{q^2}{2\pi^2 v} \tag{8}$$

$$\times\int_{-\infty}^{\infty}\int_0^{k_m}\int_{4\pi} T_{ki}^{-1}v_k v_i\delta\left(\frac{n}{c}\varkappa_j v_j - 1\right)\frac{d\omega}{\omega^2}k^2 dk\, do.$$

The integration with respect to k must be carried out up to a certain maximum value k_m of the order of magnitude of $1/b$, where b is the minimum parameter of the remote collisions.

3. Let us apply the equation obtained to the motion of a charged particle in an optically-active uniaxial crystal having a dielectric-constant tensor of the following form:

$$\varepsilon_{ik} = \begin{pmatrix} \varepsilon_1 & -i\varepsilon_2 & 0 \\ i\varepsilon_2 & \varepsilon_1 & 0 \\ 0 & 0 & \varepsilon_3 \end{pmatrix}. \tag{9}$$

In the case under consideration the tensor T_{ik} is defined by the matrix

$$T_{ik} = \begin{pmatrix} n^2(\varkappa_1^2 - 1) + \varepsilon_1 & n^2\varkappa_1\varkappa_2 - i\varepsilon_2 & n^2\varkappa_1\varkappa_3 \\ n^2\varkappa_1\varkappa_2 + i\varepsilon_2 & n^2(\varkappa_2^2 - 1) + \varepsilon_1 & n^2\varkappa_2\varkappa_3 \\ n^2\varkappa_1\varkappa_3 & n^2\varkappa_2\varkappa_3 & n^2(\varkappa_3^2 - 1) + \varepsilon_3 \end{pmatrix}. \tag{10}$$

To obtain the components of the inverse tensor it is necessary to divide the minors of the corresponding elements of tensor T_{ik} by the determinant consisting of its components. This determinant equals

$$T = (\varepsilon_1\sin^2\theta + \varepsilon_3\cos^2\theta)[n^2 - n_1^2(\theta)][n^2 - n_2^2(\theta)], \tag{11}$$

where

$$n_{1,2}^2(\theta) = \frac{(\varepsilon_1^2 - \varepsilon_2^2)\sin^2\theta + \varepsilon_1\varepsilon_3(1+\cos^2\theta) \pm \sqrt{(\varepsilon_1^2 - \varepsilon_2^2 - \varepsilon_1\varepsilon_3)^2\sin^2\theta + 4\varepsilon_2^2\varepsilon_3^2\cos^2\theta}}{2(\varepsilon_1\sin^2\theta + \varepsilon_3\cos^2\theta)} \tag{12}$$

are the ordinary and extraordinary index of refraction and θ is the angle between the optical axis of the crystal and the propagation direction k of the wave.

Equation (8) is a general expression for the energy losses of a moving particle. Let us apply this equation to the two simplest motions of a particle, along and perpendicular to the optical axis of a crystal.

4. In the case of a particle moving along the optical axis, we orient the coordinates as in Fig. 1. In this case Eq. (8) takes the following form:

$$-\frac{d\mathscr{E}}{dz} = i\frac{q^2 v}{\pi c^3}\int_{-\infty}^{\infty}\int_0^{n_m}\int_0^{\pi}\frac{n^4\cos^2\theta - n^2\varepsilon_1(1+\cos^2\theta) + \varepsilon_1^2 - \varepsilon_2^2}{(\varepsilon_1\sin^2\theta + \varepsilon_3\cos^2\theta)[n^2 - n_1^2(\theta)][n^2 - n_2^2(\theta)]} \tag{13}$$

$$\times\,\delta(n\beta\cos\theta - 1)\sin\theta\, d\theta\, n^2 dn\, \omega d\omega,$$

where k is replaced by a new variable $n = kc/\omega$. The delta function yields the integral with respect

to the angle variable, while the integration with respect to n must be restricted to a region from $1/\beta$ to $n_m = k_m c/\omega$. The integration yields

$$-\frac{d\mathscr{E}}{dz} = \frac{q^2}{\pi c^2}\,\mathrm{Re}\, i\int_0^\infty \frac{(1-\varepsilon_1\beta^2)(n_1^2-\varepsilon_1)-\beta^2\varepsilon_2^2}{\varepsilon_1\beta^2(n_1^2-n_2^2)}\ln\frac{n_m^2\beta^2-n_1^2\beta^2}{1-n_1^2\beta^2}\,\omega\, d\omega$$
$$+\frac{q^2}{\pi c^2}\,\mathrm{Re}\, i\int_0^\infty \frac{(1-\varepsilon_1\beta^2)(n_2^2-\varepsilon_1)-\beta^2\varepsilon_2^2}{\varepsilon_1\beta^2(n_2^2-n_1^2)}\ln\frac{n_m^2\beta^2-n_2^2\beta^2}{1-n_2^2\beta^2}\,\omega\, d\omega, \tag{14}$$

where

$$n_{1,2}^2 = \{(\varepsilon_1^2-\varepsilon_2^2+\varepsilon_1\varepsilon_3)\beta^2-(\varepsilon_3-\varepsilon_1)\pm[(\varepsilon_1^2-\varepsilon_2^2-\varepsilon_1\varepsilon_3)^2\beta^4$$
$$-2\varepsilon_1(\varepsilon_1^2-\varepsilon_2^2+\varepsilon_3^2)\beta^2+2\varepsilon_3(2\varepsilon_1^2+\varepsilon_2^2)\beta^2+(\varepsilon_3-\varepsilon_1)^2]^{1/2}\}/2\varepsilon_1\beta^2, \tag{15}$$

are the values of the indices of refraction in the direction of the emission maxima, determined by the following equations:

$$\cos^2\theta_{1,2} = 1/\beta^2 n_{1,2}^2(\theta_{1,2}).$$

It is evident that the energy losses of the moving charge will be caused by the frequency regions in which the arguments of the logarithms become negative, and also by frequencies at which the integrands have poles, for it is only in these cases that the real part of (14) differs from zero. We thus have

$$-\frac{d\mathscr{E}}{dz} = -\frac{q^2}{c^2}\int\frac{(1-\varepsilon_1\beta^2)(n_1^2-\varepsilon_1)-\beta^2\varepsilon_2^2}{\varepsilon_1\beta^2(n_1^2-n_2^2)}\,\omega d\omega - \frac{q^2}{c^2}\int\frac{(1-\varepsilon_1\beta^2)(n_2^2-\varepsilon_1)-\beta^2\varepsilon_2^2}{\varepsilon_1\beta^2(n_2^2-n_1^2)}\,\omega\, d\omega$$
$$+\frac{q^2}{v^2}\sum_i\frac{\omega_i}{|d\varepsilon_1/d\omega|_i}\ln\left\{1+\frac{k_m^2v^2}{\omega_1^2}\frac{\varepsilon_1}{\varepsilon_3}\right\},$$

where the integration is carried out in the first two terms over the frequency regions defined respectively by the following inequalities

$$n_m^2\beta^2 > n_1^2\beta^2 > 1;\quad n_m^2\beta^2 > n_2^2\beta^2 > 1, \tag{16}$$

and in the third term the summation is over those frequencies ω_i, at which ϵ_1, ϵ_2, and ϵ_3 vanish simultaneously. Substituting the explicit expressions for n_1^2 and n_2^2 we obtain finally

$$-\frac{d\mathscr{E}}{dz} = \frac{q^2}{2c^2}\int\left(1-\frac{1}{\beta^2\varepsilon_1}\right)$$
$$\times\left\{1\pm\frac{\varepsilon_1(\varepsilon_1^2-\varepsilon_2^2-\varepsilon_1\varepsilon_3)\beta^4-(2\varepsilon_1^2-2\varepsilon_1\varepsilon_3+\varepsilon_2^2)\beta^2-\varepsilon_3+\varepsilon_1}{(1-\varepsilon_1\beta^2)[(\varepsilon_1^2-\varepsilon_2^2-\varepsilon_1\varepsilon_3)^2\beta^4-2\varepsilon_1(\varepsilon_1^2-\varepsilon_2^2+\varepsilon_3^2)\beta^2+2\varepsilon_3(2\varepsilon_1^2+\varepsilon_2^2)\beta^2+(\varepsilon_3-\varepsilon_1)^2]^{1/2}}\right\}\omega d\omega$$
$$+\frac{q^2}{v^2}\sum_i\frac{\omega_i}{|d\varepsilon_1/d\omega|_i}\ln\left\{1+\frac{k_m^2v^2}{\omega_i^2}\left(\frac{\varepsilon_1}{\varepsilon_3}\right)_i\right\} \tag{17}$$

(integration over the regions defined by Eq. 16).

This expression determines the total energy losses

of the particle, including both the polarization and the Cerenkov losses. Let us note that Eq. (4.5) of Ref. 3 leads to the same expression for the integral of (17), which determines the Cerenkov losses.

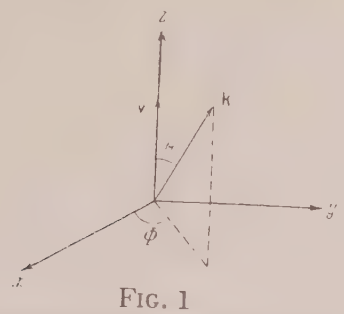

FIG. 1

5. To clarify the character of the losses given by (17), let us compute the energy flux through a cylindrical surface surrounding the trajectroy of the charge. For this purpose we shall first determine the field produced in an optically-active anisotropic medium by the motion of a point charge. Inserting Eq. (6) into Eq. (2), and using the known relationships

$$\int_0^{2\pi} e^{i\varkappa r\cos\vartheta}\,d\vartheta = 2\pi J_0(\varkappa r);$$

$$\int_0^{\infty} \frac{J_0(\varkappa r)\,\varkappa d\varkappa}{\varkappa^2+k^2} = K_0(kr); \quad \operatorname{Re} k > 0,$$

we obtain the components of the electric field intensity in cylindrical coordinates as follows:

$$E_z(\mathbf{r},t) = \frac{-iq}{\pi v^2}\int_{-\infty}^{\infty}\left\{\frac{(1-\varepsilon_1\beta^2)(n_1^2-\varepsilon_1)-\beta^2\varepsilon_2^2}{n_1^2-n_2^2}K_0(rk_1)\right. \tag{18}$$

$$\left.+\frac{(1-\varepsilon_1\beta^2)(n_2^2-\varepsilon_1)-\beta^2\varepsilon_2^2}{n_2^2-n_1^2}K_0(rk_2)\right\}e^{i\omega(z/v-t)}\frac{\omega d\omega}{\varepsilon_1};$$

$$E_r(\mathbf{r},t) = \frac{q}{\pi c}\int_{-\infty}^{\infty}\frac{1}{\varepsilon_1}\left\{\frac{n_1^2-\varepsilon_1}{n_1^2-n_2^2}k_1K_1(rk_1)\right.$$

$$\left.+\frac{n_2^2-\varepsilon_1}{n_2^2-n_1^2}k_2K_1(rk_2)\right\}e^{i\omega(z/v-t)}d\omega;$$

$$E_\varphi(\mathbf{r},t) = \frac{iq}{\pi v}\int_{-\infty}^{\infty}\frac{\varepsilon_2}{\varepsilon_1(n_1^2-n_2^2)}\{k_1K_1(rk_1)-k_2K_1(rk_2)\}\,e^{i\omega(z/v-t)}\,d\omega,$$

where $k_{1,2}^2 = (\omega/v)^2(1-\beta^2 n_{1,2}^2)$, and $n_{1,2}^2$ are given by (15).

For the magnetic field intensity we obtain analogously:

$$H_z(\mathbf{r},t) = -\frac{q}{\pi\beta v^2}\int_{-\infty}^{\infty}\frac{\varepsilon_2}{\varepsilon_1}\left\{\frac{1-\beta^2n_1^2}{n_1^2-n_2^2}K_0(rk_1)+\frac{1-\beta^2n_2^2}{n_2^2-n_1^2}K_0(rk_2)\right\}e^{i\omega(z/v-t)}\,\omega d\omega;$$

$$H_r(\mathbf{r},t) = -\frac{iqc}{\pi v^2}\int_{-\infty}^{\infty}\frac{\varepsilon_2}{\varepsilon_1(n_1^2-n_2^2)}\{k_1K(rk_1)-k_2K_1(rk_2)\}e^{i\omega(z/v-t)}d\omega; \tag{19}$$

$$H_\varphi(\mathbf{r},t) = \frac{q}{\pi c}\int_{-\infty}^{\infty}\frac{1}{\varepsilon_1}\left\{\frac{\varepsilon_1n_1^2-\varepsilon_1^2+\varepsilon_2^2}{n_1^2-n_2^2}k_1K_1(rk_1)\right.$$

$$\left.+\frac{\varepsilon_1n_2^2-\varepsilon_1^2+\varepsilon_2^2}{n_2^2-n_1^2}k_2K_1(rk_2)\right\}e^{i\omega(z/v-t)}d\omega.$$

The optical activity of the medium results in an electric field intensity component E_φ and in magnetic field-intensity components H_z and H_r which are lacking when a charge moves through an inactive medium.

Using the Poynting theorem, we now determine the quantity of energy radiated by the charge per unit path

$$-\frac{d\mathscr{E}}{dz} = \frac{c}{4\pi}\int_{-\infty}^{\infty}(E_\varphi H_z - E_z H_\varphi)\,2\pi r dt. \tag{20}$$

Inserting Eqs. (18) and (19) into Eq. (20) we obtain through simple transformation

$$-\frac{d\mathscr{E}}{dz} = \frac{q^2 r}{\pi v^2}\,2\mathrm{Re}\int_0^\infty \left\{\frac{(1-\varepsilon_1\beta^2)(n_1^2-\varepsilon_1)-\beta^2\varepsilon_2^2}{\varepsilon_1(n_1^2-n_2^2)}K_0(rk_1)\,k_1^* K_1(rk_1^*)\right.$$
$$\left.+\frac{(1-\varepsilon_1\beta^2)(n_2^2-\varepsilon_1)-\beta^2\varepsilon_2^2}{\varepsilon_1(n_2^2-n_1^2)}K_0(rk_2)k_2^* K_1(rk_2^*)\right\} i\,\omega\, d\,\omega. \tag{21}$$

If ϵ_1, ϵ_2, and ϵ_3 have no zeros in common, the real part of the expression just obtained will be made up of contributions from only those frequencies at which k_1 and k_2 are imaginary. Noting that in the case of imaginary k we have

$$k^* K_1(rk^*)\,K_0(rk) - kK_1(rk)\,K_0(rk^*) = i\pi/2,$$

the losses due to Cerenkov radiation assume the following form [compare with Eqs. (16) and (17)]:

$$-\frac{d\mathscr{E}}{dz} = -\frac{q^2}{v^2}\int_{\beta^2 n_1^2>1}\frac{(1-\varepsilon_1\beta^2)(n_1^2-\varepsilon_1)-\beta^2\varepsilon_2^2}{\varepsilon_1(n_1^2-n_2^2)}\,\omega\, d\,\omega$$
$$-\frac{q^2}{v^2}\int_{\beta^2 n_2^2>1}\frac{(1-\varepsilon_1\beta^2)(n_2^2-\varepsilon_1)-\beta^2\varepsilon_2^2}{\varepsilon_1(n_2^2-n_1^2)}\,\omega\, d\,\omega. \tag{22}$$

The second term of (22) diverges logarithmically. This is because we obtained the fields $E_z(\mathbf{r},t)$ by integrating with respect to k from zero to infinity, while macroscopic electrodynamics is not valid for $k\to\infty$. It is evident that in (22) one is restricted to the frequency region $\beta^2 n_m^2 > \beta^2 n_2^2 > 1$.

The total losses (taking the near collisions into account) in an isotropic medium are known to be independent of the parameter, $k_m \sim 1/b$. This parameter which enters logarithmically into the expression for the losses in the case of near collisions, and which also enters into the expression for the polarization losses that account for the interaction between the moving charge and the longitudinal field, cancels out in the final expression. In an anisotropic medium the losses in the case of near collisions are the same as in the isotropic medium. But now the parameter k_m enters logarithmically into the expression for the losses due to the radiation of the extraordinary waves, which are also longitudinal in the case of $n_2^2\to\infty$. Thus in an anisotropic medium the total losses, taking the near collisions into account, are also independent of the undetermined parameter k_m.

6. If a charge moves along the axis of an inactive ($\epsilon_2 = 0$) uniaxial crystal, expression (17) for the losses is considerably simpler:

$$-\frac{d\mathscr{E}}{dz} = \frac{q^2}{c^2}\int_{\beta^2\varepsilon_1>1}\left(1-\frac{1}{\beta^2\varepsilon_1}\right)\omega\, d\,\omega$$
$$+\frac{q^2}{c^3}\int\left(\frac{1}{\beta^2\varepsilon_1}-1\right)\omega\, d\omega$$
$$+\frac{q^2}{v^2}\sum_i\frac{\omega_i}{|d\varepsilon_1/d\omega|_i}\ln\left\{1+\frac{k_m^2 v^2}{\omega_i^2}\left(\frac{\varepsilon_1}{\varepsilon_3}\right)_i\right\} \tag{23}$$

(the second integral is taken over the region $n_m^2\beta^2 > (\epsilon_3/\epsilon_1)(\beta^2\epsilon_1 - 1) > 0$ and $\beta^2\epsilon_1 < 1$, while ω_i are the common zeros of ϵ_1 and ϵ_2). Expression (23) is identical with those obtained in Refs. 2 and 3. However, thanks to inequality $n_m^2\beta^2 > (\epsilon_3/\epsilon_1)(\beta^2\epsilon_1 - 1)$, the boundaries of the frequency regions, over which the integration is carried out, are so shifted that expression (23) contains no singularities. If ϵ_1 and ϵ_2 have no common zeros, the third term of (23) drops out. In this case, making the transition in the limit to the isotropic medium ($\epsilon_3\to\epsilon_1$), the second term of (23) reduces to the ordinary expression for the polarization losses.

In the case of the simplest gyrotropic medium ($\epsilon_1 = \epsilon_3$) the equation for the losses becomes (cf. also Ref. 3):

$$-\frac{d\mathscr{E}}{dz} = \frac{q^2}{2c^2}\int\left(1-\frac{1}{\beta^2\varepsilon_1}\right)\left\{1 \mp \frac{\beta\varepsilon_2(1+\beta^2\varepsilon_1)}{(1+\beta^2\varepsilon_1)\sqrt{4\varepsilon_1+\beta^2\varepsilon_2^2}}\right\}\omega\, d\omega + \frac{q^2}{v^2}\sum_i \frac{\omega_i}{|d\varepsilon_1/d\omega|_i}\ln\left(1+\frac{k_m^2 v^2}{\omega_i^2}\right). \tag{24}$$

The summation extends over all frequencies at which ϵ_1 and ϵ_2 vanish simultaneously. If ϵ_1 and ϵ_2 have no common zeros, the total losses are determined by the first term of (24). The integration in (24) is carried out over the frequency regions defined by the inequalities

$$n_m^2\beta^2 > [(2\varepsilon_1^2-\varepsilon_2^2)\beta \pm \varepsilon_2\sqrt{4\varepsilon_1+\beta^2\varepsilon_2^2}]\,\beta^2/2\varepsilon_1\beta > 1.$$

Expression (24) contains no singularities in the indicated frequency region.

7. Let us consider now a charge moving perpendicularly to the optical axis of the crystal. Choosing the coordinate system shown in Fig. 2 we obtain:

$$\varkappa_1 = \sin\vartheta\cos\varphi;\ \varkappa_2 = \cos\vartheta;$$
$$\varkappa_3 = \sin\vartheta\sin\varphi;\ \mathbf{kv} = kv\cos\vartheta.$$

Let us determine the component of the inverse tensor T_{22}^{-1}, substitute it into Eq. (8), and integrate (8) with respect to the angle σ. As a result we get:

$$-\frac{d\mathscr{E}}{dy} = i\frac{q^2}{2\pi^2c^2}\int_{-\infty}^{\infty}\int_0^{2\pi}\int_{1/\beta}^{n_m}\frac{n^2(1-\beta^2\varepsilon_1\cos^2\varphi-\beta^2\varepsilon_3\sin^2\varphi)+\beta^2\varepsilon_1\varepsilon_3-\varepsilon_1\sin^2\varphi-\varepsilon_3\cos^2\varphi}{An^4+Bn^2+C}$$
$$\times n\,dn\,d\varphi\,\omega\,d\omega, \tag{25}$$
$$A = \beta^2(\varepsilon_1\cos^2\varphi+\varepsilon_3\sin^2\varphi);$$
$$B = (\varepsilon_1-\varepsilon_3)\sin^2\varphi-\beta^2(\varepsilon_1^2-\varepsilon_2^2)\cos^2\varphi-\beta^2\varepsilon_1\varepsilon_3(1+\sin^2\varphi);$$
$$C = \beta^2\varepsilon_3(\varepsilon_1^2-\varepsilon_2^2)-(\varepsilon_1^2-\varepsilon_2^2-\varepsilon_1\varepsilon_3)\sin^2\varphi.$$

Assuming for simplicity that ϵ_1, ϵ_2, and ϵ_3 have no common zeros, we obtain finally the following equation for the total energy losses:

$$-\frac{d\mathscr{E}}{dy} = \frac{q^2}{4\pi c^2}\int_0^{2\pi}d\varphi\int\left(1-\frac{1}{\beta^2(\varepsilon_1\cos^2\varphi+\varepsilon_3\sin^2\varphi}\right)$$
$$\times\left\{1\mp\frac{B-2A\dfrac{1-\beta^2\varepsilon_1\cos^2\varphi-\beta^2\varepsilon_3\sin^2\varphi}{\beta^2\varepsilon_1\varepsilon_3-\varepsilon_1\sin^2\varphi-\varepsilon_3\cos^2\varphi}}{\sqrt{B^2-4AC}}\right\}\omega\,d\omega, \tag{26}$$
$$n_{1,2}^2 = (-B\pm\sqrt{B^2-4AC})/2A$$

(integration with respect to $d\omega$ in the regions defined by Eq. 16). The upper sign of (26) corresponds to losses due to the radiation of the ordinary waves, and the lower to those of the extraordinary ones. The conical surfaces for the ordinary and extraordinary waves are complicated in form (ex-

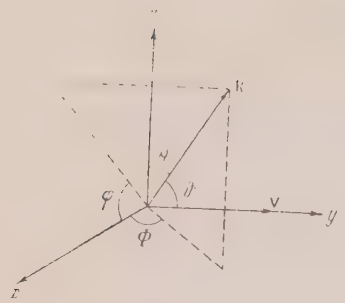

FIG. 2

hibit a dependence on the angle φ) and the intensity varies on the different generatrices of the conic surfaces.

In principle, it is possible to carry out the integration in (26) to the very end, provided the components ϵ_1, ϵ_2, and ϵ_3 of the dielectric tensor are given as the functions of the frequency.

If $\epsilon_1 = \epsilon_3$, Eq. (26) becomes identical with the result of Ref. 3, provided the integration limits are changed in that reference in the manner shown above. In the limiting case of an inactive uniaxial crystal ($\epsilon_2 = 0$) we obtain the corrected Ginzburg equation[1]:

$$-\frac{d\mathscr{E}}{dy} = \frac{q^2}{2\pi c^2}\int_0^{2\pi} d\varphi \Bigg\{ \int\limits_{n_m^2\beta^2 > \varepsilon_1\beta^2 > 1} \left(1 - \frac{1}{\beta^2\varepsilon_1}\right) \frac{\beta^2\varepsilon_1 \cos^2\varphi}{\sin^2\varphi + \beta^2\varepsilon_1\cos^2\varphi}\,\omega\, d\omega + \int \left(1 - \frac{1}{\beta^2\varepsilon_3}\right) \frac{\varepsilon_3 \sin^2\varphi}{(\sin^2\varphi + \beta^2\varepsilon_1\cos^2\varphi)(\varepsilon_1\cos^2\varphi + \varepsilon_3\sin^2\varphi)}\,\omega\, d\omega \Bigg\}. \tag{27}$$

The second integral is taken over the region

$$n_m^2\beta^2 > [\beta^2\varepsilon_1\varepsilon_3 + (\varepsilon_3 - \varepsilon_1)\sin^2\varphi]/(\varepsilon_1\cos^2\varphi + \varepsilon_3\sin^2\varphi) > 1.$$

In conclusion, we thank Prof. A. I. Akhiezer for interest in the work and for evaluation of the results obtained.

Translated by J. G. Adashko
95

The Theory of Nonlinear Effects in the Ionosphere

S. A. ZHEVAKIN AND V. M. FAIN

(Submitted to JETP editor July 8, 1954)
J. Exptl. Theoret. Phys. (U.S.S.R.) 30, 518-527 (March, 1956)

Nonlinear effects which arise in the propagation in the ionosphere of modulated and unmodulated electromagnetic waves of arbitrary amplitude have been computed with consideration of the earth's magnetic field.

1 The elementary theory of the Luxembourg-Gorkov effect has been given by Bailey and Martin.[1] Later, the theory was improved by Ginzburg, who gave a rigorous analysis of nonlinear effects in the ionosphere by means of the kinetic equation.[2]

The kinetic equation was solved by Ginzburg by means of successive approximations, in which analysis he, for well understood reasons, restricted himself to a consideration of the first approximation only. In the same paper the results were applied only for the case of sufficiently weak electromagnetic fields.* Meanwhile, the use of the velocity distribution function of the electrons, obtained in closed form in Ref. 3 for the case of propagation in a plasma of an amplitude modulated high-frequency electromagnetic wave of arbitrary intensity (in the presence of a constant magnetic field) permit us to carry out the calculation of the magnitude of cross modulation and other ionospheric nonlinear effects without any assumption as to the smallness of the field intensity. As a result of such a calculation, an essential simplification of the theory of nonlinear effects in the ionosphere can be achieved, inasmuch as we can avoid the direct application of the unwieldy method of the kinetic equation.

Suppose that a high power transmitter produces in the ionosphere the field

$$E_1 = E_0(1 + \mu \cos \Omega t) \cos \omega_1 t, \tag{1}$$

where μ is the depth of the modulation, Ω the modulation frequency and ω_1 the carrier frequency. Further, let us suppose the existence of an additional disturbing electromagnetic wave with frequency ω_2. In the quasi-stationary approximation, which exists for $\Omega << \omega_2$, and upon fulfillment of the conditions

$$\omega_2^2 \gg \nu_{ef}^2; \ |\omega_2 - \omega_H| \gg \nu_{ef}, \tag{2}$$

where $\omega_H = |(e/mc)H|$, the absorption coefficient k is proportional to ω_2. Therefore, the field of the wave with frequency ω_2 at the receiver is proportional to the expression[4]

$$E \sim \exp\{-(\omega_2/c)\int k_0 ds - (\omega_2/c)\bar{\eta}\int k_0 ds\}. \tag{3}$$

Here $(\omega_2/c)\int k_0\, ds$ is the total absorption in a wavelength for the weak field. For brevity, the notation $\eta = \Delta\nu_{ef}/\nu_{ef,0}$ is introduced, where $\nu_{ef,0}$ is the effective number of collisions in the weak field; $\Delta\nu_{ef} = \nu_{ef} - \nu_{ef,0}$ is the increment in the effective number of collisions under the action of an electric field of frequency ω_1, radiated by the transmitter; $\bar{\eta}$ is some mean value of the quantity η along the direction of propagation. We emphasize that, because of the conditions (2), Eq. (3) is equally applicable for both small and large values of $\Delta\nu_{ef}$.

We seek the quantity η, which characterizes the cross modulation, in two limiting cases. In the first case,

$$\Omega \ll \delta\nu_{ef}, \tag{4}$$

while in the second,

$$\Omega \gg \delta\nu_{ef}, \tag{5}$$

where δ characterizes the mean energy lost by the electron in a collision with a molecule or an ion. Below we shall consider only elastic collisions. Then

$$\delta = 2m/M, \tag{6}$$

where m is the mass of the electron and M is the mass of the molecule or ion.

2. We consider the case (4). If the condition

*We note that, as a consequence of the omission by Ginzburg of a solution for arbitrary magnitude of the field intensity, the very meaning of a "weak field" therein remains insufficiently defined.

[1] V. A. Bailey and D. F. Martin, Phil. Mag. 18, 369 (1934).

[2] V. L. Ginzburg, Izv. Akad. Nauk SSSR, Ser. Fiz. 12, 293 (1948).

[3] V. M. Fain, J. Exptl. Theoret. Phys. (U.S.S.R.) 28, 422 (1955). Soviet Phys. JETP 1, 205 (1955).

[4] Ia. L. Al'pert, V. L. Ginzburg and E. L. Feinberg, *The propagation of radiowaves*, Moscow, 1953.

$$\frac{(1-z)^2}{(1+z)^2}\frac{\omega_1^2}{\nu_{ef}^2} \gg 1, \tag{7}$$

is satisfied, where $z=\omega_H^2/(\omega_1^2+\nu^2)$, the isotropic part of the velocity distribution function of the electron is a Maxwell function with effective temperature[3]

$$T_{ef} = T\left[1+\frac{Me^2}{6kT\omega_1^2m^2}\left(E_\perp^2\frac{1+z}{(1-z)^2}+E_\parallel^2\right)(1+\mu\cos\Omega t)^2\right], \tag{8}$$

where $E_\perp$ and $E_\parallel$ are the components of the electric field respectively perpendicular and parallel to the earth's magnetic field H, T is the temperature of the ionosphere (more precisely, the temperature of the molecules and ions).

In a weak field, in the case of collisions with molecules,[4]

$$\nu_{ef,m,0} = \frac{4\pi a^2}{3}N_m\bar{v}, \tag{9}$$

where $\bar{v}=(8kT/\pi m)^{1/2}$ a is the molecular radius, N_m the molecular concentration. For collisions with ions,[4]

$$\nu_{ef,i,0} = \frac{2\pi e^4 N_i\bar{v}\ln\alpha}{3(kT)^2}, \tag{10}$$

where N_i is the ionic concentration, $\alpha=2kT\rho_m/e^2$ (ρ_m = the maximal impact parameter[4]).

In the strong field of the transmitter with frequency ω_1, the quantity ν_{ef} is found from Eqs. (9), (10) by simple substitution of T_{ef} for T:

$$\nu_{ef,m} = \frac{4\pi a^2}{3}N_m\sqrt{\frac{8kT_{ef}}{\pi m}}; \tag{9'}$$

$$\nu_{ef,i} = \frac{2}{3}\pi\frac{e^4N_i\ln\alpha_{ef}}{(kT_{ef})^2}\sqrt{\frac{8kT_{ef}}{\pi m}}, \tag{10'}$$

where $\alpha_{ef}=2kT_{ef}\rho_m/e^2$. Hence, for the quantities η_m and η_i, which characterize the cross modulation, in the case of collisions with molecules and in collisions with ions, we get, respectively,

$$\eta_m = \frac{\Delta\nu_{ef,m}}{\nu_{ef,m,0}} = \frac{\nu_{ef,m}-\nu_{ef,m,0}}{\nu_{ef,m,0}} = \sqrt{\frac{T_{ef}}{T}}-1; \tag{11}$$

$$\eta_i = \frac{\Delta\nu_{ef,i}}{\nu_{ef,i,0}} = \frac{T^{3/2}}{T_{ef}^{3/2}}\frac{\ln\alpha_{ef}}{\ln\alpha}-1. \tag{12}$$

In the case of propagation of the transmitter wave (frequency ω_1) close to the gyromagnetic frequency ω_H ($\omega_1\approx\omega_H$), we must consider that this wave, generally speaking, is elliptically polarized. The electric field at an arbitrary point of space is then written as

$$E_x = E_{0x}\cos\omega t(1+\mu\cos\Omega t),$$
$$E_y = E_{0y}\cos(\omega t-\beta)(1+\mu\cos\Omega t),$$
$$E_z = E_{0z}\cos(\omega t-\gamma)(1+\mu\cos\Omega t).$$

The velocity distribution function of electrons in the presence of such a field and a constant magnetic field H, directed along the x axis, is obtained by the method set forth in Ref. 3. It has the form (in this calculation, D. Ia. Kaushanskii took part) $f(\mathbf{v})=f_0(\mathbf{v})+\mathbf{v}\cdot\mathbf{f}_1(\mathbf{v})$, where the isotropic part of the distribution function is equal (we recall that we now assume the quasi-stationary condition (4) to be satisfied) to

$$\mathbf{f}_0(v) = C\exp\left[-\int_0^v dv\,mv\left\{kT+(1+\mu\cos\Omega t)^2\frac{e^2}{m^2}\left(\frac{(E_{0y}^2+E_{0z}^2)Ml}{6A}\right.\right.\right.$$
$$\left.\left.\left.+\frac{E_{0x}^2Ml^2}{6\omega^2l^2+v^2}+\frac{2E_{0y}E_{0z}\omega eH\,Ml\sin(\beta-\gamma)}{3Amc(\omega^2+\nu^2)(1+z')}\right)\right\}^{-1}\right],$$

where

$$A = \frac{l^2\omega^2(1-z')^2+v^2(1+z')^2}{l(1+z')},$$

$$z' = \frac{\omega_H^2}{\omega^2+\nu^2},\quad \nu=\frac{v}{l}$$

(l is the mean free pathlength of the electron, $e=-|e|$ is the electronic charge) and

$$\mathbf{f}_1 = \frac{e}{m}(1+\mu\cos\Omega t)\{[d_1(E_{0y}\cos\beta\mathbf{j}+E_{0z}\cos\gamma\mathbf{k})+q_1(-HE_{0z}\cos\gamma\mathbf{j}+HE_{0y}\cos\beta\mathbf{k})$$
$$+r_1(HE_{0z}\sin\gamma\mathbf{j}-HE_{0y}\sin\beta\mathbf{k})+q_1(-E_{0y}\sin\beta\mathbf{j}-E_{0z}\sin\gamma\mathbf{k})+h_1E_{0x}\mathbf{i}]\cos\omega t$$
$$+[g_1(E_{0y}\cos\beta\mathbf{j}+E_{0z}\cos\gamma\mathbf{k})+r_1(-HE_{0z}\cos\gamma\mathbf{j}+HE_{0y}\cos\beta\mathbf{k})$$
$$+q_1(-HE_{0z}\sin\gamma\mathbf{j}+HE_{0y}\sin\beta\mathbf{k})+d_1(E_{0y}\sin\beta\mathbf{j}+E_{0z}\sin\gamma\mathbf{k})+p_1E_{0x}\mathbf{i}]\sin\omega t\},$$

where

$$d_1 = -\frac{1}{A}\frac{\partial f_0}{\partial v};\quad g_1 = \frac{\omega l^2(z'-1)}{v[\omega^2l^2(1-z')^2+v^2(1+z')^2]}\frac{\partial f_0}{\partial v};$$
$$h_1 = -\frac{l}{\omega^2l^2+v^2}\frac{\partial f_0}{\partial v};\quad q_1 = \frac{e(\omega g_1-\nu d_1)}{mc(\omega^2+\nu^2)};$$
$$p_1 = -\frac{\omega}{(\omega^2+\nu^2)v}\frac{\partial f_0}{\partial v};\quad r_1 = -\frac{e(\omega d_1+\nu g_1)}{mc(\omega^2+\nu^2)}.$$

We note that in the isotropic part of the distribution function, the term $\frac{2MlE_{0y}E_{0z}\omega eH\sin(\beta-\gamma)}{3Amc(\omega^2+\nu^2)(1+z')}$ is positive if the electric field has the direction of rotation corresponding to the so-called extraordinary wave, and negative for the direction of rotation corresponding to the ordinary wave. If $\beta=\gamma=0$, i.e., if the electric field is linearly polarized, then the velocity distribution function of the electrons coincides with the function obtained in Ref. 3.

Let the condition

$$\omega_H = \omega_1;\quad \omega_1^2 \gg \nu_{ef}^2. \tag{13}$$

be satisfied. Then the isotropic part of the distribution function takes the form

$$f_0 = C\exp\left[-\int_0^v dv\, mv\left\{kT+(1+\mu\cos\Omega t)^2\frac{e^2}{m^2}\left(\frac{(E_{0y}^2+E_{0z}^2)M}{12\nu^2}\right.\right.\right.$$
$$\left.\left.\left.+\frac{E_{0x}^2M}{6\omega_1^2}-\frac{E_{0y}E_{0z}MH\sin(\beta-\gamma)}{6\nu^2|H|}\right)\right\}^{-1}\right]. \tag{14}$$

In this case, $e=-|e|$.

The effective collision number is found from the formula[4]

$$\nu_{ef} = -\frac{4\pi}{3}\int_0^\infty \frac{v^4}{l}\frac{\partial f_0}{\partial v}dv. \tag{15}$$

Normalizing f_0 to unity and substituting in Eq. (15), we find, for $l=$ const (as will be the case in the collision of electrons with molecules), that

$$\nu_{ef,m} = \frac{4\pi a^2}{3}N_m\sqrt{\frac{8kT_1}{\pi m}}\,g(u), \tag{16}$$

where

$$T_1 = T\left[1+\frac{Me^2E_{0x}^2}{6m^2kT\omega_1^2}(1+\mu\cos\Omega t)^2\right],$$
$$u = \frac{Me^2l^2}{24m^2(kT_1)^2}\left(E_{0y}^2+E_{0z}^2\right.$$
$$\left.-2E_{0y}E_{0z}\frac{H}{|H|}\sin(\beta-\gamma)\right)(1+\mu\cos\Omega t)^2,$$

and the function $g(u)$ is determined by the expression

$$g(u) = \frac{\sqrt{\pi}}{2}\frac{\int_0^\infty xe^{-x}(1+x/u)^u\,dx}{\int_0^\infty \sqrt{x}e^{-x}(1+x/u)^u\,dx}. \tag{17}$$

For integral values of u, the integrals which appear in the function $g(u)$ are expressed in elementary functions (see Ref. 5). The values of $g(u)$ for integral u are the following:

[5] I. M. Ryzhik and I. S. Fradshtein, *Table of integrals, sums, series and derivatives*, Moscow, 1951.

$u = 0$	1	2	3	4	5	7	10
$g(u) = 1{,}000$	1,200	1,314	1,379	1,431	1,475	1,571	1,629

From Eqs. (9) and (16) for the case of collision of electrons with molecules, we find

$$\nu_m = \sqrt{\frac{T_1}{T}}\, g(u) - 1; \quad (\omega_1 \approx \omega_H). \tag{18}$$

3. We proceed to the calculation of the magnitude of the cross modulation for the case $\Omega >> \delta\nu_{ef}$. In view of the fact that in this case the quasi-stationary condition (in relation to the frequency of the low power transmitter ω_2) is essentially made use of by us, the modulation frequency Ω must be limited also: $\delta\nu_{ef} << \Omega << \omega_2$.

By the method developed in Ref. 3, it is easy to find the isotropic part of the distribution function in this case. It has the form

$$f_0(v) = \Phi_{0,0} + F_{0,1}\cos\Omega t + G_{0,1}\sin\Omega t + F_{0,2}\cos 2\Omega t + G_{0,2}\sin 2\Omega t + F_{0,3}\cos 3\Omega t + G_{0,3}\sin 3\Omega t + F_{0,4}\cos 4\Omega t + G_{0,4}\sin 4\Omega t + \cdots \tag{19}$$

Expressions for $\Phi_{0,0}$, $G_{0,1}$, $F_{0,1}$ $G_{0,2}$, $F_{0,2}$, etc. have been developed in Ref. 3. When conditions (5) and (7) are satisfied, these expressions take the form

$$\Phi_{0,0} = \left(\frac{m}{2\pi k T'_{ef}}\right)^{3/2} \exp\left\{-\frac{mv^2}{2kT'_{ef}}\right\},$$

where

$$T'_{ef} = T\left[1 + \frac{Me^2\left(1 + \frac{1}{2}\mu^2\right)}{6kT\omega_1^2 m^2}\left(E_{0\perp}^2 \frac{(1+z)}{(1-z)^2} + E_{0\parallel}^2\right)\right];$$

$$G_{0,1} = \frac{1}{3\Omega v^2}\frac{\partial}{\partial v}\left[\frac{\mu e^2 v^3}{m^2\omega_1^2 l}\left(E_{0\perp}^2 \frac{(1+z)}{(1-z)^2} + E_{0\parallel}^2\right)\frac{\partial \Phi_{0,0}}{\partial v}\right];$$

$$G_{0,2} = \frac{\mu}{8} G_{0,1};$$

$$F_{0,1} = -\frac{1}{6v^2\Omega}\frac{\partial}{\partial v}\left[v^3 \frac{e^2}{m^2\omega_1^2 l}\left(E_{0\perp}^2 \frac{(1+z)}{(1-z)^2} + E_{0\parallel}^2\right)\left(1 + \frac{3}{8}\mu^2\right)\frac{\partial G_{0,1}}{\partial v}\right] - \frac{1}{\Omega v^2}\frac{\partial}{\partial v}\left[\frac{m}{M}\frac{v^4 G_{0,1}}{l} + \frac{kTv^3}{Ml}\frac{\partial G_{0,1}}{\partial v}\right];$$

$$F_{0,2} = -\frac{1}{12v^2\Omega}\frac{\partial}{\partial v}\left[v^3 \frac{e^2}{m^2\omega_1^2 l}\left(E_{0\perp}^2 \frac{(1+z)}{(1-z)^2} + E_{0\parallel}^2\right)\mu\left(\frac{9}{8} + \frac{\mu^2}{16}\right)\frac{\partial G_{0,1}}{\partial v}\right] - \frac{\mu}{16\Omega v^2}\frac{\partial}{\partial v}\left[\frac{m}{M}\frac{v^4 G_{0,1}}{l} + \frac{kT}{M}\frac{v^3}{l}\frac{\partial G_{0,1}}{\partial v}\right];$$

$$F_{0,3} = -\frac{1}{18\Omega v^2}\frac{\partial}{\partial v}\left[v^3 \frac{e^2}{m^2\omega_1^2 l}\left(E_{0\perp}^2 \frac{(1+z)}{(1-z)^2} + E_{0\parallel}^2\right)\frac{3\mu^2}{8}\frac{\partial G_{0,1}}{\partial v}\right];$$

$$F_{0,4} = \frac{\mu}{16} F_{0,3};$$

$$G_{0,3} = \frac{1}{18\Omega v^2}\frac{\partial}{\partial v}\left[v^3 \frac{e^2}{m^2\omega_1^2 l}\left(E_{0\perp}^2 \frac{(1+z)}{(1-z)^2} + E_{0\parallel}^2\right)\left(\frac{\mu^2}{4}\frac{\partial F_{0,1}}{\partial v} + \mu\frac{\partial F_{0,2}}{\partial v} + \left(1 + \frac{\mu^2}{2}\right)\frac{\partial F_{0,3}}{\partial v} + \frac{\mu^2}{4}\frac{\partial F_{0,4}}{\partial v}\right)\right] + \frac{1}{3\Omega v^2}\frac{\partial}{\partial v}\left[\frac{m}{M}\frac{v^4 F_{0,3}}{l} + \frac{kTv^3}{Ml}\frac{\partial F_{0,3}}{\partial v}\right];$$

$$G_{0,4} = \frac{1}{24\Omega v^2}\frac{\partial}{\partial v}\left[v^3 \frac{e^2}{m^2\omega_1^2 l}\left(E_{0\perp}^2 \frac{(1+z)}{(1-z)^2} + E_{0\parallel}^2\right)\left(\frac{\mu^2}{4}\frac{\partial F_{0,2}}{\partial v} + \mu\frac{\partial F_{0,3}}{\partial v} + \left(1 + \frac{\mu^2}{2}\right)\frac{\partial F_{0,4}}{\partial v}\right)\right] + \frac{1}{4\Omega v^2}\frac{\partial}{\partial v}\left[\frac{m}{M}\frac{v^4 F_{0,4}}{l} + \frac{kTv^3}{Ml}\frac{\partial F_{0,4}}{\partial v}\right].$$

Substituting all these expressions in Eq. (15), and setting l=const there, we find the effective number of electronic collisions with molecules:

$$\nu_{ef,m} = \nu_0 + \nu'_\Omega \cos \Omega t + \nu''_\Omega \sin \Omega t + \nu'_{2\Omega} \cos 2\Omega t + \nu''_{2\Omega} \sin 2\Omega t + \nu'_{3\Omega} \cos 3\Omega t + \nu''_{3\Omega} \sin 3\Omega t + \nu'_{4\Omega} \cos 4\Omega t + \nu''_{4\Omega} \sin 4\Omega t, \tag{20}$$

where

$$\nu_0 = \frac{4}{3l}\sqrt{\frac{8kT'_{ef}}{\pi m}};\ \nu'_\Omega = \frac{8e^2\mu}{3\Omega^2 l^2 m^2 \omega_1^2}\frac{m}{M}\left(E_{0\perp}^2 \frac{(1+z)}{(1-z)^2} + E_{0\parallel}^2\right)\nu_0;$$

$$\nu''_\Omega = \frac{4\mu e^2}{3\Omega l^2 m^2 \omega_1^2}\left(E_{0\perp}^2 \frac{(1+z)}{(1-z)^2} + E_{0\parallel}^2\right);\ \nu'_{2\Omega} = \frac{\mu}{16}\nu'_\Omega;\ \nu''_{2\Omega} = \frac{\mu}{8}\nu''_\Omega;$$

$$\nu'_{3\Omega} = 0;\ \nu''_{3\Omega} = \frac{m}{M}\frac{e^2\mu^2}{18\Omega^2 m^2 \omega_1^2 l^2}\left(E_{0\perp}^2 \frac{(1+z)}{(1-z)^2} + E_{0\parallel}^2\right)\nu''_\Omega;\ \nu'_{4\Omega} = 0;\ \nu''_{4\Omega} = \frac{3\mu}{64}\nu''_{3\Omega}.$$

Hence

$$\eta_m = \eta_0 + \eta'_\Omega \cos \Omega t + \eta''_\Omega \sin \Omega t + \eta'_{2\Omega} \cos 2\Omega t + \eta''_{2\Omega} \sin 2\Omega t + \eta'_{3\Omega} \cos 3\Omega t + \eta''_{3\Omega} \sin 3\Omega t + \eta'_{4\Omega} \cos 4\Omega t + \eta''_{4\Omega} \sin 4\Omega t, \tag{21}$$

where

$$\eta_0 = \sqrt{T'_{ef}/T} - 1;$$

$$\eta'_\Omega = \nu'_\Omega/\nu_{ef,m,0};\ \eta''_\Omega = \nu''_\Omega/\nu_{ef,m,0};$$

$$\eta'_{2\Omega} = \nu'_{2\Omega}/\nu_{ef,m,0};\ \eta''_{2\Omega} = \nu''_{2\Omega}/\nu_{ef,m,0} \text{ и т. д.}$$

We shall not consider the collisions of electrons with ions, because of the small practical interest of these collisions when condition (5) is satisfied.[4]

4. All the formulas we have obtained agree in the linear approximation relative to E^2 and, in the absence of a magnetic field, with the formulas obtained in Ref. 4.* The difference between our formulas and the corresponding formulas of Ref. 4 are illustrated in Figs. 1 and 2.

In Figs. 1 and 2 the quantity $x = \frac{e^2}{m^2}\frac{E_0^2}{\omega_1^2}\frac{M}{6kT} \times (1+\mu\cos\Omega t)^2$ is plotted along the abscissa and the quantity $\eta = \Delta\nu_{ef}/\nu_{ef,0}$ along the ordinate; the earth's magnetic field was not considered.

We now estimate magnitudes. In this case, we consider that we need to replace the quantity $2m/M = \delta_{el}$ which characterizes the energy lost by the electron in an elastic collision, for the calculation of inelastic collisions by a certain mean quantity δ_0. We assume, in accordance with Ref. 6, that $\delta_0 = 2 \times 10^{-3}$. Assuming that the system of the transmitter radiates upwards with a gain of g=1.5 relative to radiation isotropically radiated in the upper halfspace, we shall compute the field intensity E_0 in the ionosphere by means of the formula,

$$E_0 = \left(10^{-5}\sqrt{\frac{W_{\text{W}}}{r_{\text{км}}}}\right) \exp\left\{-\frac{\omega_1}{c}\int k(\omega_1)\,ds\right\} \text{ CGSE},$$

*In Ref. 2 the isotropic part of the distribution function $f_{00} + f_{01}$ for the case $\Omega \ll \delta\nu_{ef,0}$ was incorrectly not normalized to unity. Therefore, in this case our formulas do not agree in the linear approximation with the formulas of Ref. 2. In our work, $\Delta\nu_{ef}$ for the collision of electrons with ions has the same sign as in the elementary theory, while in Ref. 2, $\Delta\nu_{ef}$ has a different sign, because of the incorrect normalization.

[4] L. G. Huxley, Nuovo Cim. Suppl. 9, 59 (1952).

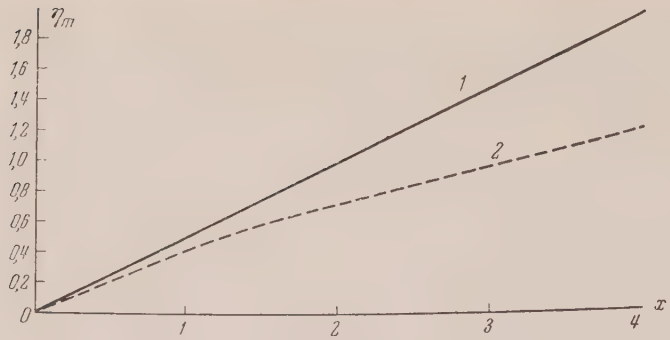

FIG. 1. Relative increase of the effective number of electronic collisions with molecules $\eta_m = \Delta\nu_{ef,m}/\nu_{ef,m0}$ as a function of the parameter x, which is proportional to the square of the amplitude of the high frequency electromagnetic wave. *1*-according to the approximate theory with consideration of terms only of order E^2; *2*-according to the exact theory.

where W_{kW} is the transmitter power in kilowatts, r_{km} is the distance in kilometers. Assuming the distance from the power transmitter to the region of the ionosphere, where the cross modulation takes place, to be equal to 85 km, the modulation factor of the field of the power station to μ=0.5, the temperature of the ionosphere T=300 °K, the circular frequency of the power station $\omega_1 = 10^6$ rad/sec, and considering that

$$\frac{\omega_1}{c}\int k(\omega_1)\,ds \approx \frac{\omega_2}{c}\int k_0(\omega_2)\,ds \approx 1,$$

we obtain a table for the comparison of the magnitudes of the cross modulation according to the exact theory and in the linear approximation relative to E_0^2.

Power W in kW	x	η				$\exp\left\{-\frac{\omega}{c}\bar{\eta}\int k_0 ds\right\}$			
		linear approximation		exact theory		linear approximation		exact theory	
		Collisions							
		with molecules	with ions	with molecules	with ions	with molecules	with ions	with molecules	with ions
125	0.53	0.26	0.72	0.24	0.44	0.77	0.49	0.79	0.645
250	1.06	0.53	1.44	0.44	0.62	0.59	0.237	0.645	0.54
500	2.12	1.06	2.88	0.77	0.79	0.35	0.056	0.465	0.455
1000	4.24	2.12	5.75	1.29	0.90	0.12	0.003	0.276	0.41

Thus, even for transmitter powers of $\sim$250 kW, noticeable deviations from the results of the linear theory are obtained. The above applies particularly to the case of collisions of electrons with ions. As a result, the linear approximation relative to E_0^2 is no longer satisfactory for transmitter powers $\geq$250 kW. We note that the amount of cross modulation in Eq. (3) is characterized by the factor $\exp\{-\frac{w^2}{c}\eta - \int ko(w_2)do\}$, and that it is impossible in the case of strong fields to limit oneself to the first two terms of the expansion of this exponent in a power series, as was

done in Ref. 4.

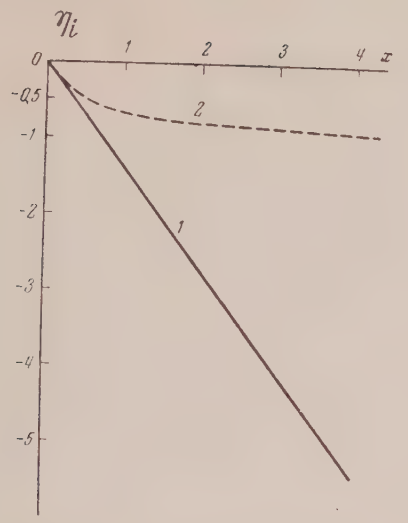

FIG. 2. Relative increase of the effective number of electronic collisions with ions $\eta_i = \Delta\nu_{ef,i}/\nu_{ef,i0}$ as a function of the parameter x, which is proportional to the square of the amplitude of the high frequency electromagnetic wave. *1*-according to the approximate theory with consideration of terms only of order E^2; *2*-according to the exact theory.

It is natural that in the two limiting cases (4) and (5), our formulas, in contrast to the formulas of Ref. 4, contain the frequencies 3Ω, 4Ω, etc., in addition to the frequencies Ω and 2Ω. It is curious that the coefficients for $\sin \Omega t$ and $\sin 2\Omega t$ in Eq. (21) (in the case l=const) agree in accuracy with the corresponding coefficients* obtained in Ref. 4. We also note that the coefficients η'_Ω, $\eta'_{2\Omega}$ which already appear in the linear approximation relative to E_0^2, but which are $\sim \delta\nu_{ef/\Omega}$ times smaller than the coefficients η''_Ω and $\eta''_{2\Omega}$, are not considered in Ref. 4.

5. Vilenskii[7] considered the phenomenon of phase and amplitude self-modulation of an electromagnetic wave which arises in its propagation through the ionosphere. This phenomenon was studied experimentally in Refs. 8,9 at a frequency close to the gyromagnetic. In these works, the phenomenon was given the name "automodulation" (see also Ref. 10). However, in Ref. 7, the normalization of the distribution function of Ref. 2 was applied incorrectly, as a result of which the author of Ref. 7 obtained wrong results for the case $\Omega << \delta\nu_{ef,0}$. For the correct calculation, the effect of phase self-modulation is some 10^3 times smaller than that found in Ref. 7.

Actually, let the transmitter radiate a modulated wave which, upon its entry into the ionosphere, corresponds to the field $E = E_0(1+\mu \cos \Omega t) \cos \omega t$. We set up the condition that the coordinate s runs along the path of the wave so that on the lower boundary of the ionosphere (for entry into it of the electromagnetic wave) $s=0$. The field of the wave at a specific point s in the ionosphere can then be represented as

$$\mathbf{E} = \mathbf{E}_1(s,t)(1+\mu\cos\Omega t)\cos(\omega t - \varphi(s,t)). \quad (22)$$

We now calculate the current arising under the action of this field. In such a case, in contrast to Ref. 7, we shall neglect not the quantity $\nu^2/\omega^2 \ll 1$, but the ratio ν^4/ω^4. The distribution function in the absence of a magnetic field and upon fulfillment of the condition $\Omega \ll \delta\nu_{ef}$ will be:[3]

$$f(\mathbf{v},t) = f_0(v,t) + \mathbf{v}\mathbf{f}_1, \quad (23)$$

where

$$f_0 = \left(\frac{m}{2\pi kT_{ef}}\right)^{3/2} e^{-mv^2/2kT};$$

$$T_{ef} = T\left[1 + \frac{M}{6kT}\frac{e^2E_1^2}{m^2\omega^2}(1+\mu\cos\Omega t)^2\right];$$

$$\mathbf{f}_1 = -\mathbf{E}_1\frac{e}{m}\left[\frac{1}{v}\frac{\nu}{\omega^2+\nu^2}\cos(\omega t - \varphi(s)) + \frac{1}{v}\frac{\omega}{\omega^2+\nu^2}\sin(\omega t - \varphi(s))\right] \times \frac{\partial f_0}{\partial v}(1+\mu\cos\Omega t)$$

$$\approx -\mathbf{E}_1\frac{e}{m}\left[\frac{\cos(\omega t - \varphi(s))}{\omega^2 l} + \frac{1}{v\omega}\left(1-\frac{\nu^2}{\omega^2}\right)\sin(\omega t - \varphi(s)\right]\frac{\partial f_0}{\partial v}(1+\mu\cos\Omega t).*$$

*Provided that the presence of a magnetic field is not taken into account.

*In the isotropic part of the distribution function, we have neglected the quantity $(\nu/\omega)^2$, because in the calculation of the current density this is equivalent to throwing away terms of order ν^4/ω^4. Just for simplicity, we have neglected the ratio $(\nu/\omega)^2$ in the coefficient for $\cos(\omega t - \varphi(s))$ also, since this leads only to an insignificant change in the calculation of amplitude modulation.

[7] I. M. Vilenskii, Dokl. Akad. Nauk SSSR 92, 525 (1953).

[8] M. Cutolo, Nuovo Cim. 9, 687 (1952).

[9] M. Cutolo, Nature 167, 315 (1951).

[10] *A new nonlinear effect in the ionosphere*, Usp. Fiz. Nauk 49, 484 (1953).

We find the total current from the formula

$$\mathbf{j}_t = Ne \int_{-\infty}^{+\infty} \mathbf{v} f(\mathbf{v},t)\, d\mathbf{v} = \frac{4\pi Ne}{3} \int_0^{\infty} \mathbf{f}_1 v^4 dv, \tag{24}$$

which yields

$$\mathbf{j}_t = \boldsymbol{E}_1 \Big\{ \sigma \cos(\omega t - \varphi(s)) - \omega \frac{\varepsilon - 1}{4\pi} \sin(\omega t - \varphi(s)) \Big\} (1 + \mu \cos \Omega t) + \boldsymbol{E}_1^3 \sigma_1 \{ \cos(\omega t - \varphi(s)) + A \sin(\omega t - \varphi(s)) \} (1 + \mu \cos \Omega t)^3, \tag{25}$$

where N_m is the molecular concentration,

$$\sigma = \frac{Ne^2 \nu_{ef,0}}{m\omega^2}; \quad \nu_{ef,0} = \frac{4}{3l} N_m \bar{v};$$

$$\sigma_1 = \frac{M}{m} \frac{e^2 \sigma}{12kT\omega^2 m}; \varepsilon = 1 - \frac{4\pi e^2}{m\omega^2} \left(1 - 1{,}10 \frac{\nu_{ef,0}^2}{\omega^2}\right);$$

$$\bar{v} = \left(\frac{8kT}{\pi m}\right)^{1/2}; \quad A = -2{,}21 \frac{\nu_{ef,0}}{\omega}.$$

In the following we shall for simplicity consider the region of the ionosphere in which self-modulation arises which is homogeneous in an isotropic medium. Then the quantities $k(\omega)$, n, σ etc., which enter into the theory are certain averages corresponding to the quantities of the real ionosphere.

For a homogeneous and isotropic medium, we get from Maxwell's equations

$$\frac{\partial^2 E}{\partial s^2} - \frac{1}{c^2} \frac{\partial^2 E}{\partial t^2} - \frac{4\pi}{c^2} \frac{\partial j_t}{\partial t} = 0. \tag{26}$$

Substituting the current (25) and the field (22) in Eq. (26) and taking into account that $\Omega \ll \omega$, we can equate separately the terms in $\sin(\omega t - \varphi(s))$ and $\cos(\omega t - \varphi(s))$. As a result we get two equations for $E'_1 = E_1(s,t)(1 + \mu \cos \Omega t)$ and $\varphi(s,t)$:

$$\frac{\partial E_1'}{\partial s^2} - E_1' \left(\frac{\partial \varphi}{\partial s}\right)^2 + \frac{\omega^2 \varepsilon}{c^2} E_1' - \frac{4\pi\sigma_1 A\omega}{c^2} E_1'^3 = 0; \tag{27}$$

$$2 \frac{\partial E_1'}{\partial s} \frac{\partial \varphi}{\partial s} + E_1' \frac{\partial^2 \varphi}{\partial s^2} + \frac{4\pi\sigma\omega}{c^2} E_1' + \frac{4\pi\sigma_1\omega}{c^2} E_1'^3 = 0.$$

It is easy to convince oneself by the proper substitution that the solution, with accuracy to E_0^3, which satisfies the boundary conditions $(\varphi)_{s=+0} = 0$ and $(E'_1)_{s=+0} = E_0(1 + \mu \cos \Omega t)$ has the form:

$$E_1' = \Big\{ E_0 (1 + \mu \cos \Omega t) - \frac{\sigma_1}{2\sigma} \frac{1 + 2Ak/n}{1 + 4(k/n)^2} E_0^3 (1 + \mu \cos \Omega t)^3 \Big\} e^{-\omega ks/c} + \frac{\sigma_1}{2\sigma} \frac{1 + 2Ak/n}{1 + 4(k/n)^2} E_0^3 (1 + \mu \cos \Omega t)^3 e^{-3\omega ks/c};$$

$$\varphi(s) = \frac{\omega}{c} ns + \frac{\sigma_1}{2\sigma} \Big\{ \frac{k}{n} \frac{1 + 2Ak/n}{1 + 4(k/n)^2} - \frac{A}{2} \Big\} E_0^2 (1 + \mu \cos \Omega t)(1 - e^{-2\omega ks/c}),$$

or

$$E = E_0 e^{-\omega ks/c} (1 - \gamma - {}^3/_2 \gamma \mu^2) \times \{ 1 + \mu_\Omega \cos \Omega t - \mu_{2\Omega} \cos 2\Omega t - \mu_{3\Omega} \cos 3\Omega t \} \times \cos\{ \omega t - (\omega ns/c) - \alpha(1 + \mu^2/2) - \beta_\Omega \cos \Omega t - \beta_{2\Omega} \cos 2\Omega t \},$$

where

$$\alpha = \frac{M}{2m} \frac{e^2}{6kT\omega^2 m} \Big\{ \frac{k}{n} \frac{1 - 4{,}42 \nu_{ef,0} k/\omega n}{1 + 4(k/n)^2} + 1{,}10 \frac{\nu_{ef,0}}{\omega} \Big\} E_0^2 (1 - e^{-2\omega ks/c});$$

$$\gamma = \frac{M}{2m} \frac{e^2}{12kT\omega^2 m} \times \frac{1 - 4{,}42 \nu_{ef,0} k/\omega n}{1 + 4(k/n)^2} E_0^2 (1 - e^{-2\omega ks/c});$$

$$\mu_\Omega = \frac{\mu(1 - 3\gamma - {}^3/_4 \gamma \mu^2)}{1 - \gamma - {}^3/_2 \gamma \mu^2};$$

$$\mu_{2\Omega} = \frac{{}^3/_2 \gamma \mu^2}{1 - \gamma - {}^3/_2 \gamma \mu^2};$$

$$\mu_{3\Omega} = \frac{{}^1/_4 \gamma \mu^3}{1 - \gamma - {}^3/_2 \gamma \mu^2}; \quad \beta_\Omega = 2\alpha\mu;$$

$$\beta_{2\Omega} = \alpha\mu^2/2.$$

If we assume that $k << n$, as is done in Ref. 7, and use the final results of this work, then the quantity α which determines the phase modulation is 1.2×10^3 times smaller than in Ref. 7, and the quantity which determines the amplitude modulation is about 4 times smaller.

Assuming the distance to the lower bound of the ionosphere to be $r \approx 100$ km, the temperature of the ionosphere to be $T = 300°$ K, the power of the transmitter $W = 200$ kw, the angular frequency of the transmitter $W = 3 \times 10^6$ rad/sec, the effective number of collisions $\nu_{ef,0} = 10^6$,, the angular frequency of modulation $\Omega = 300$ rad/sec, and replacing the value $2m/M = \delta_{el}$ (which characterizes the energy transfer in an elastic collision with a molecule) by 2×10^{-3} (Ref. 6), we get for the frequency shift $\Delta\omega$ (upon satisfying the condition $2\omega ks/c >> 1$): $d\varphi/dt = \omega + \Delta\omega = \omega - \beta_\Omega \Omega \sin \Omega t$, a quantity of the order of 2 rad/sec.

We note in conclusion that the experimental investigation of the phase self-modulation, arising in the passage through the ionosphere of an amplitude modulated electromagnetic wave would be useful for the determination of the effective number of collisions in this region of the ionosphere in which the phase self-modulation arises.

Translated by R. T. Beyer
96

Theory of the Molecular Generator and Molecular Power Amplifier

N. G. BASOV AND A. M. PROKHOROV
P. N. Lebedev Physical Institute, Academy of Sciences, USSR

(Submitted to JETP editor Dec. 10, 1954)
J. Exptl. Theoret. Phys. (U.S.S.R.) 30, 560-563 (March, 1956)

On the basis of dispersion theory, with the effect of saturation taken into account, a theory is given of the operation of the molecular generator and of the microwave molecular power amplifier. Formulas are derived for the condition of self-excitation of the generator, and for the generated frequency and the amplitude of the steady oscillation. Other problems considered are the power amplification factor of the molecular amplifier, the bandwidth of the amplifier, and the condition for operation of the amplifier in the linear range.

1. INTRODUCTION

By a molecular generator we mean a self-oscillatory system that uses the energy connected with transitions between different energy levels of molecules. The oscillatory circuit of a molecular generator is a cavity resonator. Through the cavity resonator is passed a molecular beam, in which there is a partial or complete absence of molecules in the lower level of the transition being used, so that such a beam is capable of radiating energy. A feedback coupling in the molecular generator is affected by the electromagnetic field of the resonator, which, acting on the dipole moments of the molecules that are passing through the resonator, causes induced emission by these molecules. In order to achieve a condition of self-excitation, the resonator must have a sufficiently high Q so that the power radiated by the molecules is greater than the power lost in the resonator and in the generator load.

The saturation effect in the induced emission constitutes the nonlinearity that determines the amplitude of the steady oscillation in the circuit of the molecular generator.

However, the molecular generator is not completely analogous to other generators with respect to the feedback coupling, since it is not a classical system; for the induced emission is an essentially quantum effect, which cannot be obtained by a classical method. In distinction from other generators, in the molecular generator the oscillatory energy is not produced in the generator circuit, but is carried into the generator circuit by the molecules of the beam, each of which must be considered to be excited by the oscillatory circuit; i.e., a molecular generator is an oscillatory system with a very large number of degrees of freedom. Therefore, the theory of operation of a molecular generator must be developed by a statistical quantum-mechanical method. In the present article this is done with the aid of dispersion theory, with the saturation effect being taken into account.[1,2]

The distinctive property of the molecular generator is the enormous stability of its frequency, for the generated frequency is little dependent on external conditions and is essentially determined by the frequency of the spectral line employed. Therefore the molecular generator can be used on the one hand as a standard of frequency, and on the other as a spectroscope of high resolving power.

If the conditions for self-excitation are not fulfilled, then the molecular generator can serve as an amplifier of microwave power with a small noise factor.

The theoretical possibility of constructing a molecular generator was pointed out in an article by us.*[3] A report has recently appeared of a realization of such a generator.[4] It should be mentioned that in the latter work there is no theoretical consideration of the reason for the operation of such a generator.

2. THEORY OF THE MOLECULAR GENERATOR

In this section we shall obtain formulas for the generated frequency ω of a molecular generator that uses an isolated spectral line of frequency ω_T. At the same time formulas will be obtained for the amplitude of steady oscillation of the electric field E in the generator resonator, tuned to frequency ω_0 and having quality factor Q.

The problem proposed reduces to the consideration of the behavior of a cavity resonator filled with

*The first report on the theoretical possibility of constructing a molecular generator was presented by the authors of the present article in May 1952 at the All-Union conference on radiospectroscopy.

[1] L. Landau and E. Lifshitz, *Quantum mechanics*, p. 170, (1948).

[2] R. Karplus and J. Schwinger, Phys. Rev. 73, 1020 (1948)

[3] N. G. Basov and A. M. Prokhorov, J. Exptl. Theoret. Phys. (U.S.S.R.) 27, 431 (1954).

[4] J. P. Gordon, H. J. Zeiger, and C. H. Townes, Phys. Rev. 95, 282 (1954).

a medium with negative losses in the vicinity of the frequency ω_r. In the solution of this problem we neglect the Doppler broadening of the spectral line, considering that it is always possible to choose a type of oscillation in the cavity resonator for which Doppler broadening is absent.

Let the medium be described by a complex dielectric constant

$$\varepsilon = \varepsilon' - i\varepsilon'' = 1 + 4\pi\varkappa N, \tag{1}$$

where κ is the polarizability of a molecule, and N is the number density of molecules in the cavity resonator. The value of κ, with the saturation effect taken into account, can be written in the form[1,2]

$$\varkappa = \frac{|d_{zn}^{m}|^2}{\hbar}\,\frac{\omega}{\omega_r}\cdot \times \frac{(\omega_r - \omega - i/\tau)(\rho_m^{(0)} - \rho_n^{(0)})}{(\omega_r - \omega)^2 + \tau^{-2} + |d_{zn}^{m}|^2\,|E|^2\hbar^{-2}}, \tag{2}$$

where $|d_{zn}^{m}|^2$ is the square of the matrix element of the z-component of the dipole moment corresponding to the molecular transition between levels m and n; $\tau = l/\bar{v}$ is the mean time of transit across the resonator field, l is the length of the resonator, $\bar{v}$ is the mean speed of the molecules, $\rho_k^{(0)}$ is the probability of occurrence of molecules at level k at the moment of entry into the field of the resonator.

Let N_0 active molecules cross the cross section S of the resonator in one second:* then

$$N = N_0 / S\bar{v}. \tag{3}$$

Substituting Eq. (2) and (3) in Eq. (1), we get

$$\varepsilon' = 1 - A\gamma\,\frac{\omega}{\omega_r}\,\frac{(\omega_r - \omega)\tau}{(\omega_r - \omega)^2 + \tau^{-2} + \gamma|E|^2}, \tag{4}$$

$$\varepsilon'' = -A\gamma\,\frac{\omega}{\omega_r}\,\frac{1}{(\omega_r - \omega)^2 + \tau^{-2} + \gamma|E|^2},$$

*By the number of active molecules we mean the difference between the numbers of molecules in the upper and lower levels of the transition under consideration.

where

$$A = 4\pi N_0\hbar / Sl; \quad \gamma = |d_{zn}^{m}|^2/\hbar^2. \tag{5}$$

The equation for the electric field intensity in the resonator will be written in the form

$$\frac{d^2}{dt^2}E + \frac{\omega_0}{Q}\frac{d}{dt}E + \frac{\omega_0^2}{\varepsilon}E = 0, \tag{6}$$

where

$$E = E(x, y, z, t).$$

For simplicity we consider that E does not depend on the coordinates x, y, z of the resonator, since Eq. (4) was derived on the assumption that the field E is uniform over the cross section of the resonator. When there is a dependence of the field E on the coordinates of the cross-section, it is necessary to derive new formulas. Taking account of the fact that the magnitude of the saturation effect is different for different points within the resonator. Such a calculation cannot give anything new in principle, and our solution amounts to the introduction of a certain effective field.

We seek the stationary state in the form $E = E_0 e^{i\omega t}$. Upon substituting in Eq. (6) and setting the real and imaginary parts equal to zero, we get

$$-\omega^2 + \omega_0^2\varepsilon'/[(\varepsilon')^2 + (\varepsilon'')^2] = 0; \tag{7}$$

$$\omega/Q + \omega_0\varepsilon''/[(\varepsilon')^2 + (\varepsilon'')^2] = 0.$$

By taking account of the expressions (4), it is possible to rewrite these equations in the form

$$\frac{Q^2}{(Q\omega/\omega_0)^2 + 1} = 1 - A\gamma\,\frac{\omega}{\omega_r}\,\frac{(\omega_r - \omega)\tau}{(\omega_r - \omega)^2 + \tau^{-2} + \gamma|E|^2}, \tag{8}$$

$$\frac{Q\omega_0/\omega}{(Q\omega/\omega_0)^2 + 1} = A\gamma\,\frac{\omega}{\omega_r}\,\frac{1}{(\omega_r - \omega)^2 + \tau^{-2} + \gamma|E|^2}. \tag{9}$$

By eliminating the amplitude of oscillation E from Eqs. (8) and (9), we get the following equation for the frequency of steady oscillation:

$$\omega^3 + \omega\omega_0^2(\omega_0\tau Q^{-1} + Q^{-2} - 1) - \omega_0^3\omega_r\tau Q^{-1} = 0. \quad (10)$$

From Eq. (10) it is clear that

$$\Delta = |\omega_r - \omega|/\omega_r \ll 1. \quad (11)$$

On solving the equation to terms of the first order in Δ, we find the generated frequency

$$\omega = \omega_r\left(1 + \frac{2Q}{\omega_0\tau}\frac{\omega_0 - \omega_r}{\omega_r} - \frac{1}{Q\omega_r\tau}\right). \quad (12)$$

As is clear from (12), the generated frequency does not coincide with ω_r even when the resonator is exactly tuned to the frequency of the spectral line ($\omega_0 = \omega_r$). As an example, for a molecular generator with $\omega_0\tau = 2 \times 10^7$, with $Q = 1000$, and with $(\omega_0 - \omega_r)/\omega_r = 5 \times 10^{-6}$, we get $(2Q/\omega_0\tau) \times (\omega_0 - \omega_r)/\omega_r = 5 \times 10^{-10}$ and $1/Q\omega_r\tau = 5 \times 10^{-11}$.

The values quoted can be realized for a molecular generator operating on the line $J = 3$, $K = 3$ of the NH_3 molecule, i.e., such a generator can be used as an absolute standard of frequency of accuracy $\sim 10^{-9}$.

The amplitude of steady oscillation can be determined from Eq. (9). It is equal to

$$|E|^2 = \frac{1}{\gamma\tau^2}\left\{A\gamma\tau^2\frac{1}{Q}\frac{\omega^2}{\omega_0\omega_r}\left[\left(Q\frac{\omega}{\omega_0}\right)^2 + 1\right] - (\omega_r - \omega)^2\tau^2 - 1\right\}. \quad (13)$$

If we consider that $\omega_0 = \omega_r \approx \omega$ and that $1/Q \ll 1$, then from (13) we get the following expression for the limit of self-excitation of the generator:

$$A\gamma\tau^2 Q > 1 \quad \text{or} \quad \frac{4\pi N_0}{Sl\hbar}|d_{zn}^m|^2 Q\tau^2 > 1. \quad (14)$$

The expression (14) was obtained by us earlier in Ref. 3. If $A\gamma\tau^2 Q \gg 1$, , then the amplitude of steady oscillation takes the form

$$|E|^2 = (4\pi N_0\hbar\omega_r/Sl)\,Q, \quad (15)$$

in this case the molecular beam radiates to the resonator the maximum possible power

$$W_{max} = {}^1/_2\, N_0\hbar\omega_r. \quad (16)$$

3. THE MOLECULAR MICROWAVE POWER AMPLIFIER

If the condition for self-excitation in a molecular generator is not satisfied, then such an apparatus can be used as an amplifier of microwave power. This apparatus is analogous to a regenerative receiver. A molecular generator possesses a small noise factor.

We shall find the power amplification factor of such an amplifier. The molecular amplifier is described by the same equations as the molecular generator, except that on the right side of Eq. (6) it is necessary to add the external force, related to the power being amplified:

$$\frac{d^2}{dt^2}E + \frac{\omega_0}{Q}\frac{d}{dt}E + \frac{\omega_0^2}{\varepsilon}E = \omega^2 Be^{i\omega t}. \quad (17)$$

The amplitude of the external force B is determined by the power input W_i to the amplifier resonator. We can represent by W_0 the power output from the amplifier; then the power amplification factor of the amplifier is

$$K = W_0/W_i \quad (18)$$

In the absence of the molecular beam, K is the coefficient of power transmission through the resonator.

To find the amplification (transmission) factor, we shall calculate the field in the resonator in two cases: in the presence of the molecular beam in the resonator, E_1, and in its absence E_2. Then the power amplification factor will be equal to the ratio of the squares of the field in the resonator in these two cases, multiplied by the coefficient of transmission through the resonator K_0 in the absence of the molecular beam:

$$K = K_0(E_1/E_2)^2. \quad (19)$$

From Eq. (17) we get the following value of E_1:

$$|E_1|^2 = B^2\left\{\left[\left(\frac{\omega_0}{\omega}\right)^2\frac{\varepsilon'}{(\varepsilon')^2 + (\varepsilon'')^2} - 1\right]^2 + \left[\left(\frac{\omega_0}{\omega}\right)^2\frac{\varepsilon''}{(\varepsilon')^2 + (\varepsilon'')^2} + \frac{1}{Q}\frac{\omega_0}{\omega}\right]^2\right\}^{-1}. \quad (20)$$

We get E_2 from (20) by setting $\epsilon' = 1$, $\epsilon'' = 0$.

At resonance, $\omega_0 = \omega_r = \omega$, the amplification

factor has its maximum value. It is equal to

$$K_m = K_0 / (1 - A\gamma\tau^2 Q)^2. \qquad (21)$$

From (21) it is possible to estimate the bandwidth Δ of the amplifier. We shall define the bandwidth of the amplifier as the amount of detuning of the frequency, with respect to the resonance frequency, for which the amplified power is diminished by a factor two. For $K < Q$,

$$\Delta^2 = (1 / \tau^2) K_0 / K_m. \qquad (22)$$

Eq. (22) shows that the bandwidth of the amplifier decreases with increase of the amplification factor of the amplifier. This also takes place in an ordinary regenerative receiver.

In order that the amplifier may operate in the linear range (far below saturation), the following condition must be satisfied:

$$\gamma\tau^2 |E_1|^2 \ll 1. \qquad (/)$$

Translated by W. F. Brown, Jr.
100

Magnetic Symmetry of Crystals

B. A. TAVGER AND V. M. ZAITSEV

(Submitted to JETP editor, Dec. 10, 1954)
J. Exptl. Theoret. Phys. (U.S.S.R.) 30, 564-568 (March, 1956)

The symmetry of crystals with a magnetic moment is considered. Besides coordinate transformations, transformations involving time reversal are investigated. The corresponding point groups are derived. It is shown that the structure of crystals which possess a magnetic moment is not invariant under time reversal.

1. INTRODUCTION

IN the determination of crystal symmetry, one regards the crystalline matter as a definite continuum. Such a description is statistical. In fact, the atoms and molecules of a crystal are all the time in motion. The crystalline continuum is to be understood as a time average over the state of the crystal. Below we shall be concerned with this average state.

A transformation which transforms this continuum into itself is called a symmetry transformation. The possible symmetry transformations depend on the properties of the continuum. One usually attributes to the crystalline continuum the following properties: (1) it is of infinite extent, (2) it is "rigid", i.e., under any symmetry transformation the distance between any two points of the continuum does not change; (3) it possesses a three-dimensional space lattice.

Condition (2) restricts the symmetry transformations of the continuum so as to reduce them to translations, rotations and reflections.[1] Condition (3) limits the possible symmetry transformations still further.[2] The existence of a space lattice rules out, for example, the occurrence of a rotation by $2\pi/5$.

The picture of a crystal as a continuum with the above properties is not rigorous. In a crystal some parts may move relative to the others. This motion may be described by a time averaged current density $\mathbf{j}(x,y,z)$. If charge is moving, then $\mathbf{j}(x,y,z)$ represents the time average of the electric current. In the equilibrium state of a crystal the average current density $\mathbf{j}(x,y,z)$ satisfies two conditions: (a) there must not be any sinks or sources for the current i.e., div $\mathbf{j}=0$; (b) there must be no macroscopic current, i.e., the integral $\int \mathbf{j}\, dS$, taken over the surface of a unit cell, must vanish, since otherwise the state of the crystal would be energetically unfavorable.

For the vast majority of substances[3] $\mathbf{j}\equiv 0$; this applies to nonmagnetic, as well as paramagnetic and diamagnetic substances. On the other hand, ferromagnetic, antiferromagnetic and pyromagnetic substances must have $\mathbf{j}\neq 0$.

Crystals with $\mathbf{j}\neq 0$ should not be visualized as "rigid" structures, but rather as the stationary flow of a liquid, in which the flow velocity $\mathbf{v}(x,y,z)$ represents the current density $\mathbf{j}(x,y,z)$ and satisfies the conditions (a) and (b). In this manner we arrive at a picture of a crystalline continuum which differs from the usual one. This continuum may, in general, possess symmetry transformations which are not rotations, reflections, or translations. Any symmetry transformation of the continuum which we have defined can be made up of a transformation which treats it as a "rigid" structure, i.e., which satisfies condition (2), and a transformation of the current density $\mathbf{j}(x,y,z)$ which does not change the space coordinates.

The distribution of the mean current density $\mathbf{j}$ allows a transformation which is peculiar to vector quantities, viz., a reversal of its direction. This transformation is equivalent to a time reversal.[3] Following Landau and Lifshitz,[3] we denote this transformation by R. Then our continuum allows the transformations

$$M = RB, \tag{1}$$

where B is a transformation which satisfies condition (2), i.e., consists of translations, rotations and reflections.

2. SOME PROPERTIES OF THE TRANSFORMATIONS INTRODUCED ABOVE. STATEMENT OF THE PROBLEM

Not every M can be a symmetry transformation.

[1] B. N. Delone, N. N. Padurov and A. D. Aleksandrov, *Mathematical Foundations of Structure Analysis*, Moscow-Leningrad, 1934.

[2] N. V. Belov, *Structural Crystallography*, Acad. Sci. USSR Press, 1951.

[3] L. L. Landau and E. M. Lifshitz, *Statistical Physics*, GITTL (State Tech. Lit. Press), 1951, p. 129.

If, in the expression (1) for M, which represents a symmetry transformation, we replace the time reversal by the identity operation E, M must go over into a symmetry transformation of the usual type, A.* Therefore, if M is a symmetry transformation,

$$M = RA. \tag{2}$$

In other words, a crystal with $j \neq 0$ may possess symmetry transformations of the normal type A and those of the type $M = RA$.

However, not all transformations of the type (2) may occur as symmetry transformations for a crystal with $j \neq 0$. For instance, in such a case R itself is not a symmetry transformation.[3] Indeed, if we apply R, we obtain $j \equiv -j$, which is possible only if $j \equiv 0$. Equally excluded are those $M = RA$ for which A is of odd order ν. (The order of a symmetry transformation is the smallest positive exponent ν for which A^ν equals the identity operation E.[4]) To prove this, we first note the obvious properties of R: (a) R commutes with the symmetry transformations of the usual type A, i.e., $RA = AR$, since R acts only on j; (b) $RR = R^2 = E$.

Let $M = RA$, where A is of odd order ν. Then $M^\nu = R^\nu A^\nu = RA^\nu = R$. If we assume that M is a symmetry transformation, then M^ν must also be a symmetry transformation, and we arrive at a contradiction.

It follows from this, in particular, that the transformations R, and RL_3, where L_3 is a rotation through 120°, are ruled out.

We note the following properties for later use:

$$M^n = \begin{cases} M' & \text{for odd } n \\ A'' & \text{for even } n \end{cases} \tag{3}$$

$$M'M'' = A, \quad AM = M', \quad MA = M''$$

The set of symmetry transformations of a given crystal forms a group in the mathematical sense of the word. The elements of the group are the symmetry transformations, and the products of elements represent their successive application. The set of symmetry transformations for a crystal with $j \neq 0$ also must form a group. There arises the question as to the possible groups of symmetry transformations of crystals with $j \neq 0$. We shall in the following be concerned only with point transformations. The determination of these possible groups of point transformations is the main object of the present paper.

3. ALGORITHM FOR CONSTRUCTING THE POINT GROUPS

As a preliminary, we prove the following properties of the groups under consideration.

1. If the point transformations M_k and A_i form a group, it is impossible to choose i and k in such a way that $M_k = RA_i$. Assume the contrary: $M_k = RA_i$. Multiply both sides of this equality by $A^{\nu-1}$, where ν is the order of A: $M_k A_i^{\nu-1} = RA_i^\nu = R$. Since M_k and $A_i^{\nu-1}$ form a group of point transformations, $M_k A_i^{\nu-1}$ must also be a symmetry point transformation for the crystal with $j \neq 0$. But R is not such a symmetry transformation. Hence we have arrived at a contradiction.

On the basis of this property we may adopt the following convention for the labels k and i. If M_k and A_i form a group, we shall always assume $i \neq k$, choosing $k = 1, 2, \ldots, m$; $i = m+1, m+2, \ldots, n$.

2. Assume that $M_k = RA_k$ and A_i form a group of point symmetry transformations. If we replace R by the identity E, i.e., M_k by A_k, then the resulting elements A_k and A_i form a group,[3] which must belong to one of the 32 symmetry classes, since after replacing R by E we no longer consider j, and thus arrive at the usual picture of the crystal as a rigid structure.

3. If $M_k = RA_k$ and A_i form a group of point symmetry transformations, the elements A_i form a subgroup. Indeed, A_i', A_i'' is a transformation of the normal type A, and hence not equal to M_k. Consequently $A_i' A_i'' = A_i'''$, since the A_i and M_k form a group. The subgroup of the elements A_i must belong to one of the 32 crystal classes.

The properties listed above lead to an algorithm, as yet incomplete, for finding the groups of point symmetry transformations. Take a symmetry class. Let its elements form the group G. We find a subgroup H amongst the elements of G. The sub-

*B differs from A in that B is an arbitrary combination of rotations, reflections and translations, whereas A includes only those compatible with a space lattice, which may belong to a crystal.

[4] A. G. Kurosh, *Theory of Groups*, GITTL (State Tech. Lit. Press), 1953.

Groups of point symmetry transformations for crystals with nonvanishing current density.

System	Symbol of symmetry class		Elements of symmetry class	Number of elements in the class (order)
	Shubnikov	Shoenfliess		
Triclinic	1	C_1	E	1
	$\overline{2}$	C_i	$E,\ C$	2
Monoclinic	2	C_2	$E,\ L_{2z_0}$	2
	m	C_{1h}	$E,\ P$	2
	$2:m$	C_{2h}	$E,\ L_{2z}P_z,\ C$	4
Rhombic	$2:2$	D_2	$E,\ L_{2x},\ L_{2y},\ L_{2z}$	4
	$2\cdot m$	C_{2v}	$E,\ L_{2z},\ P_x,\ P_y$	4
	$m\cdot 2:m$	D_{2h}	$E,\ L_{2x},\ L_{2y},\ L_{2z},\ P_x,\ P_y,\ P_z,\ C$	8
	4	C_4	$E,\ L_{4z},\ L_{2z},\ L_{4z}^{-1}$	4
	$4:2$	D_4	$E,\ L_{4z},\ L_{2z},\ L_{4z}^{-1},\ L_{2x},\ L_{2y},\ L_{2xy},\ L_{2-xy}$	8
	$4:m$	C_{4h}	$E,\ L_{4z},\ L_{2z},\ L_{4z}^{-1},\ P_z,\ S_{4z},\ S_{4z}^{-1},\ C$	8
	$4\cdot m$	C_{4v}	$E,\ L_{4z},\ L_{2z},\ L_{4z}^{-1},\ P_x,\ P_y,\ P_{xy},\ R_{-xy}$	8
	$m\cdot 4:m$	D_{4h}	$E,\ L_{4z},\ L_{2z},\ L_{4z}^{-1},\ L_{2x},\ L_{2y},\ L_{2xy},\ L_{2-xy}$ $P_x,\ P_y,\ P_{xy},\ P_{-xy},\ P_z,\ S_{4z},\ C,\ S_{4z}^{-1}$	16
	$\overline{4}$	S_4	$E,\ S_{4z},\ L_{2z},\ S_{4z}^{-1}$	4
	$\overline{4}\cdot m$	D_{2d}	$E,\ S_{4z},\ L_{2z},\ S_{4z}^{-1},\ P_x,\ P_y,\ L_{2xy},\ L_{2-xy}$	8
Hexagonal	3	C_3	$E,\ L_{3z},\ L_{3z}^{-1}$	3
	$3:2$	D_3	$E,\ L_{3z},\ L_{3z}^{-1},\ 3L_{2\perp}$	6
	$3\cdot m$	C_{3v}	$E,\ L_{3z},\ L_{3z}^{-1},\ 3P_{\parallel}$	6
	$\overline{6}$	S_6	$E,\ S_{6z},\ L_{3z},\ C,\ L_{3z}^{-1},\ S_{6z}^{-1}$	6
	$\overline{6}\cdot m$	D_{3d}	$E,\ S_{6z},\ L_{3z},\ C,\ L_{3z}^{-1},\ S_{6z}^{-1},\ 3P_{\parallel},\ 3L_{2\perp}$	12
	$3:m$	C_{3h}	$E,\ L_{3z},\ L_{3z}^{-1},\ P_z,\ S_{3z},\ S_{3z}^{-1}$	6
	$m\cdot 3:m$	D_{3h}	$E,\ L_{3z},\ L_{3z}^{-1},\ 3P_{\parallel},\ P_z,\ S_{3z},\ S_{3z}^{-1},\ 3L_{2\perp}$	12

Groups of point symmetry transformations for crystals with nonvanishing current density.

Groups of point symmetry transformations for crystals with nonvanishing current density
1) E
1) E, C; 2) E, RC
1) E, L_{2z}; 2) E, RL_{2z}
1) E, P; 2) E, RP
1) $2:m$; 2) 2, RP_z, RC; 3) m, RL_{2z}, RC; $\overline{4}$) 2, RL_{2z}, RP_z
1) $2:2$; 2) 2, RL_{2x}, RL_{2y}
1) $2\cdot m$; 2) 2, RP_x, RP_y; 3) m, RL_{2z}, RP_y
1) $m\cdot 2:m$; 2) $2:2$, RP_x, RP_y, RP_z, RC
3) $2\cdot m$, RL_{2x}, RL_{2y}, RP_z, PC; 4) $2:m$, RL_{2x}, RL_{2y}, RP_x, RP_y
1) 4; 2) 2, RL_{4z}, RL_{4z}^{-1}
1) $4:2$; 2) 4, RL_{2x}, RL_{2y}, RL_{2xy}, RL_{2-xy}; 3) $2:2$, RL_{4z}, RL_{4z}^{-1}, RL_{2xy}, RL_{2-xy}
1) $4:m$; 2) 4, RP_z, PS_{4z}, RS_{4z}^{-1}, RC
3) $2:m$; RL_{4z}, RL_{4z}^{-1}, RS_{4z}, RS_{4z}^{-1}; 4) $\overline{4}$, RL_{4z}, RL_{4z}^{-1}, RP_z, RC
1) $4\cdot m$; 2) 4, RP_x, RP_y, RP_{xy}, RP_{xy}; 3) $2\cdot m$, RL_{4z}, RL_{4z}^{-1}, RP_{xy}, RP_{-xy}
1) $m\cdot 4:m$; 2) $4:2$, RP_x, RP_y, RP_{xy}, RP_{-xy}, RP_z, RS_{4z}, RS_{4z}^{-1}, RC
3) $4:m$, RL_{2x}, RL_{2y}, RL_{2xy}, RL_{2-xy}, RP_x, RP_y, RP_{xy}, RP_{-xy}; 4) $4\cdot m$, $RL_{2x}RL_{2y}RL_{2xy}$, RL_{2-xy} RP_z, RS_{4z}, RC, RS_{4z}^{-1}; 5) $m\cdot 2:m$, RL_{4z}, RL_{4z}^{-1}, RS_{4z}, RS_{4z}^{-1}, RL_{2x}, RL_{2y}, RP_{xy}, RP_{-xy}
6) $\overline{4}\cdot m$, RL_{4z}, RL_{4z}^{-1}, RP_{xy}, RP_{-xy}, RL_{2x}, RL_{2y}, RC, RP_z
1) $\overline{4}$; 2) 2, RS_{4z}^{-1}, RS_{4z}
1) $\overline{4}\cdot m$; 2) $\overline{4}$, RP_x, RP_y, RL_{2xy}, RL_{2-xy}
3) $2:2$, RS_{4z}, RS_{4z}^{-1}, RP_x, RP_y; 4) $2\cdot m$, RS_{4z}^{-1}, RS_{4z}, $RL_{2xy}RL_{2-xy}$
1) 3
1) $3:2$; 2) 3, $3RL_{2\perp}$
1) $3\cdot m$; 2) 3, $3P_{\perp}P_{\parallel}$
1) $\overline{6}$; 2) 3, RS_{6z}, RC, RS_{6z}^{-1}
1) $\overline{6}\cdot m$; 2) $3:2$, RS_{6z}, RC, RS_{6z}^{-1}, $3RP_{\parallel}$
3) $3\cdot m$, RS_{6z}, RC, RS_{6z}^{-1}, $3RL_{2\perp}$; 4) $\overline{6}$, $3RP_{\parallel}$, $3RL_{2\perp}$
1) $3:m$; 2) 3, RP_z, RS_{3z}, RS_{3z}^{-1}
1) $m\cdot 3:m$; 2) $3\cdot m$, $3RP_{\parallel}$, $3RL_{2\perp}$; 3) $3\cdot m$, RP_z, RS_{3z}, RS_{3z}^{-1}, $3RL_{2\perp}$
4) $3:2$, RP_z, RS_{3z}, RS_{3z}^{-1}, $3RP_{\parallel}$

Hexagonal	6	C_6	$E,\ L_{6z},\ L_{3z},\ L_{6z}^{-1},\ L_{3z}^{-1},\ L_{2z}$	6
	6 : 2	D_6	$E,\ L_{6z},\ L_{3z},\ L_{6z}^{-1},\ L_{3z}^{-1},\ L_{2z},\ 6L_{2\perp}$	12
	6 : m	C_{6h}	$E,\ L_{6z},\ L_{3z},\ L_{2z},\ L_{3z}^{-1},\ L_{6z}^{-1},\ P_z,\ S_{6z}$ $S_{3z},\ S_{3z}^{-1},\ S_{6z}^{-1},\ C$	12
	$6 \cdot m$	C_{6v}	$E,\ L_{6z},\ L_{3z},\ L_{2z},\ L_{3z}^{-1},\ L_{6z}^{-1},\ 6P_{\parallel}$	12
	$m \cdot 6 : m$	D_{6h}	$E,\ L_{6z},\ L_{3z},\ L_{2z},\ L_{3z}^{-1},\ L_{6z}^{-1},\ 6P_{\parallel}$ $6L_{2\perp},\ P_z,\ S_{6z},\ S_{3z},\ C,\ S_{3z}^{-1},\ S_{6z}^{-1}$	24
Cubic	3/2	T	$E,\ 3L_2,\ 4L_3,\ 4L_3^{-1}$	12
	$\overline{6}/2$	T_h	$E,\ 3L_2,\ 4L_3,\ 4L_3^{-1},\ 4S_6,\ C,\ 4S_6^{-1},\ 3P$	24
	$3/\overline{4}$	T_d	$E,\ 3L_2,\ 4L_3,\ 4L_3^{-1},\ 6P,\ 3S_4,\ 3S_4^{-1}$	24
	3/4	O	$E,\ 3L_2,\ 4L_3,\ 4L_3^{-1},\ 3L_4,\ 3L_4^{-1},\ 6L_2$	24
	$\overline{6}/4$	O_h	$E,\ 3L_2,\ 4L_3,\ 4L_3^{-1},\ 3L_4,\ 3L_4^{-1},\ 6L_2$ $6P,\ 3P,\ C,\ 3S_4,\ 3S_4^{-1},\ 4S_6,\ 4S_6^{-1}$	48

Hexagonal	1) 6; 2) 3, $RL_{6z},\ RL_{2z},\ RL_{6z}^{-1}$
	1) 6 : 2; 2) 6, $6RL_{2\perp}$; 3) 3 : 2, $RL_{6z},\ RL_{2z},\ RL_{6z}^{-1},\ 3RL_{2\perp}$
	1) 6 : m; 2) 3 : m, $RL_{6z},\ RL_{2z},\ RL_{6z}^{-1},\ RS_{6z},\ RS_{6z}^{-1}, RC$;
	3) 6, $RP_z,\ RS_{6z},\ RS_{3z},\ RC,\ RS_{3z}^{-1},\ RS_{6z}^{-1}$; 4) $\overline{6}$, $RL_{6z},\ RL_{2z},\ RL_{6z}^{-1},\ RP_z,\ RS_{3z},\ RS_{3z}^{-1}$
	1) $6 \cdot m$; 2) 6, $6RP_{\parallel}$; 3) $3 \cdot m, RL_{6z},\ RL_{2z},\ RL_{6z}^{-1},\ 3RP_{\parallel}$
	1) $m \cdot 6 : m$; 2) $m \cdot 3 : m$, $RL_{6z},\ RL_{2z},\ RL_{6z}^{-1},\ 3RP_{\parallel},\ 3RL_{2z},\ RS_{6z},\ RC,\ RS_{6z}^{-1}$
	3) 6 : m, $6RP_{\parallel},\ 6RL_{2\perp}$; 4) $\overline{6} \cdot m$, $RL_{6z},\ RL_{2z},\ RL_{6z}^{-1},\ 3RP_{\parallel},\ 3RL_{2\perp},\ RP_z,\ RS_{3z},\ RS_{3z}^{-1}$
	5) 6 : 2, $6RP_{\parallel},\ RP_z,\ RS_{6z},\ RS_{3z},\ RC,\ RS_{3z}^{-1},\ RS_{6z}^{-1}$
	6) $6 \cdot m$, $6RL_{2\perp},\ RP_z,\ RS_{6z},\ RS_{3z},\ RC,\ RS_{3z}^{-1},\ RS_{6z}^{-1}$
Cubic	1) 3/2
	1) $\overline{6}/2$; 2) 3/2, $4RS_6,\ 4RS_6^{-1},\ RC,\ 3RP$
	1) $3/\overline{4}$; 2) 3/2, $6RP,\ 3RS_4,\ 3RS_4^{-1}$
	1) 3/4; 2) 3/2, $3RL_4,\ 3RL_4^{-1},\ 6RL_2$
	1) $\overline{6}/4$; 2) 3/4, $6RP,\ 3RP,\ RC,\ 3RS_4,\ 3RS_4^{-1},\ 4RS_6,\ 4RS_6^{-1}$
	3) $3/\overline{4}$; $3RL_4,\ 3RL_4^{-1},\ 6RL_2,\ 3RP,\ RC,\ 4RS_6,\ 4RS_6^{-1}$
	4) $\overline{6}/2$; $3RL_4,\ 3RL_4^{-1},\ 6RL_2,\ 6RP,\ 3RS_4,\ 3RS_4^{-1}$

group H must also belong to one of the 32 symmetry classes. Multiply by R all elements of G-H, i.e., all those belonging to G, but not to H. These give $RA_k = M_k$. If the set of elements M_k and A_i forms a group, then this is of the required type. This algorithm would allow us to derive all the required groups. However, the construction of all the required groups by means of this proposed algorithm is extremely laborious, since it involves checking the group property for many sets of elements.

In order to perfect an algorithm to derive the groups of point symmetry transformations we prove the following theorem, which makes it easy to pick out from the symmetry classes such subgroups, for which the set A_i and M_k automatically form a group.

Theorem. Let the set A_k ($k = 1,2, \ldots, m$) and A_i ($i = m+1, m+2, \ldots, n$) form a group G, and let the set A_i ($i = m+1, m+2, \ldots, n$) be a subgroup H of G. Then a necessary and sufficient condition for the set $M_k = RA_k$ ($k = 1, 2, \ldots, m$) and A_i ($i = m+1, m+2, \ldots, n$) to form a group is that the index* of H be 2.

We note that $A_k A_i$ and $A_i A_k$ do not belong to H. Consequently

$$A_k A_i = A_{k'} \in G - H, \tag{4}$$

$$A_i A_k = A_{k''} \in G - H.$$

We first prove our condition to be necessary.

$M_k M_{k'} = A_k A_{k'} R^2 = A_k A_{k'}$, which by (3) equals A_i:

$$A_k A_{k'} = A_i. \tag{5}$$

Take one A_k and multiply it successively by all the A_k. The products will according to (5) be A_i elements, which must all be different. Hence the number of elements A_k does not exceed the number of the elements A_i, i.e., the index of the subgroup must be 2.

Now we prove the condition to be sufficient.

Since the number of elements is finite, it is not necessary for establishing the group property of the set to show the existence of a unit element or of an inverse. The associative property is obvious. It remains only to prove that the set is closed. There exist the following types of products of elements: $A_i A_i$, $A_i M_k$, $M_k A_i$, $M_k M_k$.

$A_i A_i = A_{i''}$ since the set of the A_i forms a subgroup; $A_i M_k = A_i A_k R$ is by (4) equal to $A_{k'} R = M_{k'}$; $M_k A_i$ is similarly equal to $M_{k''}$; $M_k M_{k'} = A_k A_{k'} R^2 = A_k A_{k'}$. Since the index of the subgroup is 2, any $A_k = \alpha A_i$, where α is one of the A_k. Hence $M_k M_{k'} = \alpha A_i A_{k'}$ and by (4) this is equal to $\alpha A_{k''} = \alpha^2 A_{i'}$. In other words, $M_k M_{k'} = \alpha A_{i'}$. It is easy to see that $\alpha^2 = A_{i''} \in H$. Therefore $M_k M_{k'} = A_{i'''}$.

This completes the proof.

Now we can formulate the final algorithm for finding all point symmetry groups. The groups of point transformations of the symmetry of crystals with $j \neq 0$ will contain, in the first place the 32 symmetry classes. To find all the others, we take a symmetry class, select from it a sub-class (the subgroup H) which has index 2. The elements of the class A_k which do not belong to the subclass are replaced by $M_k = RA_k$. The elements A_i of the suclass and the elements $M_k = RA_k$ form the required group. In order to find all possible such groups we have to investigate all 32 symmetry classes.

We must only remember that in a crystal with $j \neq 0$ the transformations R and RL_3 cannot occur as symmetry transformations. This point will prove important in the hexagonal and cubic systems.

4. LIST OF GROUPS OF POINT TRANSFORMATIONS FOR THE SYMMETRY OF CRYSTALS WITH A MEAN CURRENT DENSITY.

We list below the groups of point transformations obtained by the method proposed above. In the table we use the following notation:

$L_2, L_3, L_3^{-1}, L_4, L_4^{-1}, L_6, L_6^{-1}$ are rotations by 180, 120, -120, 90, -90, 60 and -60 degrees, respectively. $S_3, S_3^{-1}, S_4, S_4^{-1}, S_6, S_6^{-1}$ are, respectively rotations by 120, -120, 90, -90, 60, -60 degrees together with reflection in the plane at right angles to the axis of rotation. C is the inversion, P the

*By the index of a subgroup we denote the number of classes in the expansion of the group with respect to the subgroup. The index of a subgroup equals the ratio of the number of elements of the group (its order) to the number of elements of the subgroup.[4]

reflection in a plane.

The subscripts x, y, z, xy, $-xy$ on L_i and S_i indicate the direction of the axis of rotation; the same subscripts on P indicate the direction of the normal to the plane of reflection.

The suscript $\perp$ or $||$ indicates that the axis of rotation through 180° or the normal to the reflection plane is perpendicular or parallel to the main crystal axis of threefold or higher symmetry. The table also shows the symmetry class to which each group of point symmetry transformation belongs, i.e., the class obtained from it by substituting E for R.

In the last column of the table the symbol of a symmetry class stands for the set of transformations belonging to that class.

The allocation of the groups of point symmetry transformations to symmetry classes has a definite meaning. The point is that goniometric and X-ray analysis discloses only the symmetry of the charge distribution $\rho(x,y,z)$ and does not notice the current $j(x,y,z)$. The symmetry which is found by goniometric and X-ray methods is therefore just that of the symmetry class which is obtained if we replace R by E in the group of point symmetry transformations, since for the charge density $\rho(x,y,z)$ the transformation R has the same effect as the identity operation. Altogether there are 90 groups of point symmetry transformations for crystals with $j \neq 0$; of these 32 coincide with the 32 symmetry classes, and 58 are new.

The groups obtained in this way are isomorphous with the groups of transformations of finite figures, with oriented grains, which were derived by Shubnikov[5] by a different method. There the part of time reversal is played by an "anti-identity" transformation. The 58 new groups are isomorphous with the groups of mixed polarity.*

5. POSSIBLE APPLICATIONS OF THE GROUPS OF POINT SYMMETRY TRANSFORMATIONS OF CRYSTALS

Above we have discussed the symmetry of crystals with $j \neq 0$. It is well known that a magnetic moment is equivalent to a current, and therefore the groups we have derived for crystals with $j \neq 0$ are also the symmetry groups for crystals with a magnetic moment. It has to be remembered that the magnetic moment is an axial vector. A symmetry transformation which does not contain a reflection acts on the magnetic moment as on an ordinary vector, but a reflection changes the direction of the axial vector in the opposite sense to that of an ordinary vector. The symmetry of the magnetic moment vector includes the symmetry transformations of the class $\infty : m$. In addition, the magnetic moment vector is symmetrical under the transformation $RP_{||}$, where $P_{||}$ is a reflection in a plane passing through the magnetic moment vector, and the transformation $RL_{2\perp}$ where $L_{2\perp}$ is a rotation through 180° about an axis at right angles to the magnetic moment vector.

As an example, let us find the possible symmetry of a pyromagnetic substance. We use the symmetry principle in a similar manner to the one used for pyromagnetic crystals in reference 6. Remembering what was said above about the symmetry of the magnetic moment vector, it turns out that pyromagnetic crystals cannot belong to the cubic system. This conclusion differs from that drawn in Ref. 6.

Recently the opinion has been expressed[7] that pyromagnetism, piezomagnetism, etc., are impossible. This paper starts from the assumption that the crystal structure must be symmetric under time reversal. But this does not hold for crystals which possess a magnetic moment. We therefore consider that the conclusions drawn in Ref. 7 as to the impossibility of pyromagnetism and piezomagnetism, is unfounded.

---

*Shubnikov has 57 groups of mixed polarity. Actually there are 58.

[5] A. N. Shubnikov, *Symmetry and Antisymmetry of Finite Figures*, Acad. Sci. USSR Press, 1951.

[6] A. N. Shubnikov, E. E. Flint and T. B. Bokii. *Foundations of Crystallography*, Acad, Sci. USSR Press, 1940.

[7] W. Zochera and H. Török, Proc. Nat. Acad. Sci. 39, 681 (1953).

Translated by R. Peierls
101

Deformation of Arc Column in Rarefied Gases at High Currents*

G. G. TIMOFEEVA AND V. L. GRANOVSKII
All-Union Electrotechnical Institute

(Submitted to JETP editor June 22, 1955)
J. Exptl. Theoret. Phys. (U.S.S.R.) 30,477-487 (March, 1956)

Various phenomena occurring in the arc of Hg, H_2, Ar and Kr at $p \sim 10^{-4} - 10^{-3}$ mm Hg and currents i_a up to 2000 amp were studied. By the method of a movable probe it was found that the half-width of the arc column decreases by 30% when the current i_a increases up to 10^2 amp. A further increase in current gives rise to gradually increasing vibrations first in the probe current, then in the arc voltage and finally, in the arc current, with an average frequency $f = 10^4 - 10^5$ cycles. The oscillograms of the current on two identical and symmetrically located probes show that these vibrations may be interpreted as the result of irregular propagation of the compressed arc column along the cross section of the tube. At current pulses $i_a \sim 500 - 2000$ amp with a duration of 1-10 μsec, it is possible to observe the compressed arc column visually and photographically; the column is found to be compressed into a narrow cord, curved into a helix and pressed against the walls of the tube. With the aid of a rotating photo-camera it was shown that, at prolonged ($10^2 - 10^3$ μsec) current pulses, the arc is also compressed and is repeatedly propagated along the cross section of the tube. The compression and the curvature of the arc column are of electrodynamic origin, but its propagation is of gasodynamic origin.

1. INTRODUCTION

THE passage of a strong electric current in a rarefied gas is accompanied by a number of specific phenomena which are not noticeable at lower currents. In particular, it was pointed out repeatedly that at high currents there should occur transverse compression in the flow of charge carriers under the action of the self-magnetic field[1,2].

The quantitative theory developed by Tonks led to the conclusion that, upon approaching the critical current $i_{cr}(a) \approx 6 \times 10^5 T_e^{3/2}(^\circ K)/\lambda_e(cm) \times E(V/cm)$, the current density at the axis should increase without limit. An assumption was proposed that such compression of the current into a narrow cord should be accompanied by a strong rarefication of the gas in this cord; the consequence of this simultaneous increase in the current density and of the drop in the density of the substance would result in a break in the current (pinch effect). A number of investigations have been devoted to the further development of the theory of this phenomenon[3,4].

Several attempts were also made to detect experimentally the electrodynamic compression of the arc column in a rarefied gas. With the aid of probes, the arc was studied in mercury vapor at currents up to 150 amp and at a vapor pressure $p = 10^{-1} - 10^{+1}$ μHg and up to 80 amp at $p = 2$ μHg[5]. It was found that at $i_a = 50$ amp and $p = 0.5$ μHg, the radial electric field is almost nonexistent; apparently, the electron distribution along the cross section of the tube is determined mainly by the magnetic field, which replaces the radial electric field of the arc column. The half-width of the concentration distribution is compressed by 27% at $i_a = 150$ amp[3] and by 20% at $i_a = 80$ amp[5]. Also, with the aid of probes[6] it was found that in the hydrogen arc at $p = 30$ μHg, the current distribution curves are compressed by 30% when the current increases from 20 to 102 amp. With a high-frequency nonelectrode (circular) current, there were observed in Kr and in other gases at $p < 0.5$ μHg and $i_a > 10^4$ amp (with the aid of a rotating camera) variations in the thickness of the luminous region, the frequency of which depends on the pressure, on the atomic weight of the gas and on the applied voltage[7]. The authors explain these variations as a manifestation of the

* Brief communication, see J. Exptl. Theoret. Phys. (U.S.S.R.) **28**, 378 (1955); Soviet Physics JETP **1**, 381 (1955).

[1] W.H. Bennett, Phys. Rev. **45**, 890 (1934).

[2] L. Tonks, Trans. Electrochem. Soc. **72**, 629 (1937); Phys. Rev. **56**, 360 (1939).

[3] P.C. Thonemann and W.T. Cowhig, Proc. Phys. Soc. (London) **64**, 345 (1951).

[4] M. Blackman, Proc. Phys. Soc. (London) **64**, 1039 (1951); A. Schlüter, Z. Naturforsch. **5a**, 72 (1950); M. Kruskal and M. Schwarzschild, Proc. Roy. Soc. (London) **223A**, 348 (1954).

[5] H. Fetz, Ann. Physik **40**, 570 (1941).

[6] B.A. Mamyrin, J. Tech. Phys. (U.S.S.R.) **25**, 1914 (1953).

[7] S.W. Cousins and A.A. Ware, Proc. Phys. Soc. (London) **64**, 159 (1951).

pinch effect. In the arc channel in H_2, Ar and in air at atmospheric pressure and at currents of the order of 10^5 amp, there are observed phenomena which the authors also interpret as the pinch effect[8].

We do not know of any descriptions of the considerable electrodynamic compression of the low pressure arc in simple cases, that is, at a current flowing in a single direction.

The object of the present investigation was first to establish the main fact: whether there occurs any noticeable compression in the arc of a constant, or slowly changing, current in a rarefied gas when the current is increased*. Should the answer be yes, then it would be necessary to answer 1) why this compression remained unnoticed, 2) how it can be explained, 3) whether it leads to a break in the current as predicted by the Tonks hypothesis.

2. EXPERIMENTAL PROCEDURE AND APPARATUS

In carrying out the experiment, we have used cylindrical tubes having a length of $l = 100$-500 mm and a diameter of $2R = 10$-70 mm; in all cases $l \gg 2R$. We have avoided any kind of constrictions in the tubes, since the presence of constrictions introduces new factors (double electrical layer in front of the constriction) and may lead to instability and a break in the current[2, 9]. With a small diameter of the main section of the tube, which of necessity has to be much narrower than the cathode section, the transition between these was very gradual and even.

The tubes were filled with Hg, H_2, Ar and Kr. In the experiments with Hg, a liquid mercury cathode was used. In order to avoid the flow of vapor from the cathode into the section of the arc under investigation (positive column), the tube was bent (Fig. 1*a*) and a screen (reflector) for the mercury

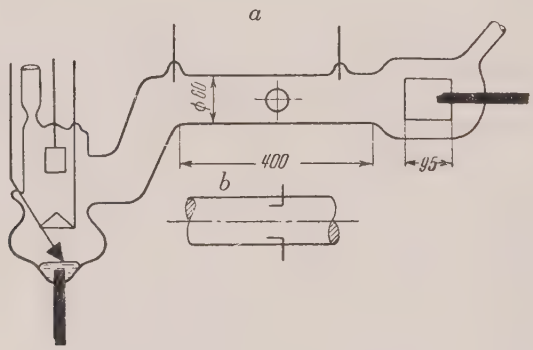

FIG. 1. *a*--mercury tube, *b*--arrangement of the two symmetrical probes with respect to the axis of the tube.

vapor was placed over the cathode. The gap between the screen and the walls remained sufficiently wide so as not to cause any narrowing of the tube. For the control of the vapor pressure in the tube, the whole cathode section was submerged into water.

In the experiments with the other gases a copper cathode of finely cut pieces of copper wire was used instead of the mercury cathode. Since the flow of vapor from the copper cathode is not significant, these tubes were made straight (Fig. 2), without any screens and without water cooling.

The arc was excited in both types of tubes by means of a semi-conductive igniter*, submerged into mercury or copper. Cylindrical tungsten probes with a diameter of 0.5 mm were introduced

* At a high gas pressure contraction (compression) of the column always occurs, but for another reason (a drop in the temperature of the gas from the axis to the periphery of the column); therefore, the electrodynamic effect here is superimposed on the ordinary contraction and it is not easy to separate it in this case[8].

[8] J.E. Allen and J.D. Craggs, Brit. J. Appl. Phys. **65**, 446 (1954).

* The igniters were supplied by the laboratory of defense apparatus of VEI (All-Union Electrical Engineering Institute).

[9] A.W. Hull, Electr. Eng. **53**, 1435 (1934); H. Kleinwachter, Arch. Elektrotechn. **34**, 523 (1940); B.N. Kliarfeld and I.A. Poletaev, Dokl. Akad. Nauk SSSR **23**, 460 (1939); V.L. Granovskii and T.A. Suetin, J. Tech. Phys. (U.S.S.R.) **16**, 1023 (1946).

FIG. 2. Tube used in the experiments with H_2 and with inert gases.

into the anode arm of the tube, their working portion being parallel to the axis of the tube, and the remaining part being coated with fused quartz. The study of the current distribution along the cross section was carried out by a probe, movable along the diameter of the tube by an iron anchor, of the external coil and of the control apparatus. In one series of experiments (see below, section 3b), two identical probes were introduced into the tube; these were placed symmetrically with respect to the tube axis and at a distance of 10 mm from it (see Fig. 1*b*). The probes were supplied with the voltage $U_p = -60$V with respect to the cathode, this ensured a purely ionic current to the probe. Under the conditions of our investigation we had to forego the measurement of the electronic currents and the determination from them of the electron concentrations, since the self-magnetic field of the arc current, approaching in these experiments 10^2 Oe, makes the interpretation of the electronic portions of the probe characteristics exceedingly difficult (see Ref. 10).

[10] G. L. Spivak and E.M. Reikhrudel, J. Exptl. Theoret Phys. (U.S.S.R.) **16**, 816 (1936).

Therefore, we concentrated on the determination of the ionic current in the probe i_p for one and the same voltage, which was sufficiently negative with respect to the cathode at various positions of the probe. The relative value of i_p at various points of the tube diameter provides the possibility of judging approximately the distribution of the ion concentration and, therefore, also of the electrons along the cross section of the column.

Sources of arc current in the various experiments were: circuit of constant current, transformers and pulse circuits. In the first case, a constant current was passed through the tube. In the second case, a single igniting pulse was passed through the igniter, which caused the passage through the tube of a single half-wave of current $f = 50$ cycles. In the third case, the discharge through the tube of a charged condenser was also produced by a pulse igniter. The resultant single current pulse in one direction in the tube had a considerably smaller duration (1-50 μsec).

The recording and the measurement of the electrical values, and first of all of the arc current and voltage i_a and U_a, and of the probe current i_p, were carried out by indicating instruments and by electronic oscillographs having electrical and mechanical resolution. The probe currents were measured with indicating instruments not only for a constant arc current, but also for single current pulses. In this case, the indicating instrument gave a ballistic reading proportional to $\int_0^T i_p dt$. The readings thus obtained were compared with each other for various conditions, for example, for various positions of the probe with respect to the axis. In addition, the probe currents, as well as the current and voltage of the arc, were oscillographed. For this purpose, coaxial-cylindrical or doubly-wound resistances of low inductance were connected into the probe and the arc circuits. In some cases, the voltage on these resistances was initially intensified by a constant current amplifier.

The external shape of the arc was photographed with an ordinary photo-camera. Owing to the comparatively low brightness of the arc at the pressures with which we were working, the photographing represented definite difficulties, particularly for the short-current pulses. It was not always possible to overcome these difficulties, even when we used a film with a sensitivity up to 250 units GOST.

For the observation of transverse compression and propagation of the arc at long current pulses a single transverse section of the arc was photographed and resolved. For this purpose, a double

screen having slits perpendicular to the axis of the tube was placed in front of the arc (Fig. 3). An image was reflected by a Zonnar objective 1:1.5; $F = 50$ mm on the photo-film of the rotating camera having a screen with a diameter of 300 mm and a number of revolutions up to 200 sec^{-1}.

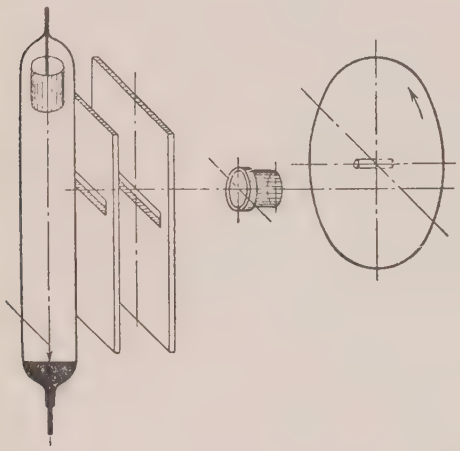

FIG. 3. Diagram for the observation of arc propagation.

3. EXPERIMENTAL RESULTS

a) Probe measurements of the distribution of charge carriers along the cross section of the tube.

We carried out these measurements with the aid of a movable probe in a tube $R = 35$ mm in mercury vapor at i_a from 13 to 1700 amp. The probe currents were determined with an indicating instrument, as well as with an oscillograph. The final form of the readings at $i_a \geq 1000$ amp was complicated by strong vibrations of the ionic current. In these cases, the average value $i_p = \frac{1}{T}\int_0^T i_p dt$ was determined. Readings were taken at 14 different positions of the probe, that is, every 5 mm. These were divided by the maximum reading of the given series, generally obtained near the axis of the tube. The ratios $i_p(r)/(i_p)_{max}$ or $\int i_p(r)dt/\int(i_p)_{max}dt$ thus obtained, expressed as functions of r/R, may characterize the distribution of the charge carriers along the cross section of the tube. The parameter characterizing the degree of arc compression may be the relative half-width of the column $(r/R)_{1/2}$, that is, the value r/R at which $i_p(r)/(i_p)_{max} = 1/2$.

Table I gives the values which we found for $(r/R)_{1/2}$ of the mercury arc column at $R = 35$ mm, at various temperatures of Hg condensation and at various arc currents i_a. The data relating to $i_a = 1$ amp were taken from old measurements[11].

TABLE I. Relative half-width $(r/R)_{1/2}$ of the arc column in Hg at various currents, determined with probes.

Temperature of Condensation °C	Saturated Vapor Pressure μHg	Arc Current in Amperes								Method of Determination
		1	22	50	85	170	680	1000	1700	
9	0.5	>1*				0.71		0.71	0.71	Oscillograph
16—17**	0.9÷1.0	~1	0.80	0.78	0.78					The Same
16—22**	0.9÷1.5	~1	0.77	0.77	0.74	0.71		0.71	0.77	Indicating Instrument
19—22**	1.2÷1.5	~1					0.71	0.66	0.75—0.78	Oscillograph

* At these conditions (n_e) column$/(n_e)_0 > 1/2$.

** Here the data of several measurements at somewhat different temperatures are taken together, since there was no great difference between them.

[11] V.L. Granovskii, *Symposium on Electronic and Ionic Apparatus*, State Energetics Press, Moscow, 1941, p. 122.

These results show that the arc compresses by approximately 30% when the current is increased up to ~ 170 amp. When the current was increased up to 1700 amp, it was not possible to observe any further compression the arc column by means of probe measurements.

b) Fluctuations of the arc parameters at high currents.

Irrespective of the fact that the results of probe observations described in Sec. a) are quite limited, the properties of the arc continued to change when the current was increased above 200 amp. This was indicated first by the large increase in the arc voltage U_a at high currents (Fig. 4), second by the resulting fluctuations (which increased with an increase in current) of all the

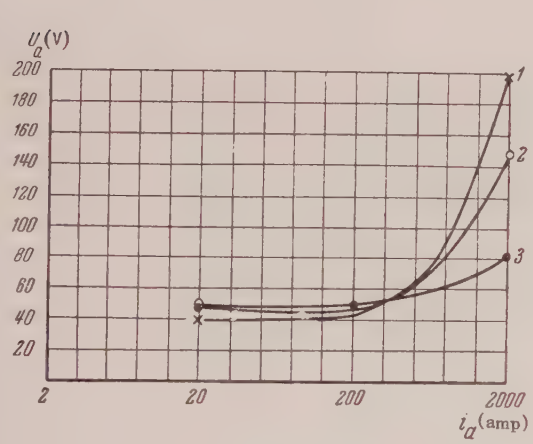

FIG. 4. The dependence of the arc voltage on the current in a cylindrical tube. *1*--$p = 1$, *2*--$p = 10$, *3*--$p = 100\,\mu$Hg.

parameters of the arc. A study of the oscillograms of the current i_a, of the arc voltage U_a, as well as of the probe current i_p, in a tube of diameter 60(70) mm in mercury vapor at pressures of 0.4 to 6 μHg when a single semi-sinusoidal current of 50 cycles is passed showed the following:

At a current up to 500 amp (current density $\bar{j}_a$ up to 12 amp/cm^2, averaged over the entire cross section of the tube) the arc is quite stable in the range of pressures investigated, the arc current and voltage (i_a and U_a), as well as the probe current i_p, do not experience any noticeable fluctuations (Fig. 5).

At $i_a \sim 1000$ amp ($j_a \sim 30$ amp/cm^2), signs of instability in the arc column begin to appear. The

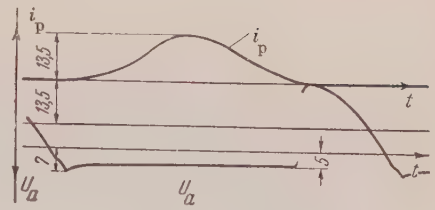

FIG. 5. The arc voltage U_a and the ionic current in the probe i_p when $(i_a)_{max} = 1.0$ amp, $p = 0.4\,\mu$Hg.

arc voltage U_a (Fig. 6) and the probe current i_p (Fig. 7) experience irregular fluctuations about

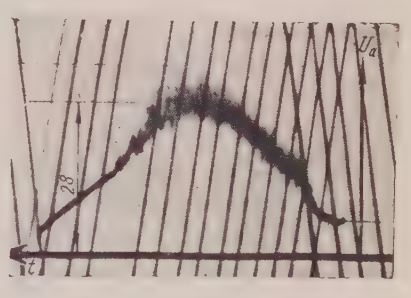

FIG. 6. Arc voltage at $(i_a)_{max} = 1700$ amp, $p = 0.4\,\mu$Hg.

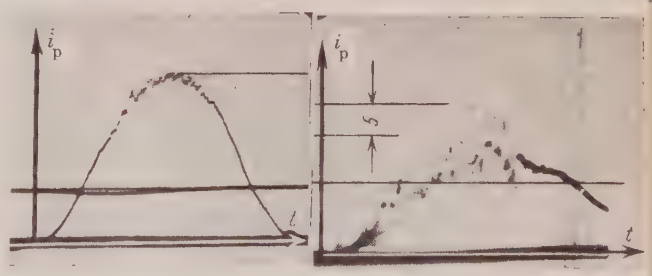

a *b*

FIG. 7. Probe current at $(i_a)_{max} = 1700$ amp, $p = 1\,\mu$Hg. *a*--at the axis of the tube, *b*--at the walls.

the average values. The absolute and relative values of these fluctuations increase as the current increases (cf. Figs. 7 and 8). Upon increasing the pressure, on the contrary, these fluctuations decrease (cf. Figs. 6 and 7*b* with Figs. 9*a* and

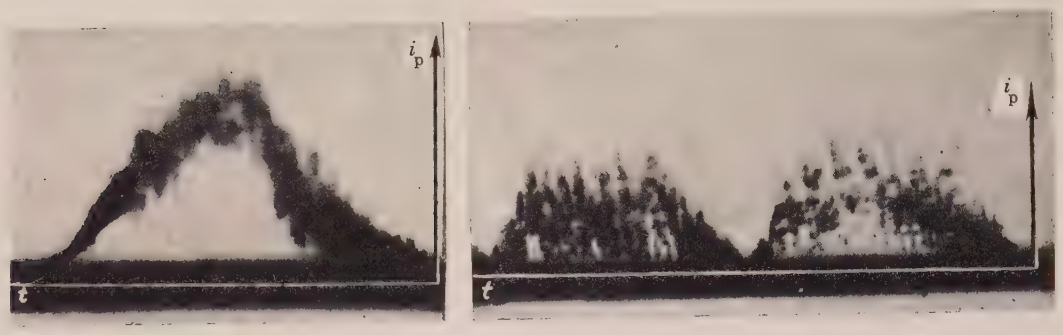

a b

FIG. 8. Probe current at $(i_a)_{max} = 2000$ amp, $p = 0.8\ \mu$Hg. *a*--along the axis, *b*--at the walls.

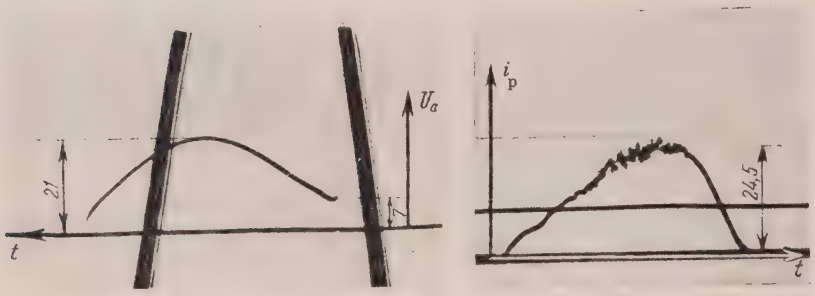

a b

FIG. 9. Arc voltage and probe current at $(i_a)_{max} = 1700$amp, $p = 10\ \mu$Hg. *a*--arc voltage, *b*--probe current at the wall.

9*b*). The fluctuations of the ionic current at the periphery (Figs. 7*b*, 8*b*) and at the walls of the tube are greater than at the axis (Figs. 7*a* and 8*a*).

However, the arc current i_a may not yet experience any noticeable fluctuations (Fig. 10). Considerable fluctuations in i_a begin even at higher currents than the fluctuations in U_a and i_p in the tube with $R = 30$ mm in Hg vapor at 1700-1800 amp ($j_a \approx 50$ amp/cm^2) (Fig. 11) when the i_p fluctuations at the edge of the tube approach 100%. Some of our observations of the relative value of the fluctuations in U_a, i_a and i_p at various conditions are compiled in Table II; the accuracy of the values is of the order of 10%. The Table shows clearly that there is an increase in the fluctuations when the current i_a is increased and the pressure p is decreased. A similar dependence of the vibrations on i_a and p was observed also in the other gases. In all cases the value most sensitive to the disturbance of the stability of arc performance was found to be the probe current, then the arc voltage and finally the arc current.

In spite of their chaotic character, these fluctuations occur with a certain average frequency f, which can be evaluated from the oscillograms. The results of such an evaluation are given in Table III. Since the frequencies of the fluctuations i_p and U_a are approximately the same, a common evaluation for both of these is given in the Table.

From the Table it is evident that the average frequency of fluctuations, other conditions being equal, decreases when the radius of the tube is increased, increases with an increase in arc current and decreases with an increase in the molecular weight of the gas.

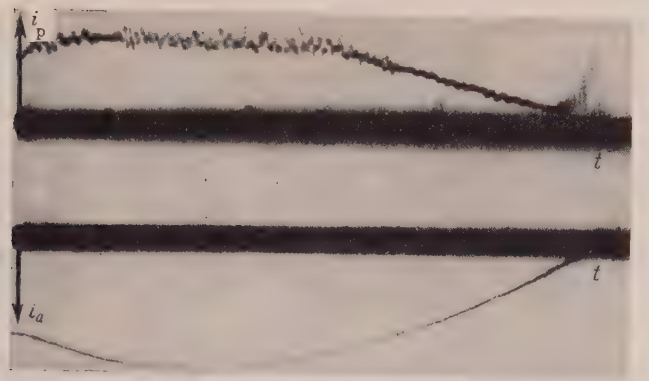

FIG. 10. Probe current i_p and arc current i_a, Ar, $R = 30$ mm, $(i_a)_{max} = 240$amp, $p = 3\,\mu$Hg.

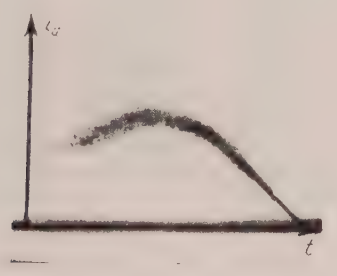

FIG. 11. Oscillogram of the arc current in Hg vapor at $R = 30$ mm, $(i_a)_{max} = 2000$ amp, $p = 0.8\,\mu$Hg.

TABLE II. Fluctuations of i_a, U_a and i_p (in %) (Hg, R = 30-35 mm)

p (μHg)	1	1	1	1	1	0.4	1	10
$(i_a)_{max}$ (amp)	190	440	1000	1700	2000	1700	1700	1700
$\Delta i_a/i_a$	0	0	0	0	25	5	0	0
$\Delta U_a/\bar{U}_a$	0	0	10	25	40	35	25	0
$\frac{\Delta i_p}{\bar{i}_p}$ at the axis	0	0	0	10	50	20—30	10	10
$\frac{\Delta i_p}{\bar{i}_p}$ at the wall	0	0	15	50	90	30—80	50	20

TABLE III. Average frequency $\overline{f}$ of the voltage fluctuations

Gas	R, mm	$(i_a)_{max}$ amp	$\overline{f}$ cycles
Hg	16	1200	$1.2—1.8\times10^5$
	16	1600	$2.6—3.6\times10^5$
	15	1200	$4.5—6.7\times10^5$
Ar	5	1000	$2.0—2.2\times10^5$
Kr	16	1000	$1.0—1.4\times10^5$
	5	1000	$1.6—1.8\times10^5$

c) Observations with two symmetrical probes.

The fluctuations of the arc parameters, described above, and primarily of the probe current, can be explained by the fact that at strong currents the arc column is compressed into a narrow cord, and that this cord does not remain stationary, but propagates along the cross section of the tube with the frequency of the fluctuations observed. To verify this hypothesis it would be expedient to register simultaneously the currents on two identical probes, placed in the same cross section of the tube, symmetrical to the axis of the tube (see Fig. 1*b*). If the arc column actually fills only a portion of the tube cross section and if it propagates with time, then the maxima and the minima of the current on both probes should not appear simultaneously. On the contrary, their synchronized appearance would indicate that there is no arc propagation, but simply fluctuations of the arc current as a whole. In Fig. 12 a sample is shown of the current oscillograms (initial sections) on the two probes registered with a double-ray oscillograph with mechanical resolution. The experimental conditions were: Hg, $R = 30$mm, $p = 1.2\mu$Hg, $(i_a)_{max} = 1000$ amp, $U_a = -55$ V. A comparison of both oscillograms shows that, in addition to the changes occurring simultaneously in both currents, there are also many peaks in each of the currents which do not coincide in time with the peaks of the other current; opposite a peak of one current there are slopes and dips of the other. Moreover, even the numbers of the peaks on both oscillograms do not agree. This and other similar photographs provide proof in favor of the above hypothesis on the irregular propagation of the arc column in the tube.

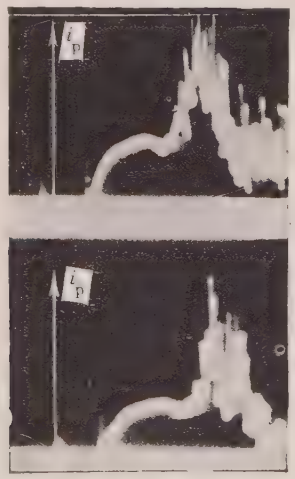

FIG. 12. Probe currents on two identical, symmetrically located probes, registered simultaneously, Hg, $R = 30$ mm, $p = 1.2\mu$Hg, $(i_a)_{max} = 1000$ amp.

d) The shape of the arc column at short pulses.

The results of the above-described observations on the behavior of the arc at strong currents, carried out with the aid of probes and of an oscillograph, require direct verification of the fact that at strong currents the arc column is actually compressed into a narrow cord. For visual observation and for photographing the compressed arc column, it is necessary to observe the arc within short time intervals, during which the column is not yet noticeably displaced. From the data on the average frequency of vibrations $\overline{f} \sim 10^5$ cycles it follows that the average period of this assumed displacement $\overline{T} \sim 10\,\mu$sec and therefore the time for observing the arc in a single position should not exceed a few microseconds. By passing strong current pulses of such duration through the tube, one could hope to observe the actual shape of the arc column at high current.

For this purpose condensers, connected to the tubes with short heavy copper conductors, were discharged through our experimental tubes. By discharging capacities of 1-2 μF, charged up to 7-8 kv, through the tubes with diameters of 10 and

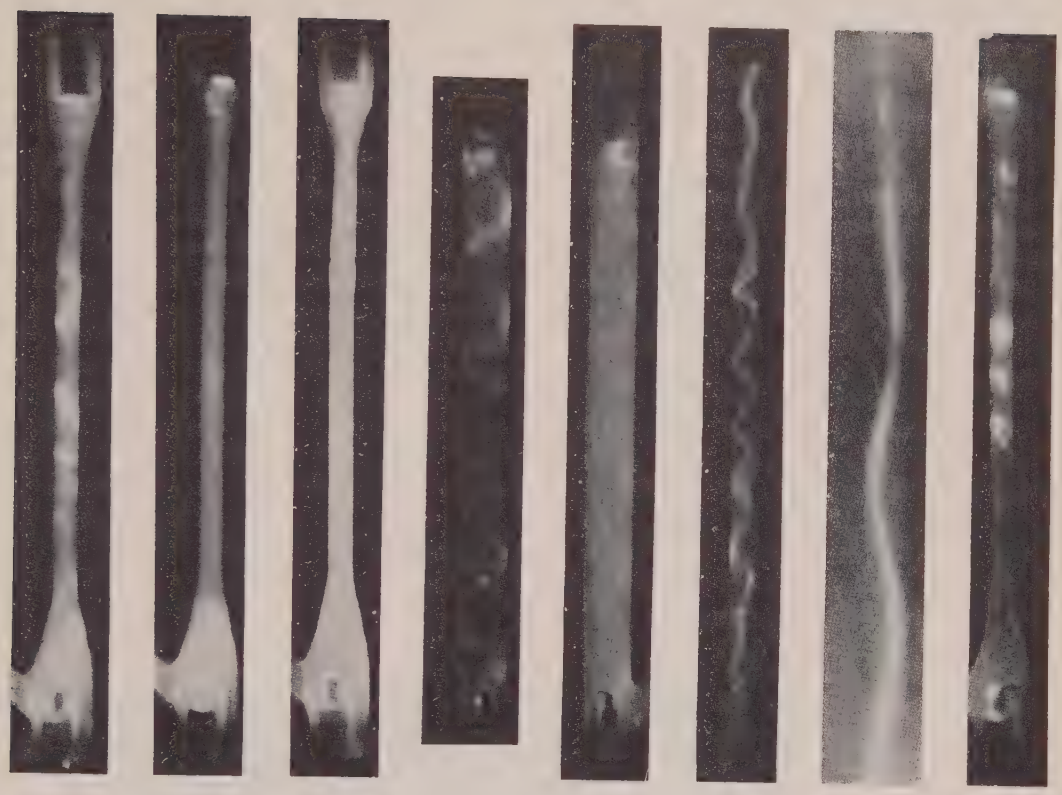

13 14 15 16 17 18 19 20

FIG. 13. The arc at a current pulse of 450amp, $\tau = 2\mu$ sec, Hg, $R = 5$ mm, $p = 1\mu$Hg.
FIG. 14. The same as in Fig. 13, $(i_a)_{max} = 220$ amp.
FIG. 15. The same as in Fig. 13, $(i_a)_{max} = 1400$amp, $\tau = 50\mu$sec.
FIG. 16. The same as in Fig. 13, $(i_a)_{max} = 2000$amp, $\tau = 7\mu$sec, Hg, $R = 16$ mm, $p = 0.4\mu$Hg.
FIG. 17. The same as in Fig. 13, $(i_a)_{max} = 2000$ amp, $\tau = 50\mu$sec, Hg, $R = 16$ mm, $p = 0.4\mu$Hg.
FIG. 18. The same as in Fig. 13, $(i_a)_{max} = 1000$amp, $\tau = 1\mu$sec, H_2, $R = 5$ mm, $p = 2\mu$ Hg.
FIG. 19. The same as in Fig. 13, $(i_a)_{max} = 450$amp, $\tau = 1.5\mu$sec, Ar, $R = 16$ mm, $p = 2\mu$Hg.
FIG. 20. The same as in Fig. 13, $(i_a)_{max} = 700$amp, $\tau = 1.5\mu$sec, Hg, $R = 5$ mm, $p = 1.6\mu$Hg.

32 mm filled with vapor of Hg, Ar, Kr and H_2 at pressures of 0.5-10μ, Hg, pulses of current were obtained of 450-2000 amp with a duration of 1-2 μsec (in some cases the pulse duration was artificially delayed up to 50 μ sec). About 100 such photographs were obtained, samples of which are given in Figs. 13-20.

In Fig. 13 a photograph is shown of an arc in Hg vapor at $R = 5$ mm, $p = 1\mu$ Hg and a current pulse $(i_a)_{max} = 450$ amp with a duration of $\tau = 2\mu$ sec. It is clearly evident that, over the major portion of the column, the brightest luminescence emanates from the comparatively narrow region or cord, the width of which is not constant, but does not exceed 2-2.5 mm (tube diameter 10 mm). This cord is bent into a three-dimensional curve approaching a helix with a nonuniform pitch along the length; it adheres closely to the glass walls of the tube.

In Fig. 14 a control photograph is given which was obtained at a current of 220 amp, all other conditions being equal. It is evident that there is no arc compression of any kind: the luminescence fills the entire tube. At a considerably greater arc duration (50 μ sec) (Fig. 15) also, no compression is observed, in spite of the even higher current (1400 amp); evidently in this time the arc has already succeeded in propagating over the entire cross section of the tube. Using a tube with a considerably larger diameter (32 mm),

similar phenomena were observed: with a current of 7 μ sec duration arc compression and its curvature in the shape of a helix are clearly visible (Fig. 16), while in the time interval of 50 μsec no compression of any kind can be observed in the photograph (Fig. 17).

This phenomenon is not specific to any particular gas (Hg vapor), it is observed also in hydrogen (Fig. 18), in argon (Fig. 19) and in krypton.

Thus, at high currents the arc column in a rarefied gas is subject to two different deformations -- transverse compression and curvature into the form of a helix, occupying the maximum space accessible to it.

In addition to the transverse compression of the column, at the very low pressures and high currents there can be observed also a longitudinal nonuniformity in the luminescence, which is also periodic in character. As an example, we can cite the photograph in Hg at $R = 5$ mm, $p = 1\,\mu$Hg, $(i_a)_{max} = 700$ amp and $\tau = 1.6\,\mu$sec (Fig. 20). The same phenomenon occurs in the other gases.

e) Propagation of the arc during prolonged time intervals.

From the earlier results one can conclude that the arc column is also compressed during a prolonged passage of current, but the compression is not noticeable because of the rapid propagation of the arc. The latter also requires substantiation by direct experiments.

Such experiments were carried out according to the diagram of Fig. 3; a "transverse section" (thin layer) was isolated from the arc column, the image of which in the form of a narrow band was photographed on a moving film. If the arc is actually compressed and is propagating, then the image of the arc cross section should be compressed into a single spot; this spot should propagate with time in a zigzag fashion along the photograph.

In Fig. 21, a photograph is shown of the arc element in a tube with a diameter of 32 mm in Hg vapor at $p = 10\,\mu$Hg and a pulse current of ~ 1200amp at $\tau = 400\,\mu$ sec obtained on a moving film. On the left, a photo is shown of the same band, but on a stationary film; below the oscillogram of the arc current is shown. The photo-resolution shows that the luminescence of the arc element at maximum currents is actually

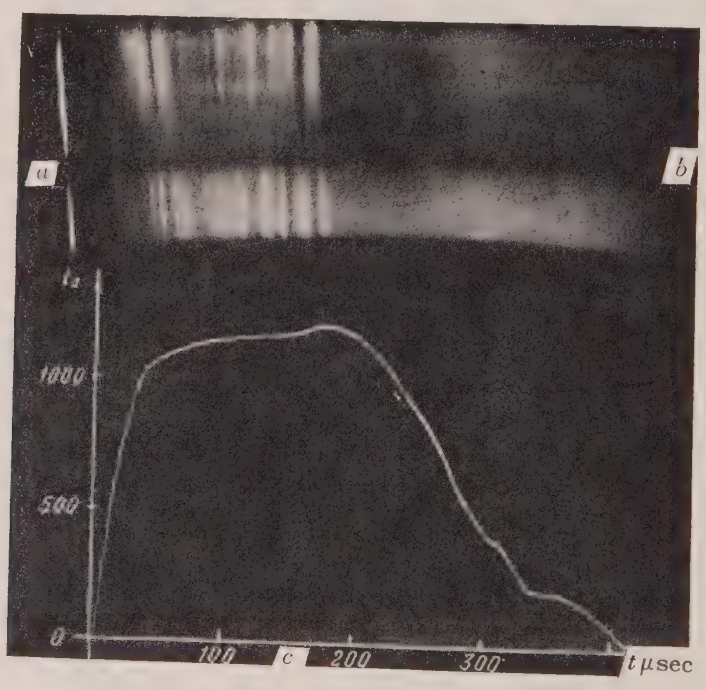

FIG. 21. *a*--photograph of the narrow band of the arc on a stationary film, *b*--the same on a moving film, *c*--oscillogram of the current.

concentrated into one spot and that this maximum of the luminescence is moving back and forth along the entire tube diameter*. The period of this propagation is on the average 13-15μ sec, which corresponds to an average frequency of $\sim 0.7\text{-}0.8 \times 10^5$ cycles. When the current drops, the arc compression and propagation break off abruptly.

The visible propagation of the arc section in a single plane in the photograph does not signify that the propagation itself necessarily takes place in a single plane. The observed horizontal propagation may be a projection of the three-dimensional propagation, for example, around the periphery adjoining the walls of the tube.

4. DISCUSSION OF RESULTS

The combination of all the results obtained by probe measurements, by oscillographic measurements and by photographic resolution of a continuous luminous arc, as well as by observations with short current pulses, leaves no doubt as to the existence of the phenomenon itself. One can consider as experimentally proved the fact that the arc in highly rarefied gases ($p \sim 10^{-3}$ mm Hg) at considerable currents ($i_a \sim 10^2 - 10^3$ amp): 1) is compressed into a narrow cord in a transverse direction, occupying a small portion of the volume of the tube, 2) it is curved into a three-dimensional helix, adhering to the inner surface of the tube walls in the majority of cases, 3) at a duration of discharge $\geq 10^{-5}$ sec, it is rapidly and irregularly propagated along the cross section of the tube.

What is the possible explanation of these phenomena?

The compression of the arc channel, other conditions being equal, may have various explanations.

a) At high gas pressures the arc column contracts towards the axis of the tube owing to the heating of the gas, which is maximum at the axis. However, in our case this interpretation does not apply. First, in our experiments the gas pressure does not exceed 10 μ Hg in Ar and Hg and a few microns in the other gases; therefore, the length of the free path of molecules in all cases was equal to or greater than the radius of the tube R. Under these conditions no considerable difference in the temperatures of the gas at the axis and at the walls could be established. Second, in the experiments with current pulses of a few microseconds duration the temperature of the gas could not increase by more than a hundred degrees or so*, as can be shown by a simple calculation. Thirdly (and this is the most important), at such low gas pressures (10^{-3} mm Hg) the rarefaction of the gas, inevitably originating at the place of the greatest heating, in this case only decreases the intensity of ionization by comparison with the neighboring, more dense reion of the gas, since the voltage of the longitudinal field E is everywhere equal and, therefore, here it will decrease and not increase the current density. Hence, the explanation of the contraction of the column, relating to the high pressure arc, does not apply here.

b) The idea about the gas focusing electron ray, through which the low pressure arc column is developed, put forward in Ref. 12, also does not apply here, since it cannot explain the prolonged stay of the column in a compressed state, when the current has already attained a maximum value; in addition, it does not explain the absence of compression at a lower current (200 amp) and the appearance of compression at the higher current (400 amp) (see Figs. 13 and 14).

c) On the other hand, the concept of the electrodynamic action of the self-magnetic field of the arc explains all of the main features of the observed phenomena. As was shown in a number of theoretical papers[2-5], the self-magnetic field sets up in the arc a radial pressure directed towards the axis and compresses the arc column. Its action should become noticeable in the time in which the motion of electrons becomes established, that is, $10^{-7} - 10^{-8}$ sec, and it should continue as

---

* Longitudinal bands of lower brightness are not associated with the processes in the arc, since they are noticeable also on the stationary photograph, but are, apparently, dependent on defects in the glass of the tube and in the slits.

* We will assume that the gas is heated as a result of the elastic collisions of electrons. The kinetic energy, transferred at each such collision, on the average is equal to $2(m_e/m_g)3/2kT_e$, the number of such collisions in the volume dV in time τ is $(\bar{c}_e/\lambda_e)n_e\tau dV$, and the energy transferred is $3(m_e/m_g)kT_e(\bar{c}_e/\lambda_e)n_e\tau dV$. If we neglect the heat exchange in the gas, then this value is equal to the increase in the internal energy of the gas, that is, $3/2n_g dVk\Delta T_g$. Assuming in $n_e = n_g$ (100% ionization), we find $\Delta T_g = 2(m_e/m_g)(\bar{c}_e/\lambda_e)\tau T_e$. If we take $m_e/m_g = 2.7 \times 10^{-6}$ (Hg), $T_e = 2.5 \times 10^5$ °C (according to some evaluations), $\bar{c}_e = 10^8$ cm/sec, $\lambda_e \sim 10$ cm, then even at $\tau = 10\,\mu$sec $\Delta T_g = 130°$ C. At lower τ, ΔT_g will be less.

[12] G.V. Spivak and E.L. Stoliarova, J. Tech. Phys. (U.S.S.R.) 20, 501 (1950).

long as the current is sufficiently high. This action should be the stronger, the higher the degree of the gas rarefaction and the higher the current; the one and the other actually take place. By a very rough approximation, currents of $10^2 - 10^3$ amp, which were used in these experiments, are sufficiently high for their magnetic field to change essentially the distribution of the carrier concentrations along the cross section of the tube. In fact, the radial component of the electric field in the column is on the average

$$\bar{E}_r \sim -\frac{d(\ln n)}{dr}\frac{D_e}{b_r} \sim \frac{kT_e}{e_0}\frac{\Delta n_e}{n_e}\frac{1}{R}$$

$$\sim 1\ \mathrm{V/cm} \sim 3\times 10^{-3}\ \mathrm{CGS}$$

The force of the magnetic field current is

$$vB/c_0 \sim 2i_a \cdot 10^8 / R \cdot 3\times 10^{10} \sim 10^{-3} i_a.$$

Hence, even when $i \sim 3$ abamp = 30 amp, it is comparable with the radial electric field; but when $i_a \sim 10^2 - 10^3$ amp, it exceeds the latter by many times.

Hypotheses a) and b) also do not explain the curvature of the column into a helix adhering to the walls of the tube. One cannot admit that the most intense heating of the gas by the current should originate along such a helix, or that along it should occur the initial breakdown of the gas. On the contrary, the electrodynamic theory explains easily also this aspect of the phenomenon as a manifestation of the fairly common property of current -- the instability of the linear form of the current with respect to the self-magnetic field.

Each deviation of the current from the strictly linear form gives rise to an electrodynamic force, increasing this deviation. According to a well known principle of electrodynamics, this change will proceed in the direction of increasing magnetic energy of the current [13], from here -- the tendency of the transition of the linear current into the helix form. For the manifestation of this it is necessary that the electrodynamic forces should exceed the elastic (in solid conductors) or the dissipative forces, counteracting the change in the form of the current. In the high pressure arc this phenomenon is well known [14]. Our experiments showed the presence of such a phenomenon also in the low pressure arc at high currents. Their results agree with the conclusions of the theoretical analysis on the stability of the arc plasma with respect to transverse perturbations [4]. They substantiate also the general conclusion [15, para 74] that at a large current the magnetic field is the main reservoir of the current energy in the gas and, therefore, the main factor determining its dynamics, by comparison with which the difference in the gas pressure begins to play a lesser role.

Regarding the rapid propagation of the arc along the cross section of the tube, the cause of this may be different -- not electrodynamic but gasodynamic. A certain small rarefaction of the gas as a result of its heating in the arc channel (above it was evaluated $< 100°$) leads to the fact that the ionization of the gas by electron collisions becomes more intense in the adjacent non-rarefied sections of the volume. It is here that the arc displaces from its previous heated channel.

According to this concept, the propagation of the arc should occur with a velocity of the order of the velocity of the motion of the gas molecules, that is, $10^4 - 10^5$ cm/sec. In that case, the average frequency of these displacements should be of the order of $c_g/R \sim 10^4 - 10^5$ cycles, and this was actually observed.

Certain details of the observed phenomena remain outside this picture; for example, the longitudinal non-uniformity of the luminescence, observed at the very low pressures and at high i_a. At present there is not enough data to formulate an opinion about these. One may only assume that here the forces of the electrostatic interaction between the charges in the plasma come into play, to which much attention has recently been paid [16].

5. CONCLUSIONS

1. Studies with the aid of a movable probe showed that the half-width of the arc column in a rarefied gas (Hg vapor) in a tube of radius R = 30-35 mm at $p \sim 1\ \mu$ Hg decreases by 30%,

---

[13] J.C. Maxwell, *Selected Works on the Theory of the Magnetic Field*, Moscow, 1952 (Russian Translation); V. F. Mitkevich, *Physical Basis of Electrotechniques*, Leningrad, 1933.

[14] L.A. Sirotinskii (editor), *High Voltage Techniques*, Part 1, State Energetics Press, Moscow, 1951, para. 11.

[15] V.L. Granovskii, *Electric Current in a Gas* 1, Moscow, 1952.

[16] A.A. Vlasov, J. Exptl. Theoret. Phys. (U.S.S.R.) 8, 291 (1938).

when the current increases up to ~ 170 amp. It was not possible by this method to observe any further compression of the arc upon increasing the current up to 2000 amp, owing to the origination of strong fluctuations in the performance of the arc.

2. Increasing the current above 10^2 in rarefied gases (Hg, Ar, Kr, H_2) gives rise to strong fluctuations in the parameters of the arc: first, in the probe current, then in the arc voltage and finally, in the arc current. The amplitude of these vibrations increases with an increase in i_a and a decrease in p. The frequency of these vibrations is of the order of 10^5 cycles; it increases with an increase in i_a and a decrease in R and in the molecular weight of the gas.

3. The oscillographic measurements of the currents on two identical, symmetrically located probes show that the above fluctuations may be explained as a result of the compression of the arc column into a narrow cord and of its irregular propagation along the cross section of the tube.

4. The compressed arc column at low pressures (a few microns Hg) may be observed visually and photographically in all the above-mentioned gases at short current pulses, in the time interval of which the arc had not succeeded in displacing ($\tau = 10^{-6}$ sec). The arc column was found to be compressed into a narrow cord, curved approximately into a helix, adhering to the walls of the tube.

5. For prolonged passage of current, the arc column, as is shown by the photo-resolution of the transverse cross section of the tube, remains compressed, but it propagates rapidly along the cross section of the tube.

6. The compression of the arc column into a narrow cord and its curvature into a helix can be explained by the electrodynamic action of the self-magnetic field of the arc.

7. Its propagation can be explained by the gasodynamic action of the arc channel -- rarefaction of the gas in the arc channel.

The authors wish to express their gratitude to V.I. Pugacheva for her assistance with all the experiments.

Translated by E. Rabkin
92

Letters to the Editor

On Alpha-decay Theory for Nonspherical Nuclei

V. M. STRUTINSKII

(Submitted to JETP editor July 24, 1955)
J. Exptl. Theoret. Phys. (U.S.S.R.) 30, 411-412 (February, 1956)

THE probability of excitation of the rotational states of a nucleus during α-decay of heavy nonspherical nuclei was calculated in the Refs. 1,2 in both of which the rotation of the nucleus was assumed to be slow compared to the motion of the α-particle (adiabatic approximation). The question whether this approximation is applicable was not really considered in either of the two works. In the case of even-even nuclei, where the moment of the total system is zero, it is possible to develop a theory which is not based on the adiabatic approximation.

The Schroedinger equation of the system α-particle + the deformed nucleus is

$$\left\{-\frac{\hbar^2}{2m}\Delta_{\mathbf{r}} + V(\mathbf{r}) + \frac{\hbar^2}{2J}\sum_{\varkappa=\xi,\eta}(I_\varkappa - l_\varkappa)^2\right\}\Psi_I(\Omega, \mathbf{r}) = \mathcal{E}\Psi_I(\Omega, \mathbf{r}). \quad (1)$$

where the independent variables are the angle coordinates of the residual nucleus and the coordinates of the α-particle relative to the residual nucleus (vector $\mathbf{r}$). The transformation of the Hamiltonian into new variables is most easily done by taking the corresponding classical problem into consideration. In Eq. (1), $V(\mathbf{r})$ is the interaction energy of the α-particle with the residual nucleus; $I_\varkappa$ and $l_\varkappa$ are the operators of the projection on the $\varkappa$th axis of the full moment of the system and the angular momentum of the α-particle (the axis of symmetry of the residual nucleus is chosen as the ζ axis); J is the moment of inertia of the residual nucleus about the ξ and η axis ($J_\zeta = 0$). The operators $I_\varkappa$ and $l_{\varkappa'}$ commute with each other, the operator $l_\varkappa$ acts only on the variable $\mathbf{r}$: $l_\xi = -i\hbar(\eta\partial/\partial\zeta - \zeta\partial/\partial\eta)$ etc. Taking into account that the result of the operator $l_\varkappa$ acting on the wave function of spin 0 vanishes we shall find the equation for $\Psi_{I=0}(r)$:

$$\{-(\hbar^2/2m)\Delta_{\mathbf{r}} + V(\mathbf{r}) + \hbar^2 l^2/2J\}\Psi_0 = \mathcal{E}\Psi_0 \quad (2)$$

(the operator l^2_ζ can be omitted as its eigenvalues vanish). Equation (2) does not contain the variables Ω; the wave function corresponding to spin 0 depends only on the relative coordinate of the α-particle. This result is fully understood, since the wave function of spin 0 should be invariant with respect to rotation of the coordinate system.

We shall develop the wave function $\Psi_0(\mathbf{r})$ in a series of Legendre polynomials:

$$\Psi_0(\mathbf{r}) = \sum_{l\,(\text{even})} \alpha_l G_l(r)\sqrt{2l+1}\,P_l(\cos\vartheta), \quad (3)$$

$$G_l(\infty) \sim r^{-1}\exp\{ik_l r\},$$

where ϑ is the angle between the direction of the vector $\mathbf{r}$ and the axis of symmetry of the nucleus. In the region outside the sphere of exit of the α-particle emerging from behind the barrier, the potential $V(\mathbf{r})$ practically does not differ from the Coulomb potential. In this region, the functions $G_l(\mathbf{r})$ fulfill the usual radial equation with energy $\mathcal{E}_l = \mathcal{E} - E_l$, where $E_l = \hbar^2 l(l+1)/2J$ is the energy of the rotational state of the daughter nucleus with spin $I' = l$, $k_l = \sqrt{2m\mathcal{E}_l}/\hbar$. We note that in the external region, at not too large l $[l \ll 2Ze^2/\hbar v(\infty)]$, one can neglect the dependence of radial function on l, so that the angular dependence of $\Psi_0(\mathbf{r})$ is the same on the surface of exit from behind the barrier and at infinity. The probability of formation of the daughter nucleus in a rotational state with spin $I' = l$ is proportional to $|\alpha_l|^{2*}$. Comparison with the observed intensity distribution in α-spectra of even-even nuclei with $A \geq 230$ (Ref. 3) gives the following values for the absolute values of the coefficients α_l:

$$|\alpha_0| = 1, \quad |\alpha_2|^2 \approx 0.33, \quad |\alpha_4|^2 \approx 0.003.$$

The case of $Re\,\alpha_2 > 0$ corresponds to an elongated nucleus (the absolute value of $\Psi_0(\mathbf{r})$ has a maximum for $\vartheta = 0$, π and consequently the predominant direction of emission of the α-particles coincides with the axis of symmetry of the nucleus); the case when the real part of $\alpha_2 < 0$ corresponds to a flattened nucleus ($|\Psi_0(\mathbf{r})|$ is greatest for $\vartheta = \pi/2$). Under the assumption that the coefficients α_l are real, it is possible to find, from the known absolute values, the width of the angular distribution of α-particles on the exit sphere from behind the barrier. The given values $|\alpha_l|$ yield for the width $|\Psi_0(\mathbf{r})|$ the values of 100° and 88° for the elongated and the flattened nucleus respectively. The difference of the angular distribution width for the

elongated and for the flattened nucleus is relatively small, and, as it will be shown below, is beyond the accuracy of the adiabatic theory. It is therefore impossible, on the basis of the adiabatic theory, to distinguish elongated and flattened nuclei from the observed intensity distribution, contrary to the claims maintained in Ref. 1.** In order to establish an actual relation between the angular distribution on the exit sphere (and consequently the intensity distribution in α-spectra) and between nuclear parameters, it is necessary to solve the Schroedinger equation (2) within the barrier region. We shall limit ourselves here only to the estimation of the nonadiabatic correction.

In the quasi-classical approximation, the Hamilton-Jacobi equation (4) corresponds to Eq. (2):

$$\frac{1}{2m}(\nabla S)^2 + \frac{1}{2J}\left(\frac{\partial S}{\partial \vartheta}\right)^2 = \mathscr{E} - V(\mathbf{r}), \qquad (4)$$

$$\Psi_0 = \exp\left\{\frac{i}{\hbar} S(\mathbf{r})\right\}.$$

The last term on the left-hand side we shall consider to be a small perturbation. Equation (4) (without the perturbation term) is the usual Hamilton-Jacobi equation of the adiabatic approximation. Let S_0 be the action function in the adiabatic approximation. Putting $S = S_0 + S'$, $|S'| \ll |S_0|$, we get the following equation for S'

$$\mathbf{v}_0 \nabla S' + (1/2J)(\partial S_0/\partial \vartheta)^2 = 0, \text{ where } \mathbf{v}_0 = m^{-1}\nabla S_0 \qquad (5)$$

with the boundary condition $S' = 0$ on the surface Σ of the nucleus. The solution of Eq. (5) fulfilling the boundary condition is

$$S' = i\int_{\mathbf{r}_0}^{\bar{\mathbf{r}}} \frac{1}{v_0}\frac{1}{2J}\left(\frac{\partial S_0}{\partial \vartheta}\right)^2 d\lambda. \qquad (6)$$

The path of integration is taken along the imperturbed trajectory, starting from the point $\mathbf{r}_0$ on the surface Σ. In the order of magnitude this integral equals $(L/\bar{v}_0)(\hbar^2\bar{l}^2/2J)$; the term added in the exponent in Eq. (4) is of the order of $\omega_0 T\bar{l}^2$, where L is the length of the path of the α-particle within the barrier, $T = L/\bar{v}_0$, $\omega_0 = \hbar/2J$, and $\bar{l}$ is the mean orbital moment of the α-particle within the barrier. In order to make the correction more exact, we have to consider the actual action function. As an example, we shall take the case of the elongated nucleus. For a sufficiently large deformation of the nucleus it is essential to assume the existence of small angles, for which the action function can be written

$$S_0 \approx -i\hbar(a(r) - b(r)\vartheta^2), \quad b > 0. \qquad (7)$$

The correction to the exponent, calculated for such an action function, amounts to $(i/\hbar)S' = 4\omega_0 T b^2 \vartheta^2$. As was to be expected, the fact that the rotation is not adiabatic broadens the angular distribution of α-particles; $b_{\text{eff}} = b - 4\omega_0 T b^{-2}$. The probabilities of transition into higher rotational levels decrease correspondingly. The non-adiabatic correction may be very essential. Thus, for $L = 3 \times 10^{-12}$ cm, $\hbar^2/2J \approx 7$ kev and the adiabatic value of $b \sim 5$, the correction is only slightly smaller than the main effect. The large value of the width of the angular distribution, found from the intensity distribution in α-spectra, is explained by the fact that the rotation is not adiabatic.

Remark added during proof: We have, together with G. A. Pik-Pichak, calculated the effective angle of emission ϑ^* of α-particles (of the angular width $|\varphi_0(\bar{\rho})|$) by numerical integration of the Eq. (4) for small angles of emission in elongated nuclei. If the deformation is not too small, ϑ^* does not depend to a great extent on it. Thus, for the case of the α-decay of U^{234}, ϑ^* changes from 65° for $a/b = 2.4$ to 80° for $a/b = 1.24$. These values are close to the "experimental" value (~ 100°). This weak dependence on the deformation of the nucleus may possibly explain the fact that the intensity distribution of the fine structure lines connected with the rotational levels is almost constant for all nuclides which are not very close to the doubly magic Pb^{208}.

* With an accuracy to terms of the order of E_l/ξ In addition, we neglect a small imaginary increment to the energy of the system.

** A straightforward answer to the question of the sign of the deformation (the sign of the quadrupole moment) can be obtained from the study of the $\alpha - \gamma$ angular correlation[4].

[1] V. G. Nosov, Dokl. Akad. Nauk SSSR **103**, 65 (1955).

[2] A. Bohr, B. Mottelson and P. Froman, Dan. Mat. Fys. Medd. **29**, 10 (1955).

[3] I. Perlman and F. Asaro, Ann. Rev. Nucl. Sci. **4**, 1954.

[4] V. M. Strutinskii. Dokl. Akad. Nauk SSSR **104**, 524 (1955).

Translated by H. Kasha,
73

Concerning Rayski's Bilocal Field Theory

V. A. ZHIRNOV
P. N. Lebedev Physical Institute
Academy of Sciences, USSR

(Submitted to JETP editor, December 2, 1955)
J. Exptl. Theoret. Phys. (U.S.S.R.) 30, 425-426
(February, 1956)

Wave equations for a Ψ-function depending on x_i and u_i are investigated in some of Rayski's papers[1,2] in a way similar to that used by Ginzburg and Tamm [3] and by Yukawa.[4] Ginzburg and Silin[5] have already made some critical notes to Ref. 2, showing in particular the incompatibility of Eqs. (22') and (22'') of that paper, as well as some other shortcomings.

The system of equations

$$L_1\Psi \equiv \left(\frac{\partial^2}{\partial x_i \partial x_i} - \varkappa^2 - 4c\left[-\frac{\partial^2}{\partial u_i \partial u_i} + \frac{1}{u_i u_i}\left\{\lambda^4\left(\frac{\partial^2}{\partial x_i \partial u_i}\right)^2 + \left(u_i\frac{\partial}{\partial u_i}\right)^2 + 2u_i\frac{\partial}{\partial u_i}\right\}\right]\right)\Psi(x_i, u_i) = 0, \tag{1}$$

$$L_2\Psi \equiv u_i\frac{\partial}{\partial x_i}\Psi(x_i, u_i) = 0,$$

$$L_3\Psi \equiv \left(\lambda^2\frac{\partial^2}{\partial x_i \partial x_i} - \lambda^{-2}u_i u_i\right)\Psi(x_i, u_i) = 0,$$

proposed in some new papers[6] is a compatible one, as L_1, L_2, and L_3 commute with each other.

However even this new system has some shortcomings. The mass spectrum derived from (1)

$$m_0^2 = \frac{\varkappa^2}{2} \pm \sqrt{\frac{\varkappa^4}{4} + \frac{4c}{\lambda^4}l(l+1)}, \tag{2}$$

$$l = 0, 1, 2, \ldots$$

not only contains imaginary masses $m_0^2 < 0$, which must be thrown out because of the condition of boundedness of the solution $\Psi \sim e^{\pm|m_0|t}$ in 4-space (see Ref. 5), but also gives the value $m_0 = 0$, in contradiction to the recipe for finding the mass spectrum (going to the center-of-mass system). Furthermore, interaction with a field cannot be introduced into the system (1) in the usual simple way, and presents an additional problem. In addition to this, we shall show that the system (1), as well as the analogous set in Ref. 5, contains solutions with spacelike momenta, corresponding to signal velocities faster than light. To do this, let us go to the system of reference where $E = 0$, $p_1 = p_2 = 0$, $p_3 \neq 0$, and let us introduce generalized spherical coordinates in u_i-space:

$$u_i = u\cosh\chi\sin\theta\cos\varphi, \quad u_3 = u\cosh\chi\cos\theta, \quad 0 < u < \infty, \quad 0 \leqslant \theta \leqslant \pi,$$
$$u_2 = u\cosh\chi\sin\theta\sin\varphi, \quad u_4 = iu\sinh\chi, \quad -\infty < \chi < \infty, \quad 0 \leqslant \varphi \leqslant 2\pi. \tag{3}$$

Then from Eqs. (1) we get

$$\left[p_3^4 + \varkappa^2 p_3^2 - \frac{4c}{\lambda^4}\left(\frac{1}{\cosh\chi}\frac{\partial}{\partial\chi}\left(\cosh\chi\frac{\partial}{\partial\chi}\right) - \frac{1}{\cosh^2\chi}\frac{\partial^2}{\partial\varphi^2}\right)\right]\Psi(x_i, u_i) = 0. \tag{4}$$

Separating the variables, $\Psi(x, u) = \Psi(x)R(\chi)Y(\varphi)$, we find

$$\left(p_3^4 + \varkappa^2 p_3^2 - \frac{4c}{\lambda^4}\mu\right)\Psi(x) = 0, \tag{5}$$

$$\frac{\partial^2}{\partial\varphi^2}Y(\varphi) = -\lambda^2 Y(\varphi).$$

$$\left(\frac{\partial^2}{\partial\chi^2} + \frac{\sinh\chi}{\cosh\chi}\frac{\partial}{\partial\chi} + \frac{\lambda^2}{\cosh^2\chi} - \mu\right)R(\chi) = 0.$$

By putting $v = R\cosh^{\lambda}\chi$, $y = \sinh\chi$, the last equation of (5) becomes

$$(1+y^2)\frac{d^2v}{dy^2} - 2(\lambda-1)y\frac{dv}{dy} + (\lambda^2 - \lambda - \mu)v = 0. \tag{6}$$

If we try to solve Eq. (6) by a finite sum

$v = \sum_{n=0}^{n_{\max}} a_n y^n$, we get the eigenvalues $\mu = l(l+1)$, $l = 0, 1, 2, \ldots$. Then from the first of equations (5) we can find the spectrum of eigenvalues of the momentum:

$$p_3^2 = -\frac{\varkappa^2}{2} \pm \sqrt{\frac{\varkappa^4}{4} + \frac{4c}{\lambda^4} l(l+1)}, \qquad (7)$$

$$l = 0, 1, 2, \ldots$$

It is clear from (7) that for $E = 0$ we can have $p_3^2 > 0$, i. e., there is a system of reference where $E^2 = p^2 - a^2$ for real E, p, and a, and $v = \partial E/\partial p = p(p^2 - a^2)^{-1/2} \geq 1$. Insofar as solutions with velocity greater than that of light can not be eliminated by the condition of finiteness, it is clear that equations (1), as they have physically unallowable solutions, cannot be considered satisfactory.

In conclusion, I express my thanks to Professor V. L. Ginzburg for valuable advice.

[1] J. Rayski, Proc. Phys. Soc. (London) 64, 957 (1951); Acta. Phys. Pol. 11, 109 (1951).

[2] J. Rayski, Nuovo Cimento 10, 1729 (1953).

[3] V. L. Ginzburg and I. E. Tamm, J. Exptl. Theoret. Phys. (U.S.S.R.) 17, 227 (1947).

[4] H. Yukawa, Phys. Rev. 77, 219 (1950); 91, 415, 416 (1953).

[5] V. L. Ginzburg and V. P. Silin, J. Exptl. Theoret. Phys. (U.S.S.R.) 27, 116 (1954).

[6] J. Rayski, Fortsh. Physik 2, 165 (1954); Acta Phys. Pol. 14, 107 (1955); Nuovo Cimento 2, 255 (1955).

Translated by E. J. Saletan
81

The Leading Role of the Vibration Properties of Plasma and the Effect of the Gas Atoms on these Properties

I. P. Bazarov
Moscow State University

(Submitted to JETP editor, February 21, 1955)
J. Exptl. Theoret. Phys. (U.S.S.R.) 30, 426
(February, 1956)

In Eq. (5) of our earlier work[1], the second term of the right-hand member should have a plus sign, and not a minus sign. The necessity for this can be easily recognized if one compares the particular case of Eq. (5) in the form of Eq. (10) with Eq. (2) which is identical to (10) and in which the sign of the second term is indicated properly; the identity of (2) and (10) are indicated in Ref. 1. The incorrectness of the sign is noted in Ref. 2, although it does not change all the Eqs. (7) – (10) which follow, or the conclusions drawn from them. The basic result of the work – the prediction of the existence of anodic strata under several conditions of charge ($I_1 < 0$) – does not depend on the sign of the second term of Eq. (5) (only the numerical value of the period d can depend on this sign), and this result was actually confirmed by experiment, as was indicated in Ref. 1. This results in the fact that, although in the developed theory of strata [1,3] the effect of the atoms of gas on the vibration of the plasma is not taken into consideration (for which reason, in part, we obtain only qualitative agreement of theory with experiment in certain cases), this theory correctly indicates, however, the leading role of the vibration properties of the plasma under certain conditions of gaseous discharge – the collective interaction between charged particles.

Calculation of the effect of atoms of the gas on the behavior of the plasma is important and necessary; however the means, borrowed from a number of other research papers, by which this calculation is carried out in Ref. 2 is unsatisfactory, since the approximation employed in Ref. 2 in the kinetic equation of the Boltzmann term for collision expressed by $-(f - f_0)/\tau = -f_1/\tau$ demands, within the frame of reference of linear approximation, the disappearance of the integral $\int f_1 d\mathbf{v}$, while in the other equation of the solved system this integral, with the same approximation, must not be equal to zero. For this reason, Ref. 2 bears a solely computational character, with no knowledge as to what sort of approximation it has with relation to a real plasma, since the solved system of equations suffers from internal contradictions.

I take advantage of this opportunity to point out that in Ref. 1, Eq. (4), the term $4\pi\rho$ must have a minus sign (and not a plus sign, as printed) and paragraph 4 should be paragraph 3. These errors bear no relationship to the correctness of the work within the frame of reference of the initial approximations.

[1] P. Bazarov, J. Exptl. Theoret. Phys. (U.S.S.R.) 21, 711 (1951).

[2] A. A. Luchina, J. Exptl. Theoret. Phys. (U.S.S.R.) 28, 18 (1955); Soviet Phys. JETP 1, 12 (1955).

[3] A. A. Vlasov, *The theory of many particles*, Gostekhizdat, 1950.

Translated by A. Certner
82

Asymptotic Meson-Meson Scattering Theory

I. T. DIATLOV AND K. A. TER-MARTIROSIAN
Leningrad Physico-Technical Institute,
Academy of Sciences, USSR

(Submitted to JETP editor October 8, 1955)
J. Exptl. Theoret. Phys. (U.S.S.R.) 30, 416-419
(February, 1956)

WHEN the method of the asymptotic theory[1,2] is applied to meson-meson scattering, a difficulty arises in that there is an infinite number of complex diagrams with four entering meson lines, each of which makes a contribution of the same order as the simplest diagrams shown in Fig. 1. The complex diagrams are "reducible" to one of the diagrams in Fig. 1, i.e., to diagrams which consist only of squares, connected by meson lines, which go over into one of the diagrams in Fig. 1 if, succesively, two squares of the complex diagram, connected by two meson lines, are substituted by one (for instance, the diagrams in Fig. 2 are "reducible" and those in Fig. 3 are "irreducible"). To any "reducible" diagram there corresponds a logarithmically divergent quantity of the order of g_0^2 and of the type $(g_0^2/4\pi i) R_n [g_0^2 (L - \xi)]$, where g_0 is the initiating charge, R_h = real numerical function, $L = \lg(\Lambda^2/m^2)$, $\xi = \lg(-k^2/m^2)$, k = momentum, intrinsic in the problem, Λ = cut off limit of the momentum[1].

"Irreducible" diagrams need not be considered since their contribution is very small – of higher order in g_0^2. In such a way the scattering amplitude $(g_0^2/4\pi i) P(k_1k_2k_3k_4)$ (k_i is the meson momentum) is determined by the infinite sum $P(k_1k_2k_3k_4) = \Sigma_n R_n(k_1k_2k_3k_4)$ extended over all "reducible" diagrams.

We considered the problem of the calculation of this sum (the so-called "parquet" problem), and discovered it was possible to construct an integral equation which determined P through the quantity R_0, corresponding to the contribution due to the simplest diagrams in Fig. 1. This possibility is connected with the fact that any complex "reducible" diagram consists of two parts, to each of which approach two external meson lines and which are connected with each other only by two meson lines. The latter becomes obvious if one considers that when one makes a "reduction" of the complex diagram, one can always reduce it to the form of Fig. 4 a, b, or c. If $F(k_1k_2, k_3k_4)$ is the sum of the contributions from all "reducible" diagrams, which are "reduced" to Fig. 4, a, and, similarly, $F(k_1k_3, k_2k_4)$ and $F(k_1k_4, k_2k_3)$ for the diagrams reduced to Figs. 4 b and c, then

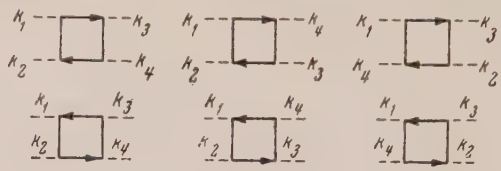

FIG. 1

it is clear that

$$P(k_1k_2k_3k_1) = R_0(k_1k_2k_3k_4) + F(k_1k_3, k_2k_4) + F(k_1k_4, k_2k_3) + F(k_1k_2, k_3k_4), \tag{1}$$

(note that P and R_0 are symmetric with respect to the arbitrary permutation k_i and $F(k_1k_2, k_3k_4)$ will not change by the mutual interchange of k_1 and k_2 or k_3 and k_4; nor by the substitution of k_1, k_2 by k_3, k_4.

One can obtain the following relation for the quantity $F(k_1k_2k_3k_4)$ (similar to the procedure for obtaining the equation for the Green's functions D, G, or Bethe-Salpeter's equation)

$$F(k_1k_2, k_3k_4) = -\frac{g_0^2}{2\pi i}\int [R_0(k_1k_2ll') + F(k_1l, k_2l') + F(k_1l', k_2l)]\, D(l)\, D(l')\, P(-l-l'k_3k_4)\, d^4l, \tag{2}$$

where $-l' = l + k_1 + k_2$, $k_1 + k_2 + k_3 + k_4 = 0$. Obviously, (1) and (2) represent a closed system of equations, with the help of which one can calculate F and P, if R_0 is known.

For large momenta the sum of the contributions, R_0, from the diagrams in Fig. 1, depends only on the biggest of the four momenta k: $R_0 = \rho_0(\alpha)\,\delta_c$, where $\alpha = [1 + (5 g_0^2/4\pi)(L - \xi)]^{3/5}$, while $\rho_0 = {}^{16}/_3(\alpha - 1)$,

and $\delta_c = \delta_{\tau_1\tau_2}\delta_{\tau_3\tau_4} + \delta_{\tau_1\tau_3}\delta_{\tau_2\tau_4} + \delta_{\tau_1\tau_4}\delta_{\tau_2\tau_3}$

depend on the subscripts τ_i $(i = 1, 2, 3, 4)$ of the isotopic spin (for calculation, Green's functions which were found in Ref. 2 are used).

For large momenta the scattering amplitude P also depends on only one quantity α. However, when any two of the four momenta, for instance k_1 and k_2, are very big but are almost opposite in direction so that their sum $k_1 + k_2 = -(k_3 + k_4)$

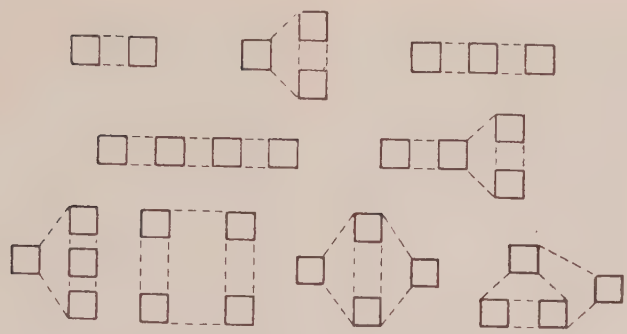

FIG. 2

is much smaller than each of them, a special case arises. (This case is essential in (2), since the integral with respect to l in (2) is logarithmically divergent, and only very big $l \approx -l'$ are of importance).

If k_3 and k_4 are the quantities of the same order as $k_3 + k_4 = -(k_1 + k_2)$, then, in this case, P depends not only on α (which corresponds to the

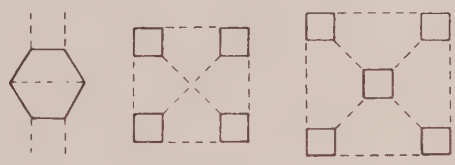

FIG. 3

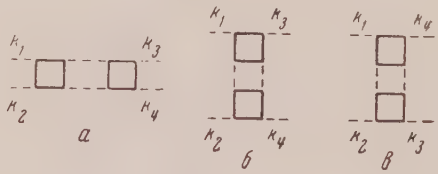

FIG. 4

quantities $-k_1^2$ or $-k_2^2$), but also on

$$\beta = [1 + (5 g_0^2 / 4\pi)\ (L - \eta)]^{2/5},$$

$$\eta = \lg [-(k_1 + k_2)^2 / m^2] = \lg [-(k_3 + k_4)^2 / m^2],$$

while

$$P(k_1 k_2 k_3 k_4) = P_c(\alpha\beta)\, \delta_c + P_{12}(\alpha\beta)\, \delta_{\tau_1\tau_2}\, \delta_{\tau_3\tau_4}.$$

If $\beta \to \alpha$, i e., if all four momenta are of the same order of magnitude, then P_{12} vanishes. Denoting $P_c(\alpha, \alpha) = P(\alpha)$, we will have in this case

$$P(k_1 k_2 k_3 k_4) = P(\alpha)\, \delta_c.$$

The limiting values of the function P_c and P_{12} can be found with the help of the system (1), (2). They have the following form:

$$P_c(\alpha,\beta) = \begin{cases} \dfrac{16}{3}(\alpha - 1)\left\{1 - \dfrac{88}{27}(\alpha - 1)^2 - \dfrac{8}{3}[(\beta - 1)^2 - (\alpha - 1)^2] + \ldots\right\}, & \beta - 1 < 1 \\ \dfrac{16}{11}\alpha\left[1 + \dfrac{5}{3}(\alpha^{40/33}\beta^{-40/33} - \alpha^{8/13}\beta^{-16/33})\right], & \alpha > 1 \end{cases} \tag{3}$$

$$P_{12}(\alpha, \beta) = \begin{cases} -\dfrac{5}{12}\left(\dfrac{16}{3}\right)^2(\alpha - 1)\{[(\beta - 1)^2 - (\alpha - 1)^2] + \ldots\}, & \beta - 1 < 1 \\ \dfrac{16}{11}\alpha(\alpha^{16/33}\beta^{-16/33} - 1), & \alpha > 1 \end{cases}$$

$$P_c(\alpha, \alpha) = P(\alpha) = \begin{cases} \dfrac{16}{3}(\alpha - 1)\left[1 - \dfrac{88}{27}(\alpha - 1)^2 - \ldots\right], & \beta - 1 < 1 \\ \dfrac{16}{11}\alpha, & \alpha > 1 \end{cases}$$

In the region $\alpha \sim 1$ or $\beta \sim 1$ the functions P_c and P_{12} can be found only by the numerical integration of the system of asymptotic equations, which follow from (1) and (2).

V. V. Sudakov succeeded in obtaining a simple equation directly for $P(\alpha)$ and in completely constructing this function. The solution found by him,

$$P(\alpha) = \frac{16}{11}\,\alpha\,\frac{1-\alpha^{-19/3}}{1+{}^{5}/_{11}\,\alpha^{-19/3}} \qquad (4)$$

for the cases $\alpha - 1 < 1$ and $\alpha > 1$ is identical with (3).

It follows from (3) or (4) that the entire sum $P(\alpha)$ is a quantity of the same magnitude as the contribution $\rho_0(\alpha)$ from the simplest diagrams in Fig. 1 (for $\alpha > 1$, $P(\alpha)$ differs from $\rho_0(\alpha)$ only by the factor 11/3).

The latter is of importance for the conclusion[4] of the pseudo-scalar theory that the meson charge of a nucleon is zero, since this conclusion is based on the results of the theory[2], in which (in the equation for the operator of the peak part) the diagram of Fig. 5 and also the infinite set of analogous diagrams obtained from Fig. 5 by sub-

FIG. 5

stitution of a square for any "reducible" diagram was not considered. Since $P(\alpha)$ and $\rho_0(\alpha)$ are quantities of the same order, the contribution of the infinite set of all diagrams of the type in Fig. 5 is a quantity of the same magnitude as that from the one diagram in Fig. 5, i.e., they can be neglected, (the contribution from the diagram in Fig. 5 is a quantity of the order of g_0^2 in comparison with the terms taken into consideration in Ref. 2).

The authors express their thanks to V. V. Sudakov for important remarks and to I. Ia. Pomeranchuk who stimulated interest in the above problem.

* Here the case when $g_0^2 \ll 1$ and $L \gg 1$ is considered, so that $g_0^2 L$ is an arbitrary quantity. When two cut off limits are introduced[3] the quantity $\tilde{g}_0^2 = g_0^2\left[1 + \frac{g_0^2}{\pi}(L_p - L_k)\right]^{-1}$ enters everywhere instead of g_0^2; $\tilde{g}_0^2$ is small for an arbitrary g_0^2 if $\frac{1}{\pi}(L_p - L_k) = \frac{1}{\pi}\lg\frac{\Lambda_p^2}{\Lambda_k^2}$ is sufficiently large.

[1] L. D. Landau, A. A. Abrikosov and I. M. Khalatnikov, Dokl. Akad. Nauk SSSR **95**, 497, 773, 1177 (1954).

[2] A. A. Abrikosov, A. D. Galanin and I. M. Khalatnikov **97**, 793 (1954).

[3] A. A. Abrikosov and I. M. Khalatnikov, **103**, 993 (1955).

[4] I. Ia. Pomeranchuk, **103**, 1005 (1955).

Translated by M. Polonsky
76

Relativistic Deuteron Disintegration in the Electric Field of the Nucleus

L. N. ROSENTSVEIG AND A. G. SITENKO
Physico-Technical Institute, Academy of Sciences, Ukrainian SSR

(Submitted to JETP editor, December 8, 1955)
J. Exptl. Theoret. Phys. (U.S.S.R.) 30, 427-428 (February, 1956)

THE disintegration of deuterons with energy of the order of 200 mev in the electric field of the nucleus was investigated by Dancoff[1] in the non-relativistic approximation. In the present communication the problem is solved, taking into account relativistic effects. It will be shown below that the relativistic corrections to the cross section for "electric" disintegration $\sigma_{1\to 1}$, found in Ref. 1, are small if $v^2 \sim 0.2$ ($E_d \sim 200$ mev)*, but are important if $v^2 \sim 1$, and that the "magnetic" disintegration investigated in Ref. 1, in which the proton-neutron system undergoes transition from the triplet to the singlet state, does not take place; the corresponding cross-section $\sigma_{1\to 0}$ is of an order of magnitude smaller than $\sigma_{1\to 1}$ in the extremely relativistic case.

As in Ref. 1, we shall make the following approximations: a) the motion of the center of mass of the proton-neutron system in the field of the nucleus is investigated in the Born approximation, which is permissible for $Z/137v \ll 1$; b) $n-p$ forces are assumed central with a zero radius of action; c) the nuclear electric field is "cut off" at $r = R_0$, the sum of the radii of the nucleus and the deuteron**; d) the deuteron radius R_d is considered small in comparison with R_0.

In the system of reference K in which the deuteron is at rest before the collision, the potentials of the field of the nucleus Ze, which has a velocity v in the z-direction, are

$$\varphi = Ze/R, \qquad A_x = A_y = 0, \qquad (1)$$
$$A_z = vZe/R,$$

$$R = R(\mathbf{r}, t) = [(1 - v^2)\rho^2 + (z - vt)^2]^{1/2}, \qquad (2)$$
$$\rho^2 = x^2 + y^2.$$

The perturbed Hamiltonian of the deuteron in the nuclear field is given by

$$V = e\varphi_p + \frac{ie}{M}(\nabla_p \mathbf{A}_p + \mathbf{A}_p \nabla_p) \qquad (3)$$
$$+ \frac{e^2}{2M}\mathbf{A}_p^2 - \mu_{\text{ядр}}(\mu_p \vec{\sigma}_p \mathbf{H}_p + \mu_n \vec{\sigma}_n \mathbf{H}_n)$$
$$\approx \frac{Ze^2}{R_p} + v\frac{Ze^2}{2M}\left\{\frac{2i}{R_p}\frac{\partial}{\partial z_p}\right.$$
$$- \frac{i}{R_p^3}(z_p - vt) - (1 - v^2)\mu_p[\mathbf{r}_p \vec{\sigma}_p]_z \frac{1}{R_p^3}$$
$$\left. - (1 - v^2)\mu_n[\mathbf{r}_n \vec{\sigma}_n]_z \frac{1}{R_n^3}\right\}$$

[in the Born approximation we drop the term $(e^2/2M)\mathbf{A}_p^2$], where M is the mass of the nucleon.

In the expressions for the wave functions of the initial and final states of the unperturbed system

$$\Psi_i = L^{-3/2}\psi_d(r)\chi_1^{m_0} e^{-iE_0 t} \quad (m_0 = -1, 0, 1), \qquad (4)$$

$$\Psi_f = L^{-3/2}\exp\{i\mathbf{q}\mathbf{r}_d\}\,\psi_{kS}^{(-)}(\mathbf{r})\,\chi_S^m e^{-iEt} \qquad (5)$$
$$\times (S = 0, 1; -S \leqslant m \leqslant S)$$

the basic states of the deuteron and the states of the continuous spectrum of the $n - p$ system which contain the scattered wave for $r \to \infty$ can (in the light of approximation b) be written in the form

$$\psi_d(r) = \sqrt{\alpha_1/2\pi}\, e^{-\alpha_1 r}/r, \qquad (6)$$

$$\psi_{kS}^{(-)}(\mathbf{r}) = \frac{1}{L^{3/2}}\left(e^{i\mathbf{k}\mathbf{r}} - \frac{1}{\alpha_S - ik}\frac{e^{-ikr}}{r}\right) \qquad (7)$$
$$(S = 0, 1).$$

We note that the orthogonality condition

$\int \psi_d(r)\psi_{k1}^{(-)}(\mathbf{r})\,d^3r = 0$ is satisfied only for $S = 1$.

For the transition that interests us, the probability amplitude is given by

$$a_{i\to f} = -i\int_{-\infty}^{\infty}(f|V(t)|i)\,e^{i\omega t}dt, \quad \omega = E - E_0. \qquad (8)$$

Introducing Eq. (3), we get, after some obvious transformations,

$$\frac{iL^3}{Ze^2}a_{i\to f} = \delta_{S1}\delta_{mm_0}A_0\left[\left(1 - \frac{vq_z}{2M}\right)B_{\mathbf{q}1} + i\frac{v}{M}C\right] \qquad (9)$$
$$- v(1 - v^2)\frac{A_1}{2M}\Big[\delta_{S1}(\mu_p B_{\mathbf{q}1} + \mu_n B_{-\mathbf{q}1})(\chi_1^m, [\mathbf{q}\mathbf{S}]_z \chi_1^{m_0})$$
$$+ \delta_{S0}\delta_{m0}(\mu_p B_{-\mathbf{q}0} - \mu_n B_{-\mathbf{q}0})\left(\chi_0^0, \left[\mathbf{q}, \frac{1}{2}(\vec{\sigma}_p - \vec{\sigma}_n)\right]_z \chi_1^{m_0}\right)\Big]$$

Here,

$$A_0 = \int d^3r e^{-i\mathbf{q}\mathbf{r}}\int_{-\infty}^{\infty}\frac{e^{i\omega t}dt}{R(\mathbf{r}, t)} \qquad (10)$$
$$= \frac{4\pi}{vq^2(1 - v^2\cos^2\alpha)}\,\frac{2\sin[(q\cos\alpha - \omega/v)L/2]}{q\cos\alpha - \omega/v},$$

$$A_1\mathbf{q} = \int d^3r\vec{\rho}e^{-i\mathbf{q}\mathbf{r}}\int_{-\infty}^{\infty}\frac{e^{i\omega t}dt}{R^3(\mathbf{r}; t)} = -\frac{i\,\mathbf{q}}{1 - v^2}A_0, \qquad (11)$$

$$B_{\mathbf{q}S} = \int d^3r\psi_{kS}^{(-)*}(\mathbf{r})\,\psi_d(r)\,e^{i\mathbf{q}\mathbf{r}/2}, \qquad (12)$$

$$C = \int d^3r\psi_{k1}^{(-)*}(\mathbf{r})\frac{\partial\psi_d(r)}{\partial z}e^{i\mathbf{q}\mathbf{r}/2},$$

where α is the angle between the z-axis and the vector $\mathbf{q}$. (Equations (10) and (11) are derived on the assumption that $L \to \infty$.)

Because of the "cut-off" of the electric field for $r = R_0$, the upper bound for the momentum q is

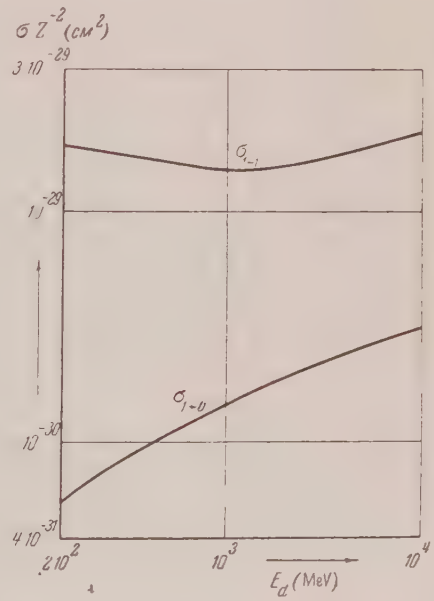

$q \lesssim q_{max} \sim 1/R_0$; condition d) gives $q_{max}/\alpha_1 \ll 1$, i.e., the coefficient of $e^{i\mathbf{q}\cdot\mathbf{r}/2}$ in the integrands of Eqs. (12) can be replaced by the first terms of the series expansion $1 + (1/2)i\mathbf{q}\cdot\mathbf{r}$. In view of the orthogonality of the functions $\psi_{k1}^{(-)}$

and ψ_d, the basic term in the integral B_{q1} is introduced by the second term of the expansion, and in B_{q0} and C by the first term.

In Eq. (9) we will keep only the basic terms, neglecting the part containing the matrix element of the operator $[qxS]_z$ and the quantity $-vq_z/2M$ in the parentheses. It is not hard to see that the terms we have here dropped give small corrections, whose calculation would hardly make sense, since we have made the approximations a) – d).

We now go over from a consideration of the probability amplitude to the cross section, sum over S and m, average over m_0, and integrate over d^3q as was done in Ref. 1. Let us write

$$\varepsilon = k^2/M, \quad \varepsilon_S = \alpha_S^2/M, \quad 1/\Gamma = v^{-1}(\varepsilon + \varepsilon_1)R_0 \leqslant 1.$$

Integration over the angle ϑ gives the distribution over ε $(0 \leqslant \varepsilon \leqslant \varepsilon_{max} = v/R_0 - \varepsilon_1)$

$$\sigma_{1\to 1}(\varepsilon)\,d\varepsilon = \frac{8}{3}\left(\frac{Z}{137v}\right)^2 \frac{\sqrt{\varepsilon_1\varepsilon^3}\,d\varepsilon}{M(\varepsilon+\varepsilon_1)^4} \times\left[\ln\frac{\Gamma^2 - v^2}{1-v^2} - v^2\frac{\Gamma^2-1}{\Gamma^2-v^2}\right], \tag{13}$$

$$\sigma_{1\to 0}(\varepsilon)\,d\varepsilon = \frac{2}{3}\left(\frac{Z}{137}\right)^2(\mu_p-\mu_n)^2 \times \frac{\sqrt{\varepsilon_1\varepsilon}(\sqrt{\varepsilon_1}+\sqrt{\varepsilon_0})^2\,d\varepsilon}{M^2(\varepsilon+\varepsilon_0)(\varepsilon+\varepsilon_1)^2}\left[\ln\frac{\Gamma^2-v^2}{1-v^2} - \frac{\Gamma^2-1}{\Gamma^2-v^2}\right]. \tag{14}$$

Equation (13) goes over into Dancoff's equation[1] if the expression in square brackets is designated by $\ln\Gamma^2$.

Integration over ϵ is carried out numerically. The figure shows the variation of the integral cross sections $\sigma_{1\to 1}$ and $\sigma_{1\to 0}$ in the energy interval $E_d = 0.2 - 10$ bev for $R_0 = 1.1 \times 10^{-13}$cm.

The authors thank Z. V. Rumiantseva, who carried out the numerical integration.

*We are employing a system of units in which $c=\hbar=1$.

**It can be shown that in this way the diffraction disintegration of the deuteron, which is not connected with the electric field close to the nucleus (see Ref. 2), is eliminated from the consideration; the whole cross section for disintegration is given by the sum $\sigma_{dif}+\sigma_{el}$, and the interference term is absent in the approximations a) – d).

[1]S. Dancoff, Phys. Rev. 72, 1017 (1947).

[2]A. I. Akhiezer and A. G. Sitenko, Dokl. Akad. Nauk SSSR 107, 3 (1956).

Translated by E. J. Saletan
83

On the Paper by N. I. Steinbok "Basic Characteristics of Ionization Chambers"

K. K. AGLINTSEV

(Submitted to JETP editor February 14, 1955)
J. Exptl. Theoret. Phys. (U.S.S.R.)
30, 429 (February, 1956)

IN the paper by N. I. Steinbok[1], it is asserted that the solution of the equation of the volt-amperecharacteristics of ionization chambers obtained by him are more rigorous and complete than those previously described in the literature (see, for example, Refs. 2, 3). This conclusion is obtained on the basis of the supposition that, if the ionization is relatively weak, it is possible to ignore the space charge ; however, no basis for the justification of this supposition is advanced in this paper and the error arising out of this supposition is not evaluated. What is more, it is possible to demonstrate that even where weak ionization exists, the part played by space charge in ionization chambers is quite significant, and therefore the conclusions drawn in Ref. 1 are in error.

Let us examine the problem of the variation in intensity of the electrical field between the anode and the cathode in a flat, air-type ionization chamber. Let us designate by h the distance between the anode and cathode and draw an axis x perpendicular to their surface. Seeliger[4] demonstrated that the value of the intensity of field E in the space between the anode and the cathode is completely determined by the numerical value of the ratio i/I_0, where I_0 is the strength of the saturation current and i is the strength of the current in the absence of saturation; upon variation of the strength of ionization and of the magnitude of I_0, only the absolute value of E changes at all points in the field. In the following table the values of E are given in relative units for various values of i/I_0 for cross sections of the chamber at various distances from the anode $x = 0$, $0.33h$, $0.42h$, $0.67h$, and h.

From this table and Seeliger's graph (Ref. 4, p. 348, Fig. 3; see also Ref. 3, Fig. 82) it can be seen that even in the vicinity of the zone of saturation $i/I_0 = 0.949$ the minimum value of intensity of the electrical field E at $x = 0.42h$ is lower by 18% than the maximum value of E at $x = h$; at $i/I_0 = 0.406$ the minimum value of the field differs from the maximum by a factor of 2.5.

From the foregoing it follows that parameter λ, which enters into the system of differential equations derived by Steinbok for ionization chambers and which contains E^2 in the denominator, cannot

i/I_0	0	$0.33h$	$0.42h$	$0.67h$	h
0.406	52	26	25	29	67
0.576	53	29	28	34	68
0.728	56	36	35	40	70
0.949	91	83	82	85	97

be considered a constant factor, but is rather a function of the coordinate $\xi = x/h$. As a result of this, in Eq. (5) the variables μ and ν cannot be separated and all the relationships subsequently given cannot be obtained. Thus, the expressions obtained in Ref. 1 are not, in fact, solutions of the equation for the volt-ampere characteristics of ionization chambers. This, of course, is the reason why the approximate expressions obtained by Steinbok differ from the approximate solutions of Mi and Seeliger.

Steinbok also gives a comparison of his experimental data which he obtained during the measurement of ionization by the compound $RaCl_2$. It is difficult to understand the fact that the experimental data for the ionization of α-particles do not conform to the dependence, characteristic for the ionization column, of the strength of the current on the difference in potential (see, for example, Ref. 3, Fig. 80) applied to the ionization chamber.

From the foregoing it follows that the volt-ampere characteristic of ionization chambers obtained in Ref. 1 and the description of the work of the ionization chambers on the basis of the characteristics derived by the author cannot pretend to rigor and accuracy. It is hardly possible to use these results in working with ionization chambers, since the question of the erroneousness of the equations is left open.

[1]N. I. Steinbok, J. Exptl. Theoret. Phys. (U.S.S.R.) 27, 5, 615, 1954.

[2]V. I. Veksler, L. V. Groshev, and B. M. Isaev. *Ionization methods of investigating radiation*, Gostekhizdat, 1949.

[3]K. K. Aglintsev, *Dosimetry of ionizing radiations*, Gostekhizdat, 1950.

[4]H. Seeliger, Ann. Physik 33, 319 (1910)

Translated by A. Certner
84

Disintegration of Positive Ions in Collision with Molecules

S. E. Kuprianov, M. V. Tikhomirov
V. K. Potapov and P. Ia. Karpova
Physico-Chemical Institute

(Submitted to JETP editor June 1, 1955)
J. Exptl. Theoret. Phys. (U.S.S.R.) 30, 569-570 (March, 1956)

In the mass spectra of some compounds broad peaks are observed whose centers of gravity do not coincide with the integral mass numbers. The apparent mass M^* is

$$M^* = M_K^2 / M_H, \tag{1}$$

where M_H and M_K – are the ionic masses before and after disintegration. The observed peaks are caused either by spontaneous disintegration of metastable ions[1,2] or by disintegration caused by collisions with molecules or atoms.[3-7]

We investigated some broad peaks in the mass spectra of carbon monoxide, carbon dioxide, methyline iodide and bromide, acetylene and ethylene (see Table). The investigation was carried out on a standard equipment MS-1 with ionic energy 2500 ev, electron energy 70 ev and electron beam current 0.5 ma. The pressure in the analyzer was 3×10^{-5} mm Hg. Mass spectra were automatically scanned by change in magnetic field and recorded by an electronic potentiometer. Ionic currents were measured at the maximum of the peaks.

We found that the intensity of broad peaks I^* in the first approximation is

$$I^* = \alpha I p. \tag{2}$$

where p is the pressure of the gas entering the analyzer of the apparatus, measured with an ionization gauge of the type LM-2, I is the intensity of the developed positive ions and α is a constant. As

No.	Disintegration scheme		M^*	Disintegration probability $\sigma \times 10^{17}$ cm^2					
				CO	CO_2	C_2H_2	C_2H_4	CH_2Br_2	CH_2J_2
1	CO^+	C^+	$5^1/_7$	1	2.8	—	—	—	—
2		O^+	$9^1/_7$	0.1	—	—	—	—	—
3		O^-	$9^1/_7$		0.6	—	—	—	—
4	CO_2^+	C^+	$3^3/_{11}$	—	4.2	—	—	—	—
5		O^+	$5^9/_{11}$	—	7.2	—	—	—	—
6	$CH^+ \longrightarrow$	C^+	$11^1/_{13}$	—	—	4.7	5	6.5	5
7	$CH_2^+ \longrightarrow$	C^+	$10^2/_7$	—	—	—	3	4	3

an example, relative peak intensities I^* / I are shown in Fig. 1, corresponding to the apparent masses $5^{1/7}$ and $10^{2/7}$ in the mass spectrum of carbon dioxide and methylene bromide in their dependence of the pressure in the analyzer.

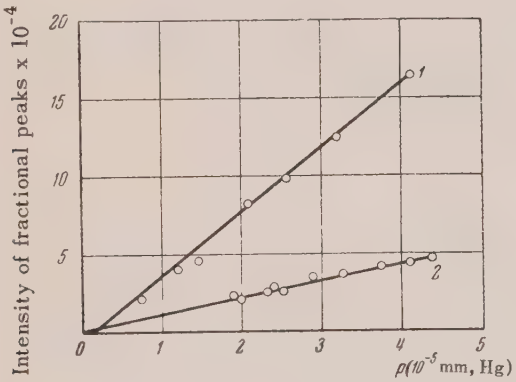

FIG. 1. 1 — $(I_{5^1/_7} / I_{28})$ (CO)×10; 2 — $(I_{10^2/_7} / I_{14})$ (CH_2Br_2)

The data given in the Table which characterize the probability of disintegration were obtained as approximations from

$$\sigma = N^* kT / Npl, \qquad (3)$$

where N^* and N are the number of disintegrated and undisintegrated ions, K is the Boltzmann constant, T is the absolute temperature, and l is the distance from the source to the magnetic field analyser. The N^* / N was determined from the height of the secondary and primary peaks. Since the fractional peaks are broad the values turn out too small. Furthermore the difference in ionization was disregarded.

The results given in the Table show that the disintegration probability of CO^+ ion according to the scheme 1 is greater than according to the scheme 2, which is in agreement with the electron affinity of oxygen and carbon. This is also confirmed by the disintegration of CO^+ from carbon monoxide according to the scheme 1 and 3. The difference of probability in processes 4 and 5 is interpreted, apart from the electron affinity influence, by the difference of the number of dissociated particles and the loss of energy connected with it. This refers also to the disintegrations according to the scheme 6 and 7.

The investigation of the influence of the electron energy up to 140 ev on the character of the dissociation processes has shown that the disintegration probability depends on the electron energy. This dependence is evidenced in the investigated cases by a decrease of the relative intensity of the fractional peaks with the decrease of the electron energy, whereby the relative intensity close to the potentials of ionic emission decreases stronger than at higher energies. The results obtained for carbon dioxide are shown in Fig. 2. A similar dependence have also other disintegrations shown in the Table where an increase of the electron

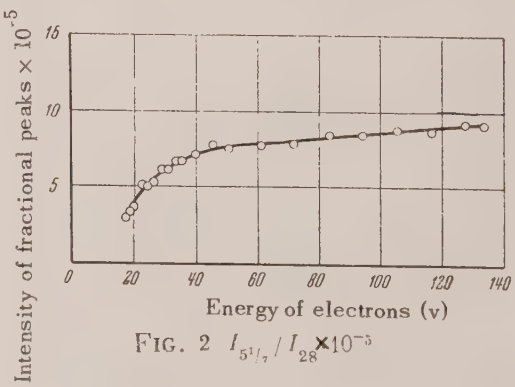

FIG. 2 $I_{5^1/_7} / I_{28} \times 10^{-5}$

energy in the region close to the ionic emission causes a disintegration increase 2-4 times. The dependence shown in Fig. 2 is similar to that of the peak with the apparent mass 1/2 investigated in the paper [8] in hydrogen ionization. We would like to mention that the influence of the electron energy on the disintegration of CH^+ and CH_2^+ in the investigated cases is different from that in methane ionization.[9] . In the last case the disintegration probability increases strongly in the region of ionic emission potentials.

The observed increase of probability of processes forming fractional peaks in disintegrations shown in the Table with an increase of electron energy is probably connected with the number and degree of excitation of emission ions. The second possible cause seems to be the increase of the initial kinetic energies of the fragmentation ions with the increase of the electronic energy.[10] An increase of ionic energy up to 3000 ev increases the probability of disintegration. The character of this dependence is influenced by the type of disintegration and by the nature of molecules involved in the collision process.

We are greatly indebted to Prof. N. N. Tunitskii for his constant interest and valuable advice during this work.

[1] J. A. Hippl, R. F. Fox and E. U. Condon, Phys. Rev. **69**, 347 (1946).

[2] V. H. Dibeler, C. Wise and F. L. Mohler, Phys. Rev. **71**, 381 (1947).

[3] G. Mattauch and F. Lichtblau, Physik Z. **40**, 16 (1939).

[4] A. Henglein and H. Ewald, *Mass Spectroscopy in Physics Research.* Nat. Bur. Stand. Circ. 522, 1953; A. Henglein, Z. Naturforsch. **7A**, 165 (1952).

[5] V. M. Kolotyrkii, M. V. Tikhomirov and N. N. Tunitskii, Dokl. Akad. Nauk SSSR 92, 1193 (1953).

[6] N. V. Fedorenko, J. Tech. Phys. (U.S.S.R.) **24**, 669 (1953).

[7] V. M. Dukel'skii and E. Ia. Zandberg, Dokl Akad. Nauk SSSR **99**, 947 (1954).

[8] N. N. Tunitskii, R. M. Smirnova and M. V. Tikhomirov, Dokl. Akad. Nauk SSSR **101**, 1083 (1955).

[9] M. V. Tikhomirov, V. M. Kolotyrkii and N, N. Tunitskii, Dokl. Aaad. Nauk SSSR **101**, 903 (1955).

[10] H. S. W. Massey and E. H. S. Burhop, *Electronic and Ionic Impact Phenomena.* Oxford, 1952.

Translated by A. Smakula
102

Beta-Spectrometer Investigation of Conversion Electrons with Aid of Nuclear Emulsions

I. A. ANTONOVA
Moscow State University

(Submitted to JETP editor November 15, 1955)
J. Exptl. Theoret. Phys. (U.S.S.R.) 30, 571-572 (March, 1956)

WITH present-day magnetic β-spectrometers, there are in use basically two methods for recording electrons --with the help of counters (gas discharge or luminescent) and photographically, by observing the intensity of darkening.[1] The photorecording method possesses the well-known advantage that it can be used in the study of very short-lived radioactive isotopes, whereas this possibility is practically excluded in work with counters. However, the sensitivity of the photographic method is low and one must use β-emitting sources of high activity.

The requirements become particularly demanding in those cases where the energy range of the β-spectrum does not exceed several hundred kev. The combination of high source activity and small thickness requires the use of compounds with high specific activity, often very difficult to obtain. A further serious drawback of the photorecording method appears to be the difficulty of measuring the relative intensities of the electron lines, due to the dependence of the intensity of darkening on the electron energy.

The above difficulties may be avoided by using thick electron-sensitive photographic emulsions and determining the number of electrons directly from the number of tracks, rather than from intensity variations. Analogous methods have been used earlier for investigating α-spectra with magmetic spectrometers, and have given positive results.*[2] The difficulty in using this method in β-spectroscopy is that the tracks are relatively thin and are quite tangled due to the strong scattering of the electrons. This makes it difficult to count the electrons against the granular background of the film.

The aim of the present work was to show the feasibility of using thick emulsions for recording electrons in a β-spectrometer, in particular for the study of conversion electrons. We employed a Danish-type spectrometer with semi-circular focussing and uniform transverse magnetic field. Its resolving power was 0.7 -1.0%. For recording

high energy electrons which produced rectilinear paths in the emulsion, a cassette was provided with a photographic plate tilted at 30° to the plane of incidence of the electrons, in order that the projected electron paths might be visible.

The source of conversion electrons was a Cs^{137} compound evaporated in layers on a mica strip 40 x 0.5 mm. to a depth of 0.2 mg/cm.^{2} The electron-sensitive plates were NIKFI type R with a grain density of 30-40 per 100 μ.

The tracks were counted with the aid of a binocular microscope, type MBI-2, having a compound drive. For convenience in counting, a grid was inserted in the microscope eyepiece. The number of electrons was recorded by a push-button counter. With this simple arrangement, scanning of the film took 2-3 hours.

In developing the method we tried out films with different thicknesses of emulsion, 200, 100, and 50 μ. The best results were obtained with the 50 μ thickness, which after developing and drying had a total thickness of 15-18 μ. This emulsion thickness proved to be quite satisfactory for distinguishing tracks against the granular background of the emulsion. In addition, the R-50 type film has the advantage that its photo-processing does not require a large expenditure of time or special equipment.

We investigated especially carefully the question of exposure time for a given source activity, and the degree of magnification in the microscope for the various films tested. The optimum exposure time for the film depended on the following: on the one hand, the number of electron tracks should not be too large, else the tracks become entangled and difficult to count, while on the other hand, for reduced statistical fluctuations, it is desireable that the number of tracks in the field of view of the microscope should not be too small. Investigation showed that with a magnification of X 300-450 the most efficient exposure was one for which the number of electrons in the microscope field of view ranged from several dozen to 300. This number could be increased to 400-500 if the film was saturated with a 5 - 10% solution of glycerin. In such swollen emulsions, the electron tracks expand toward the vertical so that the microscope focusses on a smaller region of the paths, in which the electron do not have time to scatter significantly. Such paths are easy to distinguish and count.

We used freshly poured emulsions, whose storage time did not exceed 7 days.

Figure 1 shows the β-spectrum obtained from

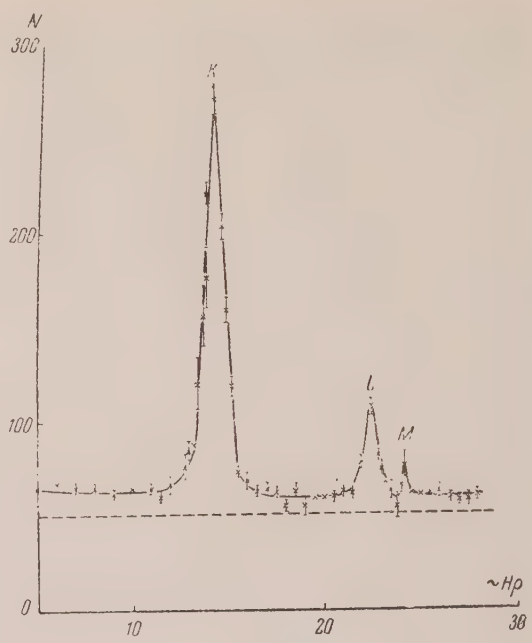

FIG. 1. Conversion Electron Spectrum of Cs^{137}

the internal conversion of γ-rays from Cs^{137} (Ba^{137*}) ($h\nu$=661. 6 kev). The numbers along the abscissa are proportional to $H\rho$, while the ordinate is N, the number of electrons in the field of view of the microscope at a magnification of X 420. The spectrum was obtained by exposing the plate for 2.5 hours to a 6 μ Cu source of Cs^{137}. It represents the average value of four curves taken from the same film. For each new curve the plate was shifted slightly toward the vertical. This made it possible to get good statistics from a single plate. As may be seen from Fig. 1 the errors in measurement do not exceed 8% and could be reduced with better statistics. A control film from the same batch showed that 51 ± 1 electrons accumulated in the background during the storage time. In the figure this background is shown as a straight dotted line. The remaining electrons in the general background, on which are distributed the K, L, and M peaks, belong to the β-spectrum of Cs^{137}, which accounts for about 8% of the total number of disintegrations.

Comparison of the areas of the K, L, and M peaks gave the ratios of the conversion coefficients for the γ-rays of Cs^{137}:

$$\alpha_K : \alpha_L : \alpha_M = (5.9 \pm 0.1) : 1.0 : (0.28 \pm 0.02).$$

The errors here represent mean square values from the processing of 7 plates. The results are in good agreement with those given by other authors[4-8] and obtained in β-spectrometers with recording by β-counters.

Thus the method of recording electrons in thick photographic emulsions proved to be entirely adaptable to β-spectroscopy. For a comparison of the exposure times necessary to darken an x-ray film appreciably, with that required by the photoemulsion method, we carried out a measurement using the same 2.65 mCu Cs^{137} preparation for both. The data obtained showed that the use of the emulsion permitted the investigation of isotopes 300-500 times weaker in intensity. This increase in sensitivity of counting, together with the other advantages of the photographic method will permit the study of many short-lived isotopes and may be of value in deciding a number of questions in β-spectroscopy.

In conclusion, I would like to thank I. M. Frank and I. V. Estulin for the interest they showed and for assistance with the work.

---

*It became known to the author afte the completion of the present work that a similar method had been used successfully by Pnievski[3] for investigating the β-spectra of RaD.

[1] L. V. Groshev and I. S. Shapiro, *Spectroscopy of the Atomic Nucleus*, GITTL, Moscow, 1952.

[2] E. S. Rosenblum, Phys. Rev. 72, 731 (1947).

[3] Ia. A. Pnievski, Acta Phys. Pol. 11, 215 (1953).

[4] W. C. Kelly, Phys. Rev. 85, 101 (1952).

[5] G. A. Graves, L. M. Langer, and R. D. Moffat, Phys. Rev. 88, 344 (1952).

[6] W. L. Bendel, F. J. Shore, H. N. Brown, and R. A. Becker, Phys. Rev. 87, 195 (1952).

[7] B. M. Dolishniuk, G. M. Drabkin, L. I. Orlov, and L. I. Rucinov, Dokl. Akad. Nauk SSSR 92,1141 (1953).

[8] R. E. Maerker and R. D. Birkhoff, Phys. Rev. 89, 1159 (1953).

Translated by C. R. Lubitz
103

Elastic Scattering of 5.4 Mev Protons by Various Nuclei

A. P. Kliucharev, L. I. Bolotin and V. A. Lutsik
Physico-Technical Institute, Academy of Sciences, Ukrainian SSR

(Submitted to JETP editor November 19, 1955)
J. Exptl. Theoret. Phys. (U.S.S.R.) 30, 573-574 (March, 1956)

A STUDY of the scattering of nucleons by atomic nuclei is one of the main sources of information about the form of a nucleus – the characteristics of the nuclear potential and the range of action of nuclear forces. Because of the success of the optical model for the scattering of neutrons by atomic nuclei[1] increased interest in proton scattering recently arose [2-5].

In the present work the elastic scattering of protons with initial energy of 5.4 mev by the following nuclei was studied: Be, C, F, Mg, Al, Ca, Mn, Ni, Cu and Zn. The measurements were made in the following manner. Fast protons, obtained from a linear accelerator, after going through a magnetic analyzer and a row of collimating diaphragms with diameters 2, 2.12, and 2.2 mm, were scattered by the target situated in a vacuum chamber. The scattered protons were registered by photoplates at various angles. The geometry of the experiment and the position of the photoplates are shown in Fig. 1. The angular resolution for the detectors nearest to the target was $\pm 2.5°$.

Because the photoplates, situated to the right and to the left of the beam (see Fig. 1), were simultaneously exposed, and the intensity of the Coulomb scattering is proportional to $\sin^{-4}(0/2)$ (where 0 is the angle of observation), the distances to the photoplates in the region of small angles were chosen in such a manner that the relationship $r \sin^2(0/2) = \text{const}$ would hold (r is the distance from the target to the detector.)

The targets for all metals studied were obtained in the form of thin foils or films of a couple microns thickness by evaporating metal in a vacuum, with the exception of nickel whose foil was obtained by electrolysis, and carbon which was prepared as a thin free film from aquadag (a graphite lubricant). For the study of scattering from fluorine thin films of MgF_2 and Li^6F were used, and for calcium films of CaF_2.

After the exposure of the photoplates and their photochemical development, first, a study of the energy spectrum of protons which were scattered by the target at 90° and 160° angles with respect to the primary beam was made. This study was made on the paths left by protons in the photoemulsion. The energy resolution of this method

was ±3.5 %. In such a way the groups of elastically scattered protons were isolated. The number of particles, corresponding to these groups, was counted afterwards on all plates. Two segments of the angular distribution curve obtained for small and large angles, were "joined together" using data for angles 50 and 60°. This was necessary in connection with the different exposure time for the "right" and "left" plates.

Previously, using this method, the angular distribution of protons scattered by gold and platinum was determined, and it was found that the distribution corresponded to the Rutherford formula within the limits of experimental error; this was to be expected since the nuclei had a greater potential barrier than the energy of incident protons.

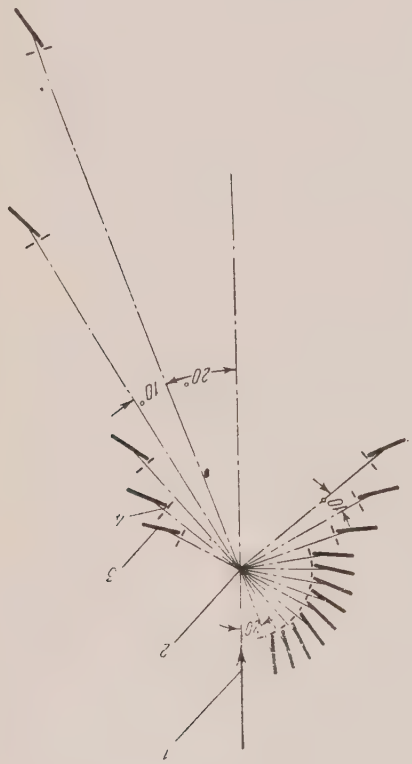

FIG. 1. *1*-proton beam, *2*-target, *3*-photoplate, *4*-diaphragm

The results obtained by us are shown in Fig. 2, where $N(\theta)$ is the number of protons scattered into the angle θ, $N(20°)$ is the number of protons scattered into the angle of 20°, θ_c is the angle in the center-of-mass system. Scattering from fluorine was obtained by excluding the effect of scattering from magnesium in MgF_2. Analogously,

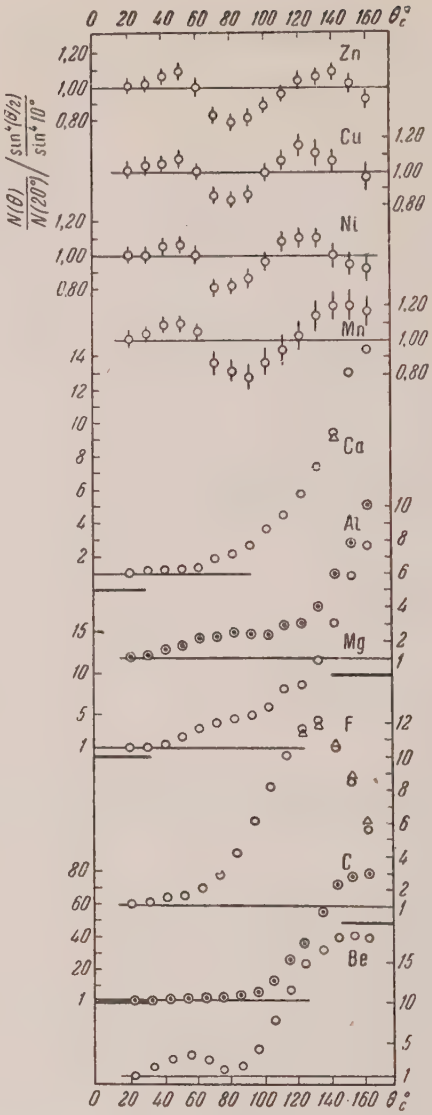

FIG. 2.

data was obtained for Ca from scattering by CaF_2. The qualitative trend of the angular distribution of protons scattered by fluorine into big angles was also measured using a thin film of Li^6F. The energy spectrum of protons, scattered from this compound, showed that for 110° it is already possible to safely divide the groups of protons elastically scattered by fluorine and Li^6. The data obtained in this way, and normalized for 110° are shown in figure 2 (the triangles). It was possible to safely separate the protons scattered by Ca and F from the target consisting of CaF_2 only for the angles of 140, 150 and 160° (the corresponding data is also shown by triangles).

The angular distribution of protons obtained by us differs very much from the Coulomb distribution and is not the same for various nuclei. Qualitative similarity in scattering by neighboring nuclei is observed. Thus, for Be and C a large scattering in the region of the angles 150-160° is obvious; however, the numerical value of the ratio for carbon is almost 4 times bigger than for beryllium. Apparently this is connected with the formation of the intermediate nucleus of N^{13}, which in this region of energies has an excitation level which gives rise to the resonant scattering of protons. Note that for an energy of 10 mev for carbon and for beryllium for 5.4 mev, a maximum at 50° [6] is observed. The curve for fluorine has a maximum for 140°. There is no data for scattering of protons from fluorine. but its neighbor – oxygen, has a big scattering maximum in the region of 120° for 9.6 mev.[5]

Scattering by magnesium and aluminum is similar, with a somewhat greater absolute value of the ratio for Mg. The angular distribution for Ni, Cu and Zn, within the experimental errors is alike in the magnitude of their ratios and in the position of maxima and minima. Similar curves for Cu were obtained by Goldman [7] for a proton energy of 6.5 mev; and by Schneider, Martin et al[8] for energies of 6, 6.5 and 7 mev. For Mn, qualitatively the curve for angular dependence is analogous to the preceding elements, but a displacement of the position of the minimum and second maximum in the direction of greater angles is observed, and the maximum is somewhat bigger. An unexpectedly large magnitude for the ratio for Ca was obtained, especially for big angles. It is possible that this was obtained as a result of two types of operation, which we were forced to do in these experiments; however, the fact is not excluded that this large effect is caused by a characteristic of the nucleus of Ca^{40}. The interesting fact is that, in spite of the small value of the ratio measured by us for heavier nuclei, the interference character of elastic scattering from these nuclei appears more clearly than for light nuclei.

Our attempts to explain the obtained results by the optical model have been as yet unsuccessful. It is possible, that the optical model in its present state is only a rough approximation for consideration of proton scattering, for which one must take into consideration a complex dependency on the potential of the nucleus, whose form can change. Obviously, further study of proton scattering at various energies and from a number of nuclei is necessary. Especially important is further study on free protons, which we are undertaking.

In conclusion the authors consider it their duty to express great thanks to Prof. K. D. Sinelnikov for discussion and constant interest in our work, and also to P. M. Seidlitz for his great attention which helped in the completion of work.

[1] H. H. Barschall, Am. J. Phys., 22, 517 (1954).

[2] B. L. Cohen and R. V. Neidigh, Phys. Rev. 93, 282 (1954).

[3] I.E. Dayton, Phys. Rev. 95, 756 (1954).

[4] R. D. Woods and D. S. Saxon, Phys. Rev. 95, 577 (1954).

[5] Y. Fujimoto and A. Hossain, Phil. Mag. 46, 542 (1955).

[6] G. E. Fischer, Phys. Rev., 96, 704 (1954).

[7] L. M. Goldman, Phys. Rev. 89,349 (1953).

[8] H. Schneider, M. Martin, M. Sempert and J. Saladin Helv. Phys. Acta, 27, 170 (1954).

Translated by M. Polonsky
104.

Photoconductivity and Luminescence of Polycrystalline CdS(Cu)

N. A. Tolstoi, B. T. Kolomets, O. I. Golikiva and M. Ia. Tsenter

(Submitted to JETP editor November 25, 1955)
J. Exptl. Theoret. Phys. (U.S.S.R.) 30
575-576 (March, 1956)

POLYCRYSTALLINE cadmium sulfide[1] with just a trace of a foreign metal represents a very convenient specimen for investigating the laws of photoconduction and luminescence. The results are summarized here of a preliminary investigation of the stationary (steady-state) and relaxation laws of a series of CdS specimens with just a trace of copper, and also copper and iron. The CdS (Cu) series consisted of 9 specimens (several of each) with various concentrations C (gms/gm) (see table)

Specimen number 10, CdS (Cu, Fe) had concentrations of Cu and Fe of 10^{-3} and 10^{-5} grams/gram, respectively.

1. Stationary (steady-state) photoconduction. The dependence of stationary photoconductivity $\Delta\sigma_0$ on the level of intensity of light E in specimens with small concentration (SC) of copper appears typical of photoconduction of the "hyper-

No.	C	No.	C
1	0	6	10^{-4}
2	10^{-6}	7	2.5×10^{-4}
3	10^{-5}	8	5×10^{-4}
4	2.5×10^{-5}	9	10^{-3}
5	5×10^{-5}		

bolic" type[2] : $\Delta\sigma_0$ grows slowly with E, showing some tendency to saturate "sublinear dependence" On the other hand, for high concentration (HC) specimens, $\Delta\sigma_0$ increases rapidly with E (''superlinear dependence''). In certain cases (No. 9 and No. 10) one observes a quadratic dependence ($\Delta\sigma_0 \sim E^2$). Specimens with intermediate concentrations show a dependence of $\Delta\sigma_0$ (E) that is nearly linear. All of these have a region of excitation that is in the ultraviolet part of the spectrum (mercury lines 365, 546 and 578 mμ; incandescent lamp with a green filter). Fig. 1 illustrates the dependence of σ (E).

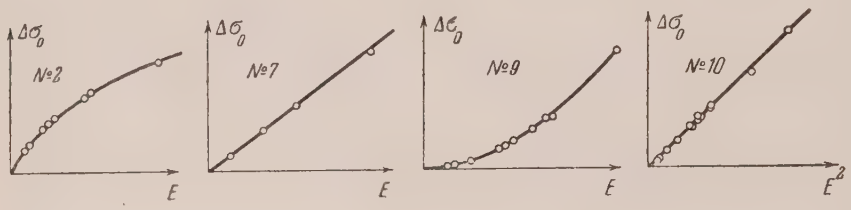

FIG. 1

The transition from sublinear to superlinear dependence takes place at a concentration of the order of several units of 10^{-4} grams/gram. As regards the dependence of σ_0 (E) for specimens with other concentrations C and different kinds of nonlinearity; comparison with photosensitivity is strictly speaking, meaningless. Nevertheless, it should be noted that through this range the values of E for specimens in the transition from LC to HC first increase the sensitivity and then abruptly reduce it. Dark conduction associated with the transition from LC to HC drops sharply.

2. Stationary luminescence. All specimens investigated were intensely illuminated in the red and infrared regions of the spectrum. Excitation was by the mercury 365 and 546 mμ lines. For samples of LC the brightness of stationary luminescence I_0 is proportional to E. For the HC specimen the dependence of I_0 (E) is superlinear. In some cases (No. 9 and No. 10) there is a quadratic relationship: $I_0 \sim E^2$. The transition from linear to sublinear dependence for luminescence is associated with somewhat smaller concentrations of activator than the transition from linear to sublinear dependence for photoconduction.

Figure 2 illustrates examples of the relationship $I_0 \sim E^2$.

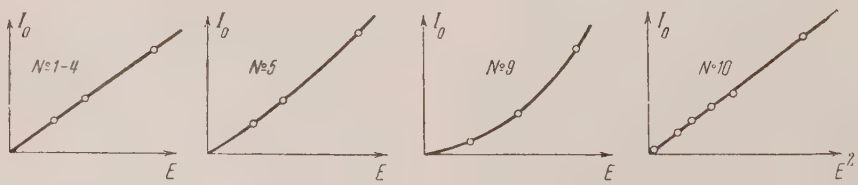

FIG. 2

3. Relaxation of photoconduction. Since the relaxation curves are not exponential, we show only the variations in their integral and differential characteristics. We first[3,4] introduced the areas above the growth curves (L_G) and the areas under the falling curves (L_F); we then[5] introduced the rate of growth of photoconduction from the instant the light was turned on (or the maximum velocity) $\Delta\sigma'_{OG}$ and the rate of decay of photoconduction from the instant the light is turned off, $\Delta\sigma'_{OF}$. Generally speaking, the above quantities are related to $\Delta\sigma'_0$, but we are interested only in the relations L_G/L_F and $\Delta\sigma_{OG}/\Delta\sigma'_{OF}$, from which $\Delta\sigma$ drops out.

For the LC samples $L_G/L_F < 1$, $\Delta\sigma'_{OG}/\Delta\sigma'_{OF} > 1$. Roughly speaking, the curves of growth increase rapidly. These results are typical for kinetic hyperbolic photoresistance, in general. For the HC specimens and No. 10 $L_G/L_F >> 1$ x $\Delta\sigma'_{OG}/\Delta\sigma'_{OF} << 1$: the growth curve increasing more slowly than the falling of the decay curve (Fig. 3). Further, the initial form of the growth curves was a parabolic character: $\Delta\sigma \sim t^2$ for small t, i.e., the growth curves have an inflection.

FIG. 3

4. Relaxation of luminescence. There is evidence of analogous characteristics for the curves of emission (flaring) and decay of luminescence, and one can ascertain the following: for the LC specimens $L_E/L_D \leq 1$, $I'_{OE}/I'_{OD} \geq 1$ (this is typical for ordinary kinetic hyperbolic phosphors in the absence of quenching). For the HC specimens and No. 10 $L_E/L_D >> 1$, $I_{OE}/I_{OD} << 1$, i.e., the curve of growth curving more slowly than the decay curve (Fig. 4). The growth curve increases parabolically at first and then twists (inflects). However, the relaxation characteristics are typical of concentration – or temperature – extinction phosphors of the hyperbolic type [for example, ZnS (Cu) and reference (6)].

5. Discussion. The alterations in the stationary and the relaxation law of photoconduction with

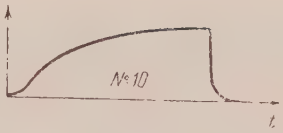

FIG. 4

increasing concentration can be seen to run parallel. Concentration quenches luminescence concomitantly with concentration quenching of photoconduction. Now, for CdS (Cu, Fe) the limit of quadratic dependence is particularly distinct, which is understandable if it is recalled that iron exhibits "classical" quenching with sulfides. The relationships $I_0 \sim E^2$, $I_E \sim t^2$ for small t, $L_E/L_D > 1$, are in agreement with the bimolecular theory of phosphorescence, in terms of lowest deterioration in the presence of pronounced quenching.[7] But it is possible to show that a value of $L_E/L_D > 3$ is not reconciliable with the bimolecular theory.[4] Experiments, however, yield values of L_E/L_D that go as far as 100. On the other hand, the dependence of $\Delta\sigma_0 \sim E^2$, $\Delta\sigma_{II} \sim t^2$ for small t and $L_H/L_C > 1$ sharply contradicts any recombination schemes, departing from the usual idea of the mechanism of excitation, but agreeing well with the theory based on the "two-stage" mechanism of excitation.[8,9]

Making a natural hypothesis suggested by this, namely, that the mechanisms of emission and photoconduction with CdS (Cu) and with CdS (Cu, Fe) exhibit a certain measure of unity, we are led to conclude that the relationships $I_0 \sim E^2$, $I_E \sim t^2$ likewise are not connected with the bimolecular degeneration mechanism of recombination, but with a two-stage mechanism of excitation (stimulation).

[1] B. T. Kolomets, Dokl. Akad. Nauk SSSR 83, 561 (1952).

[2] N. A. Tolstoi, P. P. Feofilov, Izv. Akad. Nauk SSSR, Ser. Fiz. 16, 59 (1952).

[3] N. A. Tolstoi and I. A. Litvinenko, J. Exptl. Theoret. Phys. (U.S.S.R.) 29, 507 (1955); Soviet Phys. JETP 2, 420 (1956).

[4] N. A. Tolstoi and A. V. Shatilov, J. Exptl. Theoret. Phys. (U.S.S.R.) 30, 109 (1956); Soviet Phys. JETP 3, 81 (1956).

[5] N. A. Tolstoi, Izv. Akad. Nauk SSSR, Ser. Fiz. 15, 712 (1951).

[6] V. A. Arkhangel'skaia, A. M. Bonch-Bruevich and N. A. Tolstoi, Izv. Akad. Nauk SSSR, Ser. Fiz. 15, 695 (1951).

[7] N. A. Tolstoi, Dokl. Akad. Nauk. SSSR 95, 249 (1954).

[8] V. E. Lashkarev and G. A. Fedorus, Izv. Akad. Nauk SSSR, Ser. Fiz. 16, 81 (1952).

[9] N. A. Tolstoi, J. Exptl. Theoret. Phys. (U.S.S.R.) 30, 171 (1956).

Translated by E. S. Emerson
105

ERRATA
(both of our own and of JETP)

Vol.	Page	Column	Line	Reads	Should read
2	434	2	22	27.3 μ	23.7 μ
2	557	Fig. 10			On the right hand side, abscissa values should read 0, 200 400, 600, 800, 1000.
2	591	2	7	$A = \frac{e^2 H_0^2 \delta_{00}}{mc^2}$	$A = \frac{e^2 H_{00}^2 \delta_{00}^2}{mc^2}$
2	754	1	3 ff.	———	[14] B. B. Kinsey and G. A. Bartholomew, Phys. Rev. 82, 380 (1951). [15] B. B. Kinsey and G. A. Bartholomew, Phys. Rev. 83, 234 (1951).
2	771	1	10	Intermediate State	Intermediate State of Tin
	771	1	19	sphere of lead	sphere of tin
3	145	1	1	$R = 10\ ec$	$R = 1/ec$

		Russian Reference
Letters to the Editor:		
An Alpha-decay Theory for Nonspherical Nuclei . . . . . V. M. Strutinskii	450	30, 411
Concerning Rayski's Bilocal Field Theory . . . . . V. A. Zhirnov	452	30, 425
The Leading Role of the Vibration Properties of Plasma and the Effect of the Gas Atoms on these Properties . . . . . I. P. Bazarov	453	30, 426
Asymptotic Meson-Meson Scattering Theory . . . . . I. T. Diatlov and K. A. Ter-Martirosian	454	30, 416
Relativistic Deuteron Disintegration in the Electric Field of the Nucleus . . . . . L. N. Rosentsveig and A. G. Sitenko	456	30, 427
On the Paper by N. I. Steinbok "Basic Characteristics of Ionization Chambers" . . . . . K. K. Aglintsev	458	30, 429
Disintegration of Positive Ions in Collision with Molecules . . . . . S. E. Kuprianov, M. V. Tikhomirov, V. K. Potapov and P. Ia. Karpova	459	30, 569
Beta-Spectrometer Investigation of Conversion Electrons with the Aid of Nuclear Emulsions . . . . . I. A. Antonova	461	30, 571
Elastic Scattering of 5.4 mev Protons by Various Nuclei . . . . . A. P. Kliucharev, L. I. Bolotin and V. A. Lutsik	463	30, 573
Photoconductivity and Luminescence of Polycrystalline CdS (Cu) . . . . . N. A. Tolstoi, B. T. Kolomets, O. I. Golikiva and M. Ia. Tsenter	465	30, 575
Errata	469	

CONTENTS

		Russian Reference
Toward New Successes of Soviet Physics	309	30, 433
Meson Field Theory. III. Conservation of Physical Quantities . . . A. A. Borgardt	312	30, 330
Generalized Form of the Diffusion Equation for a Single Particle . . L. Janossy	315	30, 433
The Hodoscopic Delayed Coincidence Method and Its Application to the Investigation of Slow Meson Formation in Cosmic Radiation . . . . . G. B. Zhdanov	323	30, 437
Formation of Negative Hydrogen Ions by Collision of Protons with Gas Molecules . . . Ia. M. Fogel' and R. V. Mitin	334	30, 450
Nucleomesodynamics in Strong Coupling. II. The Ground and Isobar States, Nucleon Charge and Spin . . . . . V. N. Baier and S. I. Pekar	340	30, 317
Meson Component of the Cosmic Radiation at an Altitude of 3200 m above Sea Level . . . N. M. Kocharian, M. T. Aivazian, Z. A. Kirakosian and A. S. Aleksanian	350	30, 243
Predischarge Phenomena in Liquid . . . . . I. E. Balygin	355	30, 464
Energy Spectrum of the Penetrating Particles of Extensive Cosmic Ray Showers . . . . . I. I. Sakvarelidze	361	30, 458
The Electromagnetic Field of a Linear Emitter Located inside an Ideally Conducting Parabolic Screen . . . . . G. G. Grinberg, N. N. Lebedev, I. P. Skal'skaia and Ia. S. Ulfiand	366	30, 528
Scattering of High-Energy Electrons and Positrons by Electrons . . . . . A. A. Abrikosov	379	30, 544
Meson Formation in Pb, Cu and C Nuclei by Cosmic Rays in the Stratosphere . . . . . D. Kaipov and Zh. Takibaev	385	30, 471
The Investigation of Trapping Centers in Crystals by the Method of Thermal Bleaching . . . . . Ch. B. Lushchik	390	30, 488
Nuclear Shells and Classification of Atomic Nuclei . . . . . A. V. Savich	400	30, 501
Motion of a Charged Particle in an Optically Active Anisotropic Medium. I . . . . . A. G. Sitenko and A. A. Kolomenskii	410	30, 511
The Theory of Nonlinear Effects in the Ionosphere . . . . . S. A. Zhevakin and V. M. Fain	417	30, 518
Theory of the Molecular Generator and Molecular Power Amplifier . . . . . N. G. Basov and A. M. Prokhorov	426	30, 560
Magnetic Symmetry of Crystals . . . . . B. A. Tavger and V. M. Zaitsev	430	30, 564
Deformation of Arc Column in Rarefied Gases at High Currents . . . . . G. G. Timofeeva and V. L. Granovskii	437	30, 477

(Contents continued on inside back cover)